Generic Methodology for Modeling and Simulation of Vibration, Wear and Noise in Electromechanical Drivetrains

Dissertation
to obtain the doctoral degree
in Mathematics and Natural Science

Submitted to the Faculty of Computer Science and Mathematics
Johann Wolfgang Goethe University
Frankfurt am Main

from
M.Sc. Yashwant Kolluru

Frankfurt 2020

(D30)

from Faculty of Computer Science and Mathematics
Johann Wolfgang Goethe University accepted as a Dissertation.

Dean:

Evaluator:

Disputation date:

Acknowledgements

The present doctoral thesis was conducted in a collaboration between the Robert Bosch GmbH at Reutlingen and Goethe University at Frankfurt.

In this context, I would like to express gratitude to my mentor Dr. Rolando Doelling and my manager Mr. Peter Kimmich for giving me the opportunity to work with the team. I thank my professor Lars Hedrich for the supervision at the university.

Yashwant Kolluru
Reutlingen, July 2020

Symbols

Latin Symbols

$\widetilde{a}$	mm	Constant from cantilever beam vibration equation
A	mm^2	Surface area
a	mm/sec	Acceleration vector
$\widetilde{b}$	m	Constant from cantilever beam vibration equation
B	$-$	Strain displacement matrix
$\widetilde{c}$	m	Constant from cantilever beam vibration equation
c	mm/s	Speed of sound
$\widetilde{d}$	m	Constant from cantilever beam vibration equation
d_z	Ns/mm	Tooth damping
$\boldsymbol{D}$	Ns/mm	Damping matrix
e	μm	path excitation
E	N/mm^2	Young's modulus
f	Hz	Frequency
$\boldsymbol{F}$	N	Force vector
F	N	Force
F	Nmm	Energy Functional
F_a	N	Axial force
F_r	N	Radial force
F_t	N	Tangential force
$\boldsymbol{F_n}$	N	Normal force vector
$\boldsymbol{g_C}$	mm	Total contact gap
$\boldsymbol{g_N}$	mm	Normal contact gap
h	μm	Wear depth
H	μm	Hardness
i	$-$	Space increment
$\underline{\boldsymbol{I}}$	N/mms	Complex intensity
J	$kgmm^2$	Moment of inertia
k	$-$	Wave number
K	$-$	K-factor
$\boldsymbol{K}$	N/mm	Stiffness matrix
$\boldsymbol{K_m}$	N/mm	Modal matrix
K_b	N/mm^2	Bulk modulus
k_z	N/mm	Tooth stiffness
LF_{ERP}	N/mm^2	Estimated Radiated Power Loss Factor
m	kg	Mass
M	Nmm	Driving torque
n	$-$	Number of elements
n	$-$	Time increment
N	$-$	Number of data points
$\boldsymbol{N}$	$-$	Shape element vector
o	$-$	Order
p	mm	grid potential
p	N/mm^2	Pressure
p_0	N/mm^2	Pressure at reference
p_{ERP}	N/mm^2	Estimated Radiated Power pressure
p_r	N/mm^2	Pressure at distance r
P	N/mm^2	Contact pressure
P_Q	Nmm	Acoustic power
r	mm	Pitch circle radius
$\boldsymbol{r}$	mm	Distance
S	mm	Slip
S	mm^2	Surface
t	s	Time
T	$-$	Rotation matrix
t_C	N	Contact force
$\boldsymbol{u}$	mm	Displacement vector
$\boldsymbol{v}$	mm/s	Velocity vector
v_i	$-$	Weighted sum layer
$\underline{\boldsymbol{v}}$	mm/s	Complex velocity
w	m	Deflection
w_{ij}	$-$	Weights of layers
$\boldsymbol{x}$	$-$	State space vector
y	$-$	Predicted values
$\hat{y}$	$-$	True values
z	$-$	Number of teeth
Z	Ns/m^3	Impedance

Greek Symbols

α_n	$\circ$	Contact pressure angle
β	$\circ$	Helix angle
β	–	Contact ratio
ζ	–	Damping ratio
ϵ	N/mm	Contact spring stiffness
ϵ_{mod}	–	Modified error
ϵ_V	–	Volumetric Strain
λ	–	Eigen values
μ	–	Friction coefficient
Π_C	–	Contact energy

Π_e	–	Energy potential
Γ	–	Volumetric drag
Θ	–	Modal matrix
Φ	–	Activation function
φ	$\circ$	Angular displacement
$\dot{\varphi}$	$\circ/s$	Angular velocity
$\ddot{\varphi}$	$\circ/s^2$	Angular acceleration
ρ	$kgmm^{-3}$	Density
ρ_f	$kgmm^{-3}$	Fluid density
ω	Hz	Eigen frequencies

Abbreviations

ANC	Active Noise Cancellation
ASAC	Active Structural Acoustic Control
AVC	Anti-Vibration Compound
BEM	Boundary Element Method
CFD	Computational Fluid Dynamics
COM	Component Oriented Modeling
DD	Dual Directional coupling
DOF	Degrees of Freedom
EMF	Electromagnetic Force
ERP	Equivalent Radiated Power
FEM	Finite Element Modeling
FFT	Fast Fourier Transform
FRF	Frequency Response Function

OGN	Other General Domains
LPM	Lumped Parameter Model
MBD	Multibody simulation
ML	Machine Learning
MM	Modal Model
MSE	Mean Square Error
MSLE	Mean Square Logarithmic Error
NN	Neural Network
NN	Nearest Neighbor
RSPM	Radiated Sound Power Model
SEA	Statistical Energy Analysis
SD	Single Directional coupling
TE	Transmission Error
UQ	Uncertainty Quantification

Contents

List of Figures

List of Tables

Abstract

This work describes development of a comprehensive methodology for analyzing vibro-acoustic and wear mechanisms in transmission systems. The thesis addresses certain gaps present in the fields of structure dynamics and abrasion mechanism and opens new areas for further research. The paper attempts to understand new and relatively unexplored challenges like influences of wear on the dynamics of drive train. It also focuses on developing new techniques for analyzing the vibration and acoustic behavior of the drive unit structures and surrounding fluids respectively.

The developed methodology meets the requirements of both the complete system and component level modeling by using specially identified combination of different simulation techniques. Based on the created template model, a three-stage spur plus helical gearbox is constructed and simulated as an application example. In addition to the internal mechanical excitation mechanisms, the transmission model also includes the rotational and translational dynamics of the gears, shafts and bearings. It is followed by illustration of wear among the rotating components. Different kinds of static and dynamic analyses are performed and coupled at various levels depending on the mechanical complexities involved. Furthermore, the structure dynamic vibration of the housing and the associated sound particle radiations are mapped into the surrounding fluid. Additionally, the approach for selection of the potential parameters for optimization is depicted. Final part focuses on the measurements of different system states used for validation of the model. In the end, results obtained from both simulations and experiments are analyzed and assessed for there respective performances.

Keywords : Noise, Vibration, Wear, Finite Element, Multi-domain modeling, Simulations, Neural Network, Gears, Housing, Powertrain.

Generische Methodik zur Modellierung von Vibration, Verschleiß und Geräusch in elektromechanischen Antrieben

Einleitung

Mit der Entwicklung von Elektrofahrzeugen entstehen für die Automobilindustrie neue Herausforderungen im Zusammenhang mit Lärm und Vibration. Der Wandel von Verbrennungs- zu Elektromotoren hat das Fahrzeug deutlich leiser gemacht. Im Zuge der Elektrifizierung werden durch das Ersetzen des Verbrennungsmotors bisher überlagerte Getriebegeräusche hörbar. In der Folge sind zuvor verborgene Vibrations- und Geräuschquellen dominanter geworden. Störend ist hierbei das Heulen des Getriebes, da monotones Pfeifen vom Menschen als besonders unangenehm wahrgenommen wird. Es entsteht mechanisch durch die wechselnde Anzahl von biegeweichen Zähnen im Zahneingriff sowie durch Geometrieabweichungen von der idealen Zahnform. Folgt man dem Körperschallpfad, so breiten sich die dynamischen Anregungen über die Zahnräder und Wellen bis zu den Lagern aus. Letztere übertragen die translatorischen Kräfte an das Getriebegehäuse und versetzen dieses ebenfalls in Schwingungen. Die Gehäuseoberfläche emittiert schließlich hörbaren Schall in Form von Druckschwankungen in das umgebende Luft. Bild 0.1 zeigt die vollständige Liste der im elektrischen Antrieb zu betrachtenden Herausforderungen und den hervorgehobenen Schwerpunkt (Motor) dieser Arbeit. Einflussparameter auf die Antriebseinheit sind unter anderen Temperatur, Leistung und Vibration, welche aus der Umwelt, dem Motor respektive von der Fahrbahn herrühren. Die Zeichnung HMI bedeutet Human Machine Interface. Diese Arbeit befasst sich mit der Untersuchung der Antriebseinheit und ihre Leistungsindikatoren wie Vibration, Verschleiß und Geräusch. Dadurch sollen die Strukturen werden verbessert und ein insgesamt geräuschärmerer Antriebsstrang entstehen.

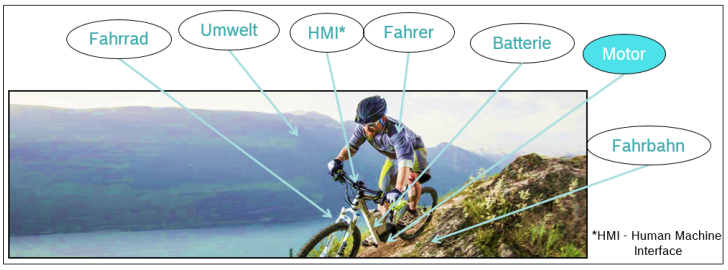

Bild 0.1: Einflussgrößen für ein eBike System

Im Folgenden ist eine Liste der Ziele und Herausforderungen dargestellt, die definiert wurde, um die Eigenschaften des Antriebsstrangs zu analysieren und zu verbessern:

- Die vibroakustischen Phänomene im Antriebsstrang können zu unangenehmen Folgen für das Endprodukt hinsichtlich der Geräuschemission führen. Die wichtige Frage hierbei ist, wie Entwickler so früh wie möglich ein umfassendes Bild über die Auswirkungen von Körperschall und Luftschall auf das Verhalten von Komponenten und Multi-Domänen erhalten können und wie das Wissen während des gesamten Entwicklungsprozesses für verschiedene Übertragungsvarianten kontinuierlich genutzt werden kann. Die erste Heraus-

forderung, um die Schwingungen der elektrischen Antriebe zu erfassen, liegt beim Aufbau einer Methodik zur präzisen Vorhersage des vibroakustischen Verhaltens.

- In zahlreichen technischen Anwendungen unterstützen Zahnräder die Kraftübertragung zwischen den rotierenden Wellen. Zusammen mit der Kraft werden auch die unerwünschten strukturellen Schwingungen durch die Wellen übertragen. Die Herausforderung besteht darin, die Einflüsse mechanischer Erregungen zu analysieren, die von Zahnradeingriffen der Wellen und Zahnräder herrühren. Das nächste Ziel besteht nun darin, die Auswirkung dieser Schwingungen auf das Gehäuse zu analysieren. Das konstruierte Modell soll hauptsächlich eine schnellere Analyse der verschiedenen Phänomene ermöglichen und die in den Prototypen schwierig wahrzunehmen sind. In Bezug auf eine physikalische oder numerische Modellierung von Übertragungen, die insbesondere die Schwingung am Gehäuse und die Schallstrahlung umfassen, ist es teilweise überaus schweig, in der Literatur Quellen ausfindig zu machen. Hierbei wird auf einzelne Mechanismen fokussiert, den vollständigen vibroakustischen Übertragungsweg, also die strukturell gekoppelte Schwingung zwischen rotierenden Getriebeteilen und Gehäuse zur Schallemission in die umgebende Flüssigkeit, wird nur teilweise und nicht als Ganzes betrachtet.
- Einer der Hauptfaktoren, der in Lauf der Zeit die Schwingungen des Antriebsstrangs beeinflusst, ist der Verschleiß der Komponenten. In den letzten Jahren hat die Berechnung und Reduzierung des Verschleißes eine immer größere Bedeutung erfahren. Bis zu diesem Punkt haben Forscher nur wenige Experimente durchgeführt, die sich mit der Herausforderung der Quantifizierung des Verschleißniveaus und seiner Verteilung befassen. Der Mangel an geeigneten numerischen Modellen, um dieses Phänomen in der Entwicklungsphase anzugehen, ist immer noch ein Problem. Das Ziel dieses Teils der Arbeit ist es, das Ausmaß und die Verteilung des mechanischen Verschleißes unter Verwendung mehrerer geeigneter Verschleißmodelle vorherzusagen sowie dessen Auswirkungen auf Vibrationen tiefergehend zu analysieren.

Die Entwicklung eines Methodenflusses, welcher nur für bestimmte Varianten oder ohne die Möglichkeit von Erweiterungen mittels verschiedener Domänen usw. anwendbar ist, erscheint nicht sinnvoll. Aus den oben genanten Herausforderungen können Modellanforderungen und notwendige Attribute definiert werden (siehe Tabelle 0.1), die für das Systemmodell erforderlich sind, um die entwickelten Techniken für alle Varianten und für verschiedene physikalische Probleme anzuwenden (mehr Information im Kapitel 2.1) [KDH19a].

Modellanforderungen	**Notwendige Attribute**
Modularität	Anregung Mechanismus
Wiederverwendbarkeit	Getriebe Vibration
Erweiterbarkeit	Gehäuse Vibration
Einfachheit	Vibration und Akustik Kopplung
Schnelligkeit	Akustik Charakteristik
Verlässlichkeit	Verschleiß Mechanismus

Tabelle 0.1: Modellanforderungen und Attribute einer Antriebseinheit

Darstellung der generischen Multi-Domänen Methodik

Um Geräusche und Vibrationen eines jeden Entwicklungsknotens zu verstehen, müssen Parameter wie Anregungsmechanismen an der Quelle, Übertragung von Geschwindigkeiten entlang der Komponenten und Vibrationen am Gehäuse gründlich analysiert werden. Das Vibrationsmodul besteht aus drei Modellkomponenten: mechanisches Getriebe, Gehäusestruktur und die dazugehörige Fluid-wechselwirkung.

Ein mechanische Getriebe enthält die internen Erregungsmechanismen im Zahngitter, die das Zahnrad in Schwingung versetzen. Innerhalb dieses Bereichs werden die angetriebenen und treibenden Wellen auf System- und Finite Element (FE)-Ebene abgebildet. Zur Modellierung der physikalischen Prozesse wird das mechanische Getriebe daher in drei weitere Mechanismen unterteilt: nichtlineares Zahngitter, Getriebekomponenten und flexibles Gehäuse. Alle drei Modellteile werden im Abschnitt 4.4.2.1 ausführlicher beschrieben (vgl. Bild 0.2). Die Schwingungen bilden Zahnräder und Wellenstrukturen, die sich in Form von Wellen auf die Lager ausbreiten. Diese Bewegungen in den Lagern erregen das Getriebegehäuse und den Deckel und lassen sie schließlich vibrieren. Die Gehäusestrukturen werden unter Verwendung der Konzepte des Flex-Body und des Submodells auf System- bzw. FE-Ebene modelliert [Hat00]. Die Gehäusestruktur hat ein Spektrum von Eigenfrequenzen und -moden und fungiert als eine Art Membran, die letztendlich Geräusche in Form von Luftschall abgibt. Schließlich werden die akustischen Infinite- und ERP (Equivalent Radiated Power) Techniken zur Berechnung der akustischen Drücke um das Gehäuse verwendet.

Abrieb in Antriebssträngen verschlechtert schließlich die NVH-Eigenschaften. Daher ist es wichtig, seine Verhaltensweisen und Formulierungen zu verstehen. Dies erfolgt durch Erstellen einer numerischen Kopplung zwischen den Vibrations- und Abriebmodulen. Anschließend werden die Konstruktions- und Materialänderungen definiert, um die Gehäusestrukturen hinsichtlich ihrer vibroakustischen Eigenschaften zu optimieren (vgl. Bild 0.2) [KDH20a].

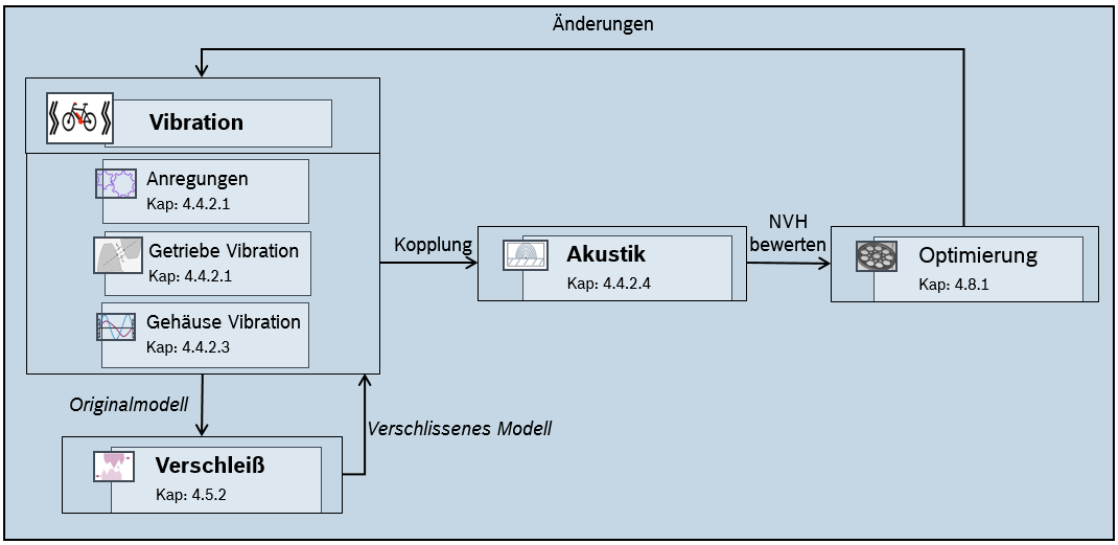

Bild 0.2: Modulare, domainübergreifende Modellbildung für eine eBike Antrieb

Eine detaillierte Ansicht der identifizierten Modellierungsmethoden für jedes dieser Module und seiner Verbindungen ist in den Kapitel 4.4, 4.4.3, 4.6 und 4.6.2 vorzufinden.

Abbildung 0.3 stellt einen generischen Prozess für den Datenfluss dar, um die beschriebenen Attribute zu realisieren. Grundsätzlich zeigt es zwei Abläufe, von denen sich einer auf den Ansatz der Mehrfachdomäne konzentriert (Ablauf-1 in Abbildung 0.3), während der andere Anwender zur Nutzung einer einzelnen Simulationsdomäne führt (Ablauf-2 in Abbildung 0.3). Beide Ansätze besitzen ihre jeweiligen Vor- und Nachteile. Diese werden im Kapitel 4.4.3 ausführlicher erläutert. Die entsprechende Schleife wird basierend auf kritischen Aspekten wie Genauigkeit, Geschwindigkeit, Komplexität im Design usw. ausgewählt. Darüber hinaus wird im Diagramm auch die Bezugnahme auf den entsprechenden Abschnitt (im Kapitel 4.4.3) der jeweiligen Modellkomponente gezeigt [KDH20b].

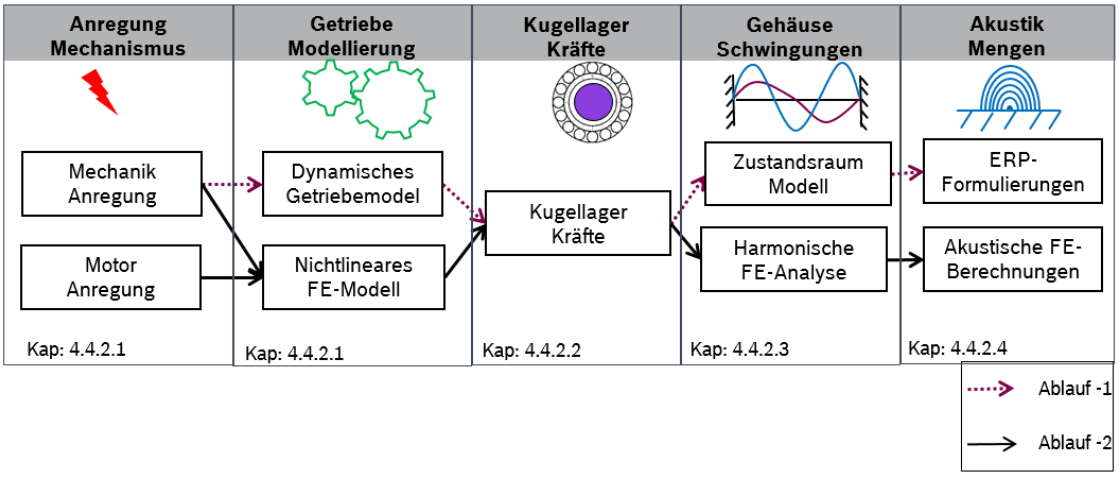

Bild 0.3: Systemmodell zur Realisierung der NVH-Eigenschaften

Abbildung 0.4 zeigt den Datenfluss für die FE-Simulation. Die Felder in der Spezifikationsebene geben die Geometrien, Materialien, Lastprofile usw. an. Die Werte für Kontakteigenschaften, Netzgrößen sowie, Last- und Randbedingungen werden im Feld FE definiert. Diese Werte spielen für die Stabilität und Konvergenz der Simulationen eine Schlüsselrolle. Werte von Parametern wie Reibung, Überlappende Domänen, Lücken und Interferenzen werden hinzugefügt, um die Kontaktdefinitionen effizienter zu gestalten. Sobald das Simulationsmodell für den Lauf verfügbar ist, wird es mit dem Subroutine-Programm gekoppelt, um den Verschleiß an den Zahnradeingriffen zu berechnen. Die jeweiligen verschleißbedingten Materialabträge werden in der Feld variablen der FE-Software gespeichert [KDH19b]. Weitere Informationen sind in Kapitel 4.5 zu finden.

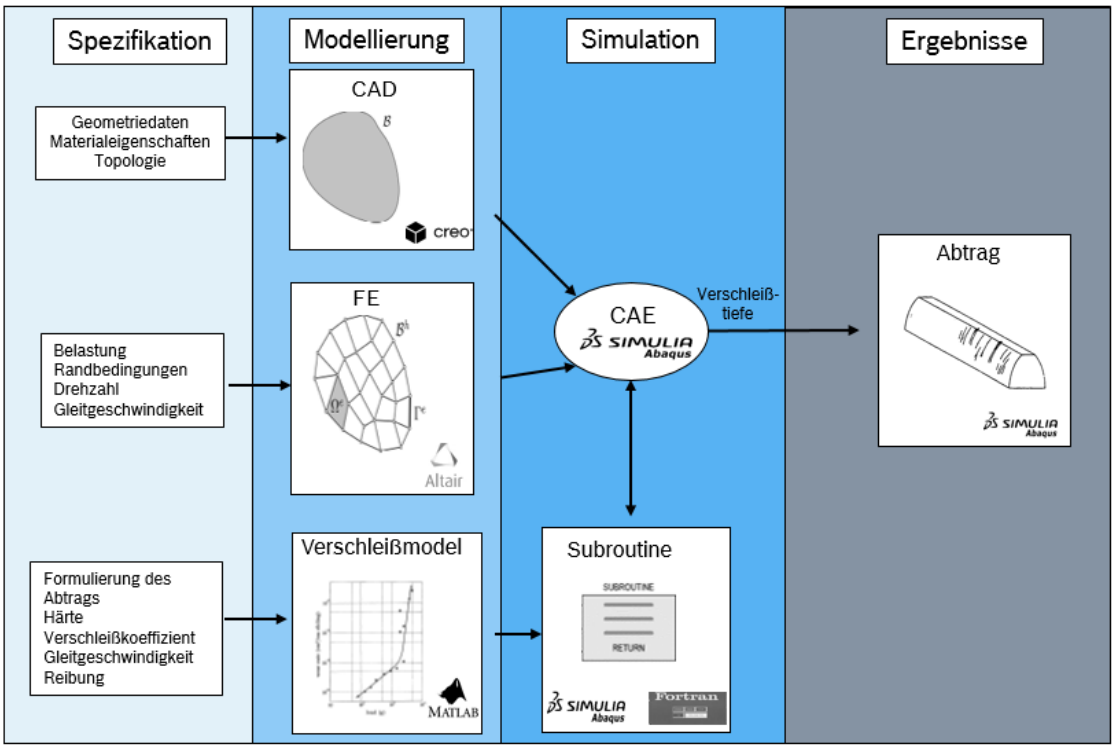

Bild 0.4: Schematische Darstellung einer Verschleißsimulation eines Antriebe

Verifikation der Methodik anhand eines Elektrischen Antriebs

In dieser Arbeit soll ein dreistufiges Getriebe für ein vibroakustisches System unter Verwendung der Methoden aus Kapitel 4 und der Techniken zur Modellierung von Instanzen aus Abschnitt 5 analysiert werden. Zur Modellvalidierung, werden Systemgrößen wie Motordrehmomente, Motordrehzahlen, Oberflächengeschwindigkeiten und Schalldruckmessungen verwendet. Schließlich wird die experimentell Validierung der Oberflächenschwingungen und akustischen Schwankungen anhand eines Laservibrometers und einer akustischen Kamera durchgeführt.

Die Vibration der Gehäuseoberfläche wird an verschiedenen Stellen mit dem Laservibrometer gemessen. Die Messprotokolle und die entsprechenden Simulationsergebnisse werden einer Auftragsanalyse unterzogen. Der Vergleich ist in Abbildung 0.5 dargestellt. Die X-, Y- und Z-Achse zeigen jeweils die Motordrehzahl, Frequenzkomponenten der Signale und die Amplitude der Oberflächengeschwindigkeit am entsprechenden Messpunkt. Zwei für die Validierung verwendete Merkmale sind zum einen die Ordnungslinien und zum anderen die Resonanzspitzen. Diagonale und horizontale Linien in der Grafik zeigen die Zahnradreihenfolge bzw. die Systemresonanzen. Größere Vibrationen an der entsprechenden Getriebekomponente treten auf, wenn ihre Reihenfolge den Systemresonanzen entspricht. Die Steigung dieser Linien korrespondiert zum ganzzahligen Vielfachen des Eingriffs pro mechanischer Zahnraddrehung relativ zur Rotorwelle betrachtet. Es gibt stärkere und schwächere Ordnungslinien. Die dominanten Ordnungen stammen aus der ersten (motorseitigen) Getriebestufe und sind in Abbildung 0.5 hervorgehoben. Die Messungen des Laservibrometers weisen zusätzliche schwächere Ordnungslinien auf, welche aufgrund der Lager der entsprechenden Wellen auftreten. Die Anzahl der Wälzkörper im Lager multipliziert mit der Geschwindigkeit entspricht der ersten Ordnung des jeweiligen Lagers. Diese Anregung durch Wälzkörper ist im Simulationsmodell nicht enthalten. Weitere Informationen sind in Kapitel 6.2.3 zu finden.

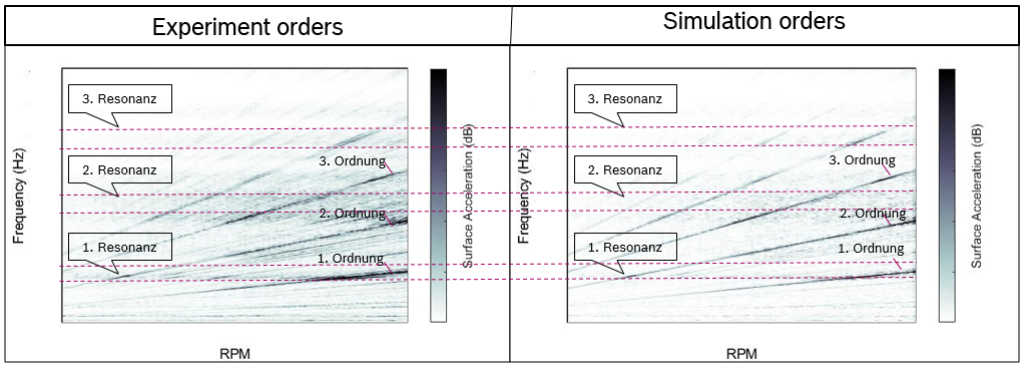

Bild 0.5: Campbell-Diagramme von Experiment vs. Simulation für das Mehrkörper-Modell

Die Graphen in Abbildung 0.6 beschreiben die Schwingungs- und Oktavediagramme, welche für den gesamten Antriebsstrang mithilfe der Oberschwingungsanalyse erhalten werden konnten. Die zuvor aus einzelnen und kombinierten Struktursimulationen erfassten Modellparameter werden in der Modellvorlage des Antriebsstrangs verwendet, um die Genauigkeit zu verbessern [KDH19a]. Zusätzlich werden vor der Durchführung der stationären Analyse die Strukturen auf Verformungen und Nichtlinearitäten überprüft, vgl. dazu Abschnitt 6.2.2. Sobald sichergestellt ist, dass die Verformungen innerhalb der Grenzen liegen, werden die Modelle in das Vibrationsmodul übertragen.

Die Werte für Experiment und Simulation stimmen jedoch nicht vollständig mit einer Genauigkeit überein, wie anhand des Diagramms 0.6 ersichtlich ist. Nichtsdestotrotz zeigt die Abbildung 0.6, dass die Simulation in der Lage ist, das Experiment, gut abbilden zu können. Die Y-Achse des Diagramms auf der linken Seite repräsentiert die Beschleunigung / Kraft, die auch

als Frequenz Response Funktion (FRF) der Schwingungsdaten bekannt ist. In ähnlicher Weise repräsentiert die Y-Achse der rechten Seite den Schalldruck / Kraft. Die X-Achse beider Diagramme entspricht der Frequenz. Die Abweichungen zwischen den Ergebnissen können durch viele Gründe, wie bspw. experimentelle Abweichungen oder Simulationsfehler verursacht werden. Insgesamt betragen die modifizierten Fehlerwerte, die unter Verwendung der Gleichung 6.3 für strukturbasierte und luftgetragene Emissionen berechnet wurden, 5,14% bzw. 3,39% [KDH20b].

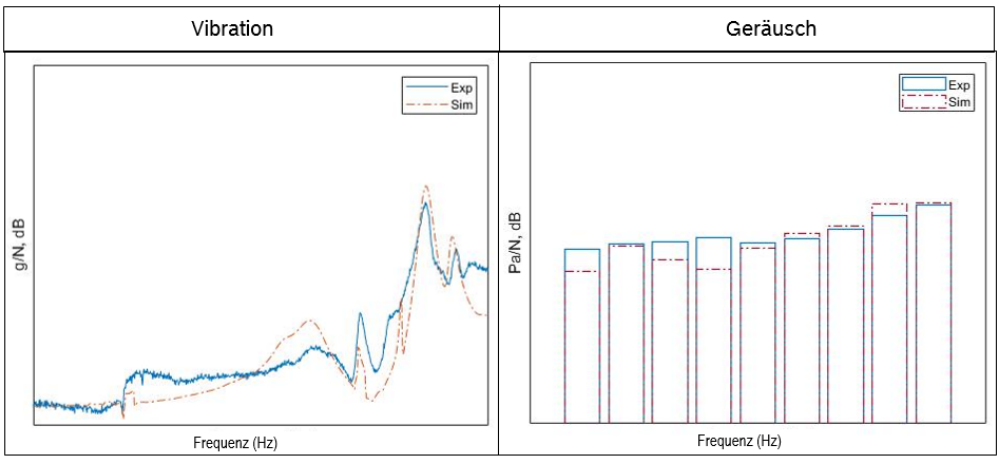

Bild 0.6: Vibration und Schalldruck des gesamten Antriebsstrangs für Experiment und Simulation, skaliert

Schließlich zeigt Abbildung 0.7 die Vergleichsdiagramme zwischen Experiment und Simulation nach dem Verschleißprozess an den Getriebewellen. Insgesamt ergeben sich aus den nach Gleichung 6.3 berechneten modifizierten Fehlerwerten für Oberflächengeschwindigkeiten und Schalldrücke 6,56% bzw. 4,27%. Weitere Informationen sind in Kapitel 6.4 zu finden [KDH20a].

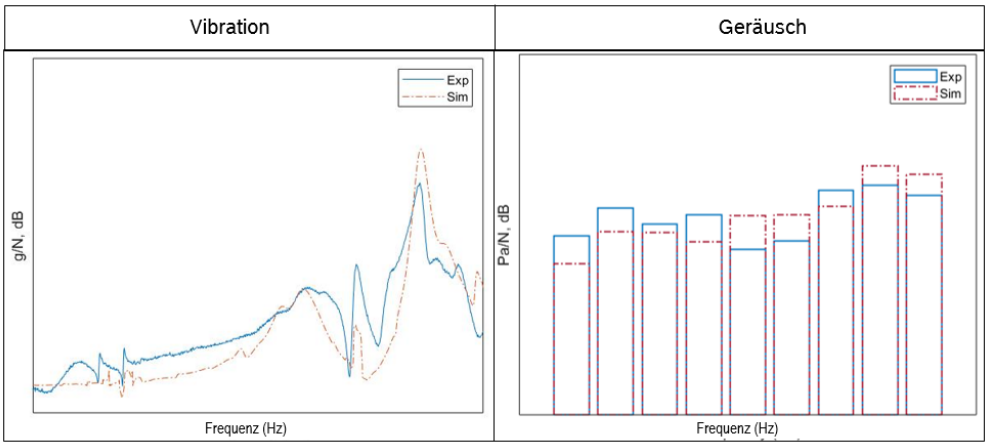

Bild 0.7: Vibration und Schalldruck des gesamten Antriebsstrangs (nach Verschleiß am Zahnradgitter) für Experiment und Simulation, skaliert

Zusammenfassung

Das Modell zur Berechnung von Vibration und Abrieb wird als Beispiel gezeigt, welches aus einem dreistufigen Stirnradgetriebe besteht. Es wird unter Verwendung einer Modellierunginstanz auf Basis der Methodik erstellt und erfüllt somit die Modellanforderungen und die er-

forderlichen Attribute aus Abschnitt 4.2. Der Nachweis der korrekten Implementierung der Modellierunginstanz wird in Kapitel 5 erbracht. Die Validierung der physikalischen Mechanismen des Modells wird in Abschnitt 6.4 geliefert.

Die Oberflächenvibration des Getriebegehäuses erzeugt den Luftschall, der in das umgebende Fluid abgegeben wird. Im Allgemeinen wird der Schall über die kinematischen Kopplungsbedingungen berechnet, wobei die Normalgeschwindigkeit der Struktur sowie des Fluids an der Grenzfläche als gleich angesehen werden. Ferner werden Impedanzen, Materialeigenschaften des Fluids usw. berücksichtigt, um die Schalldrücke an Fernfeldorten zu berechnen. Aus Systemsicht wird die ERP Technik hauptsächlich für die Berechnungen verwendet. Für die FE-Ergebnisse werden die Konzepte akustisch-finiter und -infiniter Elemente verwendet, die auf der Grundlage der Navier-Stokes-Gleichungen entwickelt werden (siehe Abbildung 4.24). Die modifizierten Fehler von etwa 15% und 5% des Schalldrucks werden für das ERP- bzw. FE-Modell berechnet. Diese Prozentsätze zeigen die Genauigkeit von FE- gegenüber der Systemmodellsimulation.

Eine weitere signifikante Herausforderung bestand in der Quantifizierung des Zahnradverschleißes. Obwohl die Simulation des Verschleißes sehr komplex ist, werden viele Annahmen getroffen, damit die Komplexität soweit verringert werden kann, sodass eine numerische Untersuchung möglich ist. Parameter wie Härte, Kontakteigenschaften, Reibung usw. werden über den Uncertainty Quantification Ansatz analysiert. Später werden die FE-Simulationen ausgeführt, um die Verschleißabträge und Verschleißraten berechnen zu können(vgl. dazu Abbildung 4.30). Darüber hinaus werden die Werte für weitere Vorhersagen mit Algorithmen für maschinelles Lernen gekoppelt. Die modifizierten Fehler von 10% und 7% gegenüber der Experimente werden für Vibrationen und Akustik im verschlissenen Simulationsmodell erhalten.

Zusammenfassend lässt sich sagen, dass ein Simulationsmodell, das nach der generischen Multi-Domänen Methode erstellt wurde, nicht nur die numerische Analyse modifizierter Übertragungskomponenten ermöglicht, sondern auch die Chance bietet, verschiedene Systemparameter zu optimieren. Aufgrund der Abbildung zwischen den Multi-Domänen Mechanismen sowie Anregung, Transmission und Strahlung können diese im Rahmen eines Gesamtsystems optimiert werden. Schließlich werden die Auswirkungen von Parameteränderungen in den Abschnitten 4.8 und 6.5 gezeigt. Ausreichende Verbesserungen der akustischen Größen um 5 bis 10% werden durch die in diesen Abschnitten gemachten Vorschläge erreicht.

Ausblick

Diese Arbeit konzentriert sich auf die Quantifizierung der akustischen Merkmale wie Druck und Intensität im Hinblick auf den Antriebsstrang. Psychoakustische Belange, d.h. das akutische Verhalten in Bezug auf das menschliche Ohr, werden in dieser Arbeit nicht betrachtet. Gleiche Amplituden von Schalldrücken sind bei Frequenz-änderungen auf völlig andere Weise wahrnehmbar. Parameter wie beispielsweise Lautstärke, Tonalität, Rauheit, Schwankungsstärke usw. sind für Charakterisierungszwecke viel nützlicher. Die Bewertung dieser Art von Luftschallemission fällt, wie oben bereits kurz angesprochen, in den Bereich der Psychoakustik. Zu diesem Zweck kann das Schallverhalten im Hinblick auf den menschlichen Eindruck weiter analysiert werden.

In Bezug auf die Verschleißsimulation können genauere Verschleißmodell-Subroutinen entwickelt werden (z. B. anwendungsspezifisch), um plausiblere Simulationsergebnisse zu erhalten. Bisher wurde eine sigmoidale nichtlineare Aktivierungsfunktion verwendet, um Vorhersage mit neuronalen Netzen treffen zu können. Diese Netze haben jedoch das Problem, dass dessen Gradienten verschwinden, wenn sie die Anfangsschichten erreichen. Dies kann Probleme beim Entwickeln eines neuronalen Netzwerks mit größeren Werten und mehreren Schichten verursachen. Um dieses Problem vermeiden und verbesserte Vorhersagen treffen zu können, wurden einige weitere alternative Aktivierungsfunktionen wie rectified linear activation unit (ReLU) oder erweiterte Faltungs- und zeitliche neuronale Netze getestet (Detaillierte Ausführungen hierzu sind im Kapitel 7 zu finden).

1 Introduction

1.1 Motivation

The automotive industry of the 21st century is portrayed by massive competition and increasing demands. One of the captivating question of this thriving industry is the carbon emissions from the vehicles. The increasing amount of greenhouse gases is leading to deterioration of the atmosphere. Usage of renewable energies is one of the methods to tackle this problem and electric mobility is a part of this huge sustainable energy umbrella. It enables the humans to shift towards a better direction. A path which has the potential of enhancing the lifespan of our planet, thereby in longer run improving the life of all the species.

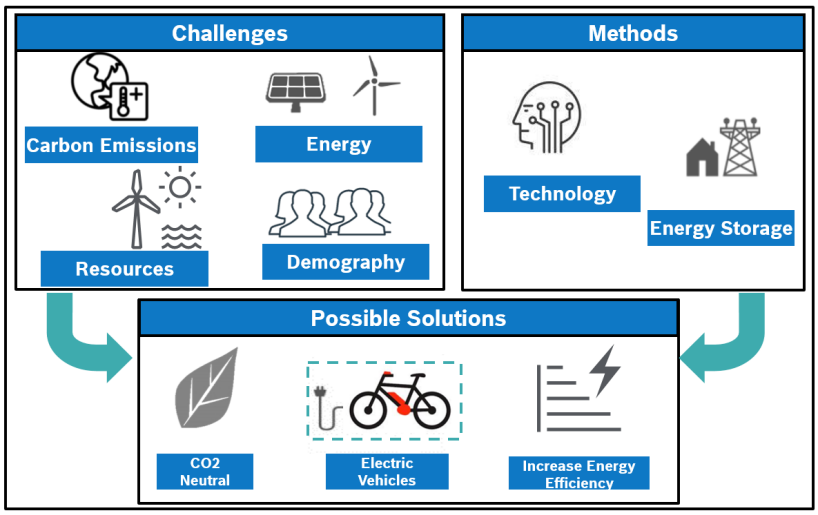

Figure 1.1: Challenges of today's world along with its possible methods and solutions

Figure 1.1 shows main challenges faced by today's world along with possible set of solutions. The growing demands of the electric mobility paved path in construction of the electrified drivetrains for the power transmission problems. The electric drivetrains like other normal automobiles posses the problems associated with the vibrations, which would discomfort the users. Analyzing the Noise, Vibration and Harshness (NVH) is a critical consideration in the design of combustion and electric vehicles for comfort. The fatigue of components arising from interior vibrational and acoustic pressure fluctuations caused by external structural or acoustic loading can bring disturbance and eventually can impact the life cycle of the vehicles.

The main source of vibrations in the electric drivetrains are the rotating components. A gear howl is described as a monotonous whistling, which is perceived by humans as unpleasant. It is created mechanically by the changing number of teeth in meshing and by geometrical deviations from the ideal tooth shape. If one observes the path of structure borne emissions, it originates from the vibrations of gears and shafts and is transferred to the bearings. The latter transmits translatory forces to the housings and would cause them to vibrate. The housing surface eventually emits audible sound in the form of pressure fluctuations on the surrounding fluid. Apart from the component excitations, the other main factor which can impact the vibrations is the

wear. Wear happens at the areas where there is repetitive contact and for our case it is the gears of drivetrain. Higher abrasion values can cause failure of the components and deterioration of the acoustic characteristics.

The noise emission of gears can be actively altered both in the concept phase and also during the subsequent development and implementation phase. In this regards, it is of interest to comprehend the influence of NVH in the early stages of product cycle. From the acoustic experts point of view, the general way to investigate this characteristic is through different numerical and experimental approaches. Accordingly, measures like avoidance of unfavorable power excitation scenarios, the vibration reduction in the transmission of structure borne noise and the absorption of sound radiation are considered to improve the performances.

Nevertheless, experimental analysis possesses many practical difficulties. An optimization, for example, is tedious, costly and requires sensitive measurement methods along with high degree of expertise. Additionally, factors like wear of the rotating components, which can impact the vibrations, makes it more and more tough. Furthermore, developers of different fields usually focus on their respective domains and in demanding products a deep understanding of the components is necessary. The fact that vibro-acoustic phenomena arise through the interaction of different physical domains is thus out of focus and can lead to unpleasant consequences for the final product in terms of noise and vibrations.

It is quite necessary to address the issue in order to render better perception of the noise emission. The most common way of achieving it is via numerical methodologies. There are complex techniques used for understanding, optimizing and predicting the vibrations of drivetrain components. Especially with regard to numerical modeling of transmission, which includes the complete path right from the origination of excitations at the shafts, structural emissions via the bearings, amount of vibrations at the housings and impact of wear on the vibrations, there is scarcity of proper approaches. Few of them deal only at individual level, like the vibrations transmission path, the noise excitations, the structurally coupled velocities between rotating gear parts and housing etc. They are mostly considered only in part and not as a whole. Accordingly, there is a requirement for developing a generic methodology that is accessible, comprehensible and applicable to developers for the numerical, vibro-acoustic analysis of transmissions systems. The method should be flexible in terms of product variants and parameter configurations, allowing for both predictive analytics and system optimization. Furthermore, it should be scalable in terms of product maturity and configurable in terms of product variants.

1.2 Outline of Chapters

The below paragraphs give a short overview of each chapter, which are used in the construction of work. It depicts the significant contents corresponding to the goals of respective chapters.

Chapter 2 shows a brief description of the problems discussed in the thesis. Firstly, the questions concerning the various numerical methodologies necessary for prediction of vibro-acoustics and abrasion behavior are discussed. Secondly, problems related to the excitations from gear mesh and motor, vibrations at housing structures and coupling at fluid structure interface are described. Thirdly, the difficulties present in perceiving wear at the gears and their potential influences on vibrations and noises are reviewed. Lastly, the system level requirements and component level attributes required for realizing the method flow are introduced.

Chapter 3 illustrates present state of research for the topics related to structure borne emissions

and abrasion. Firstly, the causes for vibrations in vehicles are introduced. Different forms of inner excitation mechanism, the transfer path of vibrations and emission of sound are shown. Secondly, various numerical modeling methods available to realize NVH characteristics are described. Also, few of the measures defined in the literature to curtail the noises are depicted. Thirdly, procedure for creating system models and Finite Element (FE) models are explained. Fourthly, the various tools like order analysis, frequency response plots, which are necessary for evaluation of the vibration and noise signals are discussed. Lastly, the current research in the field of abrasion is illustrated. It introduces to concepts like the mathematical wear models and methods for evaluating the wear plots.

Chapter 4 can be mainly divided in two blocks. The first block commences with the description of available simulation techniques to analyze vibrations and wear among the components. The model requirements and the necessary attributes for the evaluation of these numerical methods are further described. The second block introduces the developed vibro-acoustic and abrasion methodologies to address the issues discussed in chapter 2. Initially, techniques are created to study the free state and the forced vibrations associated in the gear box system. Secondly, numerical validations like stiffness, stress analysis are shown, which make the simulation templates more plausible to the reality. Thirdly, the harmonics of structures and the coupling with acoustics are discussed. Fourthly, simulation flows and techniques for the abrasion calculations are depicted. Further, the influences of wear on NVH are also illustrated. At end of the section, complete data flow across vibration, noise and wear domain is drawn. Finally, different possibilities of optimization techniques within design and simulation to reduce the noise and vibrations are discussed.

Chapter 5 aims to implement the techniques originated in chapter 4 for a example model. Chapter at first introduces the list of softwares used to simulate, analyze and evaluate the NVH and wear characteristics of the drivetrain. Initially, the solution technique is verified on a simple model for its plausibility and robustness. Vibration submodules like excitation at the gear mesh and harmonics of the structure are validated with help of convergence studies and simplified structures. Vibration and noise for FE models are verified with help of simple cube constructed. Later, the technique is extended on to the optimized cube structure as well. In regards with examining the exactitude of abrasion models, simplified 2D models are simulated.

Chapter 6 tries to analyze and optimize the vibrations for a three stage gear model. It focuses in applying all the knowledge gained with methods discussed in chapter 4 and over the simulations of simplified structures from chapter 5, on to a three stage drivetrain model. Firstly, the design layouts of the drivetrain model along with assumptions concerning the drivetrain variant are introduced. Secondly, the model is extensively used across system and FE simulations. It includes simulations of individual parts, combined components and complete drivetrain. Models illustrating the link between the NVH and wear modules are also shown. Thirdly, the improvements brought from the design improvisations of the components are also discussed. The experimental runs are carried out for the measurements of noise and wear profiles. Finally, the plots of vibrations and noises for the original-new, original-worn and improved-new power units are illustrated.

Chapter 7 summarizes the complete work discussed in the earlier chapters. Additionally, it tries to define the targets for next phase of the project.

2 Research Questions

Acoustics and vibrations are amongst the foremost indicators in perceiving the quality of automobiles. These factors enjoy a growing focus in automotive Research and Development(R&D) at the time point, where it is essential to bring fundamental changes in powertrain configurations. The powertrain systems, vehicle architectures and design models are being globally challenged since the past few years by emission standards and legislation aimed at promoting energy-efficient solutions. In the coming years, even more challenging NVH performance levels are to be achieved with lightweight structures, turbocharged engines and hybrid drivetrain models.

2.1 Objectives

The major objective of the thesis is to understand and improvise the noise and vibration characteristics of the electric drivetrain assemblies. It is done by dividing this huge vibration problem umbrella into set of smaller challenges or problem statements, which should later enable the better comprehension of the structure borne and airborne emissions. The vibro-acoustic phenomena arise through the interaction of different physical domains and can lead to unpleasant consequences for the final product in terms of noise emission. The important question here is that, how to provide developers a comprehensive picture in regards with the impact of vibrations on component, multi-domain behavior as early as possible, and also how to continuously harvest the knowledge through out the development process for different transmission variants and system configurations.

A straight answer to this is: numerical methods. The field of R&D in NVH is filled up with different numerical techniques like Finite Element Method (FEM), Multibody Dynamics (MBD), Boundary Element Method (BEM), Lumped Parameter Model (LPM), Statistical Energy Analysis (SEA) etc. These methods are mainly used in the design phase of the product to avoid potential failures at production phase. The first challenge in order to comprehend vibrations of the electric drivetrains lies in building up a methodology to predict the vibro-acoustic behaviors precisely. Construction of a robust mechanism plays a key role in connecting the different level challenges and thereby providing channels for the communication among them. It should additionally be cost and computationally effective. Coupling strategies would allow for the effective and efficient integration of the vibro-acoustic models into the system level multi-physics models. The methodology and flow developed should ultimately allow for an efficient analysis of the vibrations. It should serve as a base to apprehend different phenomena associated with the vibro-acoustics.

In numerous applications of engineering, gear wheels aid in transmission of power between the rotating shafts. Along with power the unwanted structure borne vibrations are also transmitted through the shafts. The second challenge is to analyze the influences of mechanical excitations, which originate from the gear mesh of the shafts and gears. Apart from the mechanical excitations, the electromagnetic forces arising from the rotor would also impact the structural dynamics. Creation of proper excitation mechanisms are essential for the vibro-acoustic model development. The next difficult task would be building of the necessary flex-body model, which

would characterize the drivetrain and help in predict the accelerations of the required housing surfaces. Although the Degrees of Freedom (DOF) are condensed drastically in state space model as compared with the FEM, it is vital to capture all the intricacies involved in the drivetrains with this limited number DOF. The model constructed should mainly enable the faster analysis of the different phenomena which are difficult to perceive in the prototypes. With regards to a physical or numerical modeling of transmissions, which includes in particular the vibration at the housing and the sound radiation, there are a lack of reference sources in the literature. It deals only with individual mechanisms, the complete, vibro-acoustic transmission path, the structurally coupled oscillation between rotating gear parts and housing to the sound emission into the surrounding fluid are considered only in part and not as a whole.

Most of the troublesome vibrations for the drive units occur at mid frequency range. FEM is the perceptible mode for mid frequency analysis of the drivetrain assemblies. It is widely utilized to scrutinize the load cases of various real time scenarios. It mainly aids in studying all the individual components like gears for the noise and vibration generation, bearings for their disturbance transmission, housings for their vibrations at surfaces and their impact on the surrounding fluids. Changes or improvements can be expensive and time consuming when made after the design phase, so it is important to produce accurate simulations of the product. The challenge here is to consider all the material and structural effects along with the excitations obtained from the system models to understand the vibrations for different models. Adjusting the vehicle design, followed by simulations to predict the NVH behavior would help in creation of a better product. The detailed analysis at problematic frequencies should be performed in order to understand the acceleration of structures and the influences of them on surrounding fluid.

One of the prime factors which influences the vibrations of the powertrains is wear at the components. Generally, wear is important in structures with repetitive loading and is critical for certain tribological applications. Over the past few years, the mechanics of wear are being better comprehended. The calculations and reduction of wear are becoming more and more essential. To this point, researchers have carried out few experiments addressing the problem of quantifying the amount of wear and its distribution, but the scarcity of proper numerical models to address the issue at the development phase is still a concern. Most of the analytical formulations in literature are developed using large amounts of experimental data. It just provides an equation with few variables which predicts the wear. Main problem with the experimental approach is that it requires an end product to perform the experiments. At the same time it would be too late to address the issue at the product manufacturing phase as the costs are increased (in comparison with the development phase). The potential to study and estimate the wear would bring enormous benefits in cost and safety to a wide range of industries, but there are currently no reliable, effective and efficient tools to do so. The target in this part of the work is to predict the amount and distribution of mechanical wear using several existing wear models and numerical methods in the design phase of the product. The challenge is to analyze the influence of wear at the component level and provide solutions to curtail it at accepted levels.

Estimation of wear is just one facet of the problem. The next challenge comes with understanding these effects on the acoustics of drivetrains. Abrasion among gears creates geometric deviations in their teeth and thereby modifying the load distribution on the tooth surface. Wear leads to increase the gear transmission error, generally resulting in increased dynamic loads, vibrations and noises. It is vital to comprehend the behavior of wear for predicting its influences on the vibrations. This thesis develops methods using vibro-acoustic based techniques to estimate the impact of wear on NVH of the drivetrain.

The relation between structure borne emissions and airborne noises is often a tricky and complex formulation. There is a complete possibility of observing a resonance only in vibration and not in acoustic domain or vice-versa. Or may be a smaller peak in one of the domains and a relatively larger jump in the other domain. The final objective of the work is to couple the vibrational domain with that of the acoustic domain. Only a one directional coupling (one way coupling from vibration to acoustic) is considered for this work. This condition is sufficient because air unlike water is completely lighter than the structure. The pressure created by the structure on the air is much greater than the force from the air on to the structure. Although, only a weak coupling is adequate for this thesis, it possesses problems like determining the acoustic properties at the fluid structure interface. It is necessary to find the correct impedances among the structures and fluids, acoustical and structural material properties, boundary behaviors at the interface etc., to transfer the influences of housing vibrations on to the surrounding fluid.

Furthermore, the following one line research questions can be derived for the above challenges: How can the level of physical detail for vibro-acoustic system model be configured according to the level of product maturity and the objective of a question or, if necessary, expanded? Are parameter changes of the components possible with regard to virtual product variant tests and is the complex model topology intuitively accessible for non-specialist users? How can a coupling between the vibration and wear domains be obtained? Even though coupling between different physical domains is achieved, can simulation results be obtained in an acceptable time? With regard to the vibro-acoustic behavior, does the gearbox model include not only excitation but also transmission mechanism for structure-borne noise and how can vibrations, noise emissions and abrasions be evaluated?

Developing the method flow which is applicable only to certain variants or without any possibility of extensions across different domains etc., is not meaningful. From the questions listed, model requirements and attributes necessary for the system model can be defined in order to apply the techniques developed for all variants and across different physical problems. The former describes the requirements for cross-domain mechanisms at the system level and the challenges anchored in them, such as parameter uncertainties, variety of variants and the degree of maturity of a product, while the latter represents the physical properties of the vibro-acoustic and wear mechanisms. Finally, the system models created must be able to realize model level requirements shown in table 2.1. Further, the left column of this table describes component level attributes. The method developed should be also able to perceive each of these characteristic at the individual level, which in turn would aid in constructing the numerical simulation technique to comprehend the NVH and wear characteristics within the powertrain. Detailed definitions of these system level requirements and component level attributes can be found in section 4.2 [KDH19a].

System level requirements	Component level attributes
Modularity	Excitation mechanisms
Reusability	Gear vibrations
Extensibility	Housing vibrations
Simplicity	Vibrations to acoustics coupling
Rapidity	Acoustical characteristics
Reliability	Wear mechanisms

Table 2.1: System/ model level requirements and the attributes that must be realized

2.2 Definition of the Work

The aim of present work is the development and validation of a generic, multi-domain methodology for modeling and simulation of vibro-acoustic and wear mechanisms in electric drivetrain models. The requirements for both the component level and system level model must be met. It means, that the methodology developed should enable the analysis of physical transmission mechanisms at the component level, the optimization of individual systems and prediction of different system states along with critical geometric areas for the problematic frequencies. Also, it should allow for an estimation of wear among the components, thereby enabling to study its influences on the drivetrains.

The targets defined in earlier section are met with aid of combination of different simulation techniques at various stages of the system development phase. These numerical methods must be checked for their plausibility and applicability. It should be able to perceive the underlying mechanism and also allow the transfer of values to adjacent module for the next challenges. For verification of this complete methodology, simulators must be selected and a modeling instance should be created, thereby the absent model components of simulator library must be added and the model developed must be further investigated.

Initially, a simple example model for each of the node in the simulation flow must be built and evaluated for its correctness and plausibility. Later as an application example, the modeling technique would build a multi-stage spur plus helical gear as a demonstrator and compare its simulation results with validation measurements. The simulation model must be numerically verified for various complexities like the stiffness of geometries and stress at the critical areas etc. After the model validation for NVH, a new template to numerically analyze the abrasion mechanism is developed. Within the wear module, the simulation is coupled with machine learning codes to make the predictions more robust. Later, the worn drivetrain model is coupled back to the vibration module to check for the deterioration in acoustics. Based on the transmission model, the optimization potential of different system parameters is finally discussed considering the entire generic methodology.

3 Basic Principles and State of the Art

This chapter describes the vibro-acoustic and abrasion analysis of drivetrains in the context of current research questions and industrial applications. Firstly, the causes of mechanical vibration excitation are explained and the object-oriented modeling and physical networks for cross-domain questions are presented. Secondly, the methods for modeling and simulation of transmissions are described. Additionally, different analysis tools for the noise evaluation are illustrated. Finally, the current research status for the topic wear prediction are described.

3.1 Vibration and Sound in Vehicles

The emission of noise in motor vehicles results from different physical mechanisms and can be caused, for example, by mechatronic components, road-tire contact or aerodynamic flow processes. The excitations occurring from the powertrains can be classified as shown in figure 3.1. Diagram illustrates potential sources and transmission routes across the frequency spectrum along with the main type of emission.

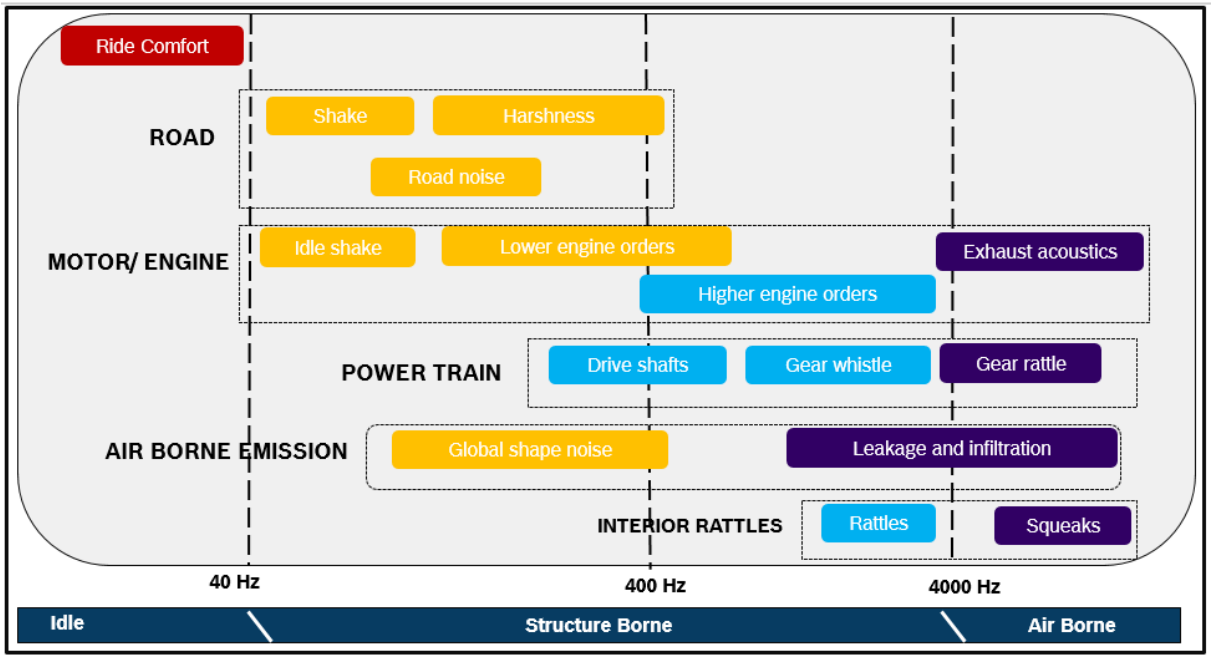

Figure 3.1: Potential sources for structure borne and airborne emissions across the complete spectrum

For a motor vehicle with an internal combustion engine, combustion represents the dominant part of the interior and exterior noise. If the combustion process is omitted in the course of electrification, subordinate noises can be perceived acoustically. Howling is one of the main noises in electrified vehicles. The howling of the gearbox is particularly annoying for humans, since the human organism reacts very sensitively to whistling, tonal noises. The presentation shown in figure 3.1 is a rough classification of sources for the motor vehicles. For better comprehension of work it is vital to understand the relevant mechanisms in gear boxes. The next section

describes the causes of emission from the gear boxes and the detailed analysis of the excitation mechanisms.

3.1.1 Causes of Vibration from Gearbox System

Generally, gear noise is either caused by internal or external excitation mechanisms [NWH05]. External excitation is understood as load fluctuations which act on the transmission from rotor or output side and consequently generate additional dynamic forces in the toothing. External excitation mechanisms are, for example, torque ripples in an electrical machine, torque fluctuations in a multi-cylinder internal combustion engine or load torque fluctuations in the output. If there is a proper design-related decoupling of external mechanisms (e.g. elastic coupling, hydrodynamic slide bearings), their influence on the gearbox is usually negligible.

In contrast, internal excitation mechanisms cannot simply be decoupled, as they are caused by the gear meshing. They occur as multiples of the meshing frequency (except for the pitch deviation) and are often perceived as so-called gear whine at high speeds. Examples of internal excitation mechanisms are fluctuations in gear stiffness, manufacturing-related deviations from the target geometry, entry and exit shocks and unbalance of gear wheels. The internal excitation mechanisms are more or less pronounced in every gear and thus generate unavoidable dynamic additional forces.

3.1.1.1 Analysis of Inner Excitation Mechanisms

There are two forms of mechanical excitation mechanisms namely: parameter and path excitation, which represent the relevant part of internal dynamic additional forces and cause gearwheels to vibrate [LB10, MDY07].

Parameter excitation occurs due to fluctuations in the tooth stiffness. The fluctuations result from the finite stiffness of the material and changing number of teeth that are in mesh. Typical overall stiffness curves of gear toothing are shown in figure 3.2 (spur gear toothing (left-hand side) and helical gear toothing (right-hand side)). In the diagrams, the x-axis describes standardized tooth pressure angle and the y-axis represents stiffness values of the gear stage.

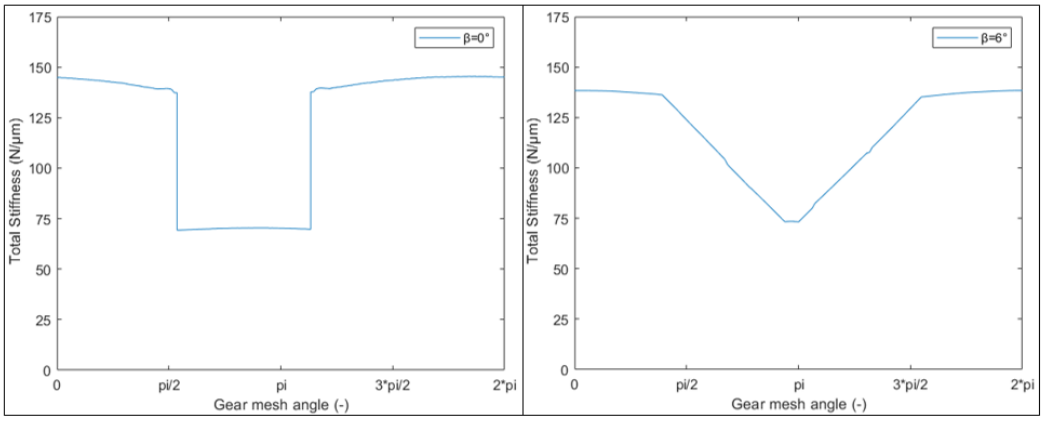

Figure 3.2: Left: total stiffness curve for a spur gear. Right: total stiffness curve for a helical gear

The course of straight toothing can be divided into two areas. When the value is approx. 140 N/ μ m, then three teeth are engaged, whereas at 75 N/ μ m only two teeth are responsible for the power transmission. This sudden change in the parameter results in a pulsed vibration excitation of the system. In comparison, the helical profile has a greater degree of coverage of

gear stage due to the helix angle $\beta = 6°$. As a result, the transition between number of teeth in mesh is more continuous, resulting in less vibration excitation. The downside is presence of additional axial forces that cause the gearbox to vibrate in the shaft axis direction.

Since the overall stiffness curve is repeated periodically per tooth revolution, the basic frequency of the excitation is made up of the number of teeth multiplied by the speed of rotation of gear. Furthermore, the harmonics of this gears and shafts and their proportions can be examined by frequency analysis.

Nevertheless, determination of overall stiffness is a complex task, since it involves nonlinearities and extremely small values that are difficult to measure. In addition, the overall stiffness curve is not additively made up as sum of all individual tooth stiffness, since the tooth connection points also shift due to the wheel center deformation [NW13]. Nevertheless, there are different numerical strategies that are available depending on the application. For example, a numerical calculation can be carried out using FE contact analysis [PAV00]. However, the accuracy of FE simulation is dependent on its relatively long simulation times. A couple of simplified models are described by [Pet89] and [WBN55] and they include not only the tooth bending but also the wheel body deformation.

Additionally, internal dynamic forces are also caused by path excitation. Generally, path excitation occurs due to tooth deviations caused by production technology and depends on the quality of position, shape and surface of individual teeth. In principle, the path excitation can only be determined experimentally, since it cannot be predicted. For parameter studies and the impact of potential geometry errors, worst-case scenarios can, however, be adopted and evaluated as part of a system simulation.

Overall, the resulting internal dynamic additional forces lead to periodic vibrations in the gearbox (like parameter excitation) and in addition, the fundamental frequency has its harmonics. Due to special tooth geometry errors, vibrations at frequencies below the fundamental frequency can also occur. As an example, a pitch deviation is given here, which imprints every second tooth in the manufacturing process. In this case, an excitation frequency of the geometry error is half the basic frequency, since the offset occurs only with every second tooth.

3.1.1.2 Structure and Airborne Emission in Drivetrains and Measures against Gearbox Noise

The effective path of structure borne noise within a gear transmission is shown in figure 3.3. The excitations originates at the gear meshes and travels to the shafts and bearings. The force exerted by bearings cause vibrations of the housing structure. These surface accelerations create pressure difference with surrounding fluid to create noise.

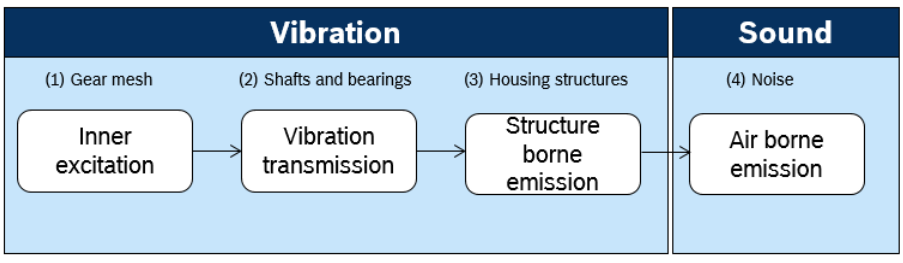

Figure 3.3: Block diagram for the representation of structure borne transmission and the formation of airborne noise

Additionally, the below points describe the system model for the vibrations right from the origination at gears to emission of sound around the housing structures:

- Due to the before mentioned dynamic additional forces in the tooth mesh, depending on the design parameters, a gearbox is set in superimposed rotational and translational directions and furthermore converted into axial, radial and tangential vibrations.
- The translatory vibrations are transmitted from the gearwheels through the shafts to the bearings. Straight gears stimulate in the tangential and radial directions, helical gears also in the axial direction.
- The housing has a spectrum of natural frequencies and is excited via the bearings as power coupling points.
- The vibrating surface ultimately vibrates the surrounding fluid and airborne noise is generated.

In principle, measures for reducing vibrations can be carried out for every mechanism that is involved in structure borne noise transmission or sound radiation. A subsequent change to the mechanics is not always trivial in practice, since they mean an intervention in the existing, entire system. As a result, noise reduction measures should be taken as early as possible in the product development phase. The basis for this is a comprehensive, physical understanding of the mechanisms. A good overview and further literature on the topic of noise reduction can be found, for example, in [Kin82, KSA06, Zel09]. In general, the measures can be divided as follows:

- Avoid unfavorable power excitation scenarios.
- Vibration reduction along the transmission path, e.g., decoupling.
- Vibration reduction using design changes, e.g., ribs for stiffening.
- Absorb sound radiation.

Furthermore, the measures for vibration reduction can be divided into passive (detuning, isolation and eradication), semi-active (switchable and continuous) and active measures (AVC: Anti-Vibration Compound, ASAC: Active Structural Acoustic Control and ANC: Active Noise Cancellation) [Zel09]. The latter tries to reduce or even eliminate annoying vibrations by introducing phase-shifted vibrations (e.g. by an actuator).

3.2 Modeling and Simulation of Vibration and Noise

Depending on the problem statement, different modeling and simulation methods are available for the numerical analysis of a physical system. In practice, however, the decision as to which method is best suited is often a challenge. In particular with regard to the vibro-acoustic modeling of gears, the choice of a suitable method is difficult. Consequently, a systematic and comprehensible procedure is required when creating a gearbox simulation model. More detailed information about the modeling techniques chosen for the work are described in the sections 4.1 and 4.2.

Within the section, initially a list of available simulation techniques are explained. After that, procedures for creating vibro-acoustic models using system modeling and FEM are illustrated.

3.2.1 Methods for Vibro-acoustic Modeling and Simulation of Gears

The numerical, vibro-acoustic analysis of transmissions is a topic that is often discussed in literature. The modeling approaches addressing this physical mechanism range from simple vibration models to finite element analysis with millions of degrees of freedom.

Since the generic, cross-domain methodology of the present work consists of specially identified combination of individual techniques, the main methods of current research are shown below.

Lumped Parameter Model

Lumped-parameter models (LPM) in the sense of gearbox modeling can be used for illustrating rotary vibration behavior of a gearbox stage using fewer degrees of freedom. System variables such as tooth, wheel and shaft stiffness, tooth mesh damping and geometry deviations are summarized as concentrated parameters. The small number of degrees of freedom as well as the generally one-dimensional (rotary) view enable an efficient simulation (faster computing times). An example of a simple LPM is shown in figure 3.4. The coupling spring with the spring stiffness k_m and damping coefficient d_m describes the flexibility of the gear stage (tooth, wheel and shaft stiffness). Since coupling sizes of LPM are generally nonlinear and dependent on the angle of rotation of the gearwheels, LPMs are particularly suitable for modeling periodic, mechanical vibration excitations. Structure borne vibrations in a three-dimensional gearbox and the imaging of the housing vibrations are not possible with this model class [OH88b, Kor07].

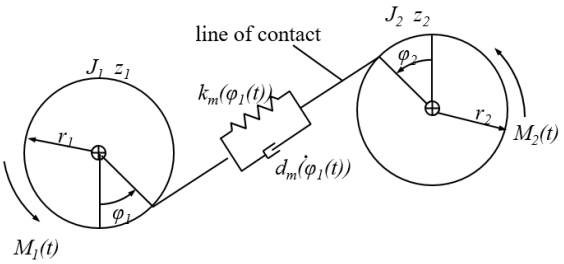

Figure 3.4: LPM gear model [OH88b]

Multi Body Model

Multibody simulation (MBD) [Cor15, Ami07, AK14] is a method that describes the kinematics and dynamics of rigid bodies in three-dimensional space (figure 3.5). Joints in the MBD model define the kinematics of the system by suppressing the corresponding degrees of freedom through constraints. Furthermore, springs and dampers represent physical coupling elements and influence the dynamic behavior of the bodies on their trajectories. Development environments for MBD models independently generate the equations to be solved taking into account the boundary conditions and are therefore suitable for an automated analysis of the system behavior. The classic MBD has its weaknesses in the mapping of complex system components, such as the nonlinear behavior of a damper or the spatial resolution of a housing vibration. The integration of complex mechanisms is the subject of many current research questions. For example, paper [Fri11] describes the modeling of a generic rolling bearing. Work in [MDY07] deals with the comparison of different excitation mechanisms of gearboxes. Paper [MBR04] uses hydrodynamic considerations for the simulation of shock absorbers. There are many more examples in the literature for expanding classic MBD models. However, this simulation method has its limits, since only the mechanical behavior can be described [Woe11].

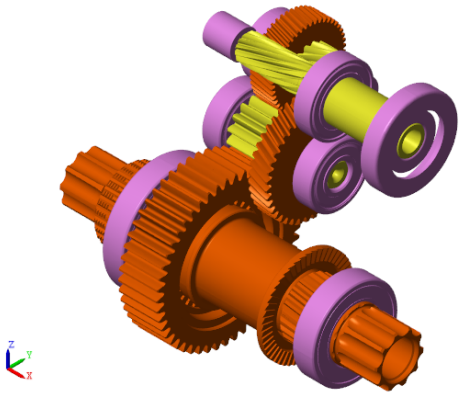

Figure 3.5: Multibody model of gears and toothed shafts (with bearings)

Finite Element Modeling

Due to the computing power of today's computers, the Finite Element Method has become a powerful numerical simulation tool for various engineering problems. Models often take into account several million degrees of freedom [Bat07].

The individual steps of a finite element simulation are as follows: The geometry examined is converted into finite elements by preprocessing. A system of differential equations is then automatically created and numerically solved during the simulation phase. Finally, post processing includes the visualization and further processing of the simulation results. Few examples of FE contact analysis are described in [PAV00, PK14, Kim15]. With regard to the vibro-acoustic behavior of gearboxes, the surface vibrations of a gearbox housing are studied in [KSO06] and paper [KWK02] deals with the sound perception of a person. All these papers attempt to solve the vibro-acoustic problem using FEM as the main tool. Overall, FEM can be used as part of a system simulation to identify individual parameters.

Figure 3.6: Finite Element Model of a gear and rotor shaft

Boundary Element Model

Boundary Element Model (BEM) uses only the edges or the surfaces, instead of the surfaces or volumes of a body (respectively). As a result, a simplified 1D or 2D problem is formulated (reducing the complexity). In contrast to FEM, resulting differential equations have fewer degrees of freedom which leads to shorter simulation times. However, fully occupied system matrices partially compensate for this property. With regard to machines and gearboxes in particular, the surfaces are responsible for the main part of the noise emission by acting as a sound membrane. Therefore, the BEM offers itself as a simulation method for various housing structures [KKB89, SWW88]. The coupling between FEM and BEM can be useful with regard to few special problems and formulations.

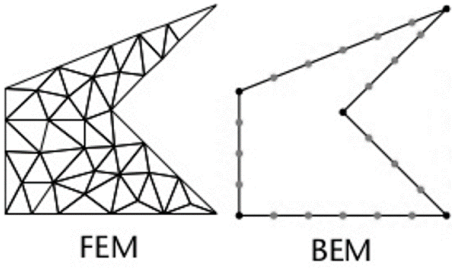

Figure 3.7: Finite Element Model vs. Boundary Element Model

Statistical Energy Analysis

Statistical energy analysis (SEA) divides a vibrating system into corresponding individual subsystems [Lyo14, Fra94]. Figure 3.8 represents an example SEA model consisting of three subsystems. The arrow marks correspond to the exchange/transfer of the energies. The energy exchange between the system components is described by a linear system of equations. A subsystem can absorb, store or transfer energy to a neighboring system and dissipate. The application range of this simulation method extends from the automotive industry for driving, interior and acoustics to aviation (e.g. helicopter interior acoustics) [Dej85, Zei06]. Since this method is preferably used in the medium to high frequency range, their robustness with regard to parameter fluctuations has proven to be advantageous. However, determination of dissipation coefficients is the most difficult part in SEA.

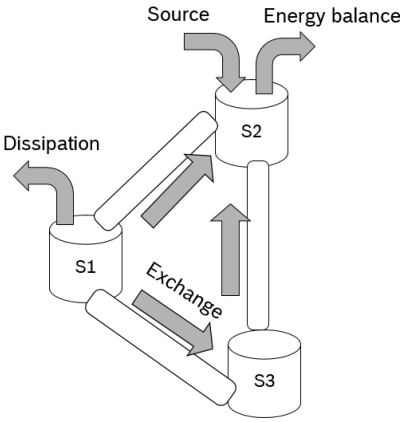

Figure 3.8: SEA example model

Computational Fluid Dynamics

The Computational Fluid Dynamics (CFD) method aims at the numerical calculation of fluid mechanical phenomena [And95]. Using this method, flow processes can be calculated, a stall (reduction in lift coefficient) can be predicted, or the distribution of pressure coefficients over an aircraft geometry can be described (check figure 3.9). This modeling technique uses Navier-Stokes equations to represent the underlying model. Other models, are the equations of potential and turbulence models which can be solved numerically faster in comparison to the basic Navier-Stokes equations. However, CFD calculations are time-consuming because of local and temporal discretization dependencies.

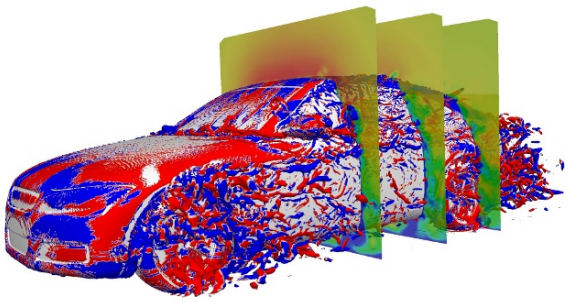

Figure 3.9: Example CFD model of a car [CFD19]

Radiated Sound Power Model

The Radiated Sound Power Model (RSPM) describes the radiated sound power of a vibrating surface [Kin82, Zel09]. Depending on the level of development and the problem statement, different levels of detail can be used. In contrast to a partial method (check figure 3.10), sound pressure is not calculated by numerical integration of the acoustic field. Instead, RSPM tries to find a solution in the form of an integral approximation from the acoustical energy by simplifying the model. From a system perspective, this approach can be faster as compared to partial integration (e.g. FE). It can be used for building efficient system simulations for models with less complexity. Few of the RSPM models available in literature are Equivalent Radiated Power (ERP), volume velocities or lumped parameter models [Kin82, FMJ09].

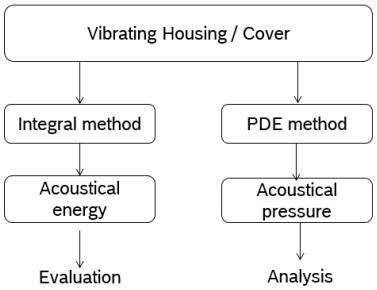

Figure 3.10: Comparison between integral and partial methods

Each of discussed methodology has its own complexities. Hence it becomes difficult to choose an appropriate simulation technique. Figure 3.11 illustrates 3 dimensional view (frequency vs. system dimension vs. complexity) with respect to the selection of different simulation models. For instance, when the frequencies of interest increase it is wise to choose the approach like SEA rather than sticking with MBD model due to the robustness offered by SEA. With increase in degrees of freedom of a model makes FEM more time consuming, therefore in this case it is wise to switch from FEM to BEM. Similarly, with increase in complexity of the problem, an analytical solution could be difficult or impossible to calculate. For the models with lesser complexity i.e., with few DOF, the solution can be computed analytically using the Partial Differential Equation (PDE) solvers.

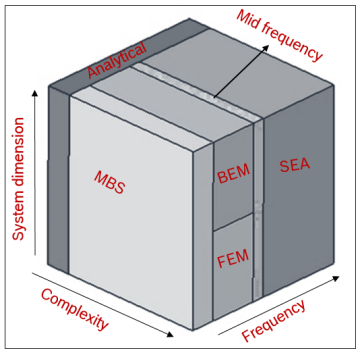

Figure 3.11: Overview of simulation methods

3.2.2 Procedure for Creating a System Model

The classic way of system modeling and simulation comprises steps like physical and mathematical modeling [Saw11]. The main advantage with this method is that, a detailed mathematical insight into physical relationships of the system can be obtained. However, the disadvantage that arises from the mathematical formulation is inflexibility in terms of modularity and scalability of models. As a result, alternative modeling methods have established which have their advantages particularly when it comes to cross-domain questions regarding complex, heterogeneous systems. One such modeling technique is Component Oriented modeling (COM).

COM is a method for building simulation models that describes the physical interrelationship before the formal creation of the mathematical model [Yef05]. Analogous to the bond graph method [MMB91, Mar85], the simulator automatically generates the differential equations of the system. Softwares like Simscape can be used as component oriented programming language [Mat8ba]. The COM has network characteristics and represents undirected signals. By defining boundary conditions, the energy flow in the system is aligned and can therefore be observed after the start of simulation.

The topology of a component-oriented model instance is referred to below as a other generalized network (OGN). A physical network consists of individual model blocks, called components, which represent real world components. These are, for example, springs and dampers (mechanics), hydraulic pipes and pressure accumulators (hydraulics) or electrical resistors and capacitors (electrics). There are also components for the coupling between domains, such as electromechanical motors or hydro-mechanical pumps.

Physical Domain	Potential (V(t))	Flow (q(t))
Electrical	Voltage	Current
Mechanical translational	Translational velocity	Force
Mechanical rotational	Angular velocity	Torque
Hydraulic	Pressure	Flow rate
Magnetic	Magnetomotive force	Flux
Gas	Pressure and temperature	Mass flow and energy flow rate
Thermal	Temperature	Heat flow

Table 3.1: Analogy variables of Component Oriented Modeling [Mat8ba]

With the COM method, complex, multi-physical simulation models can be created efficiently and clearly and cross-domain interrelationships can be analyzed. The simulator uses a generalized approach of the Kirchhoff network and mesh rules to create the mathematical equations [Cla04]. Non-electrical components are treated in the form of analogies and are listed in table 3.1. The analogy variables can be divided into flow and potential values and, when multiplied, describe a power value of the corresponding domain.

COM can be made available to a large number of developers from non-specialist domains, who then develop, integrate and test sub-components as part of an overall system simulation. The insight into the mathematical relationships remains closed at the system level and thus allows even the non-simulation experts to work with it. Furthermore, for advanced users and a detailed system analysis, commercial simulators nevertheless provide basic, mathematical relationships for model components by means of source code.

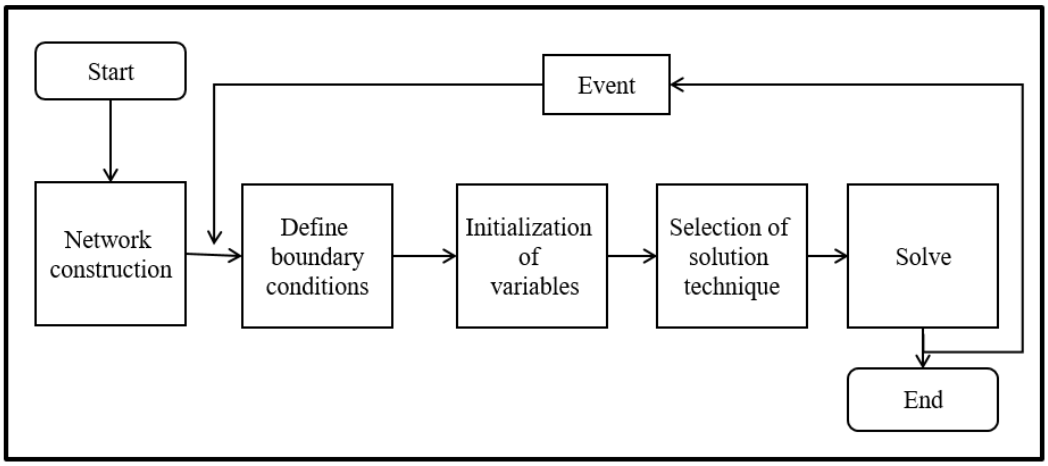

Figure 3.12: Schematic view of physical network in Simscape [Mat8ba]

The compilation and simulation process for COM environment is shown as an example in figure 3.12. The process includes formal model validation, establishing the equations (network, equation construction), defining the boundary an initial conditions (boundary conditions and initialization of variables) and the simulation process (solution technique and solve). If there is a discrete event, such as a hard mechanical stop or the closing of an electrical switch, the corresponding boundary conditions of the differential equations are reset (Event). The numerical solution process is then continued until a required termination criterion is reached (End).

3.2.3 Procedure for Creating a Finite Element Model

Apart from system modeling instances, this thesis tries to blend in the FE modeling for the evaluation of vibration and sound. Generally, engineering analysis of mechanical systems have been addressed by deriving differential equations relating the variables of through basic physical principles such as equilibrium, Newtons laws of motion, conservation of energy, the laws of thermodynamics and Maxwell's equations. However, once formulated, solving the resulting mathematical models is often difficult, especially when the resulting models are nonlinear partial differential equations. Only simple problems of regular geometry such as a rectangular or a circle with the simplest boundary conditions were tractable. Methodologies like FEM tries to circumvent these problems and determine the solutions even for complex structures [Bat07].

FE analysis obtains the stresses, temperatures, flows, or other desired unknown parameters by minimizing its own energy functional (F). An energy functional consists of all the energies associated with the particular finite element model. The FE method obtains the correct solution for any finite element model by minimizing the energy functional. The minimum of the functional is found by setting the derivative of the functional with respect to the unknown grid point potential to zero as shown in equation 3.1.

$$\frac{\partial F}{\partial p} = 0 \tag{3.1}$$

Where p is the unknown grid point potential/ displacement to be calculated. Furthermore, equation 3.2 represents the energy potential (Π_e) at element level. Here $\mathbf{u}$, B, E, V, $\mathbf{N}$, q and S represent displacement vector, strain displacement matrix, elasticity matrix, volume, shape function vector, vector of applied surface traction and surface respectively.

$$\Pi_e = \frac{1}{2}\int_{\Omega_e} \mathbf{u}^T (B^T E B)^T \mathbf{u} dV - \int_{\Omega_e} \mathbf{u}^T \mathbf{N}^T u dV - \int_{\Gamma_e} \mathbf{u}^T \mathbf{N}^T q dS = 0 \tag{3.2}$$

Taking the partial derivative ($\partial\Pi_e/\partial u$) the element equilibrium equation (3.3) can be derived.

$$\mathbf{Ku} - \mathbf{F} = 0 \tag{3.3}$$

Where $\mathbf{F} = \int_{\Omega_e} \mathbf{N}^T \mathbf{u} dV - \int_{\Gamma_e} \mathbf{N}^T q dS$ (force vector) and $\mathbf{K} = \int_{\Omega_e} (B^T E B)^T \mathbf{u} dV$ (stiffness matrix). Detailed information about the proof can be found in [Bat07, Nik04]. Table 3.2 represents physical significance of the vectors u and f w.r.t. different applications.

Application Problem	State (DOF) vector (u)	Forcing vector (f)
Structural mechanics	Displacement	Mechanical force
Heat conduction	Temperature	Heat flux
Acoustic fluid	Displacement potential	Particle velocity
Potential flows	Pressure	Particle velocity
General flows	Velocity	Fluxes
Electrostatics	Electric potential	Charge density
Magnetostatics	Magnetic potential	Magnetic intensity

Table 3.2: Representation of force and grid potential across different domains

Finally, the steps considered for creating a standard FE model are described below:

1. **Discretization of the continuum** - The first step is to divide the continuum region into finite elements. Normally, the mesh is generated by a preprocessor program. The description of mesh consists of several arrays most of which are nodal coordinates and element connectivities [Nik04].
2. **Selection of interpolation functions** - Interpolation functions aid to interpolate the field variables over the element. Normally, polynomials with certain degree are selected as interpolation functions. The degree of this polynomial depends on the number of nodes assigned to the element and it effects the stiffness of structure and there by natural modes.
3. **Element definitions** - The matrix equation for the FE should be established, which relates the nodal values of the unknown function to other parameters. This can either be done by the variational approach or the Galerkin method. Additionally, element definitions with different DOF are available in the literature (e.g. continuum, acoustic, temperature, electromagnetic). For the purpose of this thesis, mostly continuum solid/ shell and acoustic elements are chosen.
4. **Assembly of the element equations** - To find the global equation system for the whole solution region all the element equations should be assembled. Element connectivity are used for the assembly process. Before solution, acoustic and structural boundary and initial conditions (which are not accounted in element equations) should also be enforced.
5. **Solution of the global system** - The finite element global equation system is generally sparse, symmetric and positive definite. Direct and iterative methods can be used for solution. The nodal values of the sought function are produced as a result of the solution. Furthermore, few of specific solution techniques like steady state solution, transient response etc., are used to solve for the vibro-acoustic problems.
6. **Computation of results** - The main parameters considered for evaluation of noise and vibrations are the surface displacements, velocities, accelerations, acoustic pressures and intensities. Additionally, values like contact forces, stresses, strains and energies are also calculated depending on the problem.

The disadvantage is that it needs advanced users to build robust FE models for better accuracy. However, this drawback can be partially bypassed by initially, developing proper FE templates. Once these templates are made available in the standard ASCII format they can be parameter-

ized for different variables, thereby providing a channel for the non-simulation experts to study for the influence of different factors. E.g., the impact of different torque profiles can be comprehended just by updating the corresponding load table in the FE template. Once the models and solutions are made available the next question arises for the comprehension of outputs. It is done by using different evaluation techniques, which are discussed in the section 3.3.

3.3 Analysis Tools for Evaluation of Vibration and Noise

Gear vibration and noise emissions can be evaluated using different system sizes. Two common methods are described below. Initially, the transmission error is analyzed. Later, the spectral components of a vibration are then examined using order analysis.

3.3.1 Transmission Error

Transmission Error (TE) can be used as analysis parameter for the evaluation of transmission noise [Tha10, MDY07, Ake01]. Assuming that, firstly, the tooth geometry of a gear stage corresponds to that of an ideal involute and secondly, that the gearbox has no flexibility, i.e., is infinitely stiff, the input and output gearwheels would rotate exactly in proportion to one another. In reality, both assumptions are not completely fulfilled. As a result, the rotation of both the gears is also not exactly proportional. The TE describes exactly this difference and can therefore be represented by the difference between ideal assumption and the real (physical) gear according to the following equation (3.4) in its mathematical, translational definition:

$$TE = |r_1\varphi_1| - |r_2\varphi_2| \tag{3.4}$$

The terms φ and r indicate the rotation angle and the pitch circle radius of the gears in contact. Figure 3.13 illustrates the transmission error from [VD12]. The parameter TE is vital in terms of noise evaluation. The literature refers to correlative relationships between TE and noise emission [HOV94, CSA99, GRR03]. Consequently, noise optimization often implies minimizing the TE, for example through profile modification [SIH91] or through active control concepts [YTS05]. In principle, an experimental determination of the transmission error is possible [SR96]. However, the measurement-related acquisition is generally time-consuming and prone to errors, since it involves very small rotary vibration amplitudes of rotating machine parts. On the other hand, the numerical calculation with the help of the simulation, is a promising alternative, since not only its complicated measuring technology is avoided during the acquisition, but also predictive analyses are made possible long before the first prototype phase in the development process.

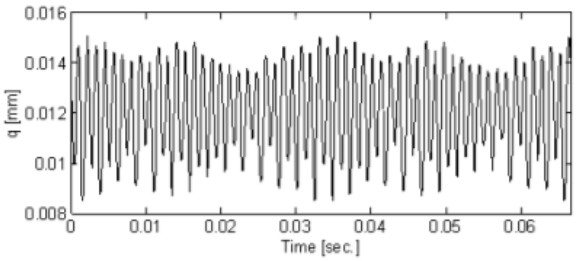

Figure 3.13: Transmission error from paper [VD12]

3.3.2 Order Analysis for System Models

The investigation of a rotating component is a complex process. Here, the speed of component varies over time and at the same time has speed-dependent vibration frequencies. For an electric motor or a transmission, for example, when the speed changes, the cogging torque frequencies or tooth mesh frequencies also shift. Performing a Fast Fourier Transformation (FFT)

over the complete, speed-dependent vibration signal would not be useful if the speed changes. Consequently, an order analysis is used which is composed of a large number of individual FFTs.

After complete detection of the vibration signal, areas are defined in which the speed can be assumed to be quasi-constant. An FFT is then carried out for each area and the frequency spectrum plotted against the speed (left-hand side of figure 3.14). The amplitude of vibration is described by the Z-axis. The frequencies, which scale proportionally to the speed, can be clearly seen. They can be identified in the representation as straight lines of origin and are referred to as order lines. System resonances, which are independent of the engine speed, can be identified in figure by horizontal lines.

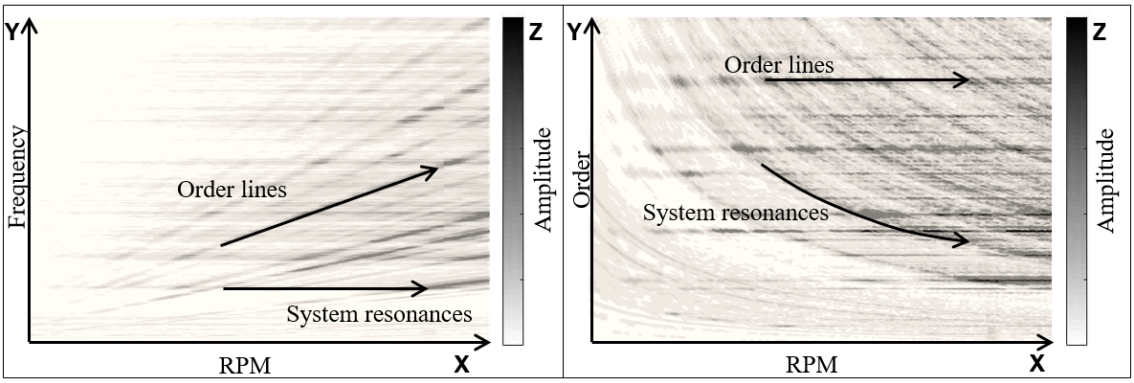

Figure 3.14: Visualization of an order analysis for speed-dependent vibration signals in different forms

An alternative representation is the visualization of the orders over the speed (right-hand side of figure 3.14). The system resonances follow a hyperbolic course. Both diagrams are also known under the term Campbell diagram or waterfall diagram [WH11]. Since they can be converted into one another by means of a transformation, only the form on the left-hand side of figure 3.14 is considered for further representations.

Order lines

Order lines of a waterfall diagram are straight lines of origin (left-hand side of figure 3.14), the slope corresponds to the respective order o. The order can thus be calculated from the quotient between frequency f and speed n:

$$o = f/n \tag{3.5}$$

For example, for a gear with 13 teeth there are 13 meshes per revolution. This corresponds to an excitation with the frequency of 13 Hz and results in the order $o = \frac{13\ Hz}{1\ s^{-1}} = 13$. If the speed doubles, the number of tooth meshes per constant time interval also doubles. The order remains invariant and can be verified by $o = \frac{26\ Hz}{2\ s^{-1}} = 13$. In general, orders do not only exist in terms of their fundamental frequency, but also have harmonics. The reason for this lies in spectral components of the excitation.

System resonances

System resonances are more or less strongly excited over the entire speed range. If the frequencies are plotted on the ordinate and the engine speed on the abscissa, they can be identified as horizontal lines:

$$f_{sys} = constant \tag{3.6}$$

Note that, due to the damping properties of material and joints, the resonances can be smeared. This makes it difficult to identify them precisely using an order analysis.

Overall, order analysis is a compact form of presentation for the visualization of different, physical phenomena of vibratory systems. For example, the speed can be recorded on a housing

surface (e.g. accelerometer or laser vibrometer), subject it to an order analysis and thereby derive the characteristics of the entire system. Few of the possible fields of application can be summarized as follows:

- The order line can be used to identify the vibration component of individual components that have speed-dependent excitation frequencies. A direct comparison of the straight lines for different embodiment of a component (e.g. ball bearings with large or small balls) provides information about their effects at system level.
- It is possible to make a statement about the natural frequency spectrum of the entire system. Natural frequencies can be identified as horizontal lines. However, the quantitative evaluation is limited due to measurement and process noise.
- With the help of order analysis, qualitatively critical operating points can be determined in relation to the noise emission. If a system resonance and an order line meet, resonance peak is created, which results in a strong sound radiation. Such phenomena should be avoided for operating points if possible.
- By averaging distributed order analyses over a housing surface, quantitative statements can be made about the radiated sound power under certain conditions.

3.3.3 Frequency Response Function and Octave Plot for FE models

Generally, FFT are used for analyzing the periodically oscillating signals, which in addition to the frequency spectrum also provide information about the amplitude of individual frequencies [Bri97, RPB08]. For the evaluation of FE outputs, like the behavior of surface accelerations and acoustic pressures Frequency Response Functions (FRF) and octave 1/3rd plots respectively are utilized.

An FRF is a frequency based measurement function which is used to identify the resonant frequencies, damping and mode shapes of a physical structure. Sometimes it is referred as transfer function between the input and output expresses the frequency domain relationship between an input and output of a linear, time-invariant system [Sie20]. Below definitions of the parameters which help in comprehending the characteristics of plots are mentioned:

- **Resonances** - Peaks indicate the presence of Eigen frequencies of the structure/components.
- **Damping** - Damping is proportional to the width of the corresponding peak. The wider the peak, the heavier is the damping
- **Mode Shape** - The amplitude and phase of multiple FRFs acquired to a common reference on a structure are used to determine the mode shape.

Many types of input excitations and response outputs can be used to calculate an experimental FRF. For example in mechanical systems (vibrations), force (Newtons) is considered as input and acceleration (mm/sec^2 or g), velocity (mm/sec) or displacement (mm) represents the output function.

The left side of figure 3.15 describes an example FRF plot. The unit of y-axis is (g/N). The acceleration is divided by the input force to obtain the FRF. The numbers indicated on the graph show the resonance frequencies. The 1st peak is tend to be very sharp indicating that there is no damping present in this frequency area. Furthermore, peak numbers 3 and 5 the peak are smoothed out competitively to the rest indicating that there is a heavier damping factor than compared to the rest of the peaks.

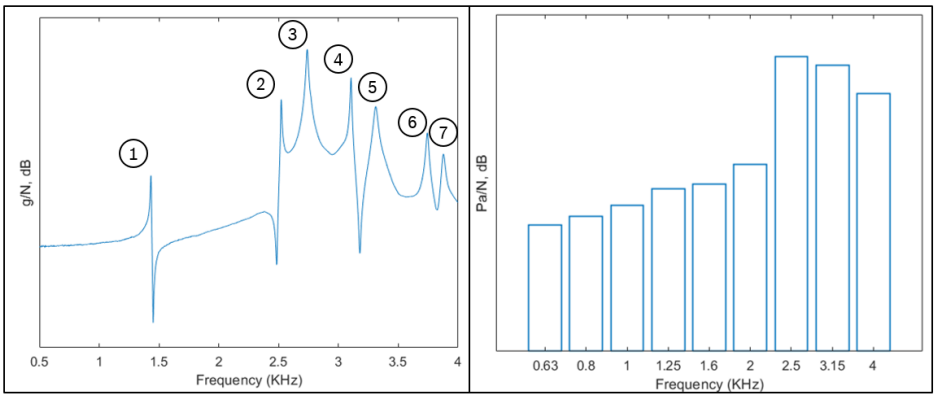

Figure 3.15: Left: FRF surface velocity plot. Right: octave 1/3rd acoustic pressure plot

Octaves are groups of frequencies that help quantify how humans distinguish across the frequency spectrum. They represent the overall level of energy over a specific frequency range. Octave analysis is an indispensable tool for sound measurement because it gives a close approximation of how the human ear responds. Right-hand side of figure 3.15 describes an octave plot corresponding to the earlier discussed FRF graph. Each rectangle corresponds to a frequency band. A band consists of a lower limit, upper limit and central frequency. Finally, acoustic 1/3rd octave limits used for the evaluation are represented in table 3.3. Generally, 1/3rd band limits are used when there are smoothly varying spectra. In case of tonals, narrow bands like 1/10th can be used. Detailed information of octave bands can be found in [Kin82].

Lower Frequency (Hz)	Center Frequency (Hz)	Upper Frequency (Hz)	Lower Frequency (Hz)	Center Frequency (Hz)	Upper Frequency (Hz)
11.2	12.5	14.1	282	315	355
14.1	16	17.8	355	400	447
17.8	20	22.4	447	500	562
22.4	25	28.2	562	630	708
28.2	31.5	35.5	708	800	891
35.5	40	44.7	891	1000	1122
44.7	50	56.2	1122	1250	1413
56.2	63	70.8	1413	1600	1778
70.8	80	89.1	1778	2000	2239
89.1	100	112	2239	2500	2818
112	125	141	2818	3150	3548
141	160	178	3548	4000	4467
178	200	224	4467	5000	5623
224	250	282			

Table 3.3: Octave 1/3rd lower center and upper frequency values

3.4 Wear in Drivetrains

Wear is referred as removal of material from a surface that increases vibration, noise or surface roughness. A large number of wear mechanisms has been identified in literature [Bhu15, Ste16, ML94]. For metals, they include deformation, adhesion, abrasion, delamination, fatigue, fracture, corrosion and oxidative wear. For brittle solids such as ceramics, they are fracture,

abrasion, tribo-chemical wear and corrosion. Broadly speaking, these can be classified into physical, melting and chemical processes and their interplay. Figure 3.16 illustrates different forms of wear being separated based on the fundamental physics [Ste16]. Wear is a huge domain and developing a general method/ setup addressing it is quite difficult. The blue highlighted (in figure 3.16) describes the focus of this thesis. Only the mechanical, adhesion and sliding wear mechanisms are considered here.

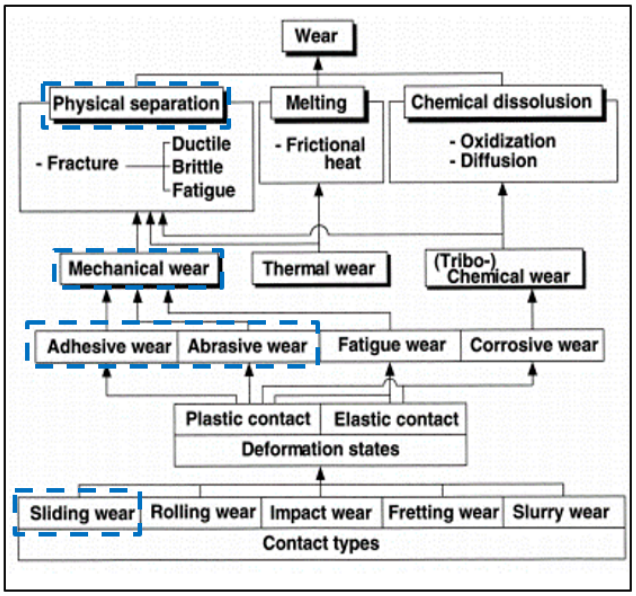

Figure 3.16: Different forms of wear mechanisms [Bhu15]

3.4.1 Wear Terminology

Wear coefficient - Wear coefficient can be understood as the probability of removal of asperities when surfaces come into contact. Wear coefficient gives the ratio of number of asperities which gets separated from the parent surface to the total number of asperities in contact [Hir16]. It is used in developing numerical formulae for the wear mechanism.
Wear rate - Wear rate is volume loss per unit distance (mm^3/mm). It is independent of the load applied. Specific wear rate is a more accurate description of the wear characteristics of any material, particularly for metals, alloys, and composites. It is defined as volume loss per unit distance per unit load (mm^3/Nmm). These are used as performance indicators to analyze the status of the wear. For instance, a higher wear rate indicates that the component is deteriorating at faster pace [Bhu15].
Wear volume - Wear volume is the total loss of volume in a component due to the underlying wear mechanism. It can be calculated using different wear models discussed in section 3.4.2. Generally, the total volume of material removed during sliding (the wear volume) is proportional to the real area of contact multiplied by the sliding distance and the wear coefficient [Arc04].
Wear maps - The factors discussed above and few other variables like sliding velocities, contact pressures etc., play key role in analyzing the effects of wear. Wear maps are nothing but the plots of these associated factors. Variables like friction, sliding velocities or loads are plotted against general outputs like wear depth or wear volume for a better picture of the wear mechanism. The common forms of wear maps which can be important to study are wear volume vs. time, wear depth vs. sliding velocity, wear vs. temperature or wear vs. load vs. time.

The relationship between wear and the operating conditions is often not linear. The transition of wear from mild to severe can occur for instance, when there are heavier loads. It would deteriorate the performances thereby increasing the noises. The part is deemed to be failed once it enters the severe zone. Hence it is important to avoid the transition from mild to severe wear. Figure 3.17 shows that the wear increases rapidly for steel once the load nears 45N (for a disc-pin-mechanism) [AH56]. This zone can be termed as transition zone and it is vital to ensure that the wear lies within the mild zone as it does not have any major impact on the performances (unlike the components in severe zone).

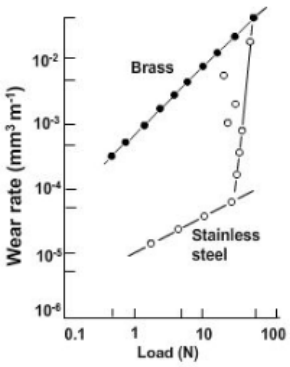

Figure 3.17: Wear transition

3.4.2 Available Mathematical Wear Models

Archards model - Archard (1953) presented the theoretical basis for the expression in equation 3.7. Consider two surfaces in a sliding contact under applied load F. Assume that during an asperity interaction, there asperities deform plastically under the applied load and that at each unit event there is a definite probability that a wear particle will be produced [AH56]. The terms h, K, S, A and H in equation 3.7 indicate the wear depth, K-factor, sliding distance, area and hardness of the softer material respectively.

$$h = \frac{K \cdot F \cdot S}{A \cdot H} \tag{3.7}$$

Rowes model - Rowe (1980) proposed a formula for the modified adhesion theory is shown in equation 3.8. This model used the effect of surface films as modification in simple adhesion theory of wear. In the equation 3.8 β and μ refer to fraction of contact area under dry lubrication and friction coefficient respectively. Here, the lubrication condition means that the shear strength of the interface is smaller than the shear strength of the bulk material [Hir16].

$$h = K \cdot \beta \cdot \sqrt{1 + \mu^2} \cdot \frac{F}{H} \tag{3.8}$$

Rhees model - The empirical equation (3.9) developed by Rhee (1971) correlates the wear of a metal-reinforced phenolic resin sliding against cast iron with the load (F), speed (v), and time (t). Within equation 3.9, ΔW is the weight loss of the friction material and a, b and c are empirical constants. Typically, these empirical relations are valid only within the range of applied test but are far more accurate in that range than other theoretical equations [Rhe71].

$$\Delta W = K \cdot F^a \cdot v^b \cdot t^c \tag{3.9}$$

In searching the literature for wear models and equations, over 300 equations were found for friction and wear [ML94]. The 2 major publications surveyed are the Wear journal between 1972 and 2012 and the ECOTRIB conferences from 2007 to 2018 [WJ12, Eco18]. These mathematical models are much complexer than the one described earlier and are specific to particular test setups. Overall, a suitable model is chosen based on the factors like operating conditions, wear type etc. For the scope of this thesis mostly the Archards approach is applied.

3.4.3 Procedure for Developing Wear FE Model

The steps for creating the FE model for abrasion is quite similar to points discussed for FE modeling of NVH. The notable addition is the coupling of FE model to the developed wear

model using the Fortran compiler and the inclusion of adaptive mesh technique to represent the wear.

1. Mesh the available geometry, define the element properties, select the appropriate shape functions and assemble the element equations as discussed in 3.2.3
2. Define the load profile of the shafts, adaptive mesh boundaries, the friction model, the contact properties etc. Adaptive meshing is a tool that makes it possible to maintain a high-quality mesh throughout an analysis, even when large deformation or loss of material occurs, by allowing the mesh to move independently from the material. It does not alter the topology (elements and connectivity) of the mesh, which implies some limitations on the ability of this method to maintain a high-quality mesh upon extreme deformation [Cor19].
3. Develop the associated abrasion model using the Fortran compilers and link it with the FE software. There will be a continuous exchange of data between the subroutine (Fortran functions) and the FE software. Values like contact pressure and slip will be transferred from FE to subroutine and the subroutine calculates the wear and sends it back to FE software.
4. Define the solution step (static, dynamic implicit etc.,) along with the information regarding step time and increment.
5. Compute the wear stored inside the field variable and also plot the contact force, slip, stress for further analysis.

3.4.4 Evaluation of Wear Plots

For the comprehension of abrasion mechanism, majorly the wear maps like wear depth vs. load, wear depth vs. time can be studied. They contain essential information to analyze the complexities and further curtail it to the mild zone. To understand them better, few of the graphs from [Kat05] are shown in figure 3.18.

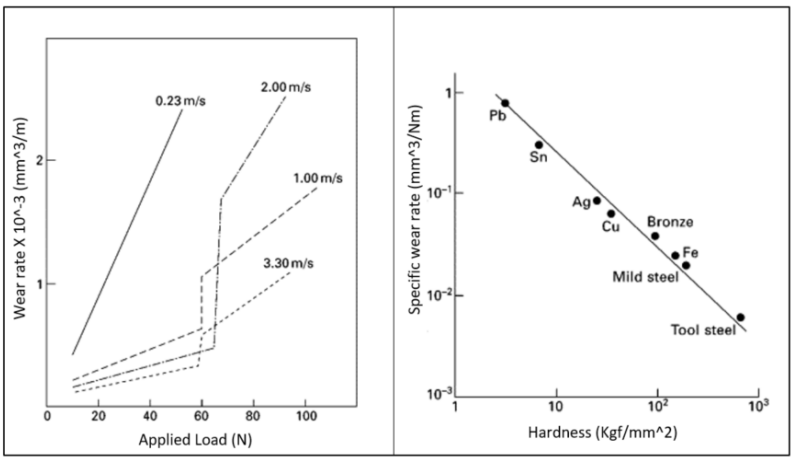

Figure 3.18: Left: wear rate vs. applied load. Right: specific wear rate vs. hardness [Kat05]

The left-hand side of figure 3.18 shows the transitions of wear rate (mm^3/m) at critical loads for high chromium ferrite steel pins sliding on austenitic stainless steel discs at 0.23, 1.00, 2.00 and 3.30 m/s. It can inferred that once the load reaches around 50N the abrasion moves to the severe zone and hence it is wise to control it having the normal load in the range [0 50]N. The right-hand side of picture 3.18 illustrates the influence of the hardness over wear rate. It can be clearly understood that as the hardness increases the removal of material becomes more difficult.

3.4.4.1 Principles of Machine Learning Algorithm

The data sets generated from Uncertainty Quantification (UQ) and FE simulations (check section 4.5) help in application of the Machine Learning (ML) techniques. Numerical simulation of abrasion model is a complex physical process. Modern software codes implement complex algorithms that solve large systems of nonlinear or partial differential equations. These computations produce a large amount of data that is usually discarded for future similar computations. The aim of this section is to leverage these data using machine learning in order to improve numerical simulation performance and get predictions at real time. Figure 3.19 describes the flowchart for machine learning models. Next part of the section focuses on the center box (Train ML algorithm) of this figure.

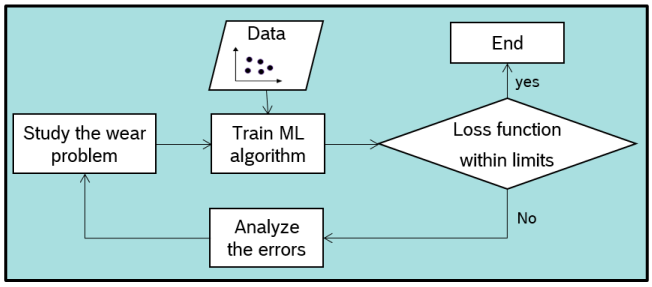

Figure 3.19: Holistic view for analyzing the wear values using artificial neural network

Consider a shallow network with 6, 4 and 2 nodes at input, hidden and output layers respectively. Equations 3.10 and 3.11 represent the weighted sum and output of the hidden and output layers respectively. Here the terms Φ and v_i correspond to the activation function and weighted sum of the corresponding node. These equations help in finding the outputs for the neural network from the given input data.

$$\begin{bmatrix} v_1^{(1)} \\ \vdots \\ v_4^{(1)} \end{bmatrix} = \begin{bmatrix} w_{11}^{(1)} & \dots & w_{16}^{(1)} \\ \vdots & \ddots & \vdots \\ w_{41}^{(1)} & \dots & w_{46}^{(1)} \end{bmatrix} \begin{bmatrix} x_1 \\ \vdots \\ x_6 \end{bmatrix} \quad \& \quad \begin{bmatrix} y_1^{(1)} \\ \vdots \\ y_4^{(1)} \end{bmatrix} = \begin{bmatrix} \Phi(v_1^{(1)}) \\ \vdots \\ \Phi(v_4^{(1)}) \end{bmatrix} \tag{3.10}$$

$$\begin{bmatrix} v_1 \\ v_2 \end{bmatrix} = \begin{bmatrix} w_{11}^{(2)} & \dots & w_{14}^{(2)} \\ w_{21}^{(2)} & \dots & w_{24}^{(2)} \end{bmatrix} \begin{bmatrix} y_1^{(1)} \\ \vdots \\ y_4^{(1)} \end{bmatrix} \quad \& \quad \begin{bmatrix} y_1 \\ y_2 \end{bmatrix} = \begin{bmatrix} \Phi(v_1) \\ \Phi(v_2) \end{bmatrix} \tag{3.11}$$

The core of neural network developed for predicting the wear in advance is the back-propagation algorithm with three layers. The importance of back-propagation algorithm is that it provides a systematic method to determine the error: difference between abrasion depth calculated by the neural network algorithm and abrasion depth provided as dependent variable in the training of hidden nodes.

Significance of activation function

Activation functions of the back-propagation also have a major effect on the neural network ability to converge. It is a mathematical formula that is activated under certain circumstances. When neurons compute weighted sum of inputs, they are passed to the activation function that checks if the computed value is above the required threshold. Mainly for the prediction of wear depth, sigmoid curves are used as activation function (check equation 3.12). The main advantage of this form of curves that is the presence of the continuous gradients, due to which the jumps

in output values are prevented.

$$\begin{aligned} \Phi(x) &= \frac{1}{1+e^{-x}} \\ \Phi'(x) &= \Phi(x)(1-\Phi(x)) \end{aligned} \tag{3.12}$$

The gradient descent technique modifies the parameters of a function to descend from a high value of a function to a low value by looking at the derivatives of the function with respect to each of its parameters, and seeing which step, via the considered parameter, is the next best step to minimize the function. Applying gradient descent to the error function helps find weights that achieve lower and lower error values, making the model gradually more accurate.

The input data of the neural network travels through the input layer, hidden layer, and output layer. In contrast, in the back-propagation algorithm, the output error starts from the output layer and moves backward until it reaches the right next hidden layer to the input layer. This process is called back-propagation, as it resembles an output error propagating in reverse direction. Equation 3.13 corresponds to the delta of output layer, where i represents the output node index.

$$\begin{aligned} e_i &= \hat{y}_i - y_i \\ \delta_i &= \Phi'(v_i)e_i \qquad \forall i \in [1\ 2] \end{aligned} \tag{3.13}$$

Moving leftward, the deltas at hidden node can be calculated using equation 3.14. Terms $v_1^{(1)}$ and $v_2^{(1)}$ are the weight sums of the forward signals at the respective nodes. It is noticeable from this equation that the forward and backward processes are identically applied to the hidden nodes as well as to the output nodes. This implies that the output and hidden nodes experience the same backward process. The only difference is the error calculation (check figure 3.20).

$$\begin{aligned} \begin{bmatrix} e_1^{(1)} \\ \vdots \\ e_4^{(1)} \end{bmatrix} &= \begin{bmatrix} w_{11}^{(2)} & w_{12}^{(2)} \\ \vdots & \vdots \\ w_{41}^{(2)} & w_{42}^{(2)} \end{bmatrix} \begin{bmatrix} \delta_1 \\ \delta_2 \end{bmatrix} \\ \delta_i^{(1)} &= \Phi'(v_i^{(1)})e_i^{(1)} \qquad \forall i \in [1\ 4] \end{aligned} \tag{3.14}$$

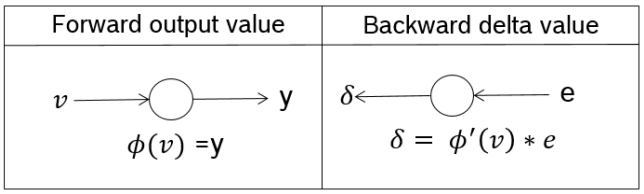

Figure 3.20: Output value calculation vs. the error calculation

In summary, the error of hidden node is calculated as the backward weighted sum of the delta, and the delta of node is the product of error and derivative of the activation function. This process begins at the output layer and repeats for the hidden layer. Moreover, once the hidden layer errors are determined, the neural network can be trained. It is done by adjusting the weights of respective layers (equation 3.15). Here, term α corresponds to the learning rate. More detailed explanation of different available weight adjustment processes can be found in [Ska18].

$$\begin{aligned} \Delta w_{ij} &= \alpha \delta_i x_j \\ w_{ij} &\leftarrow w_{ij} + \Delta w_{ij} \end{aligned} \tag{3.15}$$

Importance of loss function

The cost function (also known as error, loss function) addresses the output error of the neural network and is proportional to the error. For most part of calculations the mean square error (MSE) (equation 3.16) is used. Furthermore, cost function mean squared logarithmic error(MSLE) (equation 3.17) is developed specifically based on the complexities involved with wear profiles. Factors like wear coefficient is so sensitive that it can create large variations to small changes in the variable, thereby having a possibility of larger errors. Application of MSLE ensures that the large errors are not significantly penalized than the small ones like the variations of material properties and contact properties. This means that MSLE will treat small differences between small true ($\hat{y}$) and predicted values (y) approximately the same as big differences between large true ($\hat{y}$) and predicted values (y).

$$MSE_L(y, \hat{y}) = \frac{1}{N} \sum_{i=1}^{N} (y_i - \hat{y}_i)^2 \tag{3.16}$$

$$MSLE_L(y, \hat{y}) = \frac{1}{N} \sum_{i=1}^{N} (log(y_i + 1) - log(\hat{y}_i + 1))^2 \tag{3.17}$$

These steps (equations 3.10 to 3.17) are repeated for every data point. After that, these steps are again repeated until the model is trained properly and the cost function values are curtailed to the desired limits. Overall, back-propagation is just like any other algorithm. Even in back-propagation, the signal still flows through the connecting lines and the weights are multiplied. The only difference is how the error is handled and how the weights are updated.

Reasons for choosing back-propagation technique with sigmoid activation function to train the wear model

- It helps to assess the impact that a given input variable has on a network output.
- It simplifies the network structure by removing weighted links that have a minimal effect on the trained network. It tries to find the optimal weight for each neuron, which results in accurate solutions.
- Smooth gradient descent of sigmoid curves prevents jumps in the output values.
- Sigmoid form of the activation functions helps to normalize the outputs of neurons to a specified range, which ensures the convergence of the system model.
- It possesses an advantage of detecting the complex non-linear relationships/ patterns among the independent variables like hardness, friction etc and the dependent ones like wear depth associated in the system.
- Overall, it is fast, simple and easy to program.

3.4.4.2 Data Flow of the Neural Network for Wear Estimation

Figure 3.21 depicts flow of data across the shallow neural network (3 layers - 1 input, 1 hidden and 1 output layer) developed. The input parameters obtained from UQ are fed to step 2. Detailed information about UQ is further described in section 4.5.1. The ML algorithm divides

data into three sections mainly: training, testing and validation [SPC06]. Initially, a training set develops the required set up for calculations, followed by testing with the test data points. The back-propagation conditions define plausible values for weights and biases involved in the algorithm.

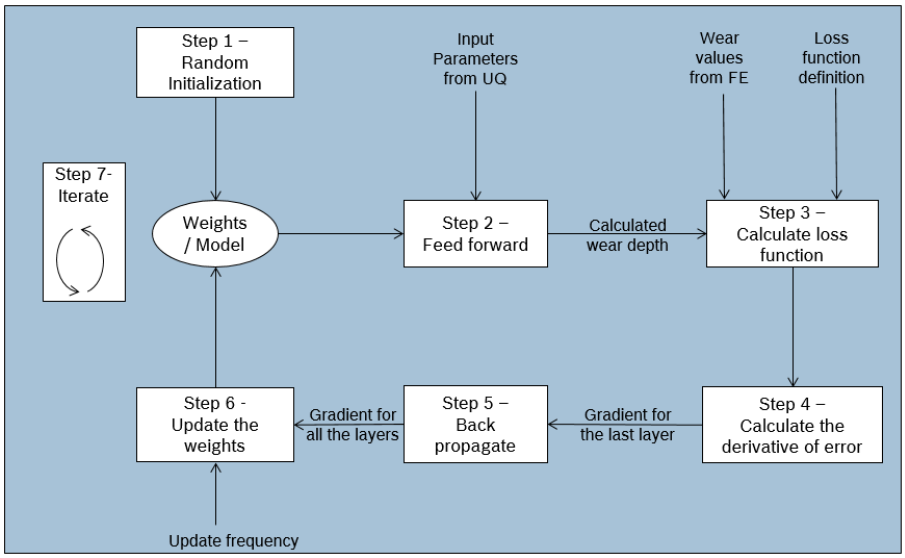

Figure 3.21: Neural network for wear calculations

The below is the summary of steps carried out training the back-propagation neural network:

1. **Initialization** - Initial weights associated with each input neuron (features like hardness, tensile modulus, yield stress, friction, wear coefficient, load etc associated with wear calculations) and hidden layer neurons are applied.
2. **Forward propagation** - The dependent and independent data values are divided into train, test and validation sets. Inputs from a training set are passed through the neural network and the wear depths are computed.
3. **Error function** - In regards with a training set, the correct output is already known. An error function is defined, which captures the delta between the correct wear depth and the actual wear depth of the model, given the current model weights.
4. **Derivatives of errors** - The idea here is to find out the amount of contribution from each of the neuron weights to the error values. This is calculated by taking the derivatives of error values obtained from desired and actual outputs.
5. **Back-propagation** - Objective of back-propagation is to change the weights for the neurons, in order to bring the error function to a minimum.
6. **Weight update** - Weights are changed to the optimal values according to the results of the back-propagation algorithm. They are updated based on the defined learning rates and activation functions.
7. **Iterate until convergence** - As the weights are updated by a small delta step at a time and several iterations are required for the network to learn. After each iteration, the gradient descent force updates the weights towards less and less global loss function. The amount of iterations needed to converge depends on the learning rate, the network meta-parameters, and the optimization method used.

4 Development of a Generic Simulation Methodology for Drive Units

As apparent from state of the art, the vibro-acoustic modeling and simulation methods of the power units are the subject of current research questions. However, no method has been identified to meet all the requirements mentioned in the chapter 2 for a multi-domain vibro-acoustic system model. This gap is to be closed in the present work by developing, implementing and validating a modular, transferable procedure in the form of a generic, multi-domain methodology. For this, a special combination of different modeling and simulation techniques are used depending on the properties offered by each of the methodology.

The first part of picture 4.1 helps in realizing the fusion of these methodologies for comprehending the structural dynamics and abrasion mechanisms. The second part majorly focuses on constructing templates and models to study, analyze and predict the vibrations at the housing structures and wear at the gear components. It additionally describes the potential optimization techniques performed to reduce the noises inside the drivetrains.

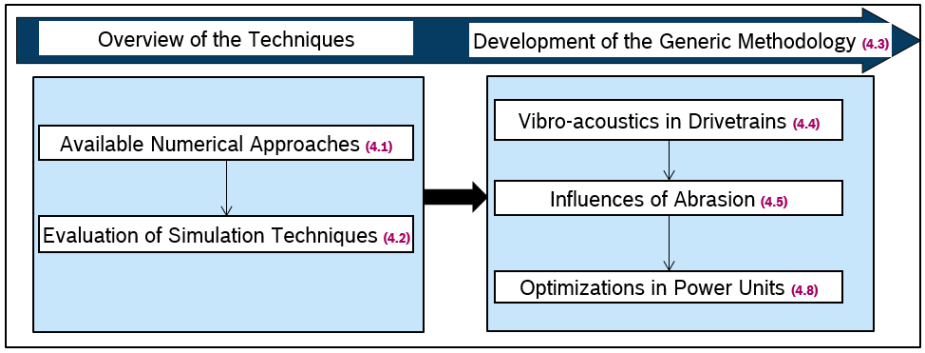

Figure 4.1: Brief overview of the sections and flow within chapter 4

4.1 Numerical Methods Available for Development of Vibro-acoustic and Wear Modeling

It is vital to comprehend the vibrations and wear mechanisms from motion inputs and the available design components in order to curtail them in the future model variants. This section introduces the methodologies available for studying vibro-acoustics and wear in drivetrains. As briefly discussed in chapter 3, the following are possible simulation techniques available for analyzing the vibrations, acoustics and wear formulations.

- Vibrations:
  - Lumped Parameter Modeling (LPM)
  - Multibody Modeling (MBD)
  - Boundary Element Modeling (BEM)
  - Finite Difference Modeling (FDM)
  - Finite Element Modeling (FEM)

  - Statistical Energy Analysis (SEA)
  - Modal Modeling (MM)
- Acoustics:
  - Equivalent Radiated Power Modeling (ERP)
  - Transfer Matrix Modeling (TMM)
  - Acoustic Finite Difference Modeling
  - Acoustic Finite/ Infinite Element Modeling
  - Computational Fluid Dynamics Modeling (CFD)
  - Ray Based Modeling (RBM)
- Wear formulations:
  - Analytical equations
  - Finite Difference Modeling
  - Finite Element Modeling
  - Boundary Value Approach
  - Machine Learning algorithms

Table 4.1 lists features corresponding to available numerical methods. It describes the properties like Degree of Freedom (DOF), linearity, type of the equation and associated solution techniques for each of the simulation method. The terms D.E. and Eq. represent differential equation and equation respectively.

Method	DOF	Linearity	Equation type	General Solution Method
LPM	very few	linear/ nonlinear	Ordinary D.E.	Trapezoidal, Implicit Euler
MBD	few	linear	Algebraic D.E.	Trapezoidal, Runge-Kutta
FDM	few	linear	Difference Eq.	Jacobi, Gauss-Siedel
BEM	few	linear/ nonlinear	Partial D.E.	Jacobi, Gauss-Siedel
FEM	many	linear/ nonlinear	Partial D.E.	Gaussian Quadrature, Newton
SEA	many	linear	Ordinary D.E.	Trapezoidal, Runge-Kutta
TMM	NA. (states)	linear	Algebraic Eq.	Jacobi, Implicit Arnoldi
ERP	many	nonlinear	Algebraic Eq.	Explicit
CFD	many	linear/ nonlinear	Partial D.E.	Finite volume
RBM	NA. (rays)	linear/ nonlinear	Ordinary D.E.	Image source

Table 4.1: Characteristics of the investigated methods for the modeling and simulation of vibro-acoustic mechanisms in gears

Furthermore, these methods (in table 4.1) are analyzed for their application on to the model level requirements and necessary attributes (section 4.2), which are later used for developing the frame work for analyzing the structure borne noises.

4.2 Evaluation of Simulation Methods Based on Model Requirements and Necessary Attributes

Model Level Requirements

In order to formulate a generic method for the work, it is vital to realize the model requirements at system level and also capture the required attributes at component and assembly level. Ensuring the model requirements aids in improving the overall applicability of methodology. The list of model level requirements are shown in table 2.1.

These factors aid in creation of a better robust model. Generally, a component is modeled separately, unconstrained from the environment where it is used ensuring the reusability. It means that, in the definition of component including its equations, only local variables and connector variables can be used. No other means of communication between component and rest of the system, apart from the connector variables is permitted. Furthermore, requirement like modularity is achieved by high levels of abstractions of system components, which are later instantiated at the usage level. Extensibility characteristic ensures the enlargement of model and its corresponding parts [Fri15, KDH19a, DDH15]. Figure 4.2 shows basic definitions of all these requirements.

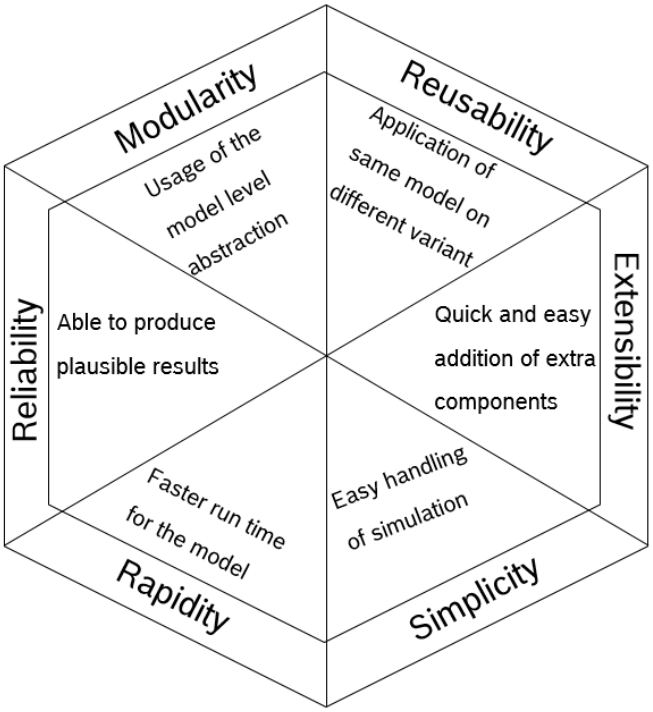

Figure 4.2: Model level requirements

All these requirements corresponds to the characteristics of object oriented modeling. Traditionally, the object oriented programming languages like C++, Java, Simulia etc., supports programming with operations on stored data. Whereas here the object orientation emphasizes on the structured mathematical modeling. This concept is mainly used to handle the complexity of large system descriptions. More information about the object oriented modeling can be found in literature [Fri15, Pet00].

Figure 4.3 gives an overview of the strengths corresponding to each numerical method. The white color indicates that the requirement cannot be fulfilled using the method. The lightly shaded boxes are used when the requirement could not be fulfilled within the own method, but has no negative influence on the whole model at the system level. The dark shaded boxes indicates that the requirements are met using the corresponding method. Furthermore, the evaluation of the methods is based on the simple logical reasoning. Below is the list of few instances along with the reasoning:

- CFD could be extended across different variants, and applied for extra components, but it is not simple and does not yield rapid results.
- The FDM method can achieve faster results but bringing it to modular level is not possible.
- Although the FEM model can be reusable for different variants, it cannot attain modularity within its own method, as only a certain level of detail for the model exists. Anyhow, at

the system level, the modularity requirement is met, since here the FE part represents a configurable level of detail.

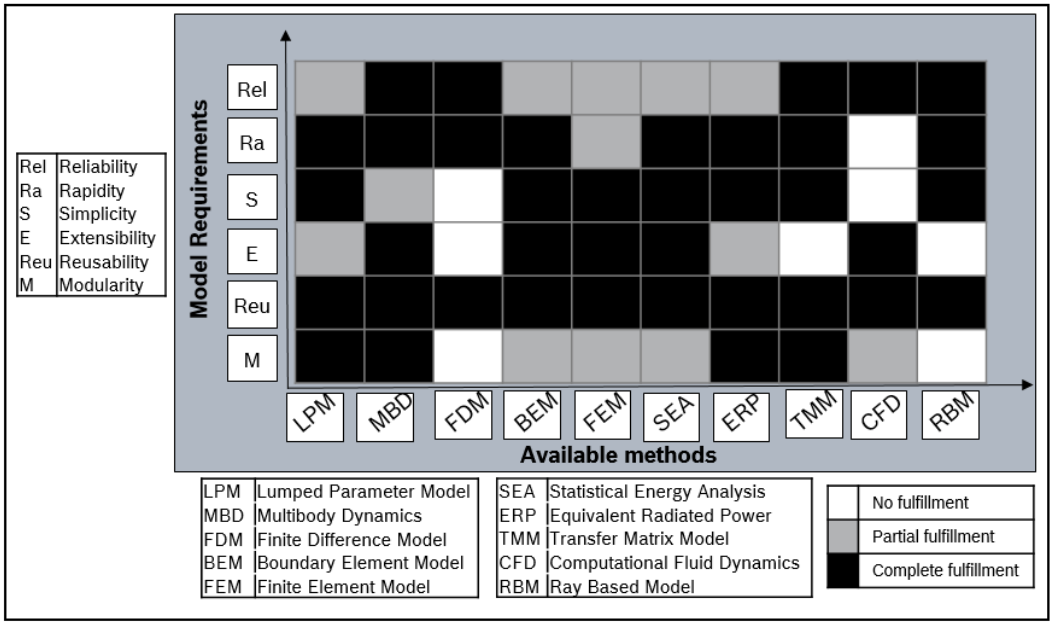

Figure 4.3: Methods vs. requirements

Finally, methods like LPM, MBD, BEM, FEM, SEA and ERP have no white colored boxes, which means these simulation techniques adheres to all the required characteristics and hence can be considered for building of the work.

Necessary Attributes

Additionally, the approach should also be able to perceive the complexities like excitation mechanisms, surface velocities and acoustical properties, which would ultimately aid in comprehending the vibro-acoustics. Following is the list of required attributes:

- Excitation mechanisms
- Gear vibrations
- Housing vibrations
- Vibrations to acoustics coupling
- Acoustical characteristics
- Wear mechanisms

Furthermore, only those sets of methods are examined, which could recognize the model level requirements. Figure 4.4 shows potential of the available methodologies to realize the necessary attributes. Below is the explanation for a few of techniques analyzed for the respective attributes:

- ERP technique can be used to estimate the acoustic pressure in both far field and near field but it is not helpful for vibrations calculations.
- MBD can be used for finding vibrations at the surface level but cannot aid in acoustical domain and also cannot be directly used for simulations of wear mechanisms.
- FEM along with vibrations is utilized for study of the wear mechanisms. This can be achieved with the connection of method to the associated wear subroutines.
- LPM can be best applied for generation of the internal excitations at the gears and toothed shafts.

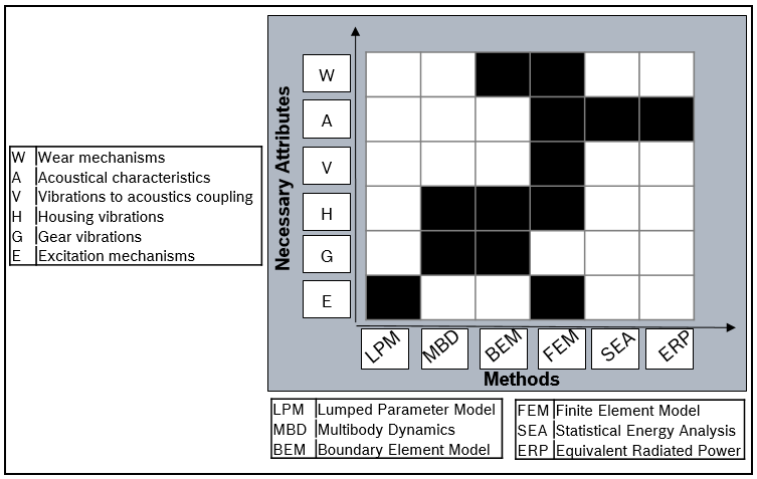

Figure 4.4: Methods vs. attributes

Graph 4.4 helps in finding a possible combination of the techniques to build a generic multi-domain method. For few of the attributes, like housing vibrations, can be perceived in MBD, BEM and FEM domains. In such cases, the particular method is selected based on the frequency spectrum of interest and for the wear mechanism it is a blend of BEM and FEM methods.

Figure 4.5 shows response along with the corresponding simulation techniques across the frequency band, which would further help in choosing the method. Finally, both the figures 4.4 and 4.5 help in selecting the method based on the attributes and frequency of interest [Alt18].

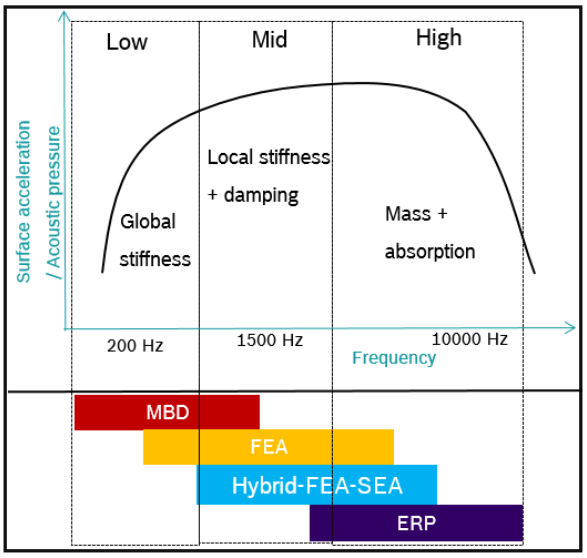

Figure 4.5: Simulation techniques mapped on the frequency spectrum

4.3 Overview of Modeling and Simulation Techniques for Vibration, Wear and Noise in Powertrains

Using the simulation techniques identified from the earlier sections (sec. 4.1 and 4.2), a generic, cross-domain methodology for comprehending the abrasion, vibro-acoustic mechanisms in drivetrains as well as sound radiation into the surrounding fluid is developed. Since the result is a complex combination of different methods, it makes sense to look at the developed methodology from two different perspectives: In the first step, the functional description is presented. Then,

a flowchart is used to illustrate the creation of each model component and there interactions.

Figure 4.6 shows overview of the data flow for the vibro-acoustic, wear and optimization module. This figure describes the detailed view of the second part of figure 4.1. This part is broadly divided into four modules mainly:

- **Structure and air borne emission** - It focuses mainly on analyzing the vibration characteristics present inside the powertrain. Eventually, the influence of surface velocity of the structures on to the surrounding fluid are also depicted.
- **Wear mechanism** - It studies the influences of wear at the areas of repetitive contacts i.e., at the gear mesh and toothed shafts.
- **Connection between abrasion and vibration module** - It describes the impact of abrasion on the surface accelerations of the housing structures.
- **Optimization flow** - It illustrates the definition and development of process used for reducing the noises and vibrations.

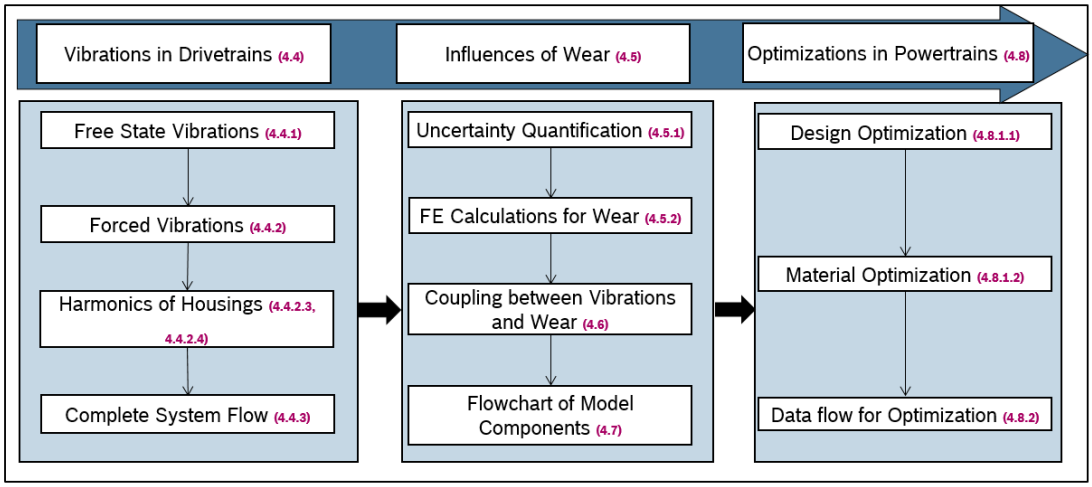

Figure 4.6: Brief overview of the sections and flow within vibro-acoustic, wear and optimization modules

The vibration module consist of three model components: mechanical gear unit, housing structure and associated fluid interaction. The mechanical gear unit includes the internal excitation mechanisms in the tooth mesh, which set the gear in vibration. Within this domain, the driven and driving shafts are mapped at system and FE level. In order to model the physical processes, the mechanical gear unit is therefore divided into three further mechanisms: non-linear tooth mesh, gear components and flexible housing. All three model parts are described in section 4.4.2.1 in more detail. The vibrations form gears and shafts structures spread in the form of waves to the bearings. These movements in bearings excite the gear housing and cover and eventually make them vibrate. The housing structures are modeled using the concepts of flex-body and submodeling at system and FE level respectively. The housing structure has a spectrum of natural frequencies and modes and functions as a kind of membrane, which ultimately emits noise in the form of airborne sound. Eventually, the acoustic infinite and ERP techniques are used for calculation of acoustic pressures around the housing.

The abrasion module consists of three fields: UQ, FE methods and neural networks. The UQ method aims in making a parameter study to understand the influences of variables present in simulations over the results like wear depth. The numerical templates try to predict the wear by coupling the wear formulations with that of the FE methods like contact algorithms, friction models etc. In the end, neural networks with back-propagation methods are created to predict the wear at faster time frames.

Abrasion in drivetrains eventually deteriorate the NVH characteristics. Therefore, it is vital to comprehend their behaviors and formulations. This is done by creating a numerical coupling between the vibration and abrasion modules. It is followed by defining the design modifications and material changes to optimize the housing structures for their vibro-acoustic characteristics.

Furthermore, a detailed view of the identified modeling methods for each of these modules and their connections are described in sections 4.4.3, 4.6 and 4.6.2.

4.4 Vibro-acoustic Behavior of Drivetrains

In order to understand noise and vibrations from each of the development node, parameters like excitation mechanisms at the source, transfer of velocities along the components and vibrations at the housing must be thoroughly analyzed. This module is further divided into three submodules. The first submodule is focused on developing a robust model to study the natural vibrations by analyzing individual and combined structures for free state vibrations. In the second submodule, the model is improved for the excitations resulting from gears and electric motor. Additionally, the model is bettered for structural properties of the components as it would influence NVH of the housings. The third submodule mainly focuses on analyzing harmonics and acoustics of the complete drivetrain.

4.4.1 Model Development for Natural Vibrations

Excitations generated at the gears and shafts need to be well comprehended and later contained at desired limits for restricting the structure borne emissions at exterior surfaces. Before analyzing the influences of excitation, it is vital to understand modal analysis for drivetrain components. It aids in evaluating vibration behaviors of the structures. A drivetrain consists of four main components, gears, motor, shafts and housings having structural influences. At the development stage, essential parameters for vehicle vibration such as mass, inertia, stiffness and damping for these structures are evaluated.

Modal analysis is a technique used for calculating the dynamic characteristics of system, like natural frequencies, damping values and mode forms. In the electromechanical transmission system, frequencies of the motor excitation and the resonance frequencies of the system components are juxtaposed with each other to perceive the vibration characteristics. There are various methods available in literature for calculation of Eigen shapes (analytical, different form of simulations) [CP14, Cor15]. Each methodology possesses its own pros and cons [And14]. Considering the factors like modeling, adaptability and accuracy, FEM is chosen as desired simulation technique to analyze the Eigen frequencies of the structures for this particular section. This approach additionally realizes the modeling requirements like reusability and extensibility mentioned in section 4.2. The degree of accuracy in FE depends majorly on selection of the element type, mesh density, material properties, constraints and load inputs. The target of the simulations is to capture the frequencies of main bending, torsion and bending plus torsion modes, as they are vital for harmonic analysis (that is the next stage of the simulations).

Eigen modes for the combined structures can be tricky and complicated as compared to the individual parts. This is due to the fact of contact between the components. The contact formulations bring additional damping into the systems. Therefore, apart from the material dampings, the contact surface dampings are also investigated and entered into the FE templates. Parameters like Young's modulus, density or contact stiffness are modified depending on the results from Experiment Modal Analysis (EMA). Finally, once the simulations for individual and combined structures are available, they are checked with the EMA, ensuring for the correctness of FE data.

4.4.2 Model Development for Forced Vibrations

Free vibrations discussed in section 4.4.1 serve as basis for understanding the surface velocities of structure in non-exciting state. The current section focuses on the impact of forced excitations in the drivetrain components. The first submodule of this forced vibration module deals with the local excitation mechanisms and associated vibrations at component level. The second section depicts the importance of analysis related to various structural components. The section after that describes the harmonics of housings and illustrates the surface velocities at critical areas. The final section gives an overview of the acoustical domain associated with the housings and covers.

4.4.2.1 Excitation of Rotating Shafts

For several engineering applications, gears and shafts help in transmission of power or energy among the rotating components. Along with this power, unwanted structure borne emissions are also transmitted. For this reason, it is necessary to understand the underlying mechanism of the gear mesh and motor, in order to curtail the vibrations at their origination. The excitations in powertrain can occur either from the mechanical gear meshes or from the electromagnetic rotor forces. Both of them influence the drivetrain vibrations and thereby the pressures of the surrounding fluid. Figure 4.7 depicts a schematic view for excitations present in the drivetrain.

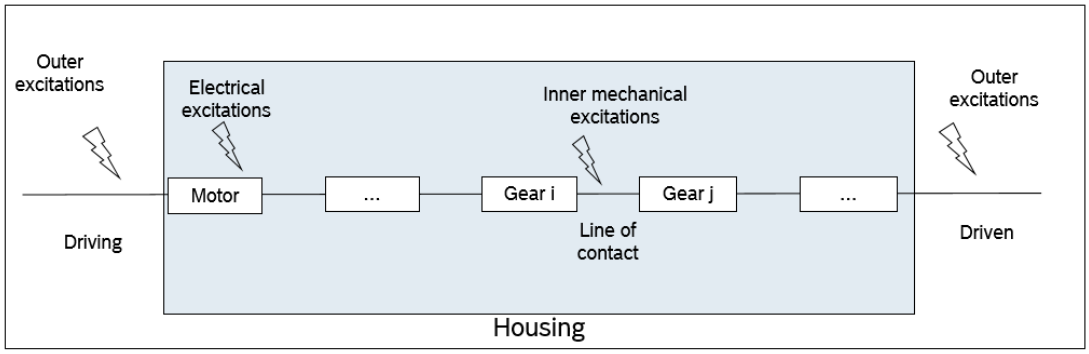

Figure 4.7: Line diagram of excitations present in drivetrain

Considering the application of mechanical excitations on system and FE model, gearbox components with different levels of detail are developed. The two types of the transmission models are listed below:

- Ideal gear transmission model
- Physical gear transmission model: Non-rigid gear model and FE gear model

For a numerical, vibro-acoustic system analysis, only the physical transmission model comes into play since it shows both the macroscopic rotation of gears and the microscopic excitation for vibration. In contrast, the ideal gear allows an efficient mapping of the macroscopic rotation and serves as a reference for the verification of the physical model (section 5.2.1).

Ideal gear transmission model
The ideal gear model has no compliance in the system (infinite stiffness of teeth) and has an ideal tooth geometry (error-free manufacture and error-free operation). Both idealizations result in a kinematic constraint for the rotational degrees of freedom of a gear. Input and output are coupled to each other by a constant gear ratio i. As generally known, the kinematic constraint of the gear pair can be determined using the pitch circle radius of both the gears (equation 4.1).

The terms φ and r indicate the rotation angle and the pitch circle radius of the gears in contact.

$$\varphi_1(t) \cdot r_1 + \varphi_2(t) \cdot r_2 = 0 \tag{4.1}$$

Both the gears move exactly proportional as radii and are predefined constant system parameters. Hence, $\varphi_1(t)$ and $\varphi_2(t)$ are linearly interdependent. Therefore, the ideal gear model has a single rotational degree of freedom and is an efficient way to map the rotation of gears on a macroscopic level. Whereas physical transmission model (simulation) allows for visualization of rotation of the gears and excitation for the surface velocities. As a result, compared to the ideal transmission, it represents a finer level of detail in the modular model design.

The excitations of the physical transmission model are modeled using two kinds of gear models namely flexible gear model and FE gear model. Both of these transmission models are developed using different approaches. Each of them would aid in design changes in early phases of the drivetrain development.

Non-rigid transmission model

For many of the scenarios, gear mesh may not be considered as being completely rigid. It is mainly due to parameter excitations, geometric excitations, backlashes, deformations in tooth etc. Parameter and path excitations (section 3.1.1.1) are used to numerically record various physical influencing factors like gear shaft bending, shaft torsion, geometric error of the tooth surface (surface topology), deviations in pitch, axle inclination etc., which generates the vibration excitation in the gearbox [DDH15, LB10].

It is necessary for a high quality analysis to a better apprehension of the intricacies. This can be achieved by introducing visco-elasticities into the models. Such an attempt is already described in papers [Ebr06, KDH19a]. Additionally for the DU, electrical components with control loops, modulations (pulsewidth), defective bearings etc., can also lead to excitations. For the current section, mainly the excitation sources of the mechanical phenomenon are considered.

The physical gear model is represented as a physical network within the framework of the methodology developed. In comparison to the direct mathematical formulation, the model requirements like extensibility and simplicity are met. The difference between the gear positions in relation to the line of contact under load can be calculated using the diagram 4.8 and equation 4.2, whereby the function f is the deviation from the ideal gear position (see also section 3.3.1).

$$\varphi_1(t) \cdot r_1 + \varphi_2(t) \cdot r_2 = f(\varphi_1, \varphi_2) \tag{4.2}$$

The dynamic gear model developed is depicted in figure 4.8. The interaction is built with aid of springs and damping elements. The terms M, J, r, z, φ, e, k and d_z represent torques, inertia, radius of pitch circles, number of tooth, rotation angle, excitation, stiffness, damping of driving and driven gears respectively. The spring stiffness and damping values are calculated using Hertzian contact analysis (check contact analysis in section 4.4.2.2).

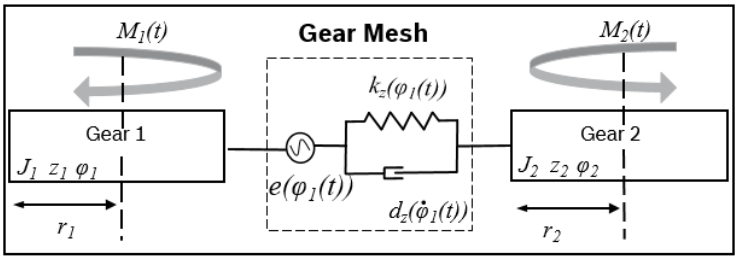

Figure 4.8: Lumped parameter gear model

The term e($\varphi(t)$) corresponds to both path and parameter excitation. It is developed as sum of mean excitation plus sinus curves, that considers the harmonics of the gear tooth with corresponding amplitudes. $\varphi_i(t)$ ($i = 1$, $i = 2$) and its first two time derivatives represent the rotation angle, angular velocity and angular acceleration respectively. The equations 4.3 and 4.4 are the dynamic Equations Of Motion (EOM) for the two lumped parts.

There are different implementation options for recording the deviations e($\varphi(t)$). Few of the common methods are using look-up tables, Fourier coefficients or analytical approximation functions. The parameters are primarily identified using numerical and analytical calculation methods, for instance using simplified models [Pet89, WBN55] or using ISO 6336 [ISO16] (check section 3.1.1.1).

$$\begin{aligned} J_1\ddot{\varphi}_1 =& \mathrm{M}_1(\mathrm{t}) \; - \; r_1 k_z(\varphi_1(t))[r_1\varphi_1(t) + r_2\varphi_2(t) + e(\varphi_1(t))] \\ & - r_1 d_z(\dot{\varphi}(t))[r_1\dot{\varphi}_1(t) + r_2\dot{\varphi}_2(t) + \dot{e}(\varphi_1(t))] \end{aligned} \tag{4.3}$$

$$\begin{aligned} J_2\ddot{\varphi}_2 =& \mathrm{M}_2(\mathrm{t}) \; + \; r_2 k_z(\varphi_2(t))[r_1\varphi_1(t) + r_2\varphi_2(t) + e(\varphi_1(t))] \\ & + r_2 d_z(\dot{\varphi}(t))[r_1\dot{\varphi}_1(t) + r_2\dot{\varphi}_2(t) + \dot{e}(\varphi_1(t))] \end{aligned} \tag{4.4}$$

In order to combine the local excitations of LPM to global MBD forces for the gear and shaft components, a transformation from normal forces of the gear tooth to translational gear forces is needed. Most of the softwares have this function as inbuilt [OH88a].

The transformation to gear forces is summarized in equations 4.5, 4.6 and 4.7. Here $\mathbf{F}$ consists of three components, namely the tangential, radial and axial forces of the gear. $\mathbf{F}_n$, $\mathbf{T}_\beta$, $\mathbf{T}_{\alpha n}$ describe the normal force, rotation matrix for helix angle and rotation matrix for the normal pressure angle respectively. More information about this transformation is described in paper [KDH19a].

$$\mathbf{F} = \mathbf{T}_\beta \mathbf{T}_{\alpha n} \mathbf{F}_n \tag{4.5}$$

$$\mathbf{T}_{\alpha n} = \begin{bmatrix} \cos(\alpha_n) & -\sin(\alpha_n) & 0 \\ \sin(\alpha_n) & \cos(\alpha_n) & 0 \\ 0 & 0 & 1 \end{bmatrix} \tag{4.6}$$

$$\mathbf{T}_\beta = \begin{bmatrix} \cos(\beta) & 0 & -\sin(\beta) \\ 0 & 1 & 0 \\ \sin(\beta) & 0 & \cos(\beta) \end{bmatrix} \tag{4.7}$$

Finite Element gear model

The non rigid gear model aids in understanding the vibrations at the system level. Sometimes, it becomes necessary to capture the gear mechanism with better accuracy in precise locations, and therefore another method variant is developed by completely building the gear model in the Finite Element. A detailed reasoning is described in section 4.4.3.

The contact enforcements between the gear tooth faces are used to generate nonlinearities in the system. Mainly, augmented Lagrangian and penalty contact algorithms are used within the simulations [Wri07]. In the penalty approach, a dummy spring with certain stiffness is introduced between the surfaces. But the main drawback with this method is that the amount of penetration between the two surfaces depends on this stiffness. Higher stiffness values decrease the amount of penetration but can lead to ill-conditioning of the global stiffness matrix and to convergence difficulties. Whereas the augmented Lagrangian method is an iterative series of penalty updates to find the Lagrange multipliers (i.e., contact traction). Compared to the penalty method, the

augmented Lagrangian method usually leads to better conditioning and is less sensitive to the magnitude of the contact stiffness coefficient. The variables like stiffness and damping of these algorithms are parameterized to study the effects of contact properties on the simulations. The deformations among the teeth would lead to transmission error. The required model parameters (like geometries, masses, inertia), material properties, load definitions and boundary conditions serve as input for the FE template. A suitable load profile is applied to get the desired torque and revolutions (RPM (Revolutions per minute) at the rotor shaft). The gear model is rotated for one complete gear ratio and then gear dynamics (velocities and accelerations) and bearing axle forces at each increment are recorded.

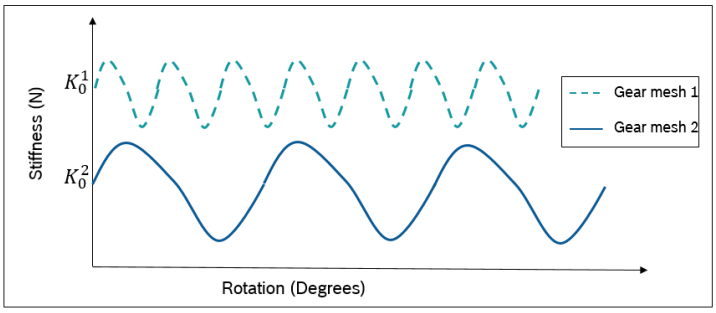

Figure 4.9: Stiffness profile of 2 sample ideal gear meshes with different mesh frequencies

Figure 4.9 illustrates the ideal stiffness profile along the line of contact versus the rotation of the rotor shaft or time. K_0^1 and K_0^2 refer to the mean stiffness values of the corresponding gear meshes. The gears at K_0^1 have higher RPM therefore the cycles (or frequency) is higher compared to the K_0^2. The difference in mean stiffness rises from the contact and geometry definitions of the gears.

The static nonlinear and dynamic quasi-static solution techniques are mainly used for running the simulations of gear model. Static analyses are used when the inertia effects are assumed to be small. They are useful for problems like contact and stiffness analysis of the components. Dynamic simulations are applied as implicit time integration schemes to calculate the quasi-static or transient dynamic responses of a system. Furthermore, quasi-static responses are applied when considerable energy dissipation is necessary in order to provide stability and improved convergence behavior for determining a final solution.

Excitations from electric motor

Electromagnetic phenomena can bring undesired effects such as NVH or heat. Factors like distorted air-gap field of an eccentric rotor can lead to electromagnetic vibrations. The irregular air gap is linked to the eccentricity, which is usual in rotating electrical machines. Eccentricity may be caused by numerous reasons, such as misalignment of the load axis and rotor shaft, relative misalignment of the rotor and stator in the fixing stage, unbalanced loads and mechanical resonances etc., [RPB08]. In order to estimate and correct electromagnetic vibrations by simulation, it is necessary to couple their forces with vibrations. To predict the vibrations caused by the electrical machines, it is vital to model not just the magnetic forces generated by the fluctuation of magnetic fields, but also the structural dynamic characteristics of the electric machines. An electromagnetic FE simulation software is used for force calculations at different nodes of stator (due to the presence of magnetic fields).

There are already few simulation techniques developed for this purpose. For instance, paper [LPW17] describes the electromagnetic simulations developed to study the characteristics of flux and EM force under different conditions using FEM. Thereby it is utilized to analyze the vibration behavior of the structures. Similarly, paper [DB12] focuses on excitations due to electromagnetic phenomena using an electromagnetic FE solver. This excitation is then

projected onto the structure mesh of the stator in order to calculate the dynamic response. But they neglect the effects of excitation due to the transmission errors. Through this work, the radial, tangential and axial forces arising at the stator due to the EM forces are coupled with the mechanical excitations for analyzing the vibration characteristics of drivetrain. The magneto-static simulation outputs magnetic forces for stator surfaces and their respective nodes. These forces are converted to the mechanical domain and are applied as loading conditions for noise and harmonic calculations for the housings (section 4.4.2.3). The values are converted to frequency domain with aid of Fast Fourier Transform (FFT) codes.

Figure 4.10 describes the flowchart for calculation of the vibration behavior for the drivetrain based on the EM characteristics. EM model is prepared using motor geometries and appropriate definitions like phase current. Apart from the calculation of flux and field lines, the simulation also generates an ITEF (Interface for Transfer of Excitation Forces) file. This file consists of information like RPM, orders and forces at each individual tooth, across discrete time points. The ITEF tool acts as an interface to transfer the forces on to the stator surfaces with radial, tangential and axial components along the frequency spectrum of interest. Later these forces are used for simulating the harmonics of the drivetrain structures.

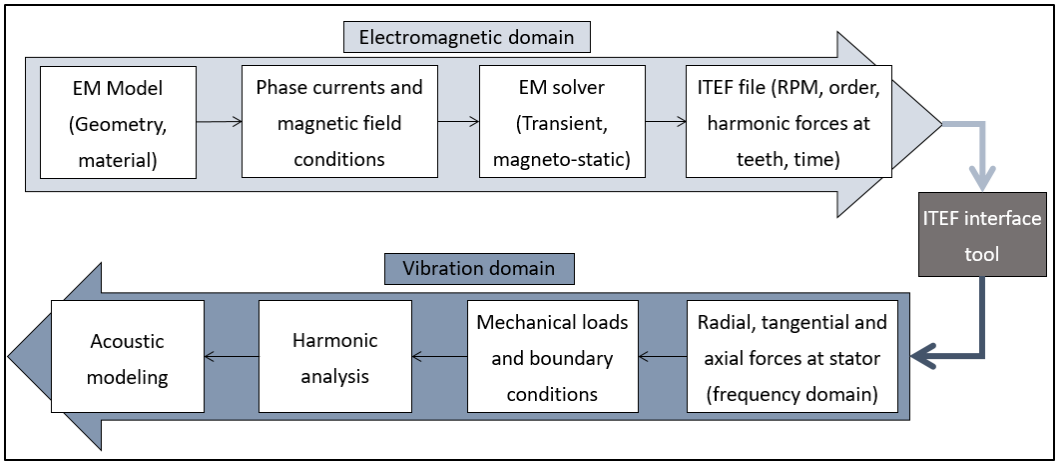

Figure 4.10: Flow for simulating vibration characteristics using EM forces

4.4.2.2 Study of the Drivetrain Components

Before analyzing the vibrations of drivetrain, it is vital to understand other properties like material strengths, damping effects, etc., of various components present in the drivetrains. The below listed are few of areas studied with the aim of building a plausible vibro-acoustic model.

- Study of bearings for equivalent spring stiffness
- Stress and stiffness analysis of the components
- Study of influences of the rotor moments on to the bearings
- Effect of material properties on the stator
- Impact of damping elements on the housings
- Contact analysis for the gear meshes

Bearing study

The simulations of the complete drivetrain with bearings can be cumbersome and could lead to convergence issues, due to the fact that bearing assemblies consists of the balls between the inner and outer rings. The idea here is to build a bearing model by replacing the balls with springs of equal stiffness (as that of the balls). Figure 4.11 shows the sectional view of the original and

simplified bearing model. The stiffness analysis on the current model (on left-hand side of the picture 4.11) is performed by fixing the outer surface of outer ring and applying a suitable load on the inner ring. Later, the deformations and stresses obtained at the balls of bearings (critical areas) are used for finding the stiffness values. Finally, these stiffness values are entered into the simplified bearing model developed (on right-hand side of the picture 4.11).

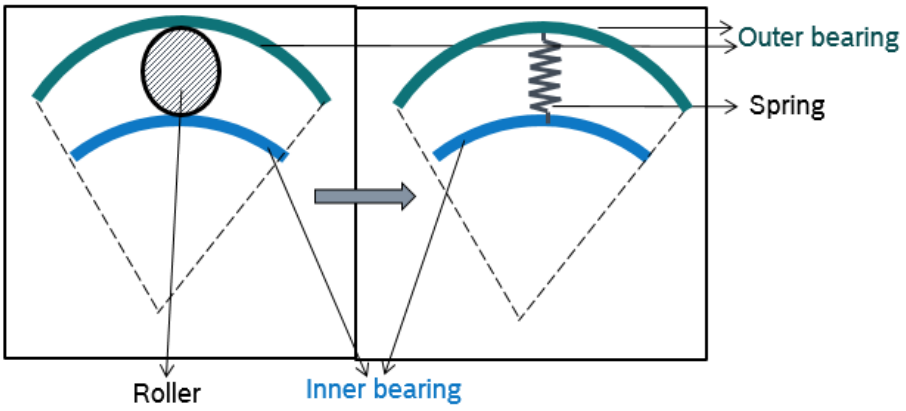

Figure 4.11: Simplified view of original and simplified bearing model

Stiffness analysis of the components

The excitations at the shafts and motor as described in 4.4.2.1, could influence other general parts like housing. For the components to be structurally safe in any domain, the stresses generated due to the load must not exceed the yield strength of the corresponding material. The stiffness of components is influenced by the plastic deformations in the drivetrain. Furthermore, the NVH characteristics will be altered once the stiffness of structure changes. Hence, it is vital to check for the plastic deformations and stresses at critical areas, when the structure is loaded. Figure 4.12 describes a flow chart for stiffness analysis of the parts. The FE model developed is first simulated for the critical stresses. If these values are below thresholds, the model can be passed on for the NVH study, and when the values are above the specified limits, the parts can be improved for their topology, materials etc.

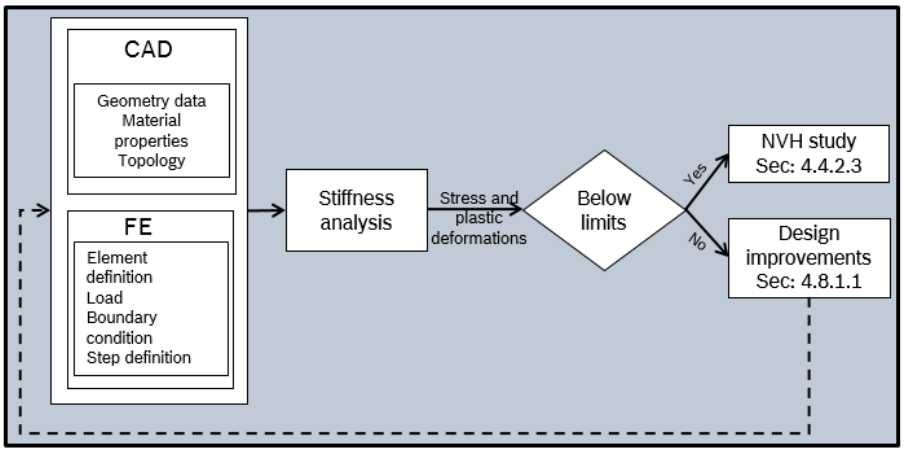

Figure 4.12: Stiffness analysis flowchart for the components

Study of influences of the rotor moments on to the bearings

Bearings are key components present between the housings and the sources of excitation. It is essential to understand their behavior before analyzing the noises around the housings. Large

deformations within the bearings may lead to change in vibration characteristics of the complete drivetrain.

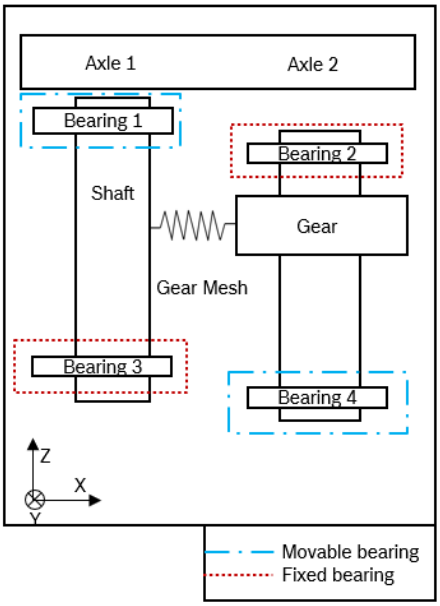

Figure 4.13: Position of bearings with respect to axle 1 and axle 2

Figure 4.13 shows the schematic diagram of the model built in order to numerically comprehend the impact of loads from earlier sections on the bearings. The boundaries applied to bearings are either fixed (only Z-axis rotation free, check figure 4.13) or movable (Z-axis translation and rotation free).

Once the deformations at bearings are curtailed at the elastic limits, the reaction forces at the axles are calculated along the time profile. Figure 4.14 shows part of the reaction forces profile in time domain at two bearings at different shafts. It is quite obvious that the bearing (2) at the outer shaft has fewer maximums due to the difference in the tooth meshing. These forces can be applied directly for analyzing surface velocities of the housings.

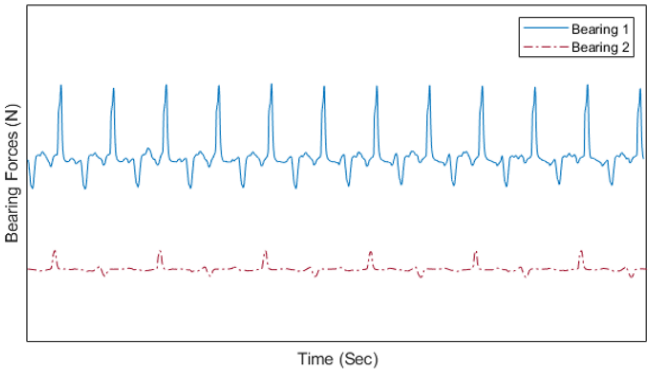

Figure 4.14: Bearing forces in time domain

Effect of material properties on the stator

Another important part of the drive is the stator. It can cause structural influences on the drivetrain assemblies, which lead to alteration of vibration properties. The material orientation plays a key role in establishment of Eigen modes of the stator. The stator material is generally orthotropic in nature, which means the material properties in orthogonal direction differ

[MSO15]. This section gives overview of the stator material model developed for the drive unit. Initially a small cube model is built with standard material properties. After that, the model is simulated to obtain the stiffness matrix from FE software package. These values are fed to the main stator modal analysis. Later, the values of simulations can be compared with that of the experiment for different Eigen forms. Finally, the C-elastic matrix is modified according to the comparisons and transferred to the cube model [HPC12] (check figure 4.15).

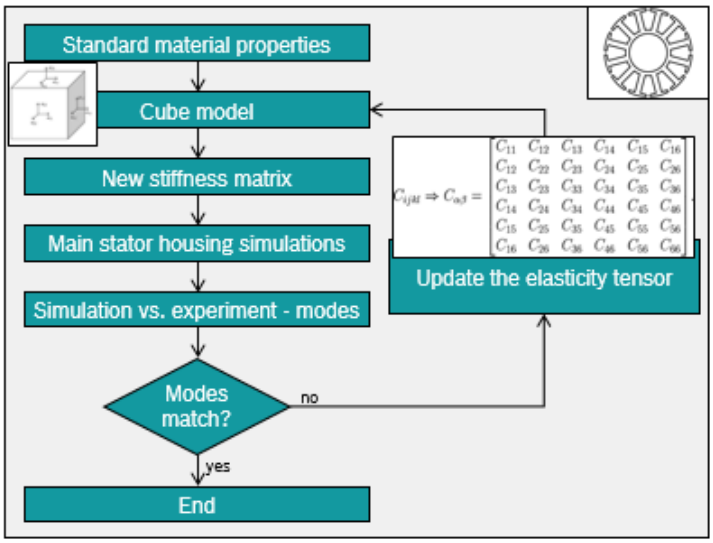

Figure 4.15: Flow for finding the correct material properties of the stator

Influences of dampers

This section describes the impact of damping elements on the surface velocities of the exterior housings. Generally, the vibrations generated inside the drivetrain are transferred to outer housing along the bearings and shafts. Introduction of dampings along the transfer path of the vibrations could damp out the amplitudes of the troublesome frequencies thereby providing a pleasant ride for the customer [TL16]. Figure 4.16 shows a schematic view of addition of dampings between the inner and outer housing of the power unit, followed by a graph depicting the reduction in amplitudes of displacements for the new model (possessing the dampers).

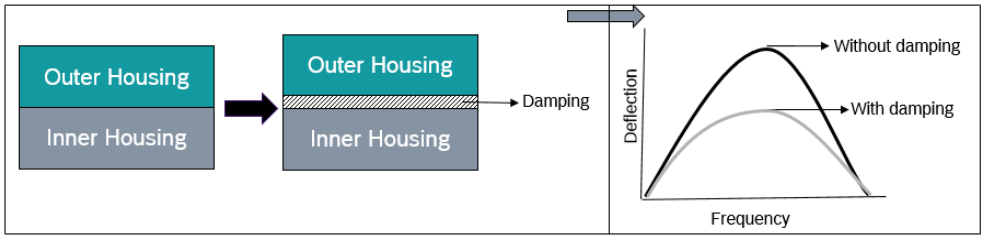

Figure 4.16: Influence of dampers on housing structures

Contact analysis among the gears

Contact formulation is classified as a boundary nonlinearity, in contrast to both material nonlinearity, which develops from nonlinear constitutive relations, and geometric nonlinearity, which appears for large deformation models. The behavior of contact would later impact the dynamic characteristics of the drivetrain. Figure 4.17 shows a line sketch of contact profile acting on a gear surface. The term σ_H indicates the Hertzian contact pressure profile. The other terms are already introduced in section 4.4.2.1.

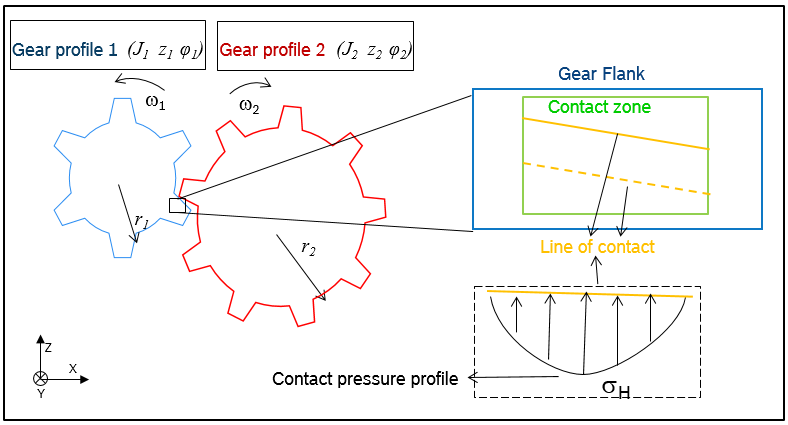

Figure 4.17: Simplified view of contact forces profile at the gear mesh

The contact nonlinearity can majorly be of two forms. Firstly, during the process of contact between two individual bodies, the plot of contact force vs displacement is zero initially (when the bodies are not connected) and increases vertically after the bodies come in contact. In this scenario, a functional relationship is not available as there is no one-on-one relationship between contact force and displacement. For e.g., in the tangential direction of contact with friction, where two bodies are stuck together until the tangential force reaches a threshold, after that a continuous sliding occurs without further increase in tangential force. This sudden change in contact slip and force makes it highly nonlinear. Secondly, in order to be a well-posed problem, either of displacement or force, but not both, should be given for every material point. Then, the FE equation solves for unknown information with given data. In the case of displacement boundary, i.e., if displacement is given, reaction force should be calculated. Similarly, for the traction boundary, displacement is calculated. Note that these two boundaries are clearly identified in the problem definition stage. Whereas, in the case of contact, however, both displacement and contact force are unknown. The user can only identify a candidate of contact boundary before solving the problem. Therefore, the FE procedure must be able to find whether a material point in the boundary of a body is in contact with the other body, and if it is in contact, the corresponding contact force must be calculated. Since the contact force at a material point can affect the deformation of neighboring points, this process needs to be repeated until finding right states for all points that are possible in contact. Because of this procedural nature, contact nonlinearity is often addressed using algorithms. The penetration approach is used not only to model contact among the gears but also to comprehend contact among the other drivetrain structures. Contact setups also play a crucial role in estimating wear among the drivetrains. Few of the contact equations represented in the section 4.5.2 , deal with analyzing the abrasion mechanisms. More detailed formulations and partial differential equations of the various other contact setups can be found in [Wri07, Kim15].

4.4.2.3 Harmonics of Drive Unit

A complete simulation of the drivetrain comprises studying the vibrations at housing and cover as well. The forces due to gear mesh errors and eccentricities of the shafts generate structure borne emissions at the gears and shafts. Furthermore, the vibrations are transferred to the housing surfaces through bearings and other middle components. This further leads to fluid pressure fluctuations around the structure thereby creating air borne noises. This section illustrates a state space model and housing submodel constructed to analyze the surface velocities of the exterior surfaces of the drivetrain assemblies.

Flex-body Model

In order to build a physical model associated with the mechanics of drivetrain, firstly a modal analysis of individual and complete assembly must be performed. The Eigen modes and frequencies obtained are then feed to the system model. Along with Eigen forms, the values of modal damping obtained from the experiments serve as basis for creation of the state-space model. Later, the excitations generated at bearings due to vibrations of the gear model are applied as forces.

Starting from the excitations at the gears, the vibrations are transmitted to the housings through the shafts, bearings and other components. Other way round, bending of the housing surfaces represents a time dependent boundary condition for bearing position. Consequently, transmission components and housing must be coupled in both directions together (DD3 in figure 4.18). Furthermore, the housing structure has natural frequencies, which gets excited due to this translational forces. In order to map the physical mechanisms of the housing structure, taking into account the system model requirements, the modal model is developed. In the following, the basic idea of modal decoupling and the generic integration into a physical network is described. A detailed view of the procedure is exemplified in [Hat00, Cor15, VA18] using simple system models.

The governing equation of motion for the housing structure can be described in the form of a 2nd order differential equation system represented in equation 4.8. The terms $\mathbf{M}$, $\mathbf{D}$, $\mathbf{K}$, $\mathbf{q}$ and $\mathbf{F}$ represent mass matrix, damping matrix, stiffness matrix, state space vector and force vector respectively.

$$\mathbf{M}\ddot{\mathbf{q}} + \mathbf{D}\dot{\mathbf{q}} + \mathbf{K}\mathbf{q} = \mathbf{F} \tag{4.8}$$

A state space representation is a simple mathematical model of a physical system as a set of input, output and state variables related by first-order differential equations. State space refers to the space whose axes are the state variables. The state of the system can be represented as a vector within that space. Equation 4.8 further be represented in the state space form as shown in equation 4.9.

$$\begin{aligned} \mathbf{x} &= \begin{bmatrix} \mathbf{q} \\ \dot{\mathbf{q}} \end{bmatrix} \\ \dot{\mathbf{x}} &= \begin{bmatrix} \mathbf{0} & \mathbf{I} \\ -\mathbf{M}^{-1}\mathbf{K} & -\mathbf{M}^{-1}\mathbf{D} \end{bmatrix} \mathbf{x} + \begin{bmatrix} \mathbf{0} \\ \mathbf{M}^{-1}\mathbf{F} \end{bmatrix} \end{aligned} \tag{4.9}$$

The problem with numerically solving the system of equations (4.9) is that all states have to be calculated for all numerical time steps, since they are coupled differential equations. For many degrees of freedom, this inevitably leads to long simulation times. In order to decouple the states of the differential equation system, the model is represented using modal matrix $\mathbf{\Phi}_m$. Equations 4.10, 4.11 and 4.12 represent the normalized modal mass matrix, modal stiffness matrix and modal damping matrix respectively. The terms ω and ζ indicate the Eigen frequencies and damping ratios respectively.

$$\mathbf{M}_m = \mathbf{\Phi}_m^T \mathbf{M} \mathbf{\Phi}_m \stackrel{!}{=} \begin{bmatrix} 1 & 0 & \dots & 0 \\ 0 & 1 & 0 & 0 \\ \vdots & 0 & \ddots & \vdots \\ 0 & \dots & 0 & 1 \end{bmatrix}, \tag{4.10}$$

$$\mathbf{K}_m = \mathbf{\Phi}_m^T \mathbf{K} \mathbf{\Phi}_m \stackrel{!}{=} \begin{bmatrix} \omega_1^2 & 0 & \dots & 0 \\ 0 & \omega_2^2 & 0 & 0 \\ \vdots & 0 & \ddots & \vdots \\ 0 & \dots & 0 & \omega_n^2 \end{bmatrix}, \tag{4.11}$$

$$\mathbf{D}_m = \mathbf{\Phi}_m^T \mathbf{D} \mathbf{\Phi}_m \stackrel{!}{=} \begin{bmatrix} \zeta_1\omega_1 & 0 & \dots & 0 \\ 0 & \zeta_2\omega_2 & 0 & 0 \\ \vdots & 0 & \ddots & \vdots \\ 0 & \dots & 0 & \zeta_n\omega_n \end{bmatrix}. \tag{4.12}$$

Since all these matrices only have entries on their diagonals, the state vector $\mathbf{x}$ can be decoupled from equation 4.9 and the system of differential equations is simplified as shown in equation 4.13.

$$\dot{\mathbf{x}}_m = \begin{bmatrix} \mathbf{0} & \mathbf{I} \\ -\mathbf{K}_m & -\mathbf{D}_m \end{bmatrix} \mathbf{x}_m + \begin{bmatrix} \mathbf{0} \\ \mathbf{F} \end{bmatrix} \tag{4.13}$$

For the connection of the model, there are different methods available. The technique described by Chudnovsky in paper [VA18] (modal superposition in state-space form) is mainly applied because of its direct analogy with respect to the system model equations. The integration of the model is visualized in figure 4.18. In addition to the state space model, the gear housing and dual directional coupling between transmission components and the housing structures are shown. The single direction coupling SD-2 represents the housing vibration, which in turn represents the entrance to the noise emission model. Similarly, DD-3 represents dual direction link used for transfer of the bearing forces obtained from the MBD system into the modal model for harmonic analysis of flexible housing.

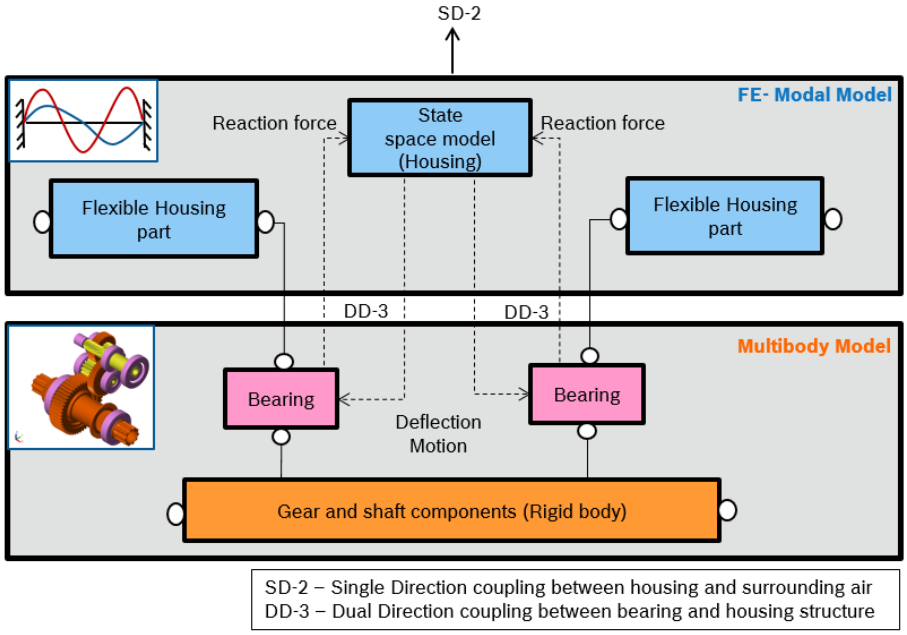

Figure 4.18: Coupling between the multibody model and modal model for the representation of housing vibrations [ZT17]. Detailed information of the coupling directions are discussed in section 4.7.

A system model can be represented as linear time invariant (LTI) using the state space model. Figure 4.18 shows state space flex-body system embedded into the simulation package. Initially, the bodies are modeled as rigid bodies with aid of the body blocks and associated Coordinate Systems (CS). A body is connected to another body using a joint that includes the primitives associated with the deflections specified in the modal model. The modal results are incorporated into a physical model by superimposing the flexible-body deflection on the rigid-body motion. These primitives are motion-triggered by a black box subsystem. The output of this system is the deflection obtained using the FE data. The input to the black box is the load acting on

body. This load can either be from a connected body or an applied external load. Detailed information about the technique can be found in [Hat00, Cor15, VA18].

The output from the state-space model steers the velocities of its adjacent bodies relative to the unflexed (rigid-body base) position of the flexible body. Therefore, joints with the appropriate DOF are inserted at the corresponding coordinates of the rigid body base. These joints are later driven by the results of state-space model. Furthermore, the joints are coupled to other side of the flexible housing body blocks.

Note that superimposing the Eigen modes on to rigid body motions is based on basis of small strain theory [ZT17].

Submodel of Housing

One of the problem with flex-body is, that it just considers only few sets of critical nodal positions to capture the modal deformations and ignore the others, which could lead to incomplete representation of the structures. Hence, if a detailed level of analysis is needed, housing must be further analyzed in the FE. The excitations available at bearing surfaces (section 4.4.2.2, 4.4.2.1) can be brought on to the housing submodel (leaving out bearings and gear shafts). Submodeling technique would allow the engineer to execute faster simulations and reduce the computational costs [Cor16]. With the aid of this method, the bearing forces of different variants can be calculated explicitly and can be applied on various housing models, instead of simulating the gear and housing modules together. The bearing forces from figure 4.14 are converted to frequency domain and used in the harmonic analysis of the housings.

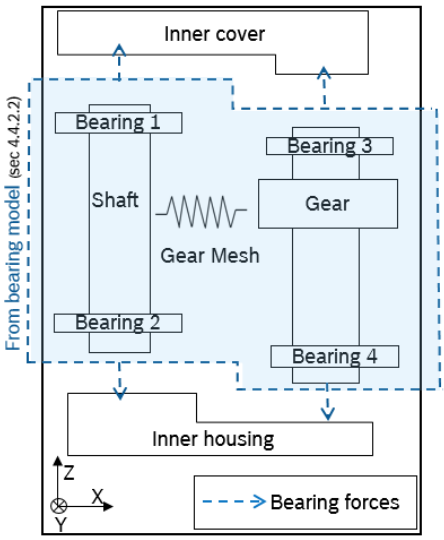

Figure 4.19: Housing, shaft and bearing structures along with the axial forces

Figure 4.19 shows line sketch of a housing surface and the direction of axial bearing forces acting on to its interior surfaces. Majorly, steady state dynamics solution method is used in analyzing the vibrations at housing and covers. When a damped structure, which is initially at rest, is excited with harmonic load, it has a transient response at first and then fades out quickly. Furthermore, the structure attains steady state, which is characterized by harmonic response with the same frequency as that of the applied load. The analysis is performed across a frequency sweep by applying the loading at series of different frequencies and logging its response. This procedure provides solutions to the linear equations of motion when the loading is harmonic.

4.4.2.4 Sound Emission

The structure borne emissions at the exterior surfaces create pressure fluctuations of the air around it. These disturbances result in noises and understanding them is also necessary to improve the performance of the DU. The idea here is to build an acoustic finite element mesh in the near field and use infinite, ERP techniques to estimate for far field distances. Detailed explanations about the link among the various structural FE models, state space models, acoustic finite mesh and Radiated Sound Power are further described in section 4.4.3.

Figure 4.20 shows coupling between the vibrational and acoustic domain. The acoustic mesh is kinematically coupled to housing [Abi19]. The acoustic particle velocity at fluid structure interface is assumed to be equal to the structural velocity of the component. It can be considered as decent assumption because the structural particles cannot penetrate into the fluid particles nor it can lead to backward opening between the structure and the fluid.

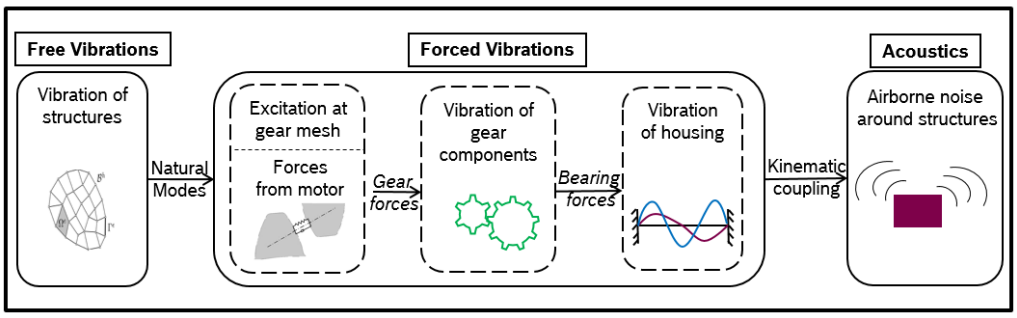

Figure 4.20: Coupling between vibration and acoustic domain

Acoustic Finite Elements

Acoustic elements model the propagation of acoustic waves and are active only in dynamic analysis procedures. The acoustic medium can be considered similar to linear elastic medium with no shearing rotation. This modeling approach considers few assumptions in order to simulate the acoustic models. Firstly, the fluid is considered to be Newtonian, i.e., the viscous stresses arising from the flow are linearly related to the local strain rate. Secondly, the flow is considered to be irrotational, i.e. vorticity would be zero. Thirdly, the bulk and shear viscosity can be modeled only to the extent that they attenuate the waves. Fourthly, the effect of body forces on the fluid medium is considered negligible. Finally, for acoustic waves the amplitude of the disturbance of field quantity is considered small. In human tolerable sound, the fractional changes are in the order of 10^{-6}, therefore this assumption of small changes can be justified. Further detailed explanation can be found in [Kin82]. Restriction to dilatation motions allows a single Degree of Freedom (DOF), to describe the acoustic pressure of the wave at given point in space. Within this domain, considering these assumptions, the pressure (p) can be linearly related to the volumetric strain (ϵ_V). Check equation 4.14, K_b is bulk modulus of the fluid.

$$\begin{aligned} p &= K_b \cdot \epsilon_V \\ \epsilon_V &= \epsilon_{11} + \epsilon_{22} + \epsilon_{33} \end{aligned} \tag{4.14}$$

Figure 4.21 represents schematic view of acoustic mesh developed around the drivetrain structure. The terms $\mathbf{n}_s$ and $\mathbf{n}_a$ indicate the normal vectors of the structural and acoustic mesh, respectively. The length of the acoustic elements should be able to capture maximum frequency of interest (freq_{max}). Higher frequency response requires smaller elements. In equation 4.15, c, n, h correspond to speed of sound, number of elements required to capture the wave (generally 5-8) and wavelength respectively.

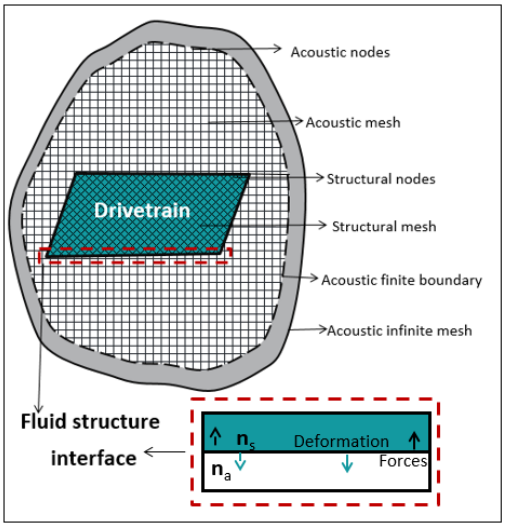

Figure 4.21: Structural, acoustic finite and infinite element model

$$freq_{max} = \frac{c}{n \cdot h} \tag{4.15}$$

Differential formulations of the surrounding air

Equation 4.16 represents the governing equation for small motions of a compressible fluid with velocity and acceleration dependent resistance [Pie89]. Volumetric drag Γ is used for representation of the attenuation present in the acoustic waves. It is used for defining the flow resistance present around the drivetrain. The terms p, $\mathbf{x}$, $\mathbf{v}_f$, ρ_f and $\mathbf{a}_f$ represent acoustic pressure (excess of ambient), Cartesian coordinates vector, particle velocity vector of air, density of air and acceleration vector of air respectively.

$$\frac{\partial p}{\partial \mathbf{x}} + \Gamma \mathbf{v}_f + \rho_f \mathbf{a}_f = 0 \tag{4.16}$$

By default, the energy is transferred without any loss between the structure and the acoustic medium. Impedances are used to define loss between air and housing structures. The acoustic velocities of nodes can be altered by introducing impedances between the surfaces. Impedance (Z_n) at the drivetrain and air interface is modeled with equation 4.17. It gives an algebraic relation between the steady state normal velocity and the pressure at the interface. The terms $\mathbf{v}_s$,$\mathbf{v}_f$ and $\mathbf{n}$ corresponds to structural velocity, acoustic velocity and normal vector at the interface respectively. It can be understood from the equation that the relation between structural motion and acoustic pressure need not be continuous. Note that, the impedance properties are defined based on absorbing characteristics of the housing structures.

$$Z_n = \frac{p}{(\mathbf{v}_s - \mathbf{v}_f).\mathbf{n}} \tag{4.17}$$

It also aids in defining the acoustic energy that dissipates from the infinite mesh. Overall, it helps in controlling the transmission of sound through the system.

Equation 4.18 represents the formula used for calculation of the acoustic pressure derived from linear perturbation theory. The terms ρ_0, c_0 and v_0 indicate the reference density, speed of sound and velocity of the base state respectively. This equation assumes no reflection of the acoustic waves at the boundaries of the finite and infinite mesh and at the same time no dissipation. Hence, the waves move to the right with no loss at constant amplitude and the pressure is in phase with specified velocity.

$$\underline{p}(\mathbf{x}) = \rho_0 \cdot c_0 \cdot v_0 . e^{-i\frac{\omega}{c_0}\mathbf{x}} \tag{4.18}$$

Furthermore, equation 4.19 is used to include the dissipation effects for the pressure equation. The term $\underline{Z}$ indicates the complex impedance used for calculation of the acoustic fluctuations around the housing assembly.

$$\underline{p}(\mathbf{x}) = v_0 \cdot \underline{Z} \cdot e^{\frac{\omega}{K_f}(b-ia)\mathbf{x}} \qquad where\ \underline{Z} = a + ib \tag{4.19}$$

Relation between structure and acoustic finite mesh

Unlike fatigue, which is a local phenomenon, acoustics is a global phenomenon where all the structures may contribute to sound radiation. Housing air coupling occurs at the interface where the acoustic medium adjoins the structure. This is called as the fluid structure interface (check figure 4.20). Here, the nodes at the exterior surfaces of the housing are tied to the inner surface of the finite acoustic mesh. The surface normal component of the housing structure velocity is used as the driving factor for calculating acoustic fluctuations around the drivetrain. The acceleration field in structure creates the natural forcing term at the acoustic boundary. Hence, the velocities at structural surfaces are transferred to the pressures at acoustic elements. This condition is also termed as kinematic coupling condition at the housing structure and surrounding air interface.

This coupling between housing structure and air medium is modeled by conservation of linear momentum. Equation 4.20 shows the set of general formulations of the housing and surrounding air at its interface. The coefficients in coupled stiffness matrix K_{fs} and coupled mass matrix M_{fs} are frequency independent but in contrast with an uncoupled structural or uncoupled acoustic finite element model, these coupled matrices are no longer symmetric. This is due to the fact that the force loading of the fluid on the structure is proportional to the pressure, resulting in a cross-coupling matrix K_{fs} in the coupled stiffness matrix. Similarly, the force loading of the structure on the fluid is proportional to the acceleration, resulting in a cross-coupling matrix M_{fs} in the coupled mass matrix. The terms u, M, M_f, K, K_f, F_s and F_a indicate the displacement of housing, mass of the housing, mass of the fluid/ air, stiffness of the structure, stiffness matrix of fluid, force applied by the structure and force exerted by the air respectively. Detailed information about the coupling finite element models can be found in paper [DV05].

$$\begin{bmatrix} M & 0 \\ M_{fs} & M_f \end{bmatrix} \begin{bmatrix} \ddot{u} \\ \ddot{p} \end{bmatrix} + \begin{bmatrix} K & K_{fs} \\ 0 & K_f \end{bmatrix} \begin{bmatrix} u \\ p \end{bmatrix} = \begin{bmatrix} F_s \\ F_a \end{bmatrix} \tag{4.20}$$

Relation between acoustic finite and infinite mesh

Acoustic infinite mesh is used for models with larger domains. Detailed properties of these elements can be found in [Cor18a]. For instance, simulating acoustic fluctuations with acoustic finite elements at distance 1000 mm away from the drivetrain could consume lots of computational effort. The acoustic measuring point for the work is defined at a farther distance from the housing structure, i.e., the drivetrain structure is small compared to the size of surrounding acoustic domain. In such cases infinite elements can be used to predict the noises at the desired distance from the housing. The acoustic infinite elements are defined on the terminating surface of acoustic finite mesh (check figure 4.21). By means of these elements, the exterior domain is interpreted as wave bearing domain identical to that used on finite element side.

The formula in equation 4.21 corresponds to the acoustic complex pressure (p) for single element set up calculated at a distance r. The values p_0, r_0 and k represent the pressure at reference, radius at reference and wave number corresponding to a frequency. Note that, the infinite elements can have linear behavior only. The values at the nodes of this single element is considered as the reference point values.

$$\underline{p}_r = p_0 \cdot \frac{\mathbf{r}_0}{\mathbf{r}} \cdot k \cdot e^{(ik(\mathbf{r}_0 - \mathbf{r}))} \tag{4.21}$$

Transmission of acoustic disturbances

Figure 4.22 describes the behavior of structural and acoustic velocities of the drivetrain structures and the surrounding fluids. Initially, the structural velocities ($\mathbf{v}_{s1}$) are generated at gears and shafts due to the excitations present in the model. They are transmitted to the housing structures along the bearings and other components present in the drivetrains. This creates vibrations $\mathbf{v}_{s2}$ at the outer surfaces of drivetrain. The term FSI indicates the fluid structure interface. It acts as an interface for transferring the structural velocities to acoustic disturbances. The terms $\mathbf{p}_1$ and $\mathbf{v}_{f1}$ represent the pressure and velocity of the finite mesh developed. These acoustic velocities are transferred further to the infinite mesh with system state of pressure $\mathbf{p}_2$ and velocity $\mathbf{v}_{f2}$, which is later used to calculate the acoustic values at larger distances. Relevance of coupling direction SD-2 is further discussed in section 4.4.3.

Note that, the reflection boundary conditions at all interfaces are neglected in this work. When acoustic behavior is numerically simulated, it has to be represented on a truncated, finite domain or in our case, using finite and infinite meshes. So, in addition to solving the governing equations inside the domain, appropriate boundary conditions are also needed. The nonreflecting boundary means that outgoing waves should be allowed to exit the domain without being reflected back in a nonphysical manner and thereby corrupting the solution. This can be considered as a valid assumption as the drive unit is used in an open atmosphere, where there is no real reflection of the acoustic waves back on to the drivetrain housings.

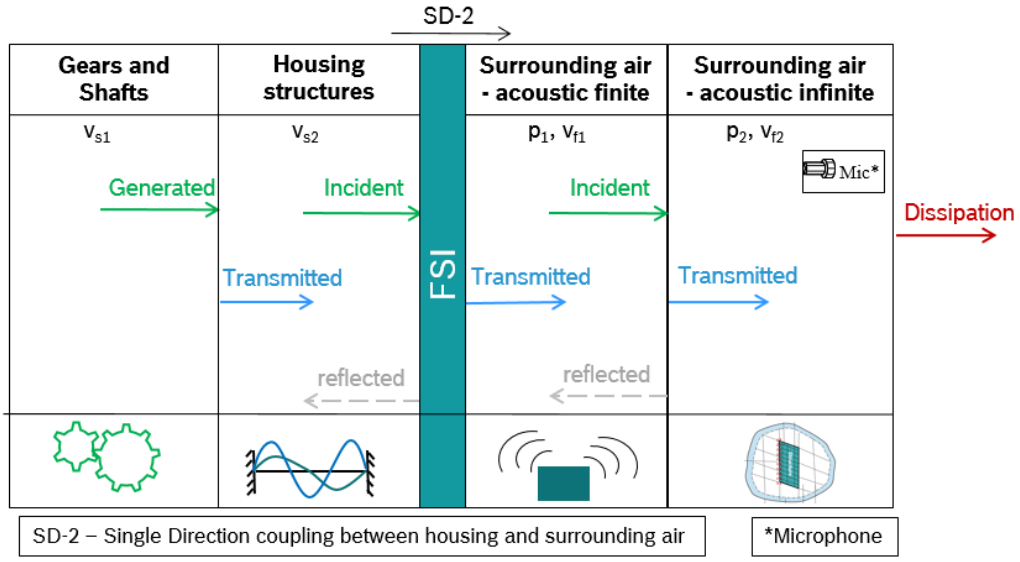

Figure 4.22: Transmission of structural and acoustic velocities in the simulation model. Detailed information of the coupling directions are discussed in section 4.7.

Conclusively, the flowchart in figure 4.23 illustrates the complete steps for realizing the acoustic pressure around the drivetrains using finite and infinite meshes. The CAD models developed are transferred to FE modeling package. Once the model is developed using appropriate element types and material information, a modal analysis (check section 4.4.1) is performed to obtain natural modes of the structures. Further, the drivetrain model is applied for the frequency load and boundary accordingly. The harmonic analysis is simulated via the modal superposition technique. Later the structural velocities are coupled with acoustic velocities at the housing and air interface. Once the acoustic conditions are obtained at the inner layers of the finite mesh, its behavior is altered with the aid of material impedance, volumetric drag coefficient, non reflecting boundary conditions etc. Lastly, using the acoustic initial conditions from the structure and acoustic model definitions, the acoustic pressures are predicted at desired distances from the drivetrain structures.

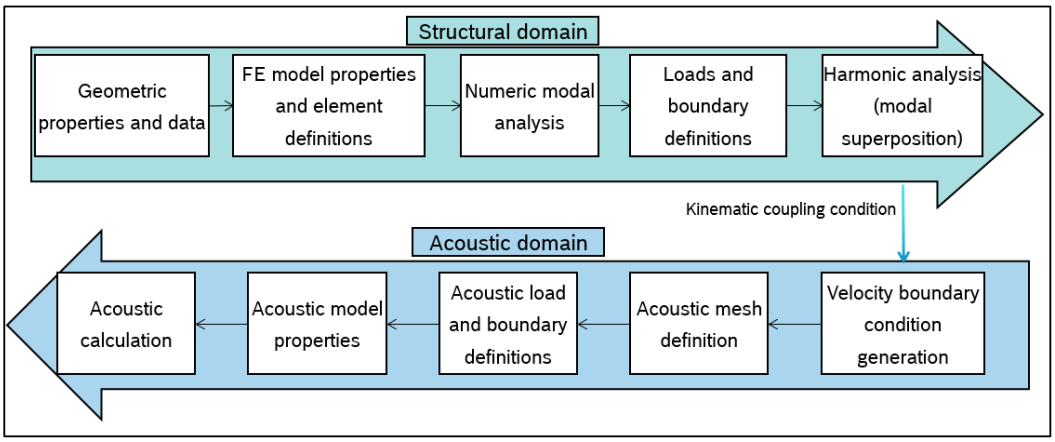

Figure 4.23: Flowchart for acoustic finite element simulation

Radiated Sound Power

In order to predict the pressures for the state-space system model, radiated sound power formulations are used. Equations 4.22 and 4.23 correspond to the acoustic power (P_Q) and complex acoustic intensity ($\underline{\mathbf{I}}$) calculated using Radiated Sound Power (RSP) [Kin82]. Here the terms A, p, v, n correspond to area, complex pressure and complex acoustic velocity and surface normal of vibrating structure.

$$P_Q = \oint_A \underline{\mathbf{I}} \cdot \mathbf{n} \, dA \tag{4.22}$$

$$\underline{\mathbf{I}} = \underline{p}.\underline{\mathbf{v}} \tag{4.23}$$

RSP model is aimed at calculating the radiated sound power as an integral quantity. Calculation of complex pressure is difficult without the aid of high end computational software. Nowadays, there are few alternate techniques for this problem. One method is with Equivalent Radiated Power (ERP) formulations and is described below.

Equivalent Radiated Power

This method is built on an assumption that the acoustic velocity and acoustic pressure are in phase with each other (far field condition). Hence, the acoustic pressure can be approximated as shown in equation 4.24. Here the terms p, Z_0, v represent the acoustic pressure, field impedance, acoustic velocity respectively. Equation 4.25 depicts formula used for calculation of the ERP power (P_{ERP}). The terms LF_{ERP}, c, ρ, A, v and n correspond to loss factor, speed of sound, density of the fluid, surface area, velocity of the structure and number of critical areas respectively.

$$p \approx Z_0.v \tag{4.24}$$

$$P_{ERP} = LF_{ERP} \cdot \left(\frac{1}{2}\, c \cdot \rho\right) \cdot \sum_{i=1}^{n} A_i \cdot v_i^2 \tag{4.25}$$

For the calculations LF_{ERP} is considered as 1. This is a conservative approach, since it calculates an upper limit of P_{ERP}. An advantage of this procedure is that even in an early development phase, different product variants can be evaluated and compared with regard to the noise emission. It has advantages like modular implementation, extremely fast simulation times and the robustness against model and parameter uncertainties when calculating acoustic characteristics. This fulfills important requirements for system and gearbox modeling mentioned in section 4.2.

4.4.3 Overview of System Flow

So far, separate methods for the modeling and simulation of vibro-acoustic mechanisms in drivetrains as well as the functional relationship among the individual model parts have been described. Figure 4.24 describes generic process for flow of the data to realize the attributes discussed in section 4.2. Basically it shows two flows, one concentrating on the approach of multi-domain (Flow-1 in figure 4.24), the other guiding researchers towards use of single simulation domain (Flow-2 in figure 4.24). Each of them have there own advantages and disadvantages. They are discussed in detail in the next paragraphs (figures 4.25 and 4.27). A respective flow is chosen based on critical aspects like accuracy, speed, complexities in design etc. Furthermore, within the diagram, reference to corresponding section of the respective model component is also shown in paper [KDH20b].

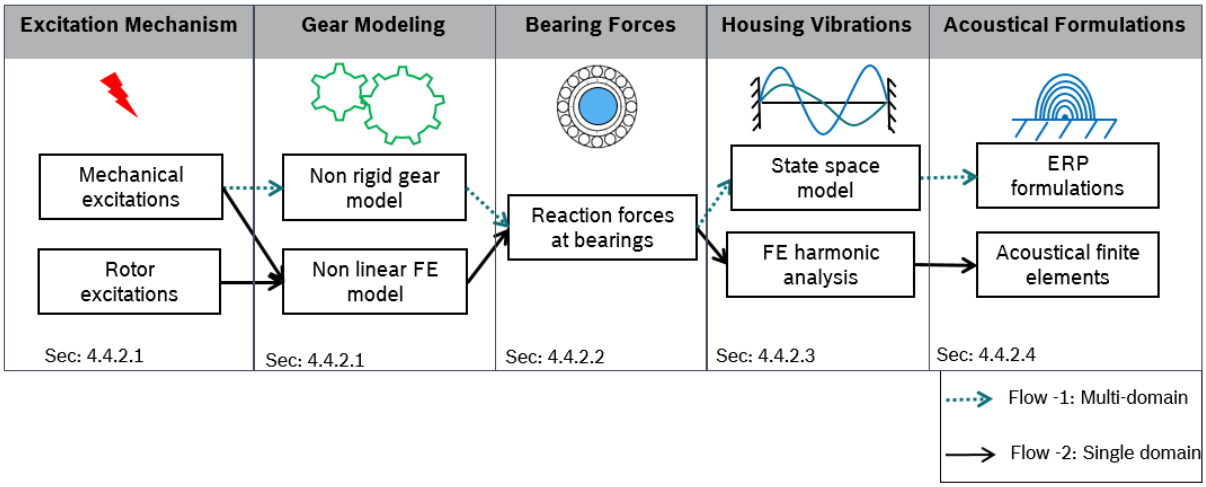

Figure 4.24: System model for realizing the NVH attributes

Multi-domain

Figure 4.25 shows system model built for analyzing the vibro-acoustics using different numerical methodologies. Other general domains include the rest mechanisms being part of the heterogeneous system model except they belong to either to vibration or acoustic modules. The other possible mechanisms and components that could influence NVH of the drivetrains are electric motor, user interaction, thermal convection, environmental condition, and control algorithm. It should be considered that few excitations for mechanical vibration can originate from other domains, for instance, torque ripples generated from the electric machine can influence the vibrations. In few scenarios, coupling in other direction could also be possible. For instance, rotational vibrations impact electric motor current dynamics and vice-versa [DDH15]. Thus, two directional interaction between other general and vibration domain must be considered. Nevertheless, once the system model features physical network characteristics, the vibrations can be modeled independent of the other mechanisms. Furthermore, few of the mechanisms also generate sound around the electromechanical drive, for instance, rattling of components, tire road noise, or aerodynamic flow noise. Nevertheless, as the other general domains offer a huge amount of diversities and complexities, this link will not be further discussed. Below is the list of few advantages offered by multi-domain:

- Faster simulation times due to the presence of fewer Degrees of Freedom in the model (lesser complex than FE).
- Can be coupled and extended for other domains like thermal, electrical, mechatronics, control systems etc., which enable the physical modeling of complete vehicle.
- Object Oriented Programming in Matlab can be used to create a tool on the outer surface

of the system model to make it possible for the non-expert users to utilize the simulations.

- Connectors help in for creating connections between submodels . It is based on variables, which define proper relations and influences between movements, flows, temperatures, etc. By joining connectors the submodels are connected. During processing the tool generates appropriate equations from connect statements and connector definitions.
- Best suites in initial phases of the design, when there is no deep insight on the modeling and simulation. For e.g., the influence of different helical angles on the vibrations of gear models does not require the complete geometry of the gears.
- Perfect modeling technique for domain specialists, as it provides common software platform (like Simscape) in order to analyze vibrations of power unit.

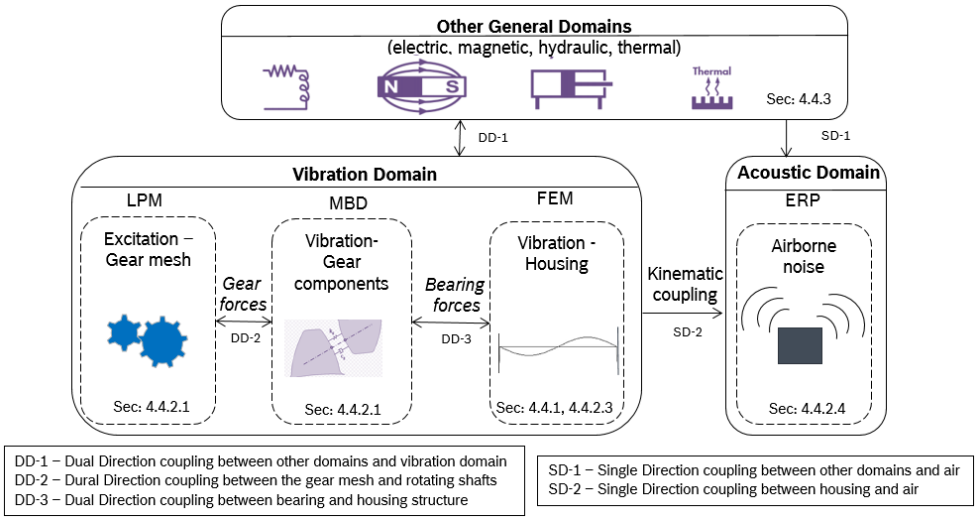

Figure 4.25: Heterogeneous system model of DU (for vibro-acoustics). Detailed information of the coupling directions are discussed in section 4.7.

Additionally, within flow-1 from figure 4.24, dual directional coupling among the simulation domains is achieved (as shown in figure 4.26). The translational forces of the transmission components are transmitted through the shafts to bearings which eventually vibrate the housing. Conversely, the deflections of housing components represent a time-variant boundary condition of the bearing position. Consequently, transmission components and housing must be bidirectionally coupled together. Furthermore, the housing structure has a spectrum of natural frequencies which can be stimulated by the translational forces.

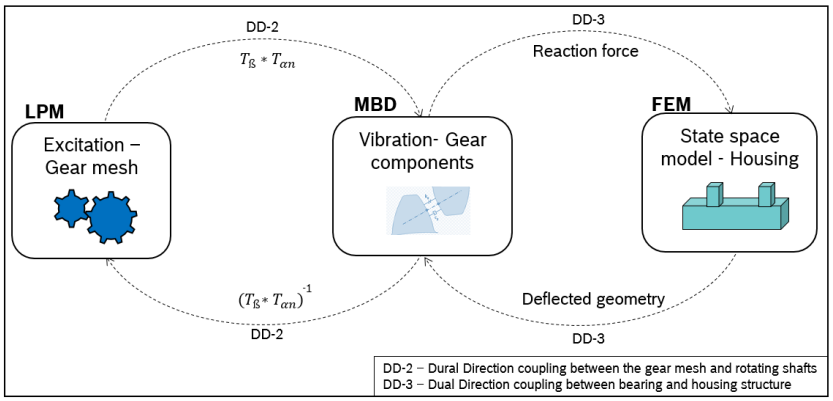

Figure 4.26: Dual direction coupling among LPM, MBD and FEM domains. Detailed information of the coupling directions are discussed in section 4.7.

Single domain

Even though flow-1 possesses advantages as stated above, it has backlogs like accuracy. Additionally, for physical mechanisms such as wear, it can be complicated to couple them into the multi-domain approach, because factors like position and orientation of abrasion are needed more precisely to analyze the wear. But multi-domain simulation approach can render the results in a generic system model frame of reference rather than pinpoint the area of trouble.

On the other hand, flow-2 shown in figure 4.24 mainly uses one simulation domain. Here FEM lies in the heart of simulation. All the values are passed to finally solve in FE (check figure 4.27). Each submodule in figure 4.27 is solved using respective analysis methods, for e.g., natural frequencies are obtained by a simple modal analysis step and similarly the housing vibrations are solved using the steady state dynamic calculations. It mainly helps in coupling wear (sections 4.5 and 4.6) with the vibrations. It can be difficult to link the wear module to the multi-domain approach as it depicts the solutions in a generalized domain compromising the accuracy and precision for time, which can be vital for understanding the abrasion influences in a better way. Below is the list of few advantages offered by FE domain:

- Detailed level of analysis like the stresses, deformations and stiffness at critical areas of drivetrain for different load profiles can be calculated.
- It is best suited for structural simulations. Wider range of analysis like transfer path vibrations, influence of acoustic impedances etc., can be studied more accurately.
- It additionally helps in optimizing the structures only at the necessary junctures (for e.g., where the deformations are large). Whereas the system model provides the results as a whole, which makes it difficult to get the root causes of the problem.
- FE package provides special assistance to connect the wear codes to its simulations. Later the wear solutions are coupled with vibrational domain to study their influences.
- It is helpful in later stages of design, when template models (alpha version) are made available for further analysis.

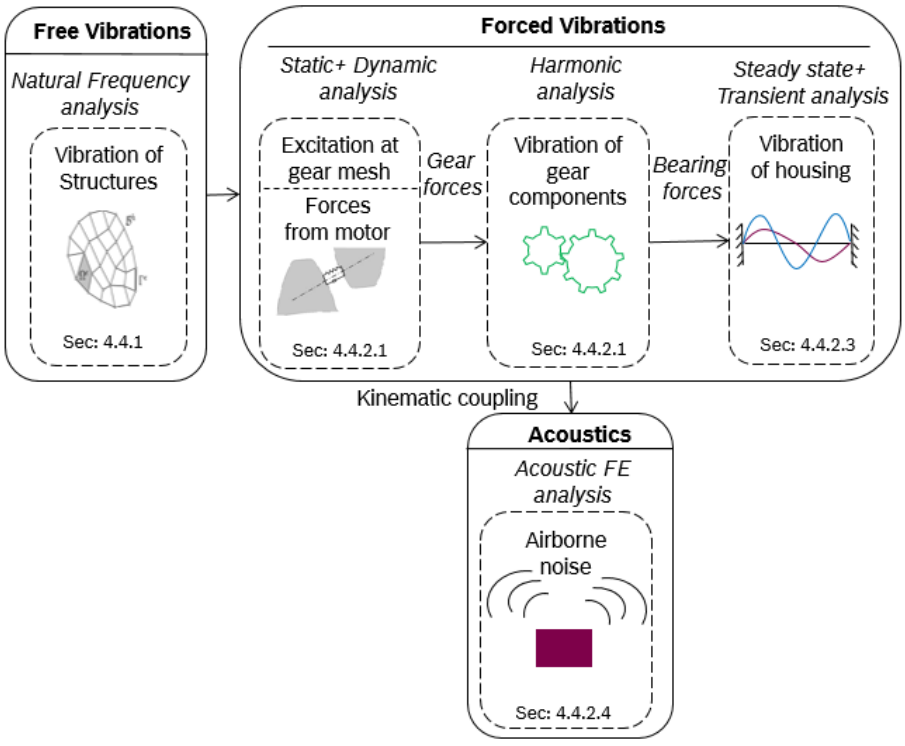

Figure 4.27: Coupling between vibration and acoustic domain

Finally, flow-1 (multi-domain) is chosen, when the engineer is just interested in the NVH characteristics as whole system point of view and for topics like gear design. Model requirements (from figure 4.3) like rapidity and simplicity are better for flow-1 compared to flow-2. It is useful especially in the early phases of the development to make a plausible layout.
On the contrary, flow-2 (single domain) can be utilized for detailed level of analysis like to understand the critical areas of stresses, check the transfer paths of the vibration etc., in the later stages of design (when a detailed level of results are needed). The flow-2 has precedence in model requirements parameters like reliability as it tries to improve the accuracy of solutions. Overall, in the life span of the design and development phase, firstly flow-1 must be executed, followed by flow-2 with main target of reducing the vibrations of the drivetrain.

4.5 Influences of Wear in Drivetrain

So far, the methods developed for vibro-acoustic modeling are described. However, the NVH of drivetrains is seldom influenced by many other factors and one of the major influencer is the wear among components. Wear is a complex process and understanding this phenomenon is vital for vibro-acoustics. The removal of material impacts behavior of the system and its components, which later influences the responses as well. This section aims in analyzing the intricacies involved in wear mechanisms, so that it could be curtailed in the design phase of the product life cycle.

There are countless analytical formulae and numerical techniques available in the literature for calculations of wear, but none of them can be applied across all systems [LA87, Bhu15]. Figure 4.28 shows the methods analyzed within the work for prediction of the wear.

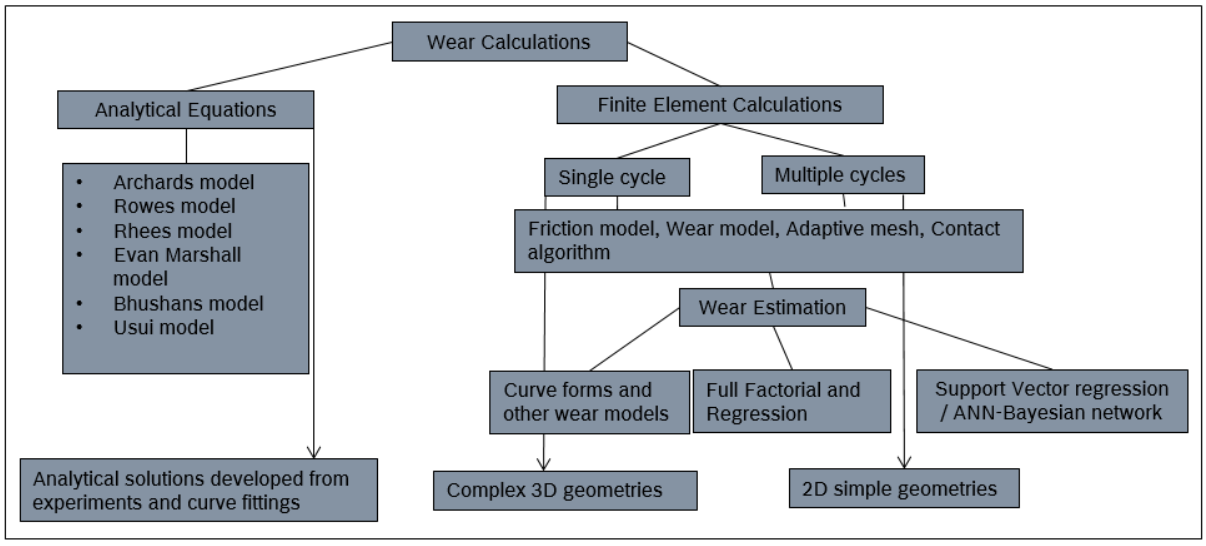

Figure 4.28: Data flow for numerical calculation of wear at the gear shafts

The factors impacting wear are mainly dependent on the system behavior. For instance, the influence of temperature is predominant at high sliding velocities, when heat is sufficiently generated. Some of the most important parameters affecting the wear are materials, gear contacts, lubrication, heat generation, electric currents etc. The influencing factors considered for the work are mainly mechanical and are depicted in figure 4.29.

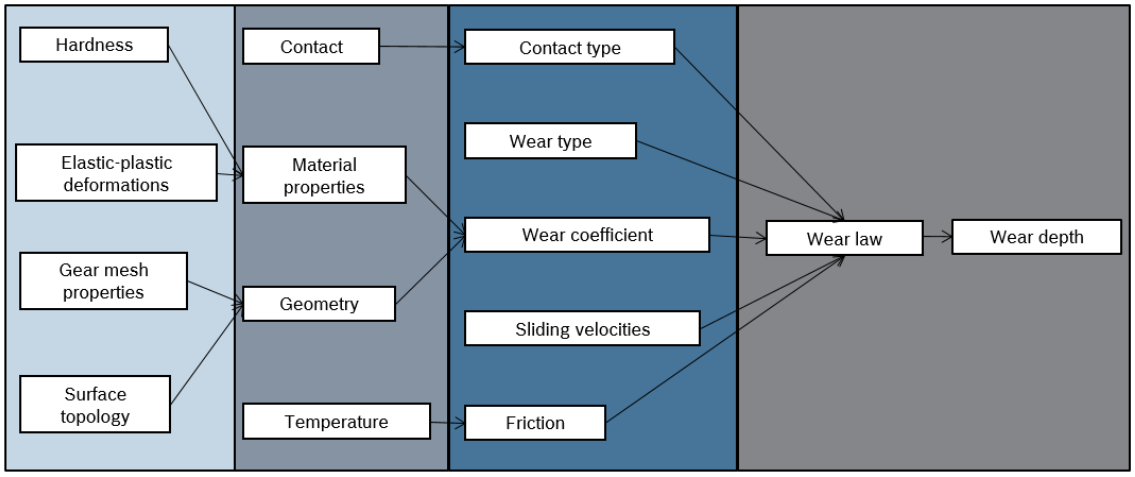

Figure 4.29: Model parameters considered for wear simulations

Figure 4.30 shows the different domains used for calculations of abrasion. It is mainly divided into UQ, FE and ML sections. The parameters defined by the means of UQ method serve as input for the FE template. Additionally, the wear subroutine developed is also connected to the FE. The responses of FE are later passed on to the machine learning algorithms for the wear predictions.

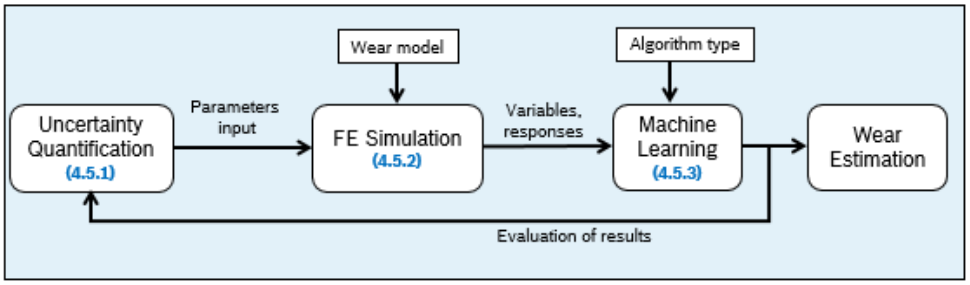

Figure 4.30: Overview of wear model calculations

4.5.1 Uncertainty Quantification Technique

The FE simulation of the complete model developed is computationally costly and consumes lots of time. The UQ approach helps in running the simulations in an optimized environment. Initially, parameters like material properties, tooth geometries, contact properties, etc., are defined using the beta and random distributions within the UQ method. Later, these values are passed on to the FE template and subroutines to run the simulations. This parameter study approach optimizes the simulation counts to realize all the complexities involved within the system. Methodologies from UQ like Non-Intrusive Spectral Projection (NISP), Latin Hypercube Sampling (LHS) and Adaptive Pseudo-spectral-Projection (APSP) are used for the reduction of uncertainties in the computations. It tries to build mathematical methods for representing uncertainties of random variables and to quantify their effect on the solution of the underlying physical problem [WKB16, Sul16].
The NISP technique tries to define ranges for all the parameters like material properties, contact properties etc., with the aid of beta and random distributions. The values from NISP model are transferred to the FE template to run the simulations. Later, FE results are passed back to the UQ for understanding the influence of parameters. Figure 4.31 shows the data flow across the APSP approach. The term DoS corresponds to Design of Simulations. The APSP starts with

a single design point (a nominal value for all parameters involved) (iteration 0). Afterwards, it performs a UQ analysis on the simulation results and estimates which parameters contribute most to the overall statistical fluctuations. In the next iteration, the parameters with bigger fluctuations are concentrated. Once the simulations are run for the iteration, the error estimators are updated. This scheme is repeated until a convergence criteria is achieved.

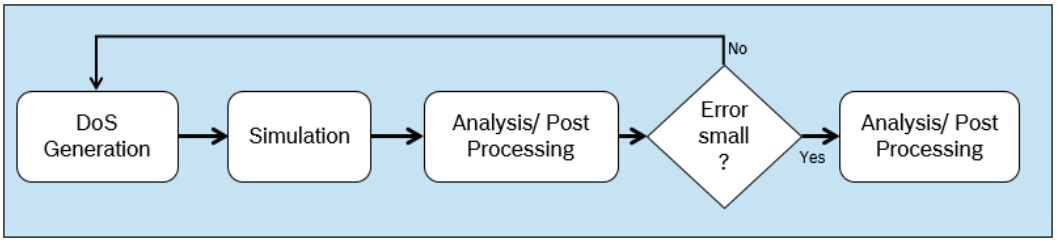

Figure 4.31: Data flow across APSP approach

4.5.2 FE Calculations for Wear

With regards to the FE calculations, initially, a convergence study to find out the correct element lengths is performed. FE analysis possesses a problem of increasing the stresses and reaction forces with decreasing element lengths. Hence, it is vital to find the element properties and dimensions such that the changes in them should not impact the results. Figure 4.32 shows an example of a convergence plot for decreasing element lengths vs parameter of interest. For our case, the target parameter is mostly contact force or von-Mises stresses or contact pressures depending on the problem. More about convergence criteria can be found in [Cor18b].

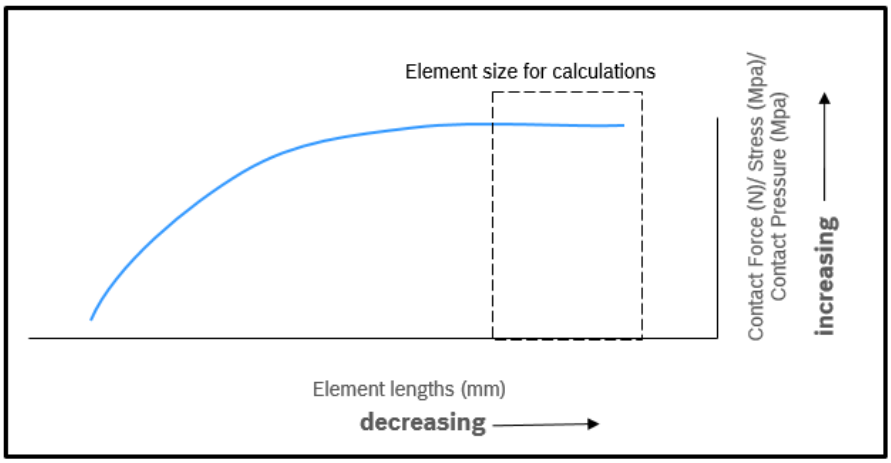

Figure 4.32: Convergence study for finding the correct element lengths

Figure 4.33 describes the link between softwares and transfer of the data among them. Initially, the FE model and wear subroutine are developed and made available in FE software and Fortran compilers (ifort and visual studio) respectively. After that, the model is validated for element qualities and other data checks, the subroutine is compiled and linked to the FE software. Once the simulation is triggered, the linked routine obtains the information like contact properties, K-factors, etc., necessary to calculate the wear and wear rate. These values are coupled back to the simulation software to displace the nodes (adaptive meshing) and represent the wear contour. Information about the adaptive meshing and the flow within the subroutine can be found in figure 4.36.

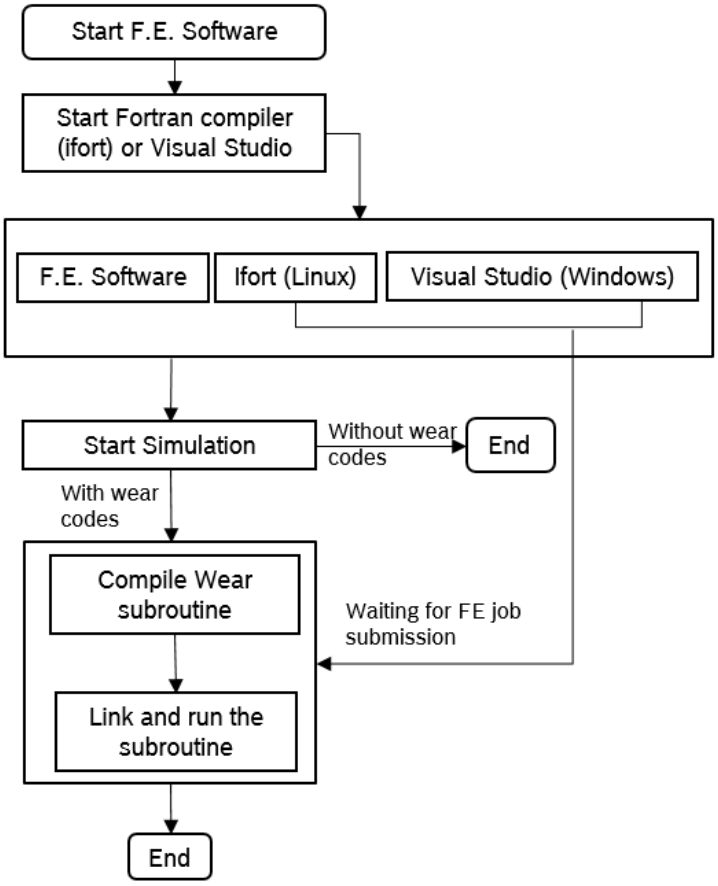

Figure 4.33: Coupling between simulation software and abrasion subroutine

The FE approach is further focused on wear model, friction model, contact algorithms and adaptive meshing techniques. The subroutines are developed for the abrasion and adhesion types of wear. The forward integration scheme is used for the calculations of wear (h) and is represented in equation 4.26. Here, i and n are the index corresponding to space and time respectively. K, P, S and H are the K-factor, contact pressure, slip and hardness at the respective node.

$$h_{i,n+1} = h_{i,n} + \frac{K_i \cdot P_i \cdot S_{i,n}}{H_i} \cdot \Delta t \tag{4.26}$$

The wear rate ($\frac{dh}{dt}$) is calculated using equation 4.27.

$$\frac{dh}{dt} = K\Big(P \cdot (dS/dt) + S \cdot (dP/dt)\Big) \tag{4.27}$$

The contact behavior influences the wear volumes. Majorly, penalty and augmented Lagrangian approaches are used to define the contact formulations. Penalty method is imagined as a weak spring with a stiffness of ϵ at the contact interface. Equation 4.28 represents the contact force $\boldsymbol{t_C}$ for penalty approach, where d_N is the normal intersection distance and $\mathbf{n}_P$ is the normal of the closest projection point of the slave node on to the master surface. Using this formulation and shape functions, the contact stiffness and contact force at each element are found out, which are later transferred into the wear subroutines [Wri07].

$$\boldsymbol{t_C} = \epsilon \cdot d_N \cdot \boldsymbol{n_P} \tag{4.28}$$

Equation in 4.29 shows the contact energy (Π_C) of the Lagrangian formulation. Total contact gap, normal contact gap, magnitude of contact force and variation are represented as $\boldsymbol{g_C}$, $\boldsymbol{g_N}$, λ and δ respectively. The terms $\lambda \boldsymbol{n_P}$ and $\boldsymbol{n_P}.\boldsymbol{g_C}$ correspond to $\boldsymbol{t_C}$ and $\boldsymbol{g_N}$ respectively. These equations are extended to element level with aid of shape functions for $\delta \boldsymbol{g_C}$ and $\delta\lambda$. Furthermore, the contacts also differ based on the choice of contact discretization, tracking approach, master and slave assignment and initial over-closure defined [Wri07].

$$\delta\Pi_C = \int_{\partial_C B_0} \Big(\delta \boldsymbol{g_C}.\lambda \boldsymbol{n_P} + \delta\lambda \boldsymbol{n_P}.\boldsymbol{g_C}\Big) \tag{4.29}$$

The friction model present at the interface also impacts the surface properties. Lubrication try to reduce the frictional forces and thereby the removal of material. Within the simulations, along with Coulomb and shear friction models, Usiu-Shaw models are used for calculating the frictional stresses. Figure 4.34 shows behavior of friction coefficient along the normal stress vs shear stress graph and equation 4.30 depicts Usui friction model. τ_R, k, μ and σ_N correspond to shear stress from friction, yield stress, coefficient of friction and normal stress respectively [Klo16].

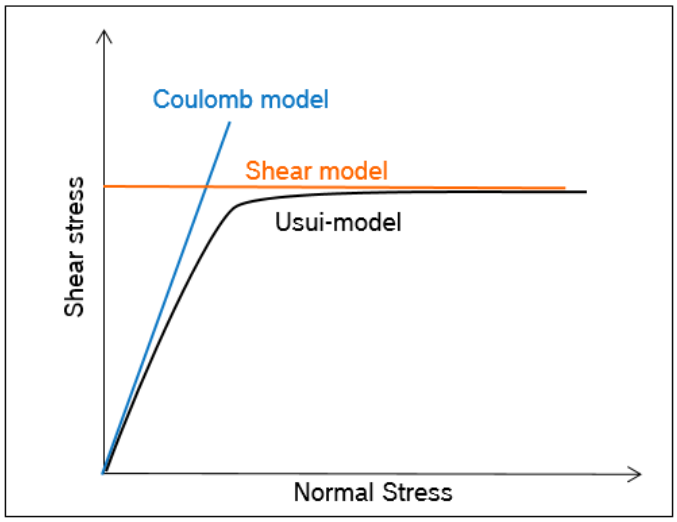

Figure 4.34: Friction model considered for wear calculations

$$\tau_R = k\Big(1 - exp(-\mu\frac{\sigma_N}{k})\Big) \tag{4.30}$$

Figure 4.35 shows flow of data for the FE simulations. The two boxes on the left-hand side indicate the geometries, materials, load profiles etc. The values of contact properties, mesh sizes, load and boundary condition (such as rotation at the shafts) inputs are defined at the FE box. These values play a key role for the stability and convergence of the simulations. Values like friction, over-closures, gaps and interference are added to make the contact definitions more efficient. Once the simulation model is available for the run, it is coupled with the subroutine in order to calculate the wear at interface of the gear mesh. The wear depths are stored inside the field variable NT. More information can be found in [KDH19b].

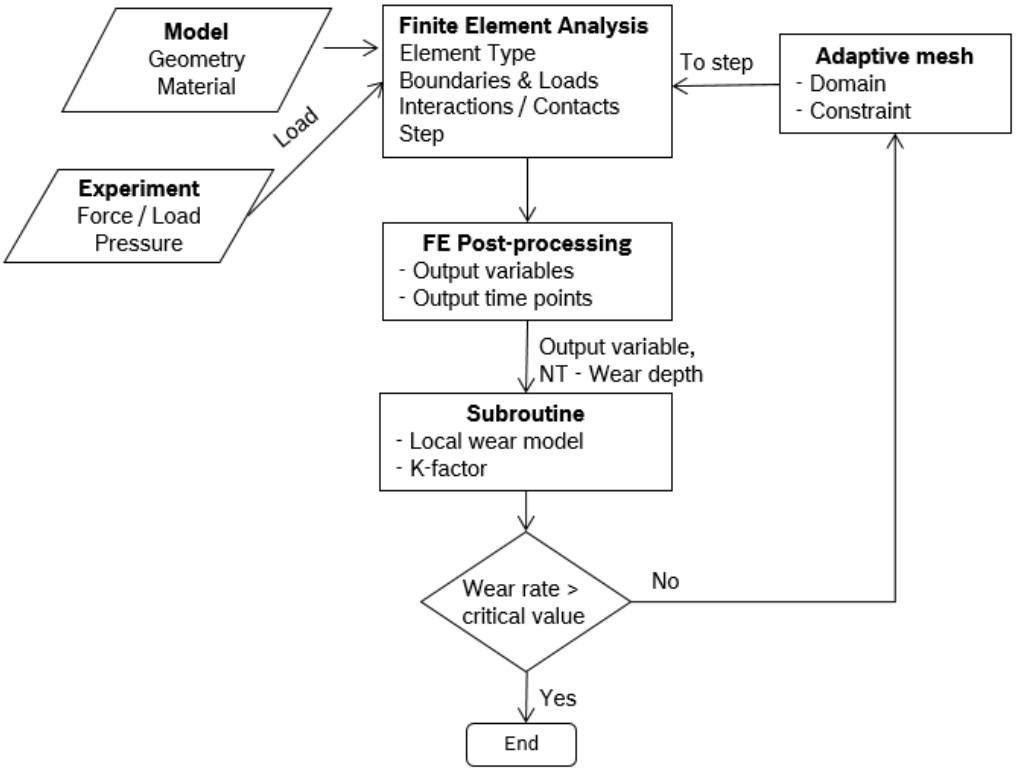

Figure 4.35: FE data flow for wear calculations

Figure 4.36 illustrates the flow of variables to calculate wear using the subroutines developed. The numbering shown in the diagram describes the flow chain of information. The Fortran codes like Ufield, Umeshmotion and Utemp are predefined in the simulation software, whereas the KAbrMas and Nearest Neighbor (NN) are developed separately. Initially, Ufield allows to store the K-factor values of both the gears defined in the parameter file (input) into the subroutines(2). Secondly, these values are passed on to the Umeshmotion subroutine, where the wear at respective node is calculated (5). The subroutine uses adaptive meshing technique to represent the abrasion at nodes. It aids in maintaining equivalent mesh topologically and provides solution for the problems of Lagrangian type or the wear. With aid of adaptive mesh, high quality mesh even at large deformations or loss of materials is obtained. This is achieved by allowing the mesh to move independently from the material. More information about adatpive meshing technique can be found in [Cor19]. Along with the K-factor values, contact pressures and contact slips are calculated within the Umeshmotion. Thirdly, values are shared with Utemp subroutine via the common block data, where the abrasion is stored inside a field variable and is represented in the GUI of software (6). Additionally, two user defined subroutines are developed to calculate the wear on the master side of the contact. Generally, when two surfaces come in contact, one is represented as slave and the other is said to be master. Most of the tools cannot predict the values of slips present on the master side of the interaction [Rog15]. Hence, an extra step is required to predict the wear on master surface. The KAbrMas subroutine (8) tries to calculate the wear on the master based on the values present on the slave. The NN subroutine (9) tries to find two nearest slave nodes having certain wear depth for every master node in contact. These values are passed on to KAbrMas subroutine (10), which uses the algorithm written in figure 4.37 to calculate the wear h_{m1} on master surface. Later, the iteration is checked for the convergence of solution (12) and once successful, the necessary output values are stored in result files (7), (13). Finally, the process is repeated for the next iterations (14) for predictions of wear at different increments.

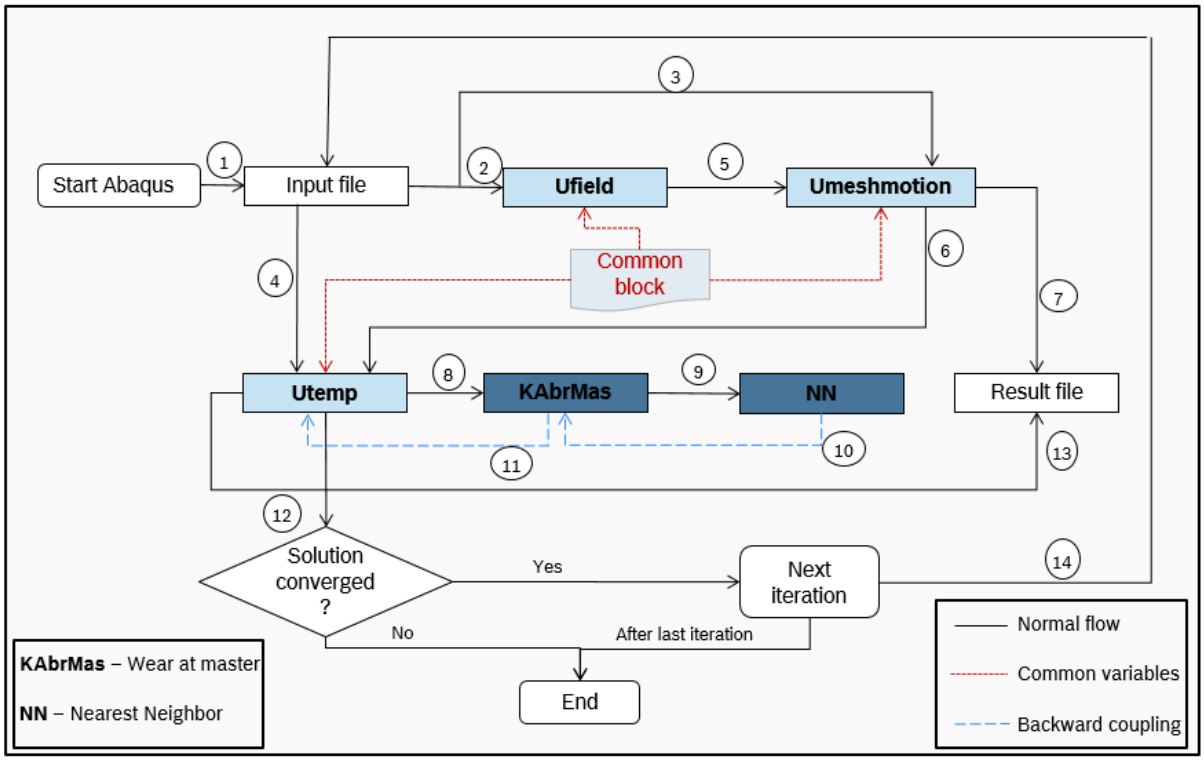

Figure 4.36: Flow of data for wear subroutine

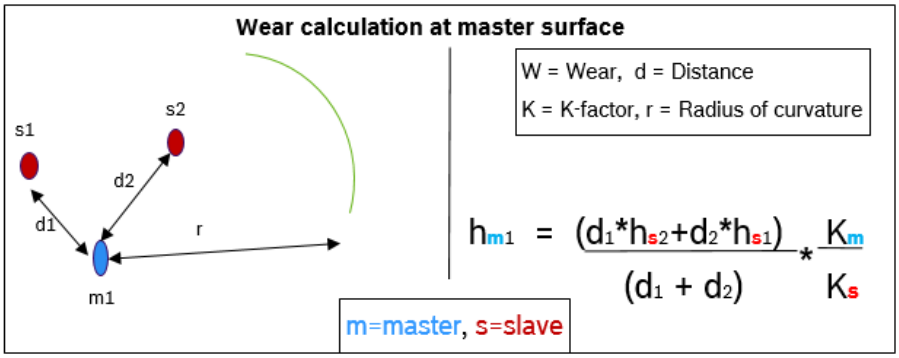

Figure 4.37: Algorithms for calculation of abrasion at the master surface

Finally, figure 4.38 illustrates the schematic view of wear calculations developed using the FE approach. It describes the process flow from specification to modeling to simulations to results. Additionally, the main softwares used for each of these phase are described in the figure. Detailed information regarding the software packages is further discussed in 5.1 [KDH20a].

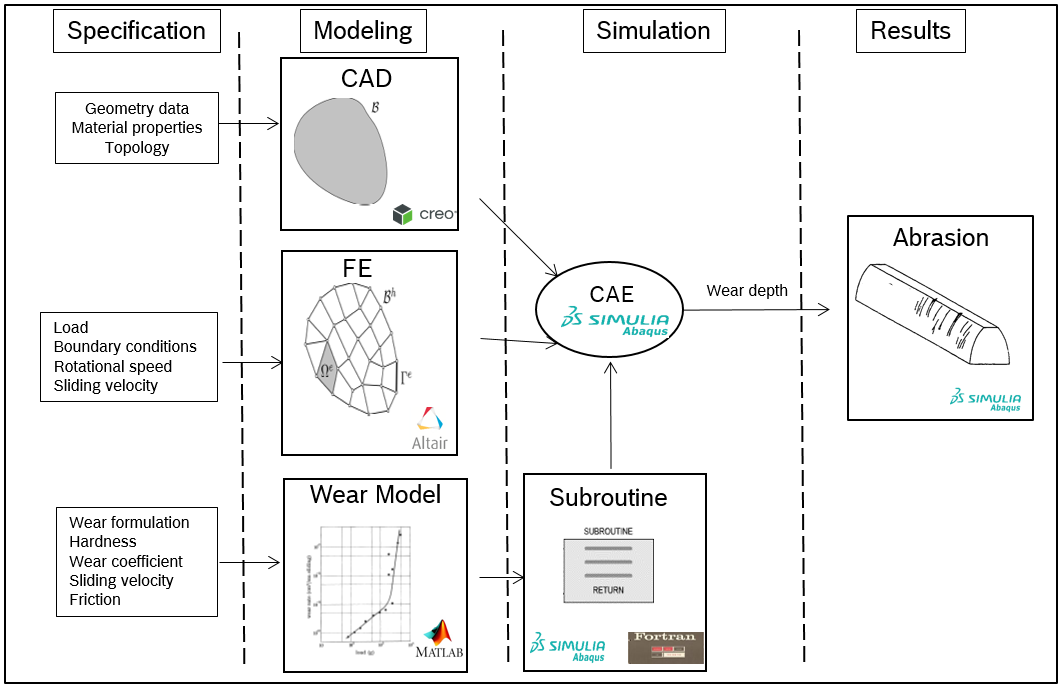

Figure 4.38: Schematic view describing the specification, modeling and simulations associated with wear setup

Forecasting for cycles

It is impossible to run the 3D simulations of wear for multiple cycles as it is computationally costly. In most cases, ablation/ abrasion wear takes the form of graph presented in the picture 4.39 before transforming to severe wear. It increases rapidly initially, followed by steady growth with respect to time [Hir16].

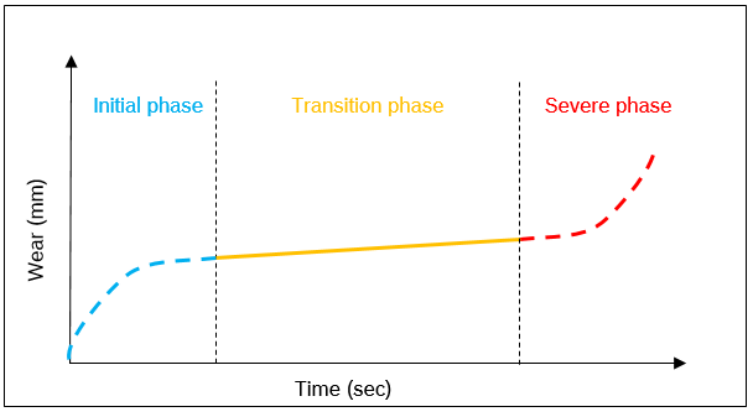

Figure 4.39: Wear profile vs. time

$$h_T = h_{FE} * \left(1 + \frac{C1}{(1 + e^{-C2/T})}\right) \tag{4.31}$$

Finally, equation 4.31 is used for estimation of wear along the time axis (h_T) (for the initial and transition phase). The term h_{FE} represents the wear calculated from the FE simulations using the figure 4.36. The approximate values of C1 and C2 are predicted using the curve fittings performed on the experimental data.

4.5.3 Training of Multi-Layer Neural Network for Wear Calculations

In general, a single FE simulation on cluster with 28 cores and 90GB memory consumes 1.5 days of time in average. This is computationally costly and hence the data generated from the FE simulations are connected with basic algorithms in order to get an idea of the wear in shorter frame of time. Within the ML algorithm (supervised learning), the available data is categorized into two sections mainly: dependent and independent data sets. Independent and dependent variables (also referred as features) are the input and output for the process that is being analyzed [Mat17, Ska18, Kim17].

Figure 4.40 describes an example neural network with hardness, tensile modulus, yield stress, contact properties, wear coefficient and torque as independent features. Furthermore, the output layer consists of wear depth and wear rate variables. The terms x_j, y_i and w_{ij}^k indicate the input features, output features and the corresponding weights. It is a shallow network with 6, 4 and 2 nodes for input, hidden and output layers. Hence, the equations described in section 3.4.4.1 can be directly used to develop the algorithms [KDH19b].

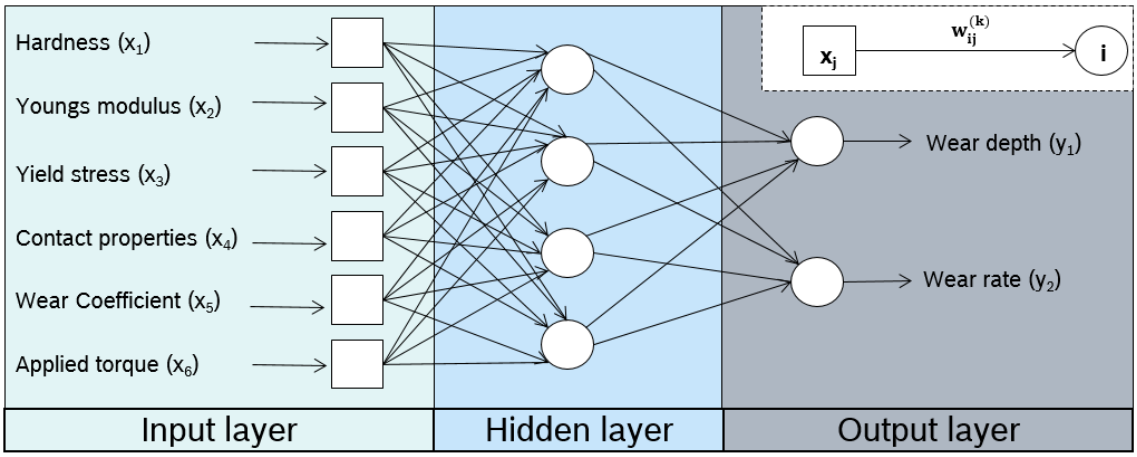

Figure 4.40: Neural network with 6,4 and 2 nodes for the input, hidden and output layers respectively

Finally, below a list of steps carried out for the prediction of wear using FE data is given:

- Ranges and the distribution of parameters like tensile modulus, wear coefficient, friction, torque etc., are developed via the UQ approach (section 4.5.1).
- A wear template model with parameters like material properties, contact properties, load profiles, step definitions etc., is created in the FE modeling package. The meshed model is defined with corresponding boundary conditions (like RPM) and load definitions (like torque profiles). A FE instance is created by passing the parameter values obtained from the earlier step (section 4.5.2). The coupling between the FE and UQ is defined with the aid of general purpose programming language.
- The subroutines for calculation of the wear depth and wear rate are developed using complied imperative programming languages. It also contains variables like wear coefficient which are parameterized.
- For all the instances generated, simulations are performed with coupling of the subroutines to the FE modeling package.
- The parameters defined and results obtained are passed through the machine learning algorithms as independent and dependent data sets respectively (section 4.5.3). In addition, the flow described in figure 3.21 is used for the prediction of the abrasion values.

Coupling of FE technique with the ML algorithms gives the flexibility of obtaining the solutions in a relatively shorter frame of time. It is vital to comprehend the fact that the experimental values for large data sets cost lots of investments and effort. With plausible data sets, including independent and dependent values from FE available, it is sensible to couple them with ML techniques. Once enough data points are discovered, the ML methods can be improvised to make the predictions of wear conceivable as it has higher probability to capture the complexities with more data points.

4.6 Numerical Coupling of Wear and Vibrations

Wear among the components can potentially deteriorate the NVH characteristics of drivetrains. For this reason, it is vital to understand the influence of abrasion on the vibrations of DU. This section gives an overview of the complex relationship among these two modules. Additionally, data flow across the modules is also described.

Figure 4.41 shows the numerical coupling among the wear and vibrations. It consists of four modules namely: FE, vibration, abrasion and acoustic module. Initially, a template with required boundaries and loads is developed in the FE. Arrow 1a represents the transfer of model from FE module to the next domain to execute harmonic analysis. Later, the analyzed results are coupled to the acoustic module to understand the effect of air borne emissions (1b). The second flow (2a, 2b, 2c) indicates that the FE template developed is first transferred to the wear module (2a) for the estimation of abrasion among the components. Furthermore, the deformed wear model is shifted to vibration (2b) and acoustic modules (2c) for the analysis of surface vibrations and fluid fluctuations.

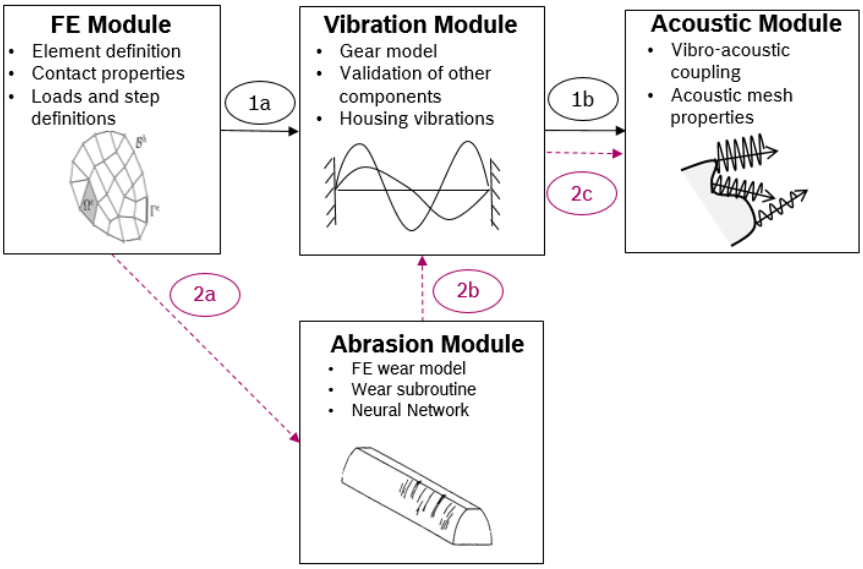

Figure 4.41: Link between vibration and wear domain [KDH20a]

4.6.1 Impact of Wear on NVH Characteristics

Gears assembled with improper mounting will abrade excessively, which leads to vibrations, noises and possible failure of the product. At gear model level, wear causes transmission errors and changes the contact formulations among the gear. Additionally at system level, it alters the orders of gear meshes, which shifts the amplitudes and frequencies of vibrations and acoustic pressures, thereby influencing the NVH properties of drive unit.

Technically, the wear mechanisms and dynamic properties of gears are influenced by each other. But for the scope of the work, only a single directional coupling is considered (i.e., influence of wear on vibration). The wear phenomenon is closely linked to the involute gears, due to the fact that every point on the tooth flank of the gears possesses a sliding velocity except the pitch point. At pitch point, a pure rolling condition occurs as there is no sliding velocity. This sliding action among the gears can cause abrasive surface wear. Furthermore, it changes the gear tooth profile geometry and thus the dynamic load. As a result, the vibrations will increase, and eventually a failure may occur [HK07]. Moreover, due to the changes in tooth surfaces caused by wear, the gear transmission ratio would no longer be static. Especially for the spur gears, the transmission error is easily influenced by the wear at tooth surfaces [WO03].

There are few studies on prediction of gear wear in quasi-static conditions [FA97, BKA04]. Nevertheless, dynamic responses are completely different from the quasi-static models. The dynamic meshing forces are of bigger magnitude than the corresponding quasi-static loads and the waveforms are completely different [HK07]. The dynamic responses of gears are influenced by geometrical deviations and elastic deformations of the tooth surface profiles. The geometric deviation results from material removal at the surface. Elastic deformation is determined by contact force and mesh stiffness. Within the simulations, a periodically time-varying mesh stiffness function and an external excitation to represent the effects of dynamic response on the gear wear process is used. Furthermore, a torsional model of the gears and shaft in contact is created and then it is combined with a static and quasi-static wear models. Finally, these models are capable of estimating the influences of surface wear on gear system dynamics.

4.6.2 Data Flow across Abrasion and Vibration Domain

In the proposed method, a dynamic system model of electromechanical drivetrain is developed with the goal to generate realistic vibration. The system model is coupled with abrasion module for a quantitative study of the effects of gear tooth surface wear on housing and gearbox vibration responses. Figure 4.42 shows flow of the data/ variables across vibration, acoustic and wear modules. The template is represented by faster times for direct estimation of vibration and sound and with slower times for inclusion of wear module. Faster time flow initially aims to calculate the associated loads pressures, tensions etc. These are than imported into the wear module (which has the slow time constant) and the result is later fed back into the vibrating domain.

Within the wear module, models with quasi-static and static solution types are used to realize the abrasion among the gears. Quasi-static can be used for realizing a mechanism that is moving so slowly, that it is practically static and wear is one such phenomenon. The elements are defined using second order shape function to get better accuracy of contact forces. The contact pressures and sliding velocities at each node of the wear model are fed into the Archard wear model to calculate the wear rates and depths. Once the abraded gear model is made available (from section 4.5.2), it is then looped back into the linear dynamic module as a new geometric transmission error. The error represents deviation of gear profile from an ideal involute curve. Furthermore, changes in the gear stiffness are incorporated into each gear and shaft model during the global dynamic simulation of the complete system. The vibrations of system are evaluated by solving for the steady state dynamics of each gear mesh model simultaneously with the vibration of exterior structures. Within the harmonic analysis, modal superposition technique is applied to improve the computational costs of the simulations [CPZ96, Cor17a]. The modal superposition analysis uses the natural modes of the system to calculate the linearized response of the model to harmonic excitations. Finally, these modules are linked to the acoustic domain with a tie connection between structural and acoustic nodes at the fluid-structure interface.

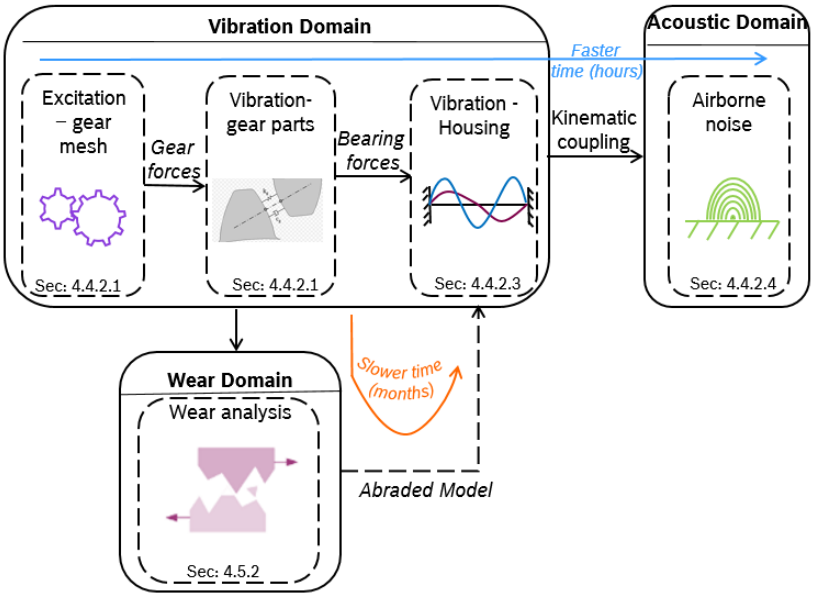

Figure 4.42: Coupling among vibration, acoustic and wear domain

4.7 Flowchart for Parameter Identification of Model Components

So far, the individual methods for the modeling and simulation of vibro-acoustic, abrasion mechanisms in drivetrains as well as the functional relationship among the individual model parts are described. The procedure for accessing the model components is subject of this section and is shown in figures 4.43, 4.44 and 4.45. Firstly, a holistic view concerning the vibration, acoustic and wear is depicted in 4.43. Secondly, the flowchart in figures 4.44 and 4.45 describes generic process to identify individual system parameters. Furthermore, reference to respective sections of the model component is shown. The figures also consists of Single Direction (SD) and Dual Direction (DD) arrows, which represent coupling among the domains. Below is brief overview of the coupling directions:

- SD-1 coupling describes the single direction link between the other general domain and acoustic module (check figure 4.25).
- SD-2 illustrates the fluid structure interface, where the structural velocities obtained from the harmonic simulations of the DU are transferred to the acoustical domain (check figures 4.18, 4.25, 4.22 and 4.43).
- SD-3 describes the exchange of information between the acoustic FE and ERP techniques for calculations of acoustic behavior at farther distances (check figure 4.45).
- SD-4 links the vibro-acoustic domain with that of the abrasion module. It tries to find out the influence of wear among the gear unit on the NVH characteristics of the drivetrain (check figure 4.43).
- DD-1 illustrates the coupling between other physical domain and the mechanical gear unit (check figures 4.25 and 4.44).
- DD-2 describes the energy exchange within the mechanical gear unit. It tries to couple the excitations from the LPM domain on to the vibrations of the MBD module (check figures 4.25 and 4.26).
- DD-3 indicates that there is transfer of data between MBD and FEM domains. The stiffness from the contact analysis and convergence studies are used as inputs for the MBD

model developed. Also, the bearing forces obtained from the MBD system are used as excitations for harmonic analysis and therefore the DD coupling is created (check figures 4.18, 4.25, 4.26 and 4.44).

In conclusion, the implementation of the methods illustrated in figures 4.44 and 4.45 is done in form of a modeling instances as shown in chapters 5 and 6.

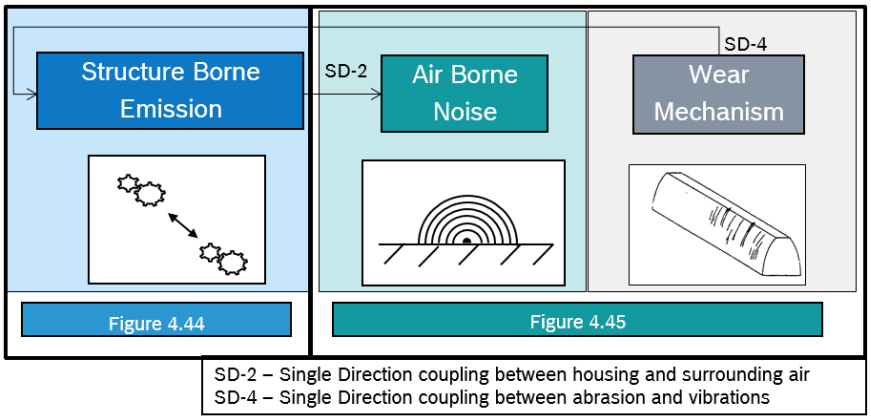

Figure 4.43: Overview of the pictures 4.44 and 4.45

Based on the chart, the methodology developed owns a paramount advantage of parallelization. Different teams of experts can work simultaneously on the identification of system parameters. For instance, a transmission team during the gear design can determine excitation mechanisms. This event corresponds to the node gear force calculation in figure 4.44 (LPM, MBD). Synchronously another team can focus on calculation of modal parameters and their experimental validation works This event corresponds to node natural vibrations of components in figure 4.44 (FEM, experiments). Additionally, different experts could work on the same vertical in a domain. For instance, the method FEM inside structure borne emissions umbrella consists of events like bearing study and harmonic analysis. One group can prepare the model for structural improvements like bearing model validations and, simultaneously the other can focus on developing the dampings necessary for harmonic analysis. The other advantage of this technique is that, few of the events like contact simulations as wells as convergence study can be used for both vibration and wear domains (multi-domain).

Optimization inside the individual system components can also be executed with this method. For example, if the influence of different materials on gear and shaft needs to be investigated for their effect on dynamics of the other components, it can be performed by calculating the masses and inertia tensors (LPM, MBD), followed with gear and bearing forces (using MBD, FE), thereby selecting the optimized model parameters for the component. More about the optimization method can be comprehended in section 4.8.

At this point, it can be understood that, all model requirements like extensibility, modularity, etc., mentioned in section 4.2, are fulfilled within and across the model components. Also, the attributes like excitation mechanisms, gear vibrations etc. introduced in section 4.2 are calculated using the techniques described. The sections discussed until now illustrated multi-domain approach in a general view, the next challenge arises for improvements in the components to curtail the unwanted noises around the exterior surfaces of the drivetrain.

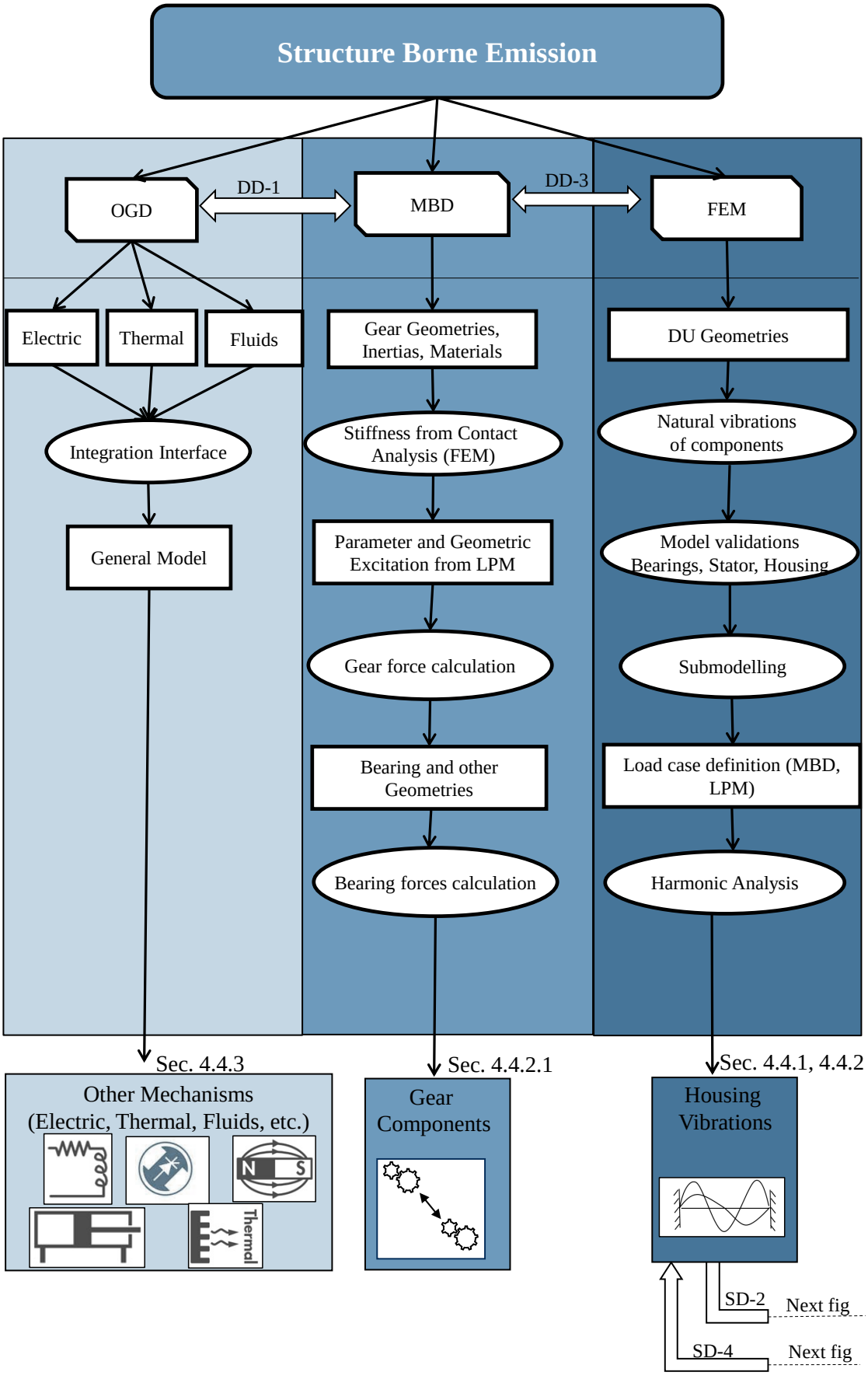

Figure 4.44: Data flow among the vibration, acoustic and wear domains

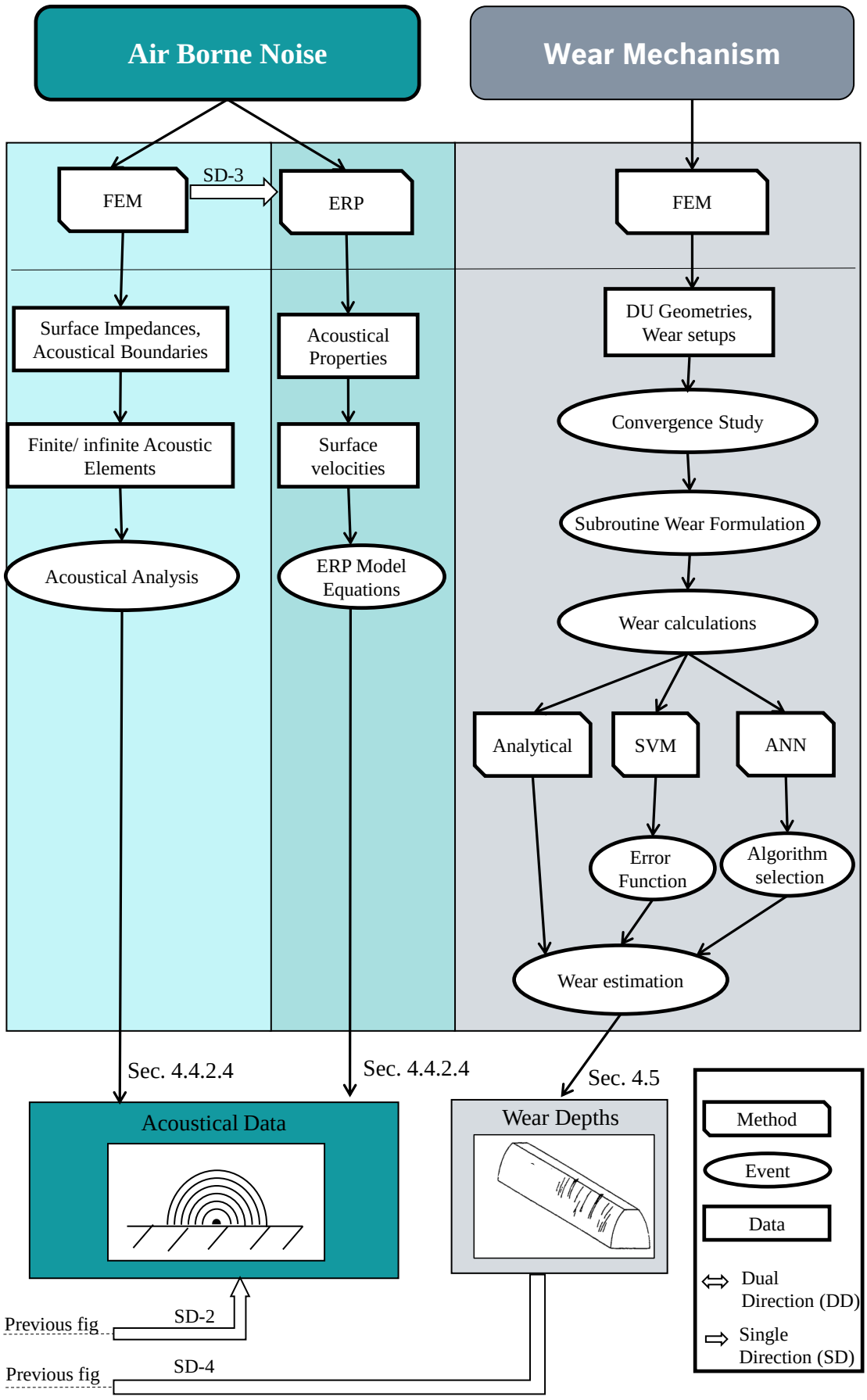

Figure 4.45: Data flow among the vibration, acoustic and wear domains - continuation

4.8 Optimization of Powertrain for NVH

Until now, methodology to understand the NVH and wear characteristics of the electromechanical drivetrain is described. The next major step of this methodology is to build a robust optimization method with the goal of improving the vibro-acoustics in drivetrain. A motive of this section is to optimize the peak responses of low and mid frequency vibrations for improving NVH performances. This section describes the optimization methods applied and eventually the flow of data in this module.

4.8.1 Numerical Optimization Techniques

Higher surface velocities of components would deteriorate the quality of drivetrain, thereby causing an inefficient ride performance. Hence, it is essential to optimize the NVH characteristics of power unit. Numerically analyzing various complexities and thereby optimizing the required parameters addresses this issue. The main available numerical optimization techniques are namely:

- **Topology** - Modification of general structure layout
- **Size** - Modification of thickness for sheet metal structures
- **Shape** - Modification of component surfaces
- **Bead** - Creation of bead structures for shell components
- **Material** - Modification of component materials

Detailed explanation of each optimization technique can be found in [Cor18c]. The size and bead optimization methods are majorly used on 2D elements (like shell, plate - sheets), whereas the power unit majorly consists of components which are represented using 3D elements. The methods of modifying dimension and shape of structures, or covering damping materials are effective to reduce structure borne noise. Within the scope of work, mainly topology and material improvements are considered for enhancing the NVH characteristics.

The vibro-acoustic optimization task is represented using three characteristics. Below a list of characteristics along with the concerning questions is given:

- **Design variables** - How can the structure be modified? Values like frequencies, weight, volume and stiffness that can be altered to obtain better vibrations.
- **Design constraints** - Which restrictions must be implemented on the model? Variables like mass and volume that could be limited to certain ranges.
- **Design objective functions** - What should be minimized, maximized, optimized etc.? Function of natural frequencies (variable) to push them out of critical spectrum domains, thereby avoiding vibrations.

Equations in 4.32 represent mathematical form of the optimization task. The term $f(x_j)$ represents objective function developed to maximize the design variable x, which in our case are the natural frequencies of the model. Terms $g_i(y_i)$ are the design constraint equations applied on variables y_i, which in our task would be weight, mass and volume mainly. The LL and HL terms in equation 4.32 represent lower limits and higher limits imposed on the design constraints respectively.

$$\begin{aligned} &Maximize\ f(x_j) \quad j = 1..m \\ &Considering\ LL \leq g_i(y_i) \leq HL \quad i = 1..n \end{aligned} \tag{4.32}$$

4.8.1.1 Design Optimization

One of the methods to improve the structural dynamic responses in the low and mid frequency spectrum is with the help of geometrical changes for the components of drivetrain. It is essential to analyze the influence of each component on the drivetrain acoustics and there by building a counter measure at the component responsible for the vibration. The optimization is built with aid of simple design sensitivity analysis, which helps in determining better model parameters. Ultimately, relevant Eigen values and vectors of the structures identified at the initial design are modified during the optimization process.

Developing a sensible combination of objective functions and constraints is one of the most challenging steps in applying topology optimization. For the design of dynamic systems, structural vibration control is the most essential consideration. The objective of this type of optimization is to achieve the optimal material layout for the load-bearing components. The surface velocities calculated in section 4.4.2.3 are then transferred into the dynamic optimization domain in order to reduce the surface accelerations of the drivetrain structures. Figure 4.46 describes the flow of the optimization module to optimize the structural dynamics of the components such as housing and cover, thereby improving the drivetrain. Minimizing the displacements at the frame and drive unit interface are considered as the objective functions. The design constraint is defined for the mass of the housing and cover. Additionally, the cast direction, i.e., a manufacturing constraint, is defined in the parameter file. This constraint ensures the manufacturability of the drivetrain component.

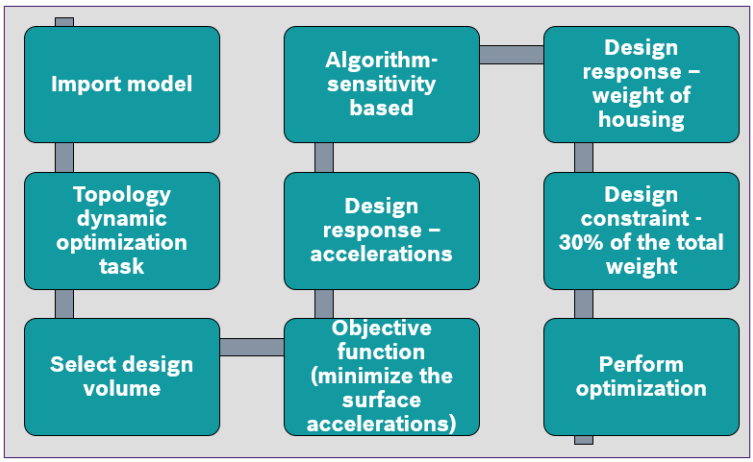

Figure 4.46: Optimization flow for performing design changes

In a real electromechanical drive, a larger number of components are used to build the model completely. If all the parts are considered as design variables, the structure modifications for drives become complicated and sometimes even impossible. Hence, the effect resulting from a small fluctuation in the current design on the objective and constraint functions must be perceived when an optimization problem is solved. Below is the list of few structural improvements considered further for the design optimization:

- New and modified rib geometries on the existing housing surfaces.
- Addition of new components between the vibrating parts.
- Other general geometrical changes on inner housing surfaces.

The improvements in design are suggested considering the manufacturing feasibility. The modifications mentioned above mainly cause changes in stiffness and masses of the parts and assemblies. The natural frequencies of structures are functions of these variables and hence the alterations in them would move the Eigen frequencies to different values.

4.8.1.2 Material Optimization

The other approach considered to improve the NVH of drives is by means of material changes corresponding to various parts. Few of the materials like foams and polymers possess the properties to damp out the problematic vibrations. Such materials are utilized for there superior damping acoustic characteristics. Choosing of an appropriate material would reduce the surface velocities of the components, thereby improving the performances of drivetrains. Below is the list of improvements considered for the material section.

- Material modifications on elements like washers, o-rings and damping rings, which are placed between the shafts and housings
- Elements with acoustic absorption properties along the transfer path of the disturbances

The modifications mentioned above alter the vibration characteristics mainly due to the changes in material variables. The material variables that can influence the vibrations can be categorized into two branches namely: mechanical and acoustical. The main mechanical properties considered for analysis are Young's modulus, density and viscous damping. Similarly, acoustical properties like volumetric drag, material impedance influence the dynamic characteristics of electromechanical drives. A part of this optimization approach is also discussed in section 4.4.2.2 under the subtitle Influence of dampers.

4.8.2 Data flow for the Optimization Technique

In the previous sections (4.4.2, 4.5, 4.6), methods for simulation of vibro-acoustic and abrasion mechanisms in drivetrains are described. This part illustrates the flow of optimization module developed (described in section 4.8.1) and its connection with modular diagram shown in section 4.6.2.

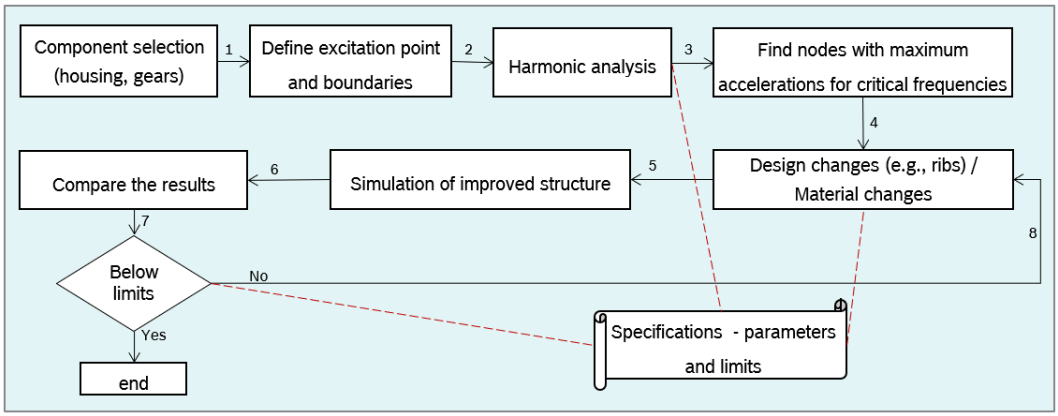

Figure 4.47: Optimization flow of electromechanical drivetrain for improved NVH performance

The flow diagram in figure 4.47 describes a common process for identifying individual system parameters and thereby altering them to improve the vibrations. Initially, a simulation on current components is executed with help of the modules developed in section 4.4.2. After that, the critical areas across the interest of spectrum are analyzed for extra vibrations. Furthermore, design and material alterations are performed depending on the underlying challenge. Later, the updated model is looped back into the flow to obtain the new dynamic characteristics. This procedure is repeated until the vibrations are curtailed to desired limits. Information about the parameters like density, Young's modulus, damping properties and acceleration limits are further found in specification sheet.

The modular diagram in figure 4.48 is an extension of figure 4.42. It helps in selection of the right model for curtailing the NVH below certain limits. The dynamic characteristics obtained

from the vibration and acoustic module are transferred to the optimization module. Later, these values are analyzed and altered with the changes in design variables. Additionally, a manual design sensitivity analysis is performed to understand the effects of changes. In the end, best suited model parameters are chosen as improvements to the drivetrain assemblies.

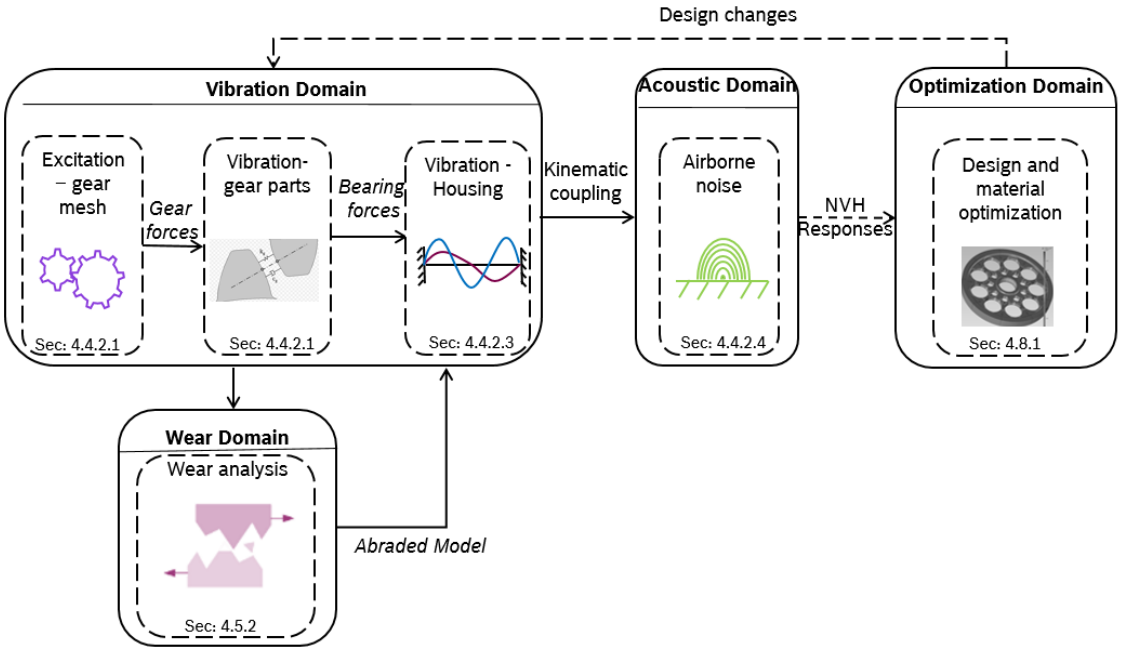

Figure 4.48: Coupling along vibration, acoustic, wear and optimization modules

Finally, it is stated that the optimization module along with vibration, acoustic and wear modules satisfies the system level requirements mentioned in section 4.2. The purpose of work to realize the method attributes in section 4.2 are also investigated using the methodology. Since the present chapter describes the multi-domain approach in a generic and quite common view, the question arises for method verification using a modeling instance and validation of real time power unit.

5 Implementation of the Method with a Modeling Instance

In the framework of the developed, generic methodology for imaging vibro-acoustic mechanisms in gearboxes, the individual modeling and simulation methods as well as the physical model components have been presented. Since the result is a complex, cross-domain methodology, the question of feasibility inevitably arises in the form of a modeling instance. Consequently, a simulator is selected for the verification which can model the model components in a multi-domain system model and, if necessary, can be extended by the corresponding model components.

Previous chapter illustrated the idea of NVH simulation template along with the complexities of abrasion in a simple generic way. This chapter aims in creating the instances for template classes developed in chapter 4. Figure 5.1 describes flowchart for simpler implementation and validation for the methodologies via modeling instances. This is achieved with the aid of simple structures and analogies. In regards with vibro-acoustics, the methods are instantiated for the multi-domain and FE simulations. Furthermore, the wear simulations are implemented on simple 2D structures. Overall, this chapter helps in comprehending the modules in a better way in contrast to the complex drivetrain structures.

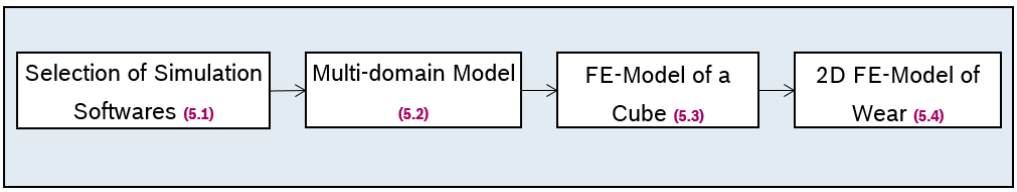

Figure 5.1: Brief overview of the sections and flow within chapter 5

5.1 Selection of Simulation Softwares

There are different possible modeling environments for verification. The simulator is chosen based on the component and module of interest. Table 5.1 shows few of the softwares available for realizing the aims of the project. Majorly, two main softwares are used for calculations: Simscape (from Matlab) for system level modeling and Abaqus (from Dassault Systemes) for FE calculations. Apart from the two, softwares like general Matlab programming, SimMechanics and Hypermesh (from Altair) are used for model preparations and FE pre-processing respectively.

System modeling packages	FE modeling packages
Altair Activate	Ansys
Dymola	Abaqus
Matlab - Simscape	Comsol
Matlab - Simulink	Hyperworks
Modelica	LS-Dyna
MSC Adams	Nastran

Table 5.1: Brief list of the softwares available to realize the targets of the work

Reasons for selection of Simscape to create the modeling instance are:

- Comprehensive and transparent model libraries.
- Modular connection for a multibody simulation.
- Object-oriented programming to extend existing libraries.
- Model-based c-code generation.
- Automated handling of physical units.
- Hardware-in-the-loop simulations.
- Various numerical solution methods like implicit, explicit etc.

Similarly for Abaqus:

- Detailed level of model characterization.
- Combination of nonlinear simulations with linear dynamics.
- Different solution techniques like static, dynamic quasi-static etc.
- Able to simulate acoustic behavior and its coupling with vibration.
- Modular representation of models.
- Platform for automation using Python.
- Special Fortran functions to calculate mechanisms like wear and acoustics.

Most importantly, Simscape and Abaqus fulfill all requirements for the system model from section 4.2. Additionally, tools like Python, Shell scripting, Fortran etc., are used for automation of tasks and debugging of errors. E.g., the wear calculations discussed in section 4.5.2 are triggered, solved and presented completely with the aid of automation. Initially, scripts aim to create the required variant models for the simulation by defining and re-initializing parameters like wear coefficient, contact definitions (these values are created in sec 4.5.1) etc., of the template model. Once the shell scripts solve for the results of respective models, Python post processing scripts are triggered to get the corresponding target values like wear depth, contact pressures, slips etc., at each step and at the respective nodes and elements. The scripts later convert the Abaqus result data to curve data and are presented with graphs like wear depth vs. time, contact pressure vs. time etc.

5.2 Multi-domain Model

Simscape includes several block libraries, which are divided into different physical domains such as SimMechanics for mechanical multibody simulations or Simscape Fluids for fluids. Hence, the tool covers a large part of the functions required for creating a model instance for vibro-acoustic transmission model. In addition, Simscape provides the possibility for extension of the modular template library. Furthermore, this section discusses three areas mainly:

- Non-rigid gear model
- Flex-body vibrations
- Equivalent Radiated Power (ERP)

The following is a detailed description of the implementation and verification of each library extension.

5.2.1 Non-rigid Gear Model

The flexible gear mesh model discussed in section 4.4.2.1 is implemented in SimMechanics. Furthermore, the verification is executed using a convergence study.

Implementation

The hierarchical implementation of the transmission model is described in figure 5.2. It consists of three levels namely: system, intermediate and transformation. At system level, the gearbox model can be integrated directly into a bigger system model and subsequently be parameterized, which fulfills the model level requirements of reusability and simplicity (check figure 4.2).

The intermediate level describes the mechanical stimulation present inside the system in the form of parameter and path excitations. Since additional excitation mechanisms can be added without further effort due to the network characteristics, the model requirement extensibility is also achieved.

The transformation level consists of equations 4.5, 4.6 and 4.7. It depicts the connection between gear mesh and gear components. Modular implementation and ease-of-use at system level of the flexible model in Simscape enables efficient, vibro-acoustic system analysis. For this purpose, the gearbox function is designed as a configurable subcomponent of the overall model. Additionally, the parameters of model include not only the gear design parameters, but also the characteristics of the excitation mechanisms. Since they are nonlinear quantities, they are loaded from an external file. More information about the section can be found in [KDH19a].

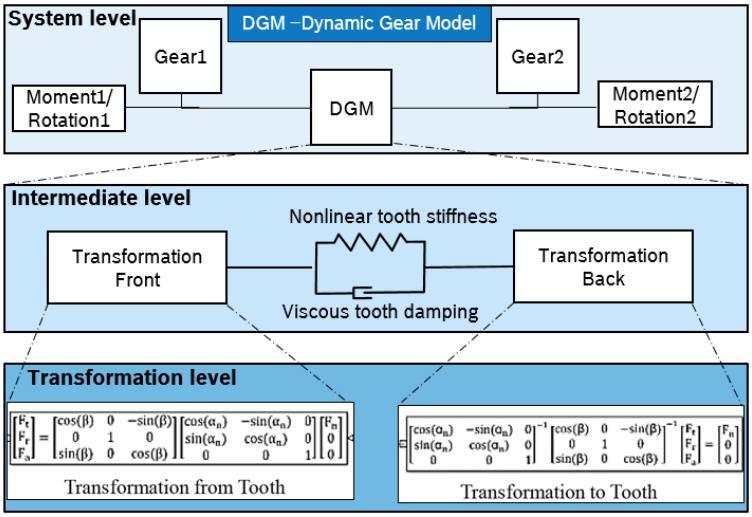

Figure 5.2: Abstract model of dynamic gear module

Validation

Purpose of the validation is to prove that the flexible gearbox model reflects correct physical action mechanisms. For this reason, simulation results of the ideal and physical transmission are compared. A study is performed by linearly increasing the constant overall stiffness of the spring at the gear mesh. The difference between simulation results of ideal (rigid) and flexible gear model is calculated and plotted against the stiffness. The difference is used as convergence criterion because there is no transmission error for an ideal model as it is zero. Figure 5.3 shows convergence plot for the transmission error. The X and Y axes represent the stiffness and percent difference between the ideal and physical gears. By the means of figure it can be illustrated that the absolute error converges to zero, which validates the interaction of non-rigid transmission implementation. This is to be expected as ideal transmission due to the existence of infinite stiffness at the gear mesh. When the stiffness values of the flexible gearbox are increased, their

results approach those of the ideal transmission. The verification of non-rigid gear model can thus be considered as successful.

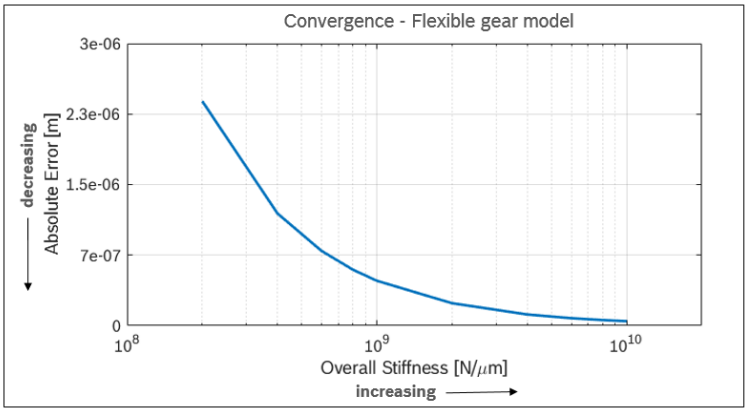

Figure 5.3: Convergence of flexible gear model

5.2.2 Flexible Structures

The flexible vibration model discussed in section 4.4.2.3 is implemented as a modal model in SimMechanics and later verified. For this purpose, a simple beam element is defined with appropriate boundary conditions. Since the Eigen frequencies and modes for this structure with respect to a given force are analytically computable, it provides itself as proof for correct implementation of the modal model (in general form) in SimMechanics environment. The three-dimensional motion of the housing is composed by superposition of individual spatial directions. Therefore, the verification of the modal model in one spatial direction suffices our purpose as shown below with the help of a cantilever beam.

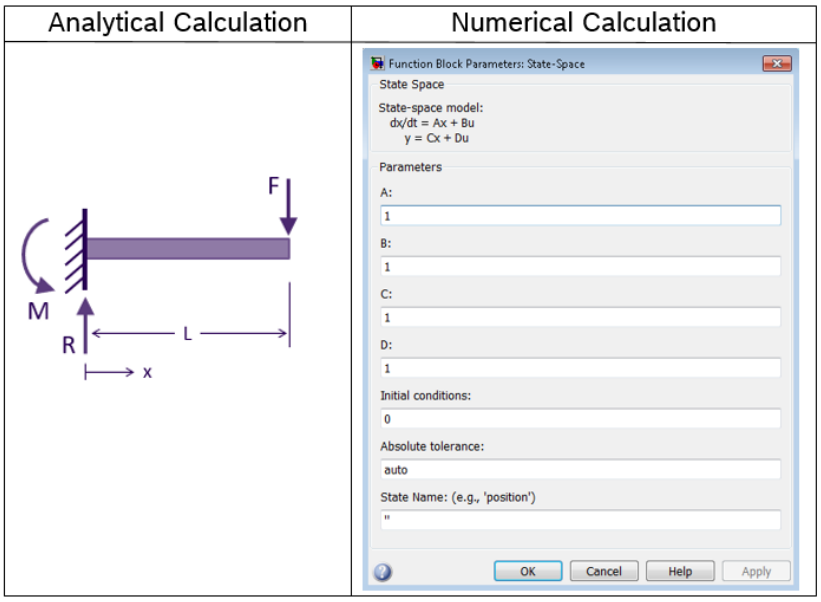

Figure 5.4: Analytical and numerical calculations for the beam modal model [Hat00]

In the simulation model of a real transmission, the natural frequencies and modes of the housing structures are not calculated analytically due to their complexities (rather they are calculated using Abaqus). Detailed information can be found in section 6.2.3. For most part of the

simulations (in this section), the existing functions of the SimMechanics standard library are utilized. The model is developed using the state-space form equations, through which linear systems of differential equations are mapped (check right-hand side of figure 5.4).

For the verification of model in SimMechanics and the correct parameter calculation in pre-processing, analytical calculations for the bending beam are computed and compared with the model. The relative error between the analytical solution and the numerical simulation results is evaluated. As part of implementation, a cantilever beam is considered and a force F is applied at the free end (check left side of the figure 5.4). The beam is considered to be homogeneous and statically determined.

The general equation for the 1-D beam structure is given by formula 5.1. Where E, I, w, m, x and t represent Young's modulus, moment of inertia, structural displacement, mass, space direction and time respectively. Deriving further, the bending wave number k_b and natural frequencies of the structure are given by the equations 5.2 and 5.3 [GHS12]. L, b, h and λ describe length, breadth, height and the mode of oscillation equation.

$$EI\frac{\partial^4 w}{\partial x^4} = m\frac{\partial^2 w}{\partial t^2} \tag{5.1}$$

$$k_b = \left(\frac{mw^2}{EI}\right)^{1/4} \tag{5.2}$$

$$f = \frac{\lambda^2}{2\pi L^2}\sqrt{\frac{EI}{\rho bh}} \tag{5.3}$$

Equation 5.4 represents general solution for the equation represented in 5.1, where $\widetilde{a}$, $\widetilde{b}$, $\widetilde{c}$, and $\widetilde{d}$ represent necessary constants. These constants can be calculated according to the boundary conditions and forces in the system. Equation 5.5 represents the analytical solution for deflection of cantilever beam.

$$w(x,\lambda) = \widetilde{a}\cos\lambda x + \widetilde{b}\sin\lambda x + \widetilde{c}\cosh\lambda x + \widetilde{d}\sinh\lambda x. \tag{5.4}$$

$$w(x) = \frac{Fx^2}{6EI}(3L - x) \tag{5.5}$$

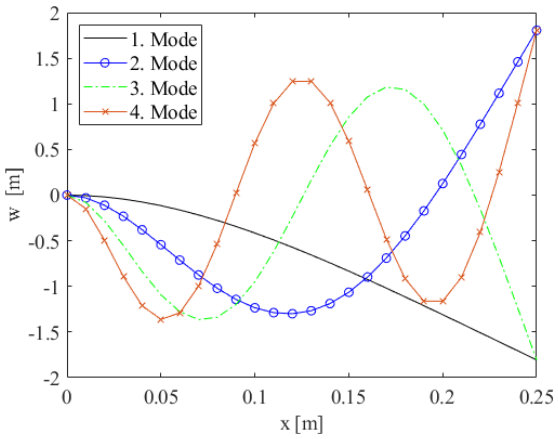

Figure 5.5: Eigen modes obtained by numerical simulation (values correspond to steel)

The model is evaluated for the first four Eigen modes and are shown in figure 5.5. Furthermore,

considering constraints, the static deflection of the beam can be analytically calculated [KHA09]. As part of the verification force of 1000 N and position L/2 are selected. Table 5.2 shows the parameter values for steel and aluminum necessary to execute the calculations.

Name	Value (Steel)	Value(Aluminum)	Units
Length	250	250	mm
Width	25	25	mm
Height	25	25	mm
Young's modulus	200000	70000	MPa
Density	$7.85*10^{-6}$	$2.70*10^{-6}$	$Kgmm^{-3}$

Table 5.2: Parameter assignment of the beam element for the verification of modal implementation in SimMechanis

For numerical simulation of the deflection in SimMechanics, different levels of detail are considered. In the first step, only one natural frequency is considered, in the second, the first two natural frequencies and so on. Considering different number/ count of modes, the analytical solutions of deflection are compared with simulation results of the modal model. These deflections calculated at x=L/2 via numerical method vs. analytical solution for steel and aluminum are shown in figure 5.6. It can be found out from the graph that even considering the first four modes, the error (difference between the analytical and numerical solution) becomes close to zero. Lower density and Young's modulus of aluminum would alter the values mass and stiffness matrix in the state space equations (shown in equations 4.9 and 4.13) and would cause greater amount of deflection in comparison with steel. Hence, the error values shown in the graph are higher for aluminum. However, the error percentages ((analytical - numerical)/analytical*100) are the same for both the materials.

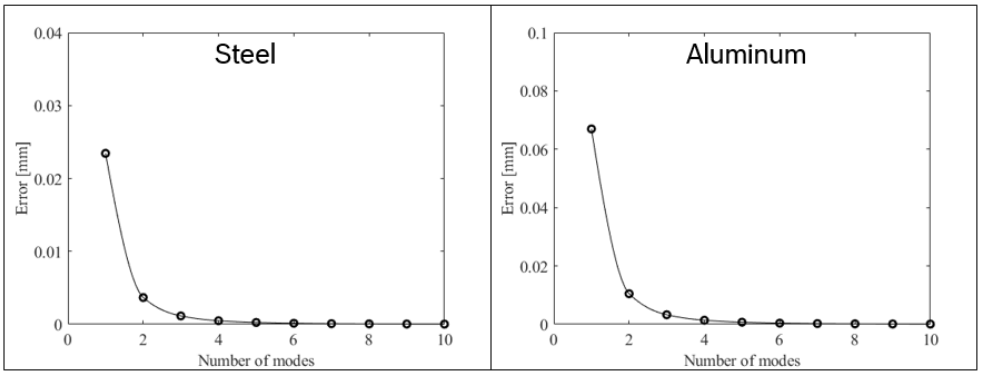

Figure 5.6: Numerical vs. analytical deflection - Steel and Aluminium

Finally, a convergent match between analytical solution and numerical simulation can be demonstrated. Therefore, for further consideration, a correct implementation of the modal model in SimMechanics can be assumed.

5.2.3 Equivalent Radiated Power

Equivalent Radiated Power (ERP) model is implemented using Matlab m-scripts applying the equations 4.24 and 4.25. If the housing surface is considered as a combination of discrete equidistant grid cells, the resulting surface velocity can be calculated as the average velocity of all points. On the other hand, when these distances between the simulation points are random,

a weighting must be defined for each point. The weight is calculated from the proportion of the area that can be assigned to that point. The values for ERP can then be plotted against the frequency. In principle, the evaluation by means of ERP is useful in post-processing and it does not consider backward coupling of aerodynamic forces to the structure. Overall, using ERP scripts, simulation times can be shortened and the model part can be considered as a modular extension from figure 4.2.

5.3 FE Model of Cube

So far, the illustrated instances represent the validation of multi-domain approach (from section 4.4.3). This part strives to verify the FE methodologies discussed in chapter 4. The modeling and simulation of the structures are executed with help of softwares like ProE (for design), Hyperworks (for building the simulation model) and Abaqus (for solving and results). The templates developed for the verification can easily be transferred and applied on the drivetrain structures, ensuring the modularity and extensibility objectives mentioned in section 4.2.

5.3.1 Cube Model Construction

Here, instead of simple beam structure (as in section 5.2.2), a hallow cubic element (check figure 5.7) is modeled. The dimensions of constructed cube are comparable to that of the drivetrain housing components. The aim here is to eliminate the design complexities and to completely focus on technique.

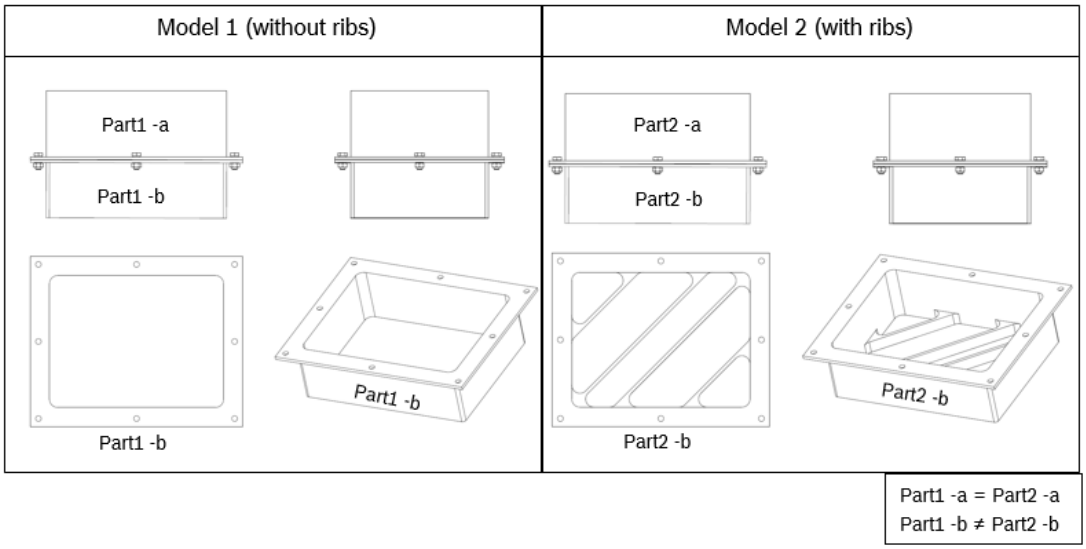

Figure 5.7: Design layout of simple and optimized cube structures

Figure 5.7 describes two models mainly: one without ribs and the other with ribs on one of the part. Model 1 is a simple cube (consisting of Part1-a and Part1-b) with a thickness of 3mm and screwed at 9 points. Model 2 (optimized structure) is similar to Model 1 (simple structure) except that it consists of new ribs to stiffen the structure and thereby moving the Eigen frequencies to a higher spectrum. The idea stems from the fact that the models should be improved for the structural dynamics and sound. It can be considered as a design optimization step (check section 4.8.1.1) for the modeling instance (with the goal of increasing the stiffness and thereby the values of natural frequencies).

Table 5.3 describes the parameter information required for the construction of the cube. The values 55 + 65 in volume tab indicate heights of the two parts respectively.

Name	Values	Units
Volume	124 X 164 X (55+65)	mm^3
Thickness	3	mm
Structure - Young's modulus	70000	MPa
Structure - density	2.7×10^{-6}	$Kgmm^{-3}$
Fluid - bulk modulus	0.142	MPa
Fluid - density	1.3×10^{-9}	$Kgmm^{-3}$

Table 5.3: Dimensions and material information (aluminum) of the cube model

The cube is just a structural component of the simulation. In order to calculate the acoustic intensities and pressure, an acoustic FE model must be developed. The (left-hand side) of figure 5.8 shows acoustic mesh developed around the outer surface of the cube. The nodes of acoustic mesh placed near the structures are tied with structural nodes. Therefore, the velocities of both the nodes at fluid structure interface are equal. Furthermore, the losses in acoustic quantities are developed using the volumetric drag, material and surface impedances. The right-hand side of figure 5.8 shows the excitation load of the structure. A load of unit magnitude across 0 to 5000 Hz is applied and later compared with the Frequency Response Function (FRF) plots of the experiment.

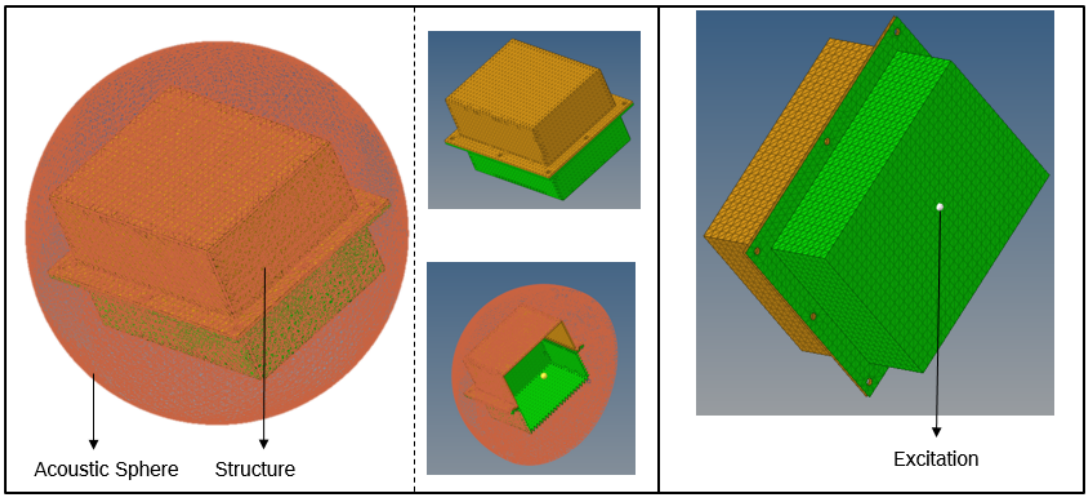

Figure 5.8: Acoustic mesh developed around the cube for harmonic analysis

5.3.2 Overview of Experimental Setup for Cube Structure

Figure 5.9 describes the setup used for analyzing the surface velocities using the experiments. Initially, the cube structures are excited with help of modal hammer at specific areas. Later, the acceleration sensors, vibrometers and acoustic camera are used for capturing the surface accelerations and acoustic pressures at critical areas determined. More information about these devices and complete schematics of the experiments are further discussed in section 6.2.1.

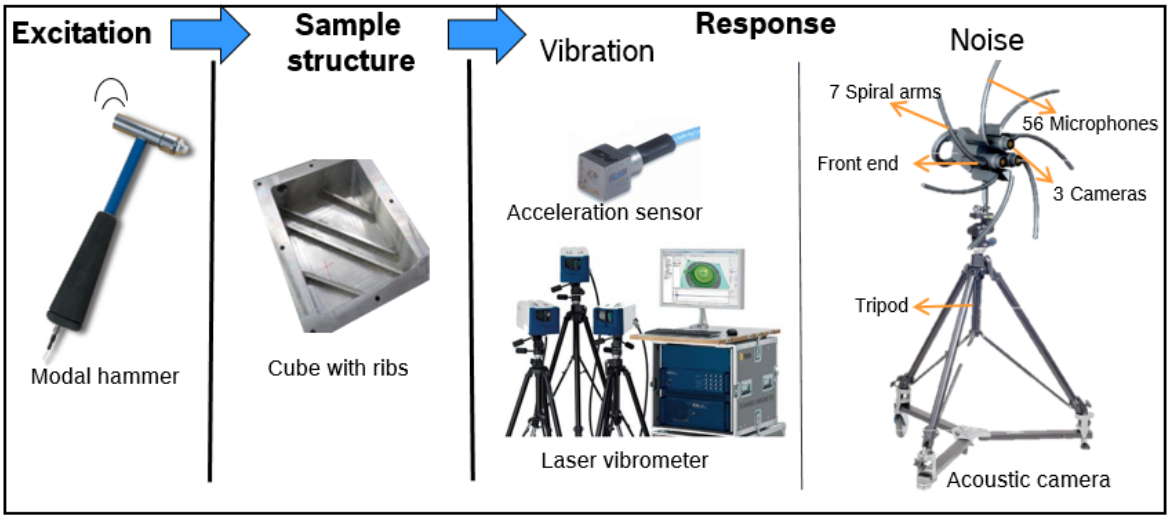

Figure 5.9: Experimental setup for calculating vibration and noise associated with the cube structure

5.3.3 Calculation of Surface Velocities

The method verification is carried out by means of experimental setups developed, instead of the analytical formulae. Initially, an Experimental Modal Analysis (EMA) (as described in section 5.3.2) is performed with the aid of different load profiles and later these values are compared with the modal analysis results of the FEM. Table 5.4 describes the values of frequencies and other properties considered to define the experimental setups and FE templates.

Name	Value	Unit
Frequency spectrum	50 - 5000	Hz
Sampling frequency	12500	Hz
Frequency resolution	1.5625	Hz
Windowing	Hanning	-
Noise type	White	-
Number of measurements (at each node)	40	-

Table 5.4: Properties of the experimental and simulation template for the cube model

Tables 5.5 and 5.6 describe the normalized Eigen modes obtained from the experiments, simulation, the difference between them and the damping of frequency points. Once the damping values obtained from the experiments are passed on to the simulation, a harmonic analysis step is defined and simulated for checking the kinematics of structure. Figures 5.10 and 5.11 show the displacement contour plots attained from the simulations and experiments. Keenly observing values of frequencies from the tables 5.5 and 5.6 or from the plots 5.10 and 5.11, it can be clearly seen that the inclusion of ribs (optimized structure) pushed the Eigen modes to a higher spectrum. E.g., the frequency value of mode 4 was initially at 0.487×SF1 Hz and after the improvement it was pushed to 0.507×SF1 Hz. This corresponds to a relative increase of 4.7%.

Eigen modes	EMA Frequencies × SF1 (Hz)	FEA Frequencies × SF1 (Hz)	Percent diff (%)	Damping (%)
Mode 1	0.213	0.209	1.88	0.304
Mode 2	0.236	0.230	2.79	0.281
Mode 3	0.380	0.377	0.95	0.445
Mode 4	0.487	0.479	1.62	0.431
Mode 5	0.536	0.539	0.60	0.740
Mode 6	0.607	0.603	0.74	0.547
Mode 7	0.649	0.639	1.45	0.244
Mode 8	0.665	0.664	0.21	0.218
Mode 9	0.735	0.736	0.12	0.279
Mode 10	0.902	0.907	0.58	0.240

Table 5.5: Eigen frequencies of cube model without ribs scaled by a factor SF1

Eigen modes	EMA Frequencies × SF1 (Hz)	FEA Frequencies × SF1 (Hz)	Percent diff (%)	Damping (%)
Mode 1	0.221	0.225	2.04	0.190
Mode 2	0.367	0.369	0.49	0.780
Mode 3	0.426	0.427	0.31	0.230
Mode 4	0.507	0.521	2.86	0.500
Mode 5	0.632	0.632	0.00	0.530
Mode 6	0.738	0.738	0.00	0.600
Mode 7	0.782	0.776	0.82	0.530
Mode 8	0.807	0.806	0.17	0.300
Mode 9	0.829	0.830	0.11	0.520
Mode 10	0.897	0.899	0.25	0.390

Table 5.6: Eigen frequencies of cube model with ribs scaled by a factor SF1

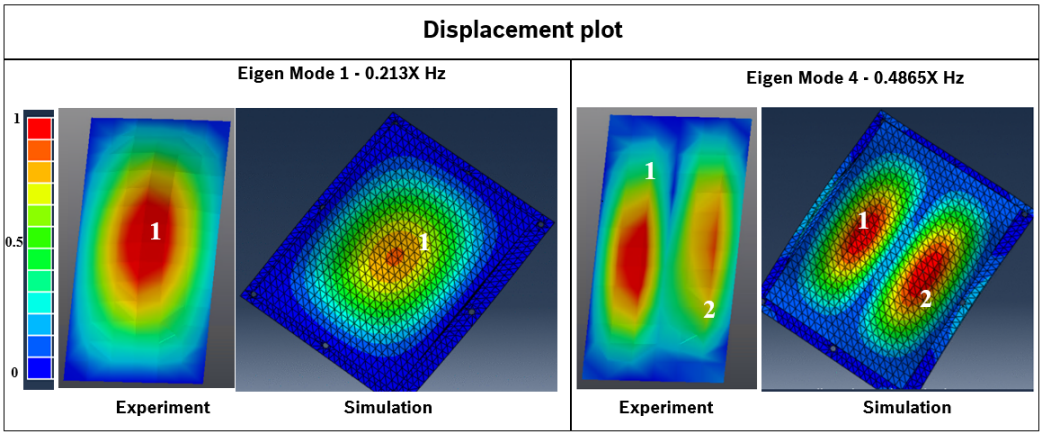

Figure 5.10: Displacement contour plots of Eigen mode 1 and 4 for the simple cube model. Experiment setup is described in sections 5.3.2 and 6.2.1.

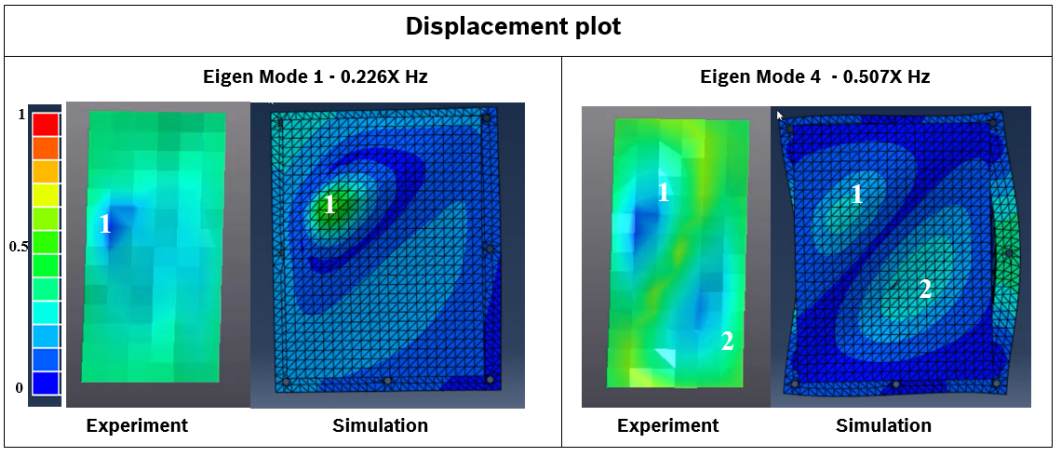

Figure 5.11: Displacement contour plots of Eigen mode 1 and 4 for the optimized cube model. Experiment setup is described in sections 5.3.2 and 6.2.1.

The graphs in diagram 5.12 illustrate response function plots of surface velocities for experiment vs. simulations (for the simple and optimized model). The simulation values are slightly more damped in comparison to the experiments, but the differences are well below 5% limits and hence these models are considered for further comparisons.

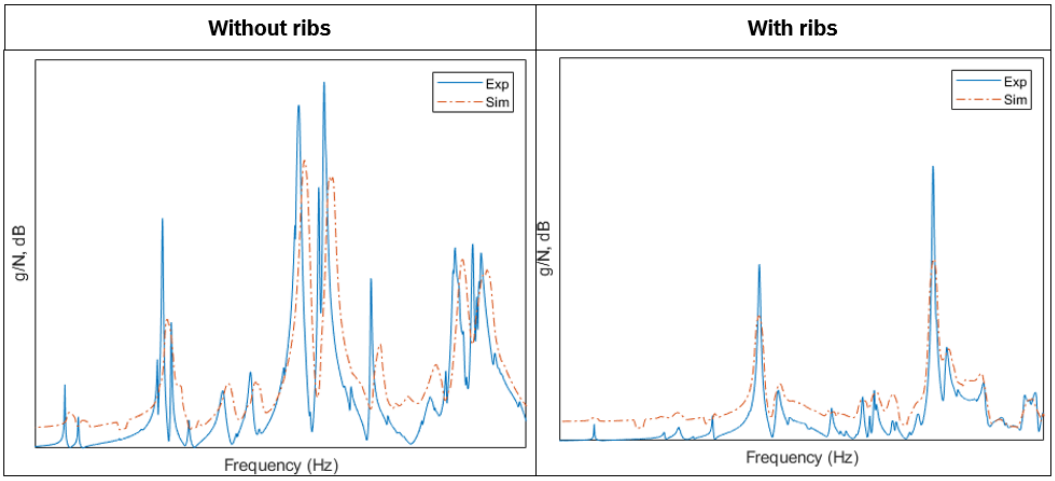

Figure 5.12: Vibration FRF plots of experiments and simulations for simple and optimized model represented with same y-axis limits. Experiment setup is described in sections 5.3.2 and 6.2.1.

5.3.4 Calculation of Acoustic Quantities

With the similar blueprint as in earlier section, the acoustical quantities are juxtaposed for comparison between the experiments and simulations (check figures 5.13 and 5.14). The volumetric drag and surface impedance (at the fluid structure interface) are modified to obtain the loss effects.

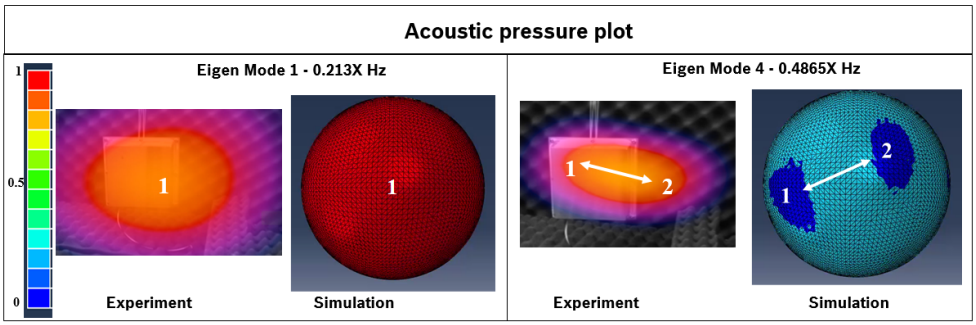

Figure 5.13: Acoustic contour plots of Eigen mode 1 and 4 for the simple cube model. Experiment setup is described in sections 5.3.2 and 6.2.1.

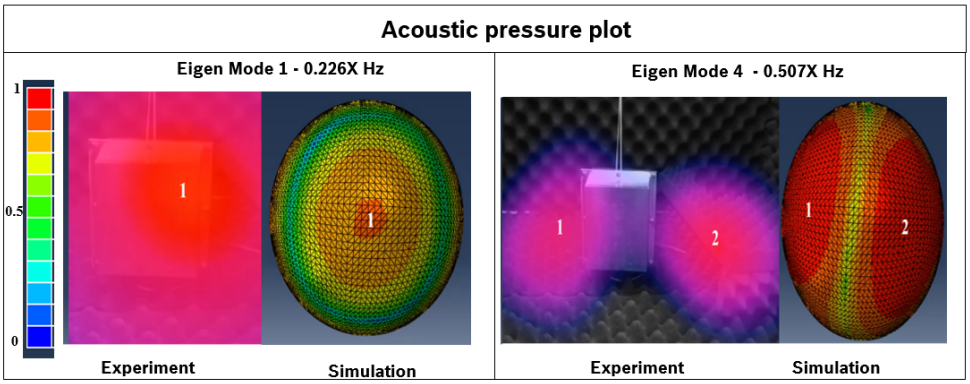

Figure 5.14: Acoustic contour plots of Eigen mode 1 and 4 for the optimized cube model. Experiment setup described in sections 5.3.2 and 6.2.1.

The plots in figure 5.15 describe FRF plots of acoustic pressure for the experiment vs. simulation measured with microphone at a distance of 500mm. There were few problematic frequency spectra where the simulation results are slightly deviated. This can be attributed to the fact that experiments conducted are in real time conditions with discrepancies like calibration errors etc., whereas the simulations performed are under ideal conditions.

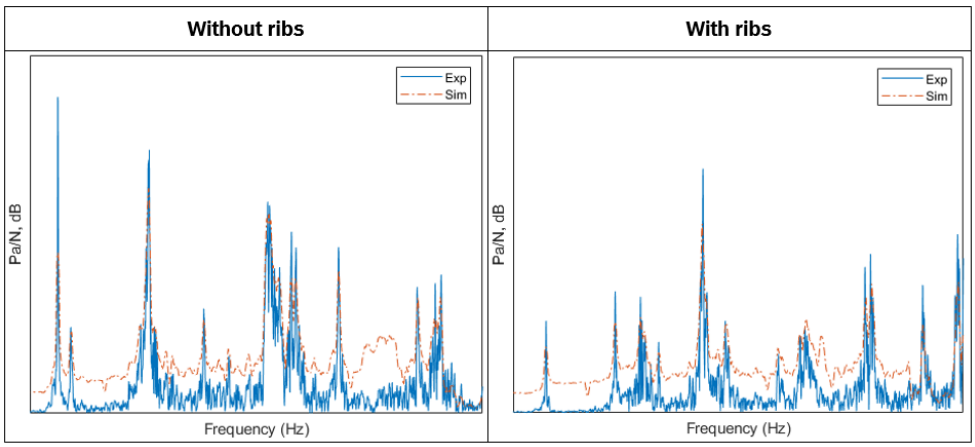

Figure 5.15: Sound FRF plots of experiments and simulations for simple and optimized model represented with same y-axis limits. Experiment setup is described in sections 5.3.2 and 6.2.1.

Finally, graph 5.16 shows improvements brought by ribs in a holistic view. The graph is obtained

by summing the FRF values of all the nodes for simple and optimized cube models. The optimized model had 19.31% less vibrations than that of the simple cube. Therefore, it can be said that the addition of ribs improves the dynamics of the structure.

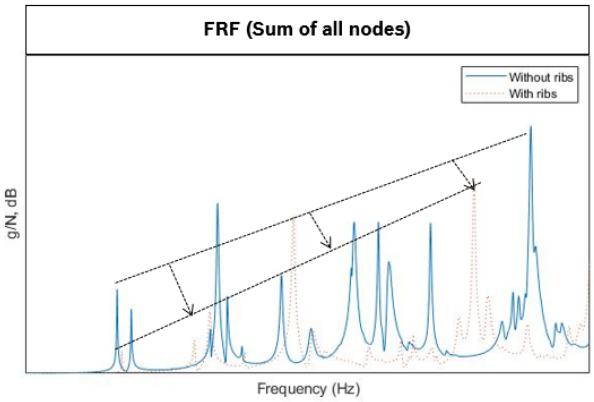

Figure 5.16: FRF plots as sum of all nodes on the surface of structure (ribs vs. without ribs). Experiment setup is described in sections 5.3.2 and 6.2.1.

Overall, the simulation frequencies are in the proximity of EMA values with a maximum difference of 2.86% (check tables 5.5 and 5.6). Furthermore, the simulation amplitudes fit well with that of the experiments (with an average difference of 5.45%). Hence, this method can be considered as an acceptable approach to analyze the drivetrain structures.

5.4 2D FE Model of Wear

So far, the modeling instances aided in comprehension of multi-domain modeling and that of the FE methodologies developed from chapter 4. These sections concentrated on dynamic behaviors of the structure. The next instance helps in understanding the abrasion mechanism of the gears. As part of the methodology, scripts developed in section 4.5.2 must be better comprehended. For this reason, a 2D gear model is developed and simulated. Figure 5.17 shows the gear model instance created.

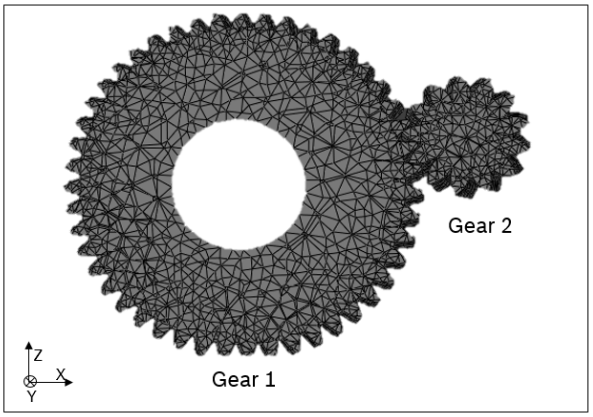

Figure 5.17: 2D diagram of gear mesh model used for wear calculations

Below are the boundary and load definitions for the problem, where U1, U2, U3, UR1, UR2 and UR3 correspond to DOF translation X, Y, Z and rotation X, Y, Z respectively:

- Gear 1 − Fixed about DOF (U1=U3=UR1=UR2=UR3=0).

- Gear 2 – Fixed about DOF (U1=U3=UR1=UR2=UR3=0).
- Gear 1 – Torque about the y-axis (M2=Constant).
- Gear 2 – Rotational velocity about the y-axis (UR2=Constant2).

The values in table 5.7 describe the wear obtained from the subroutine defined in figure 4.36 vs. values calculated analytically. The first column Inc. represents the increment. Further columns in the table indicate K-factor, contact pressure and contact slip respectively. From the results, it can be interpreted that the model code developed agrees completely with the analytical solution and hence can be used for the 3D gear geometries of the drivetrain.

		Subroutine Values				**Analytical Formula**
Inc.	**Torque**	**K-factor**	**Pressure**	**Slip**	**Wear (at node)**	**Wear**
	N · mm		MPa	mm	mm	mm
1	0	4.00E-5	274.42	0.00E+00	0	0
2	120	4.00E-5	228.85	8.42E-03	7.72E-05	7.72E-05
3	300	4.00E-5	194.24	8.23E-03	1.40E-04	1.40E-04
4	620	4.00E-5	182.01	8.14E-03	2.03E-04	2.03E-04
5	950	4.00E-5	171.29	8.06E-03	2.56E-04	2.56E-04
6	1200	4.00E-5	146.92	7.86E-03	3.02E-04	3.02E-04
7	1600	4.00E-5	147.77	7.86E-03	3.50E-04	3.50E-04
8	2100	4.00E-5	165.51	8.01E-03	4.02E-04	4.02E-04
9	2500	4.00E-5	166.39	8.02E-03	4.55E-04	4.55E-04

Table 5.7: Wear calculated with Fortran code used for the FE simulation vs. analytical formula

5.5 Interim Conclusion

From the need to predictively analyze transmission components in terms of vibro-acoustic behavior in the overall system and to perform numerical parameter studies, different system, transmission and FE model requirements are defined. Based on this, various methods for modeling and simulation of physical mechanisms could be evaluated. The result showed that, none of the techniques singly meet all the requirements. Consequently, a complex simulation process is developed in the form of a generic, multi-domain methodology for mapping vibro-acoustic and wear mechanisms in drive units. After a detailed presentation of individual model components, a modeling instance is created in Simscape and Abaqus. Later, the numerical verification of the methods is also attempted. The instances enable vibro-acoustic analysis of gearboxes, abrasion at gear surfaces, optimization of individual system parameters and the prediction of system states.

By integrating individual methods as a physical network and FE template decks, developers of other domains gain easy access to the simulation model. The modular and extensible execution of functions such as those of the ideal and physical transmission allow the mapping of different stages of product development. The reusability of model parts also allows the analysis of different component layouts. Finally, the computation time depends on the investigated system and the flow chosen from figure 4.24.

6 Validation of the Method using an Example Drive Unit

This chapter aims to analyze a three-stage gearbox for vibro-acoustic system using the methods from chapter 4 and techniques used for modeling instances from chapter 5. Figure 6.1 shows the different sections described in this chapter.

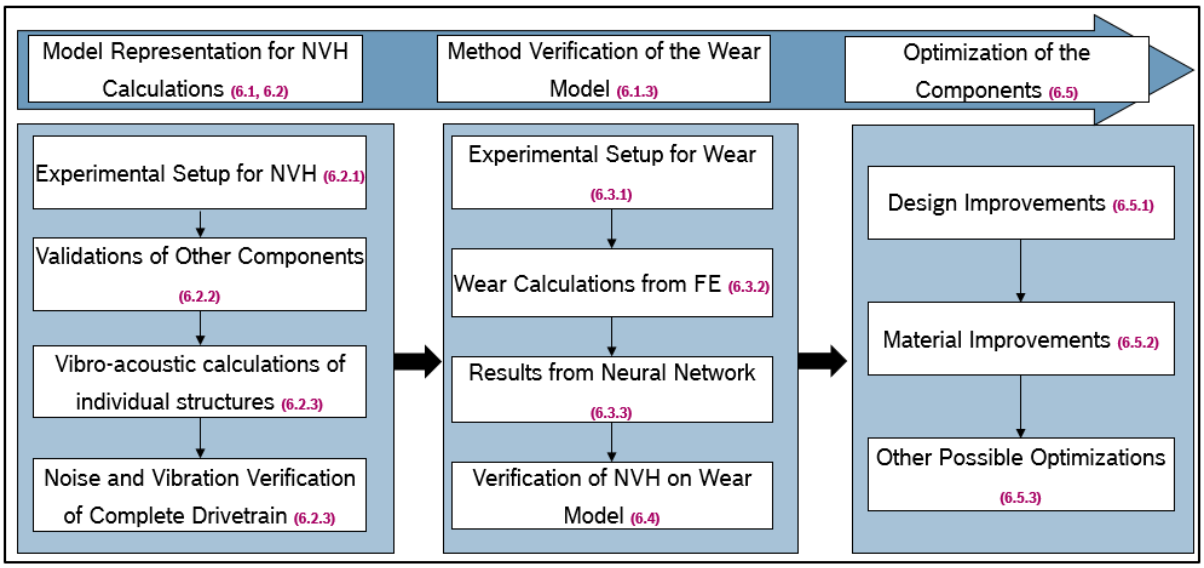

Figure 6.1: Brief overview of the sections and flow within chapter 6

Points that are discussed in this chapter are mainly the excitation of gears and motor, the dynamics of drivetrain components, vibration of the housing structure and the sound emission that is mapped into the surrounding fluid. For model validation, engine torques, engine speeds, surface velocities and acoustic pressure measurements are used as system quantities. Eventually, the experimental validations for surface vibrations and acoustic fluctuations are performed with the aid of a laser vibrometer and an acoustic camera. Subsequently, numerical analysis and also the selection of potential system optimizations will be demonstrated on basis of the model.

6.1 Model Representation

The assumptions made when creating a three-stage gearbox are explained. Subsequently, the model topology and the determination of model parameters are presented.

6.1.1 Model Assumptions

Below is a list of assumptions considered to build the modeling instance of drivetrain:

- Viscous dampings at gears and material dampings at housings.
- Small deflections of vibration amplitudes at housings.

- No backward coupling from acoustic to vibrations at fluid structure interface.
- Wear only at one tooth in simulation.
- Wear at single area (as a patch) on a tooth instead of multiple regions.
- Ideal power supply from motor.
- Experiment deviations (noises) are not considered in simulation.

6.1.2 Model Topology

The model topology of the three-stage gear unit is described in 6.2. The gears and toothed shafts are indicated with an alphabet "Z". In addition to the gear stages, the diagram includes bearings, clutch, brake, housing, the electric motor and its control [KDH19a].

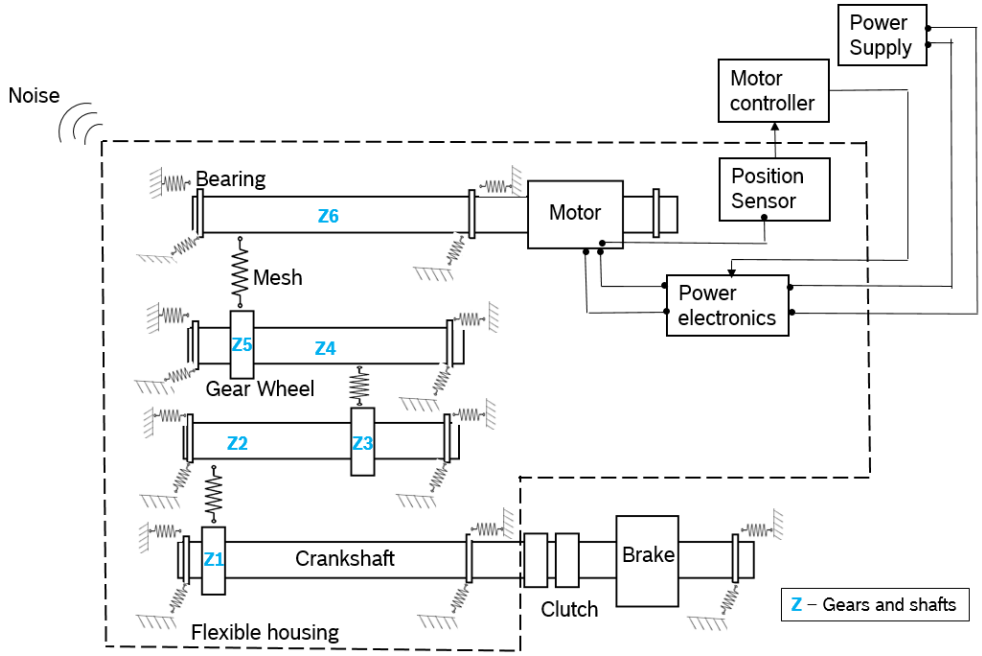

Figure 6.2: Model layout of the three stage drive unit with associated power electronics

The topology in computer is developed using softwares like Hypermesh, Abaqus, SimMechanics etc., and methods discussed from the previous sections (modeling instances). Furthermore, the extensions of dynamic gearbox model (section 4.4.2.1), the housing oscillation (section 4.4.2.3) and the sound emission model (section 4.4.2.4) are used as model components to understand the NVH characteristics.

6.2 Method Verification of the NVH Model

This section describes the test setups built to understand the structure and airborne emissions of drivetrain components. Furthermore, in order to build robust numerical models, validations like stiffness and stress analysis of the components are described. In the end, numerical solutions obtained from the methodologies developed are verified with experimental data.

6.2.1 Experimental Setup for NVH

Different profiles and combinations of RPM and motor torque are considered as inputs for the experimental runs and later are used for simulations as well. The experiments are conducted for

three different load definitions. Each of them can be identified using RPM and torque profiles as described below. More information of the test cases is described in table 6.3.

- Load case 1 - time[0 30] sec; torque= 2.4 N · m; speed= 2500 RPM.
- Load case 2 - time[0 50] sec; torque= 1.4 N · m; speed= 4300 RPM.
- Load case 3 - time[0 50] sec; torque= 0.0 N · m; speed= 4400 RPM.

Polytec laser vibrometer assists the measurement of exterior vibrations on the housing and cover surfaces [Tec19]. Alongside with vibrometer, acceleration sensors are also placed at critical points for better precision of results. The absorber box in figure 6.3 is used to isolate the powertrain vibrations from the rest. The power unit is connected to CANape via the Human Machine Interface (HMI) and the magnetic brakes equipped within the system. Different loads for the drivetrain can be defined and controlled using the CANape software [CAN19]. The different form of the dashed lines indicate the surface velocities and recorded acoustic fluctuations. Acoustical characteristics like pressure are measured using the acoustic camera (from Head acoustics) and microphones mounted at distances of 500 mm and 1000 mm [Aco16]. LMS software serves as a central node to send and control the force reference signals and also record the vibrations and noises [Sie15]. In the end, after the analysis of multiple DU variants for different kinds of torque and RPM profiles, the Campbell and spectral plots are generated.

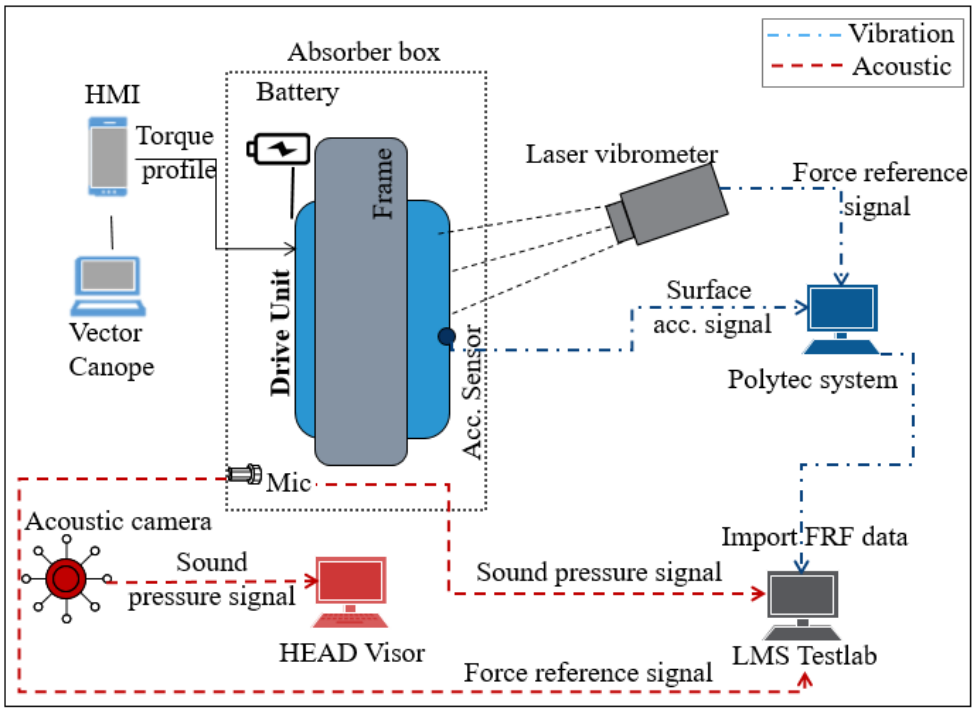

Figure 6.3: Experimental setup for measuring surface vibration and noise of the drive unit described in figure 6.2

6.2.2 Validation of Other Model Components

Before analyzing the drivetrains for their structure borne emissions, the numerical models built must be robust enough to capture the complexities and hence, few validations like stress-strain analysis of the components are performed to make sure there are no damages, failures or high deformations in critical areas. This part mainly addresses the points mentioned in 4.4.2.2.

Bearing study for equivalent spring stiffness

Here the rollers of bearing are replaced by equivalent springs to reduce the computations and eradicate the convergence problems which can arise from the rollers. Figure 6.4 illustrates the bearing assembly considering one roller (since it is symmetrical). For non-disclosure purpose the roller profile is modified from spherical to cylindrical.

Below are the boundary definitions for the problem, where U1, U2, U3, UR1, UR2 and UR3 correspond to DOF translation X, Y, Z and rotation X, Y, Z respectively:

- Inner bearing – Fixed about vertical edges at center (U1=U3=0).
- Roller – Fixed about vertical edges at center (U1=U3=0).
- Outer bearing – The topmost face is encastred (U1=U2=U3=UR1=UR2=UR3=0).

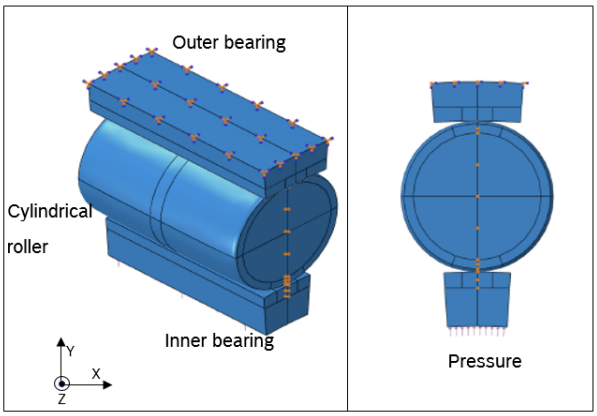

Figure 6.4: Simulation model for the bearing study. More information in section 4.4.2.2

A static simulation step is created with a pressure load of 50 to 200 N/mm^2. Following the simulation, deformations and stresses obtained at the roller are used to calculate the stiffness values of the components and apply them to the equivalent spring model.

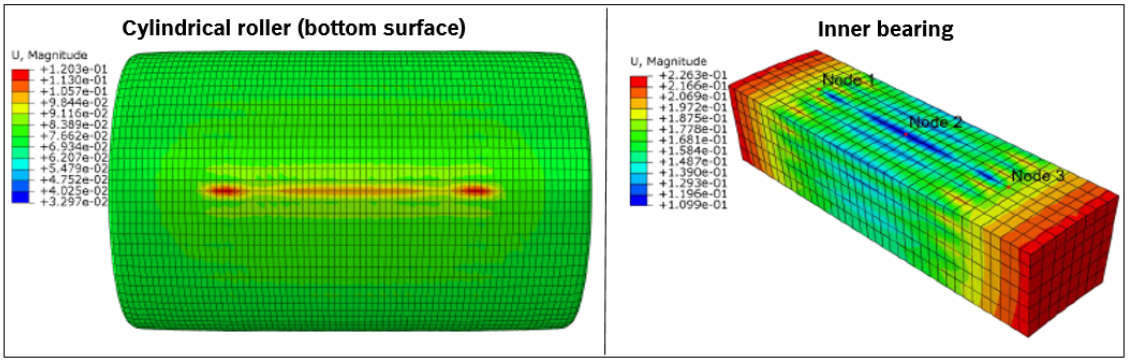

Figure 6.5: Deformations at roller (bottom surface) and inside bearing displayed in mm

Figure 6.5 describes the displacement contours obtained at the cylinder roller and the inner geometry. The deformations obtained from the interface nodes (check table 6.1) and forces are used to calculate the equivalent stiffness of the roller. For this particular load case and for few particular points (node 1, 2, 3), as described in figure 6.5, the stiffness calculated is given in equation 6.1, where the values in numerator and denominator correspond to the force and deformation respectively.

Time (Sec)	Node 1 (mm)	Node 2 (mm)	Node 3 (mm)
0.1	5.95E-02	4.49E-02	5.88E-02
0.2	7.78E-02	5.42E-02	7.82E-02
0.3	9.41E-02	6.25E-02	9.35E-02
0.4	1.08E-01	7.00E-02	1.08E-01
0.5	1.22E-01	7.74E-02	1.22E-01
0.6	1.35E-01	8.43E-02	1.35E-01
0.7	1.47E-01	9.09E-02	1.48E-01
0.8	1.60E-01	9.74E-02	1.60E-01
0.9	1.73E-01	1.04E-01	1.73E-01
1	1.86E-01	1.10E-01	1.87E-01

Table 6.1: Deformations at nodes of inner bearing defined in figure 6.5

$$
\begin{aligned}
K_{node1} &= \frac{(100000 - 10000)}{(0.186 - 0.0595)} = 711462.45\ N/mm \\
K_{node2} &= \frac{(100000 - 10000)}{(0.11 - 0.0449)} = 1382488.50\ N/mm \\
K_{node3} &= \frac{(100000 - 10000)}{(0.187 - 0.0588)} = 702028.08\ N/mm
\end{aligned}
\tag{6.1}
$$

Finally, figure 6.6 describes the stress profiles obtained for inner bearings with rollers and with springs. There is a small difference of 2.8% in the values. It can be argued that this is effected due to the amount of springs present. A design sensitivity analysis should be further studied to reduce the deviations in stresses and deformations of this particular bearing simulation.

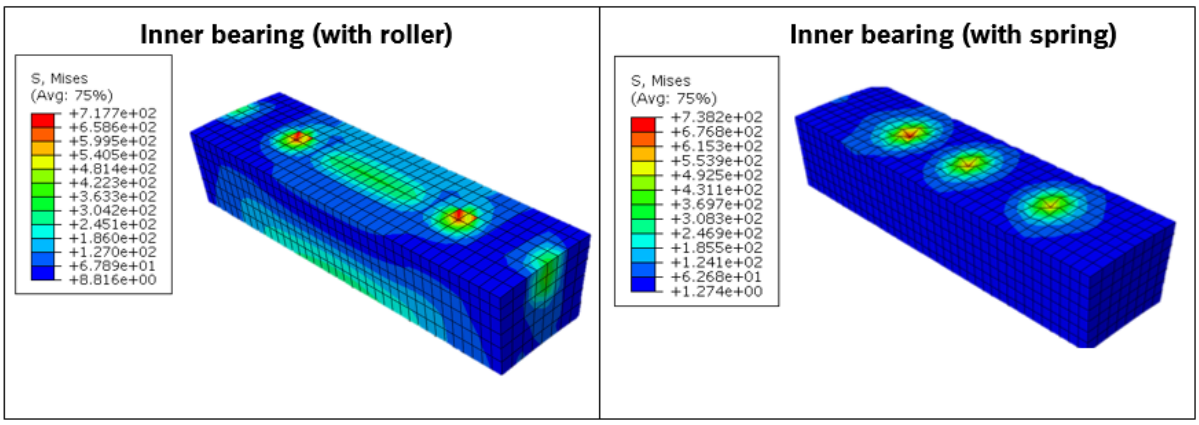

Figure 6.6: Von-Mises stress of inner bearing (with roller vs. with springs)

Stress-strain and stiffness analysis

This section describes the stiffness analysis performed on few of the components to comprehend their structural behavior under different load cases. Larger deformations in them would impact the NVH characteristics and therefore it is necessary to perform these simulations. Figure 6.7 describes the design layout of the gears, shafts and the housing components which influence the vibrations. More information is given in section 4.4.2.2.

Critical areas to analyze in the drivetrains regarding deformations are housing and covers. The following is a list of combinations which are analyzed for their stresses and deformations:

- Outer housing + Outer cover
- Inner housing + Inner cover
- Outer housing + Inner housing + Inner cover
- Inner housing + Inner cover + Gears + Shafts (= Gear box)

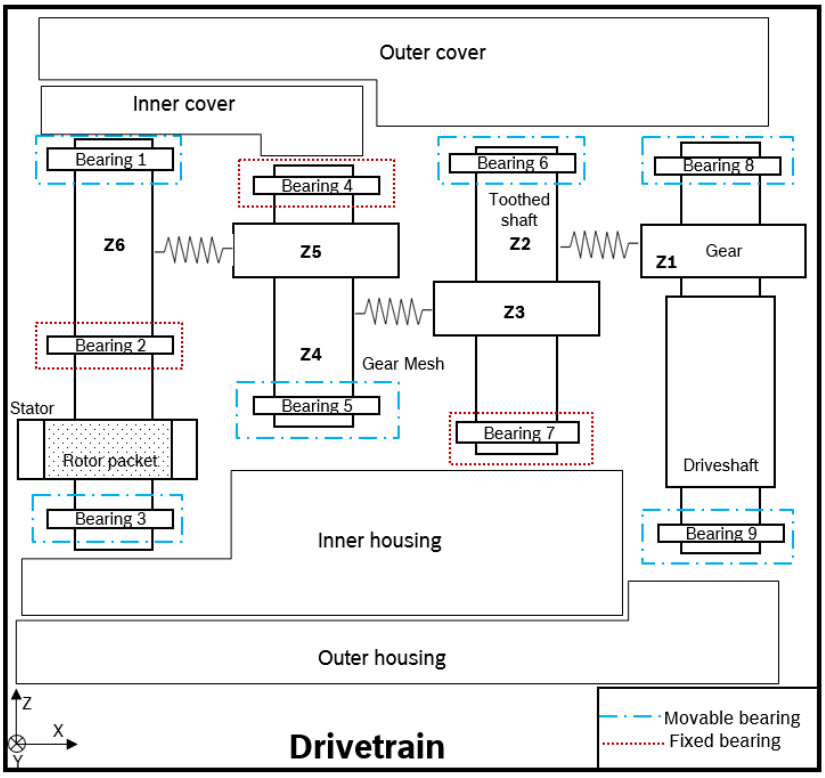

Figure 6.7: Architectural layout of housings, gears, toothed shafts and bearings of the drivetrain

For each of the problem, appropriate loads and boundaries are defined to check for the deformations and stiffness values. The list of displacements and von-Mises stresses obtained for these combinations is shown in table 6.2. For all the analyses, a static solution is defined neglecting inertia effects. Detailed load points, constraints and result plots are not illustrated due to the non-disclosure agreement.

Combined structures	Maximum deformation (mm)	Maximim von-Mises stress (MPa)	Yield stress (MPa)
Outer housing + Outer Cover	1.54E-01	82.65	150
Inner housing + Inner cover	2.38E-02	60.23	160
Outer housing + Inner housing + Inner cover	3.12E-02	73.68	150
Inner housing + Inner cover + gears + shafts	1.87E-02	45.69	160

Table 6.2: Deformations and stresses induced in the structures for their respective load cases

It can be clearly seen that the model doesn't undergo any plastic deformations. Hence, it can

be directly analyzed for the vibration module for free state analysis. Furthermore, the results obtained in this step (table 6.2) can be transferred to the next step to analyze the structure borne emissions in a loaded/ excited environment.

Study of influences of the rotor moments on to the bearings
The other analysis performed with bearings at its center is the influence of shaft moments on to the associated bearings. The model illustration for the three stage drivetrain with bearings is already shown in figure 6.7 (shafts, gears and connected bearings). It is built with the principles mentioned in section 4.4.2.2. The boundaries applied to the bearings are either fixed, thus Z-axis rotation is free, or movable, thus Z-axis translation and rotation is free (check figure 6.7). Apart from the load profiles defined in section 6.2.1, simulations are executed for an extra load i.e., case4. It is defined to check for the worst possible scenario with application of maximum torque (check table 6.3).

	Shafts	**Torque (N · m)**	**RPM**
Load case 1 (High Torque)	Rotorshaft	0.026	0.578
	RE4	0.093	0.160
	RE2	0.250	0.059
	Crankshaft	0.868	0.017

	Shafts	**Torque (N · m)**	**RPM**
Load case 2 (Low Torque)	Rotorshaft	0.011	0.991
	RE4	0.038	0.274
	RE2	0.103	0.100
	Crankshaft	0.357	0.029

	Shafts	**Torque (N · m)**	**RPM**
Load case 3 (No Torque)	Rotorshaft	0.000	1.000
	RE4	0.000	0.277
	RE2	0.000	0.101
	Crankshaft	0.000	0.029

	Shafts	**Torque (N · m)**	**RPM**
Load case 4 (Worst case)	Rotorshaft	0.031	0.494
	RE4	0.109	0.137
	RE2	0.292	0.050
	Crankshaft	1.000	0.014

Table 6.3: Load cases for the drive unit along with torques of other shafts (scaled)

The stress values obtained are well below the plastic limit proven by the yield stress limit of 550 MPa according to table 6.4. Hence, the bearings modeled can be directly used for numerical simulation of vibrations.

	von-Mises stress (MPa)			
	Worst Case	**High Torque**	**Low Torque**	**No Torque**
Bearing 1	122.22	96.24	76.25	0.10
Bearing 2	210.25	183.10	127.11	0.19
Bearing 3	175.76	130.25	98.21	0.12
Bearing 4	120.32	90.80	78.21	0.11
Bearing 5	75.00	68.45	53.21	0.08
Bearing 6	45.31	41.28	32.00	0.05
Bearing 7	67.28	53.65	44.63	0.07
Bearing 8	30.21	27.32	22.18	0.00
Bearing 9	28.10	21.43	19.21	0.00

Table 6.4: Von-Mises stress values of the bearings displayed in figure 6.7

Furthermore, the ideal gear model from the SimMechanics standard library cannot display translational forces. As a result, the bearing force is zero. This problem can be bypassed with the

aid of dynamic gear model developed in section 4.4.2.1 and 5.2.1. This gear model would help in calculation of the dynamic translational bearing forces at each of the axles.

The force profiles of the rotorshaft and crankshaft for different load cases are detailed in figure 6.8 and 6.9. In the figures shown, six and three maxima can be counted for the load case 1 and 2 respectively. This is to be expected when the speed is halved, since the number of tooth meshings are halved and thus also internal excitation impulses take place within the same time period. The average bearing force increases by approximately 3.2% for load case 1 compared with load case 2.

Furthermore, it can be stated that the difference between minimum and maximum force values is approximately 60 to 160 mN (for load case 1 of figure 6.8). These values describe the dynamic force which causes the housing to vibrate. The corresponding dynamic forces for the output shaft are lower in comparison to the rotor shaft. Although the viscous damping is reflected in the same way, the high frequency components are hardly noticeable. As a result, the dynamic excitation of the housing structure by the last gear stage is significantly less.

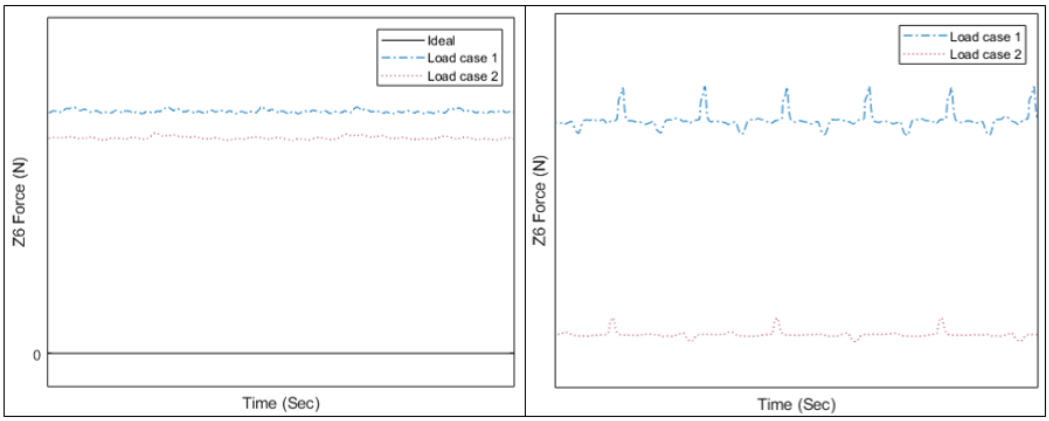

Figure 6.8: Representation of the axial bearing forces at Z6 shaft (check figure 6.2) of the ideal and dynamic gear model for load case 1 and 2 from the table 6.3

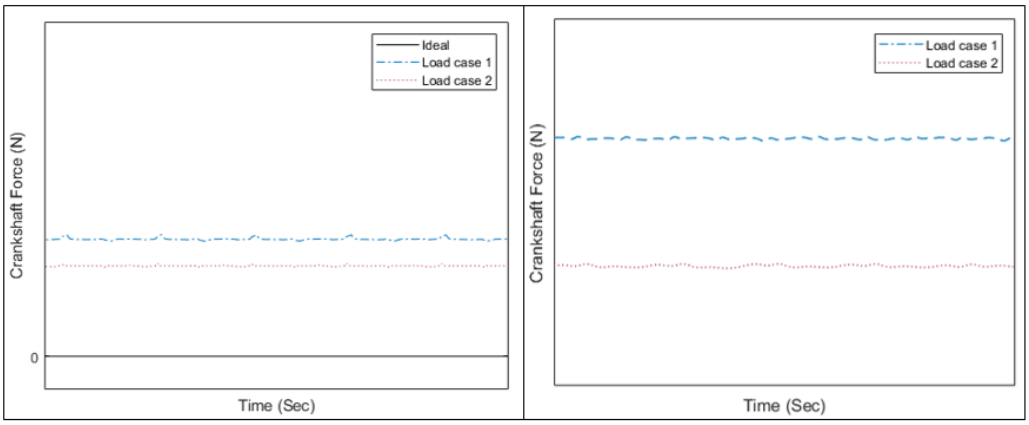

Figure 6.9: Representation of the axial bearing forces at crankshaft (check figure 6.2) of the ideal and dynamic gear model for load case 1 and 2 from the table 6.3

These reaction forces obtained along the time domain at each of the axle are converted to frequency domain. These values are later used for forced excitation of the housing structures and thereby obtaining the vibrations for different load profiles.

Figure 6.10 describes the axial forces in frequency spectrum obtained at drivetrain and Z2 axles for load case with low torque (table 6.3). The position of each axle can be returned by means of figure 6.2. Note that the frequency scale can be replaced alternatively with order spectrum as well.

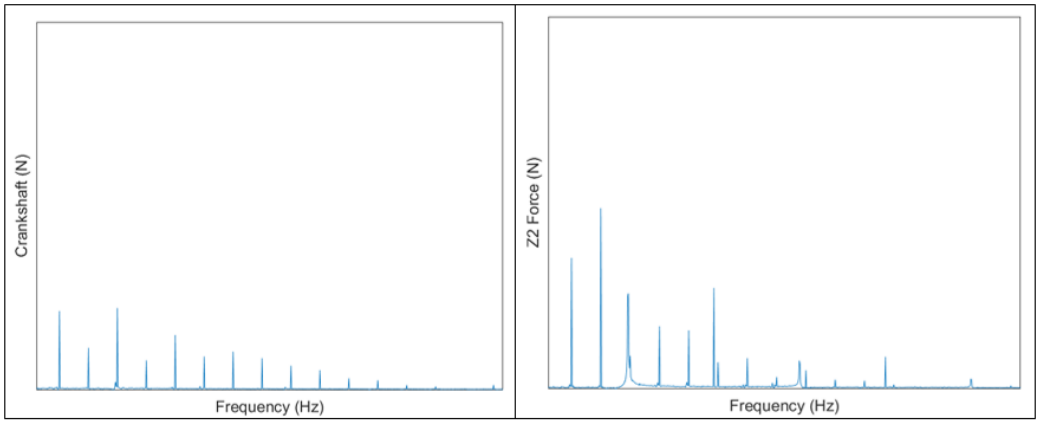

Figure 6.10: Axial forces at crankshaft and Z2 axles converted in frequency domain for load case 2 from the table 6.3

Figure 6.11 illustrates the forces for Z4 and rotor shaft axles. As already mentioned, the dynamic forces are high for the rotor shaft and thus the amplitudes are also higher compared to Z4 axis forces.

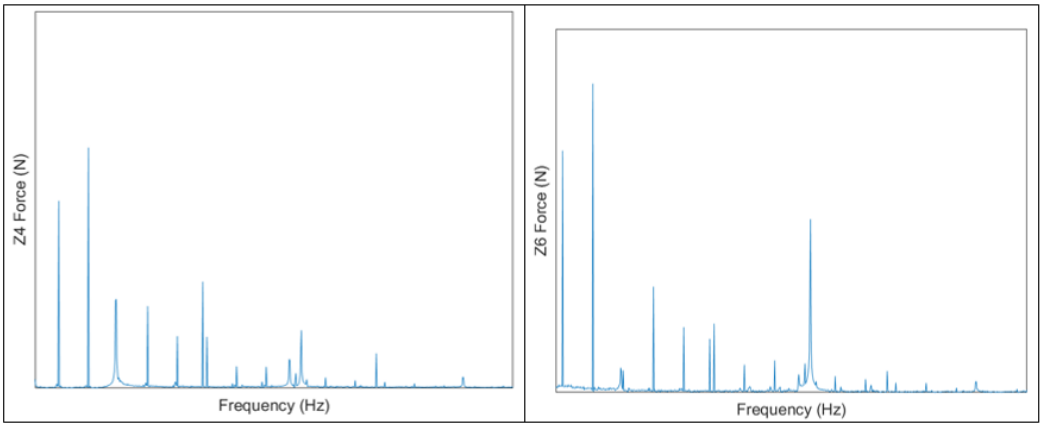

Figure 6.11: Axial forces at Z4 and Z6 axles converted in frequency domain for load case 2 from the table 6.3

Contact analysis

When using the multi-domain technique (check section 4.4.3) for comprehension of NVH characteristics, KISSsoft design software is used for obtaining the contact stiffness values [KIS16]. It aids in finding the values in faster time frames unlike FE analysis (and therefore used for multi-domain approach).

The tooth geometry of the gears is generally modeled using KISSsoft software. This creates a * .Z12 file. Using the contact analysis tool, the total stiffness can be calculated and exported as a text file. The excitation curves can be transferred into Fourier coefficients. The first ten Fourier coefficients are shown for the three gear stages in figure 6.12 and they serve as input parameters for the dynamic gearbox model (y-axis is of the same limits for all the three plots). Note that the same amount of load is applied on each of the shafts for comparison of deviations among the

gear meshes. The reason for obtaining higher amplitudes for the first gear stage is due to the presence of spur gear profile. Whereas the second and third gear stages are built as helical gears, which reduces the amplitudes of orders. Furthermore, KISSsoft does not include the calculation of gear damping d_z. This is calculated by equation 6.2, where D_z, b_z, k_z and m_{red} describe the degree of damping, tooth width, average meshing stiffness and equivalent mass relative to the mesh plane respectively [LB10].

$$d_z = 2D_z b_z \sqrt{k_z m_{red}} \tag{6.2}$$

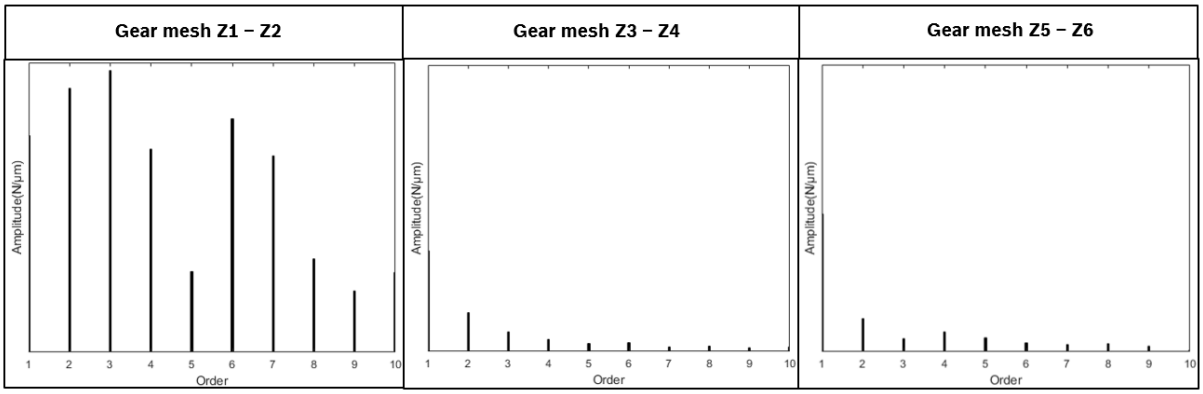

Figure 6.12: Fourier coefficients of the overall stiffness of the 1st, 2nd and 3rd gear stage of the dynamic model from figure 6.2. More information in section 4.4.2.2 (under Contact analysis among the gears).

When using the single domain (check section 4.4.3), a detailed contact analysis is performed in FE. Contact is form of nonlinearity and it influences both the dynamics of structural components and wear among the gears. Hence, various models built are initially brought to contact before researching the vibrational characteristics of the DU. As an example, the model from earlier section (tables 6.3 and 6.4) are extended with a contact step between the gear meshes. Eigen modes of the models are compared for their changes after contact. The exact values are described in table 6.12 (after introducing the concepts of structural vibrations in sec 6.2.3). One more topic concerned with contact is the convergence of the contact parameters like contact forces and contact pressures. Complete details with regard to convergence in contact studies are described in section 6.3.2.

Furthermore, the results of the damping elements introduced in section 4.4.2.2 are illustrated in section 6.5.2.

6.2.3 Vibro-acoustic Model Validation

Once the models are verified for instances (chapter 5) and made robust and plausible using the templates mentioned in section 6.2.2, an attempt to understand vibrations is made. As a part of it, the first step is to validate the model components for their natural frequencies. It falls into the section housing vibrations of figure 4.24. It aids in building the state space model for the housing structures in multi-domain approach and perform detailed harmonic analysis in the single domain approach.

Table 6.5 describes scaled masses, Young's modulus and yield limits of different structures available in the drivetrain. It sums up to about 92% of the total mass of the power unit. The structural validation of these components individually and combined would aid in understanding the vibrations of the entire drivetrain in later stages.

Component	Mass (Kg)	Young's modulus (MPa)	Plasticity limit (MPa)
Outer housing	0.086	0.119	0.140
Outer cover	0.068	0.119	0.140
Inner housing	0.027	0.119	0.140
Inner cover	0.009	0.119	0.140
Stator	0.268	0.952	0.651
Z1	0.063	1.000	1.000
Z2	0.065	1.000	1.000
Z3	0.019	1.000	1.000
Z4	0.010	1.000	1.000
Z5	0.015	1.000	1.000
Z6	0.023	1.000	1.000
Crankshaft	0.065	0.938	1.000
Driveshaft	0.044	0.933	0.940
Rotor packet	0.079	0.881	0.417
Brackets	0.045	1.000	0.515

Table 6.5: Modeling information of individual components shown in figure 6.7 (scaled)

Before analyzing the influences of forced vibrations originating from shafts, the structures are verified for natural states and simple excitations. Analyzing the complete drivetrain at the first go can be extremely hard due to numerous complexities associated in the system. Hence, it is advised to start with validations of the individual structures and slowly increase the complexities. Firstly, the individual structures described in figure 6.7 are simulated to find there natural frequencies (check table 6.6). The simulations focus only on the structures that can bring major impact on the dynamics of the drivetrain.

Eigen modes × SF2 (Hz)	Mode 1	Mode 2	Mode 3	Mode 4	Mode 5	Mode 6
Outer housing	0.021	0.030	0.040	0.050	0.058	0.064
Outer cover	0.023	0.030	0.055	0.058	0.067	0.080
Inner housing	0.049	0.060	0.087	0.107	0.117	0.132
Inner cover	0.054	0.078	0.094	0.152	0.157	0.193
Stator	0.035	0.036	0.036	0.040	0.042	0.046
Z1	0.118	0.118	0.152	0.152	0.308	0.308
Z2	0.482	0.482	0.666	0.829	0.830	0.945
Z3	0.268	0.269	0.457	0.465	0.465	0.607
Z4	0.454	0.455	0.724	0.725	0.774	1.000
Z5	0.444	0.445	0.559	0.559	0.759	0.975
Z6	0.110	0.110	0.272	0.272	0.302	0.454
Crankshaft	0.087	0.087	0.176	0.198	0.198	0.275
Driveshaft	0.185	0.186	0.237	0.238	0.243	0.243

Table 6.6: Simulated natural frequencies of the main structural components of the drivetrain that influence the dynamics with scale factor SF2

Values described in table 6.6 are scaled with a scale factor SF2. These simulations for individual structures often have modes above 5 kHz and don't require any experiments to validate as they are straight forward to calculate.

The problems and difficulties originate when the multiple components are simulated. Tables 6.7 and 6.8 describe the natural frequencies for different set of component combinations, slowly increasing the complexities.

Eigen modes × SF3 (Hz)	**Outer housing + Outer cover**	**Outer housing + Outer cover + Bearings**	**Outer housing + Outer cover + Brackets**
Mode 1	0.207	0.336	0.136
Mode 2	0.287	0.408	0.147
Mode 3	0.333	0.439	0.162
Mode 4	0.375	0.536	0.252
Mode 5	0.427	0.561	0.296
Mode 6	0.452	0.610	0.319

Table 6.7: Simulated natural frequencies of combined structures scaled with a factor SF3 - I

Eigen modes × SF3 (Hz)	**Inner housing + Inner cover**	**Outer housing + Inner housing + Connector elements**	**Outer housing + Motor**
Mode 1	0.372	0.186	0.148
Mode 2	0.483	0.324	0.298
Mode 3	0.756	0.356	0.328
Mode 4	0.802	0.409	0.344
Mode 5	0.901	0.428	0.405
Mode 6	1.000	0.487	0.454

Table 6.8: Simulated natural frequencies of combined structures scaled with a factor SF3 - II

Once the simulations for various structural combinations are executed, they are compared with experimental results. The test setups are described in section 6.2.1. Tables 6.9, 6.10 and 6.11 describe the natural modes obtained via the EMA, difference with simulation values and the damping factors calculated using the internal LMS software. LMS is a tool utilized to perform the EMA, more information is given in section 6.2.1. It is found that the frequencies calculated in simulations fit very well with the experiments as the percent difference is mostly below 5%. The next interesting question is to validate the amplitudes between the simulations and experiments.

Eigen modes × SF3 (Hz)	**Outer housing + Outer cover**			**Outer housing + Outer cover + Bearings**		
	Experiment (Hz)	Percent diff (%)	Damping (%)	Experiment (Hz)	Percent diff (%)	Damping (%)
Mode 1	0.210	1.30	1.97	0.342	1.73	1.26
Mode 2	0.293	2.09	2.25	0.412	0.88	1.35
Mode 3	0.332	-0.38	0.61	0.453	3.12	2.61
Mode 4	0.382	1.77	0.30	0.525	-2.05	4.51
Mode 5	0.427	-0.03	0.42	0.558	-0.47	0.42
Mode 6	0.458	1.13	1.24	0.596	-2.37	1.24

Table 6.9: Experimental Eigen frequencies, percent difference with the simulations and damping factor values of combined components of the drivetrain (which influence the dynamics) with scale factor SF3 - I

Eigen modes × SF3 (Hz)	Outer housing + Outer cover + Brackets			Inner housing + Inner cover		
	Experiment (Hz)	Percent diff (%)	Damping (%)	Experiment (Hz)	Percent diff (%)	Damping (%)
Mode 1	0.131	-3.86	0.17	0.370	-0.47	1.23
Mode 2	0.152	3.34	0.25	0.494	2.37	0.65
Mode 3	0.164	2.33	0.03	0.743	-1.75	3.51
Mode 4	0.266	1.45	3.21	0.786	-1.98	2.03
Mode 5	0.308	3.05	1.32	0.907	0.72	0.89
Mode 6	0.340	4.08	2.46	1.010	1.03	0.98

Table 6.10: Experimental Eigen frequencies, percent difference with the simulations and damping factor values of combined components of the drivetrain (which influence the dynamics) with scale factor SF3 - II

Eigen modes × SF3 (Hz)	Outer housing + Inner housing + Connector elements			Outer housing + Motor		
	Experiment (Hz)	Percent diff (%)	Damping (%)	Experiment (Hz)	Percent diff (%)	Damping (%)
Mode 1	0.187	0.40	0.25	0.143	-2.36	0.23
Mode 2	0.328	1.23	0.28	0.292	-2.29	1.35
Mode 3	0.356	0.00	0.29	0.327	-0.48	2.12
Mode 4	0.403	-1.69	0.16	0.339	-1.42	0.29
Mode 5	0.429	0.20	0.54	0.389	-4.10	0.98
Mode 6	0.486	-0.21	0.36	0.446	-1.80	1.19

Table 6.11: Experimental Eigen frequencies, percent difference with the simulations and damping factor values of combined components of the drivetrain (which influence the dynamics) with scale factor SF3 - III

Finally, table 6.12 describes influence of contact on to the vibrations. For model definition, refer to the part contact analysis in section 6.2.2. It can be observed that the natural frequencies are moved due to the contact between the components. The global stiffness of the assemblies is modified due to this nonlinearity. The result is a change of the natural modes.

Eigen modes × SF3 (Hz)	Model (Gears + Shafts + Bearings)	
	Before contact (Before Torque)	After contact (Load case 4)
Mode 1	0.083	0.088
Mode 2	0.121	0.116
Mode 3	0.130	0.128
Mode 4	0.152	0.149
Mode 5	0.159	0.179
Mode 6	0.173	0.200

Table 6.12: Shift in natural frequencies after contact between gears and shafts calculated using FEM. Load case 4 is shown in table 6.3

Surface velocities of combined structures

This part of the section illustrates vibration graphs obtained for the combinations defined in tables 6.9, 6.10 and 6.11. Plots in figure 6.13 illustrate the accelerations obtained for experiments and simulations for the combination "Outer housing + Outer cover" and "Outer housing + Outer cover + Bearings". The x-axes of the graphs represent the frequency spectrum of interest and y-axes represent the surface acceleration measured at the point of interest. The surface accelerations are displayed in decibel format for better representation and validation purposes.

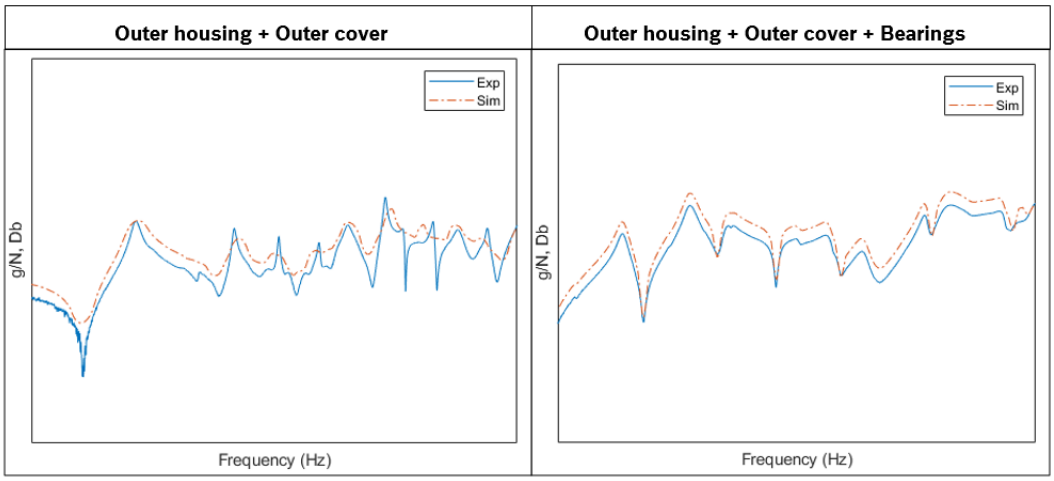

Figure 6.13: Surface velocity plots of "Outer housing + Outer cover" and "Outer housing + Outer cover + Bearings" obtained for their appropriate load cases (represented with scale factor SF3v). Simulation and experimental setup are described in sections 4.4.2.3 and 6.2.1 respectively.

For both left and right-hand side of figure 6.13 the resonant frequencies from the simulations match with the experiments but the amplitudes are found out to be slightly higher. The complete difference between the experiments and simulations is further described in table 6.13.

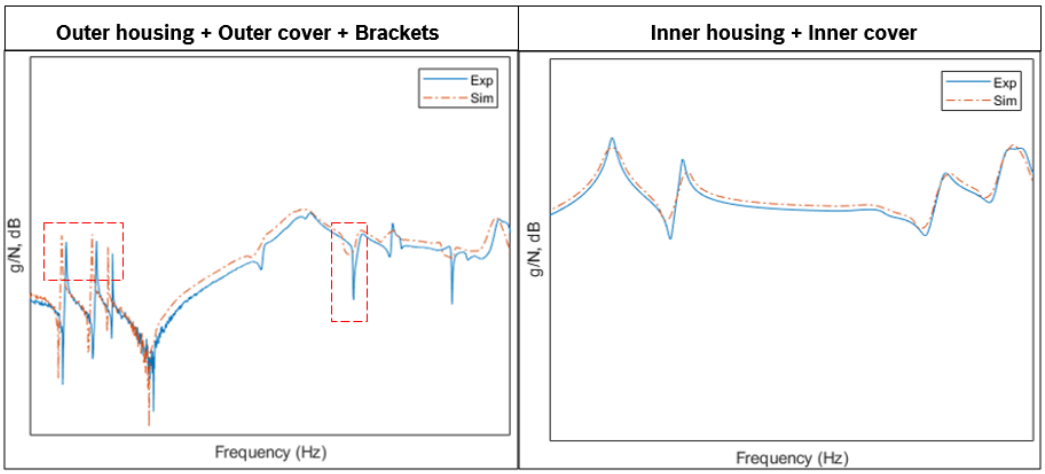

Figure 6.14: Surface velocity plots of "Outer housing + Outer cover + Brackets" and "Inner housing + Inner cover" obtained for their appropriate load cases (y-axis is represented with scale factor SF3v). Simulation and experimental setup are described in sections 4.4.2.3 and 6.2.1 respectively.

Similarly, plots in figure 6.14 describe the validations for "Outer housing + Outer cover + Brackets" and "Inner housing + Inner cover". The left-hand side plot has few resonant frequencies, which are slightly displaced from the experiment values. The deviations in FRF plots can arise due to the complexities in material properties like stiffness and damping coefficients or the intricacies in geometries. In this case, the material level damping parameters present in the models are responsible for these shifts. But as they fall within the acceptable limits, the values are considered for further simulations.

Furthermore, plots in diagram 6.15 illustrate the last two examples "Outer housing + Inner housing + Connector elements" and "Outer housing + Motor". The y-axis is again represented with scale factor SF3v. Except for one or two frequency ranges, the simulation amplitudes for both plots fit well with those of the experiments and hence the model parameters can be accepted and further used for simulations of complete drivetrains.

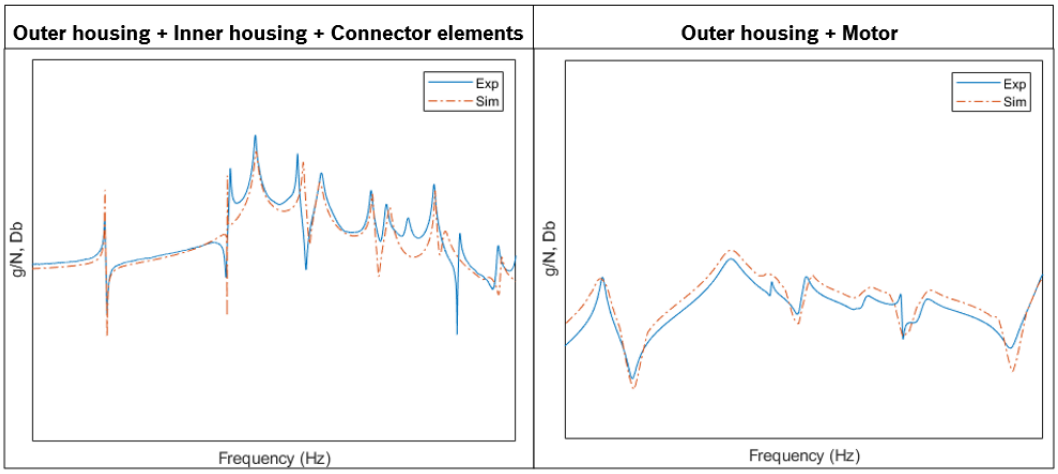

Figure 6.15: Surface velocity plots of "Outer housing + Inner housing + Connector elements" and "Outer housing + Motor" obtained for their appropriate load cases (y-axis is represented with scale SF3v). Simulation and experimental setup are described in sections 4.4.2.3 and 6.2.1 respectively.

The y-axis limits for plots in 6.13, 6.14 and 6.15 are equal but the frequency scales are altered, since the spectrum of interest varies with the parts considered. All these plots help in studying parameters like Young's modulus, material damping and contact damping, which are modified within the numerical templates to bring simulation values on to the experiment contours. Overall, by this way, different structures are validated and made available for the simulations of the entire drivetrain assembly.

Sound emission of combined structures

Once the vibrations of combined structures are validated, the model can be analyzed for studying the acoustics (line 1b of figure 4.41). The acoustic model around the structure is constructed as described in figure 5.8. Here, the octave plot with bandwidth of 1/3rd is used for representation of the acoustic pressures. Once again, the y-axis limits for plots in 6.16, 6.17 and 6.18 are equal but the frequency scales are changed, since the spectrum of interest varies with the parts considered in the simulation.

The left and right-hand side of figure 6.16 describe acoustic pressure bands for the "Outer housing + Outer cover" and "Outer housing + Outer cover + Bearings" respectively. The x-axes of the graphs represent the frequency spectrum of interest and y-axes represent the acoustical quantities measured at a distance of 500 mm. Furthermore, the pressures are displayed in decibel format for better representation and validations of the results.

Overall, it can be understood that, except for few lower frequencies, the simulation results are pretty close to those of the experiments. The whole deviations between the experiments and simulations are described in table 6.13.

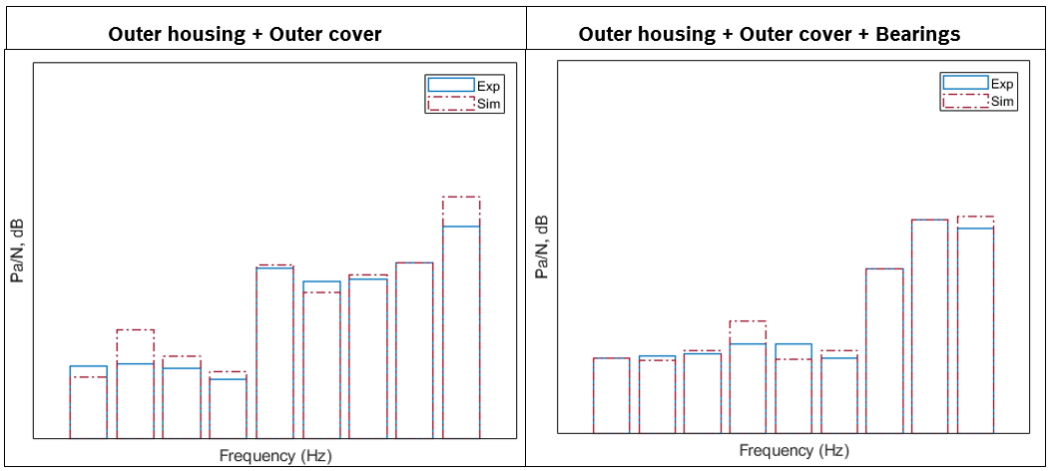

Figure 6.16: Sound octave plots of "Outer housing + Outer cover" and "Outer housing + Outer cover + Bearings" obtained for their appropriate load cases (y-axis is represented with scale factor SF3a). Simulation and experimental setup are described in sections 4.4.2.4 and 6.2.1 respectively.

Similarly, the left and right-hand side of figure 6.17 describe acoustic pressures for the "Outer housing + Outer cover + Brackets" and "Inner housing + Inner cover" respectively. The amplitudes obtained for the right-hand side of this figure are relatively high in comparison with the other combined structures. The reason for this is the geometry structure and material of the inner housing and inner cover.

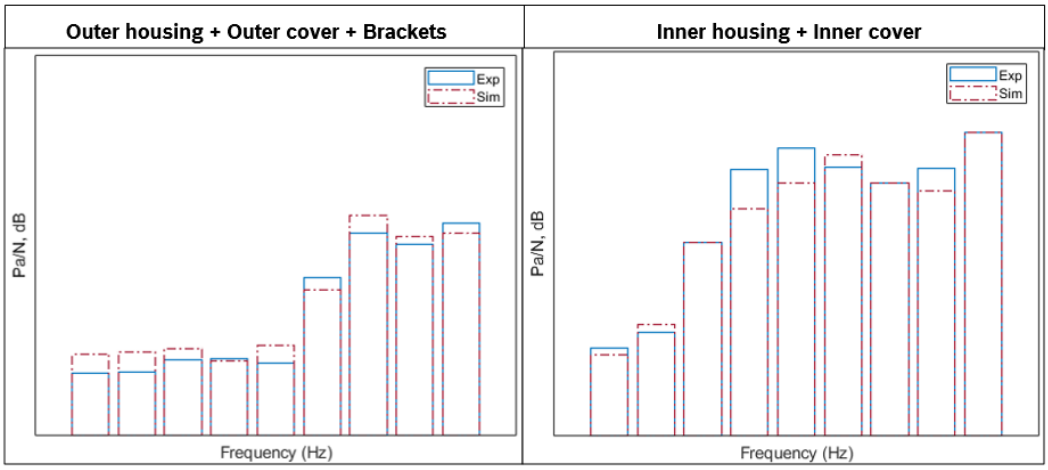

Figure 6.17: Sound octave plots of "Outer housing + Outer cover + Brackets" and "Inner housing + Inner cover" obtained for their appropriate load cases (y-axis is represented with scale factor SF3a). Simulation and experimental setup are described in sections 4.4.2.4 and 6.2.1 respectively.

Furthermore, the left and right-hand side of figure 6.18 describe acoustic pressure values for the "Outer housing + Inner housing + Connector elements" and "Outer housing + Motor" respectively. All these graphs try to support the fact that simulation results are in admissible

limits, thus the associated variables from these models can be further used for a next step of more complex simulations of structures.

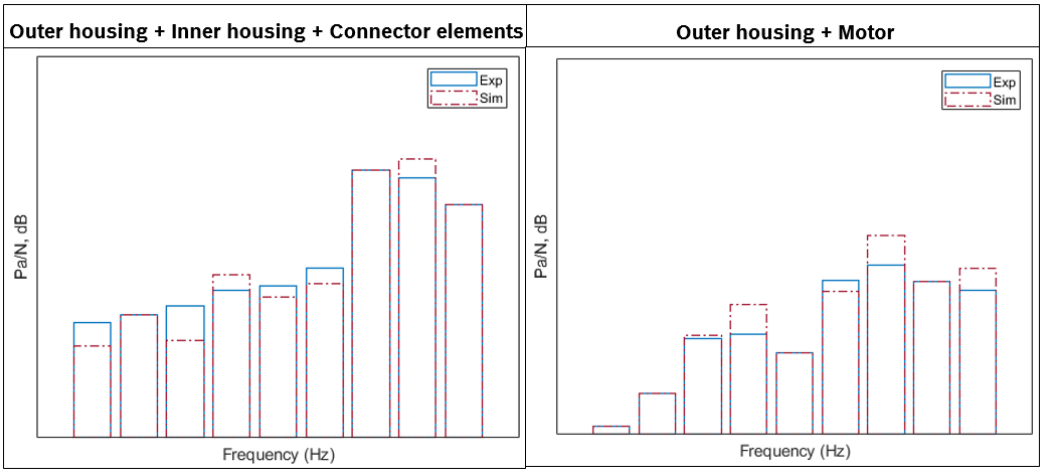

Figure 6.18: Sound octave plots of "Outer housing + Inner housing + Connector elements" and "Outer housing + Motor" obtained for their appropriate load cases (y-axis is represented with scale SF3a). Simulation and experimental setup are described in sections 4.4.2.4 and 6.2.1 respectively.

Finally, table 6.13 describes the deviations in amplitudes among the experiment and simulations for the list of combined structures discussed. From this table, it can be inferred that the values are well within the accepted limits and hence the model parameters studied in these simulations can be further used for the analysis of complete drivetrain structures.

Percent diff (%)	Vibration	Sound
Outer housing + Outer cover	4.30	4.51
Outer housing + Outer cover + Bearings	4.11	1.56
Outer housing + Outer cover + Brackets	4.32	4.20
Inner housing + Inner cover	2.02	3.14
Outer housing + Inner housing + Connector elements	4.62	3.59
Outer housing + Motor	3.34	3.43

Table 6.13: Differences among the experiment and simulation amplitudes for the list of combined structures described in tables 6.7 and 6.8

Results from multi-domain

This part depicts the vibro-acoustics results obtained for the complete drivetrain assembly using the multi-domain approach as described in section 4.4.3. The housing is measured at different locations using the laser vibrometer. The measurement records and the corresponding simulation results are subjected to order analysis. The comparison is illustrated in figure 6.19. The x-, y- and z-axes show the engine speed, frequency components of the signals and amplitude of the surface velocity at the corresponding measuring point.

Two characteristics used for validations are firstly the order lines and secondly the resonance peaks. Larger vibrations at the corresponding gear component occur when its order meets the system resonances. Slope of these lines corresponds to the integer multiple of the meshing per

mechanical gear wheel rotation relative to the rotor shaft.

There are stronger and weaker order lines. The dominant orders originate from the first (engine-side) gear stage of the gear unit and are highlighted in figure 6.19. The measurements of laser vibrometer have additional weaker order lines, which occur due to the bearings of corresponding shafts. The number of balls in the ball bearing multiplied by the speed corresponds to the first order of the respective bearing. These excitations by the bearings balls is not included in the simulation model.

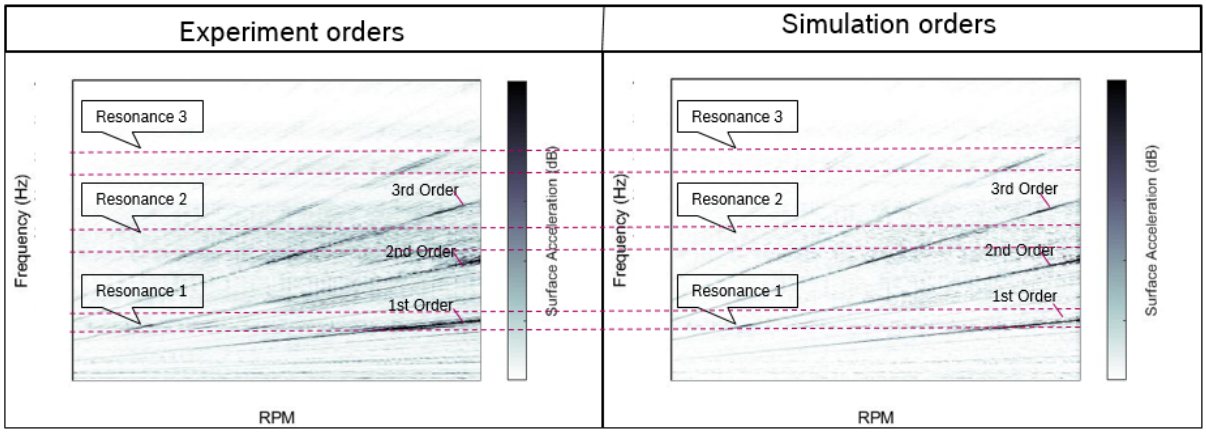

Figure 6.19: Experiment vs. simulation with DD-3 (check figure 4.26) for load case 2 (check table 6.3). Multi-domain and experimental schematics are described in sections 4.4.3 and 6.2.1 respectively.

The course of an order line has different resonance peaks. Higher vibration amplitudes result from the interfaces between an order line and a natural frequency of the housing structure. These amplitudes can be used for calculation of differences between the simulations and experiments. Note that the few of the deviations in the results can be caused by parameter uncertainties in the model, component tolerances at the measurement object and by experiment inaccuracies.

In further analysis, the effects of housing vibration on the rotating gear components are investigated. For this reason, the dual direction coupling (DD-3 from figure 4.26) is commented out in the simulation model. The link is therefore only in one direction, i.e., from the gearbox to housing. Since this represents a physical simplification in the simulation model, the newly calculated results will differ from those previously obtained. The magnitude of difference will be decisive for the relevance of DD-3 and its consideration in the simulation model.

The left-hand side plot of figure 6.20 illustrates the spectrogram for the model without DD-3. The x-axis of this plot corresponds to the speed (or frequency) and the y-axis corresponds to the vibration amplitude. Comparison of the left-hand side of figure 6.20 with figure 6.19 can be extremely difficult as any differences are not recognizable by the three-dimensional visualization. Hence, the ordercuts (right-hand side of figure 6.20) for three of the dominant orders are generated, which can be used for quantification of the deviations. These graphs describe the surface vibration profile corresponding to each of the orders. Furthermore, this plot helps in comparison of resonance points of the orders (position of the resonances with respect to the rotational speed) and their amplitude.

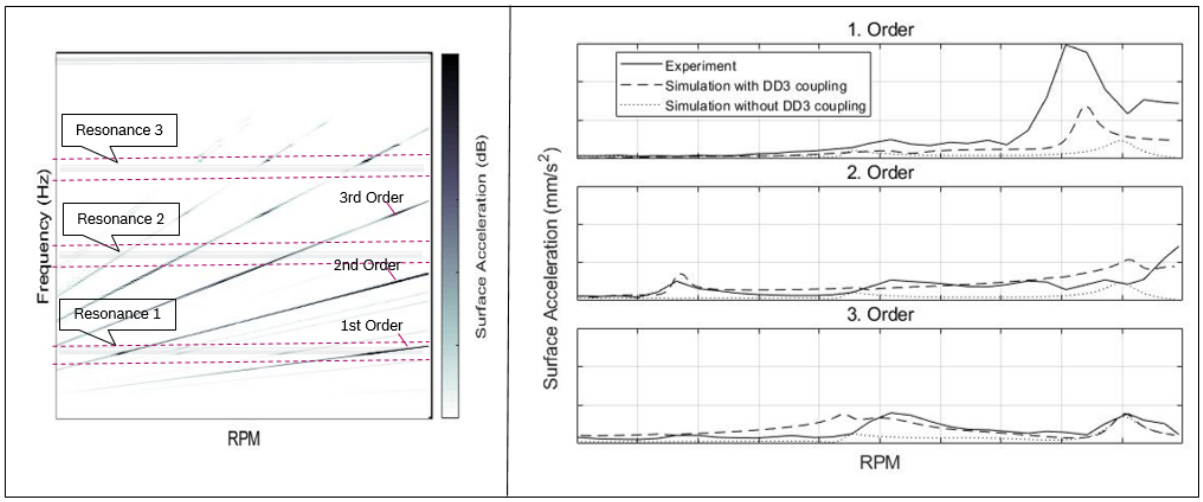

Figure 6.20: Left - Simulation without DD-3 for load case 2 (check table 6.3). Right - comparison of the ordercuts for first three orders for a measurement and simulation point with and without DD3. Multi-domain and experimental schematics are described in sections 4.4.3 and 6.2.1 respectively.

Since most of the measurement and simulation values are close to zero, the direct mean error is relatively big. Therefore, this direct mean error is transformed to modified mean absolute error (equation 6.3). The modified error neglects the small amplitudes thereby enabling the comprehension of influences from backward coupling. For the interpretation of results, this property seems to be sensible from a physical point of view, since these small surface velocities of housing emit only very little sound into the surrounding fluid and hence are neglected. Basis for this is the quantification of deviation between simulation and experiment as well as between the model variants with and without backward coupling.

$$\epsilon_{mod} = \frac{1}{N}\sum_{i}\left|\frac{y_{exp} - y_{sim}}{mean(|y_{exp}|, |y_{sim}|) + R}\right|, \quad where\ R = max(y_{exp,sim}) - min(y_{exp,sim}) \tag{6.3}$$

Modified error (%)			
	1. Order	**2. Order**	**3. Order**
With DD-3	9.9	8.4	12.7
Without DD-3	13.8	17.2	16.3
Improvement with DD-3 (%)			
Percentage difference	39.4	104.8	28.3
Average	57.5		

Table 6.14: Evaluation of deviation between experiment and simulation results and percentage improvement with backward coupling

Table 6.14 describes the difference of simulation values w.r.t. the experiments. For the orders studied, an average improvement of 57.5% for the simulation is recorded (when DD-3 is applied). Hence, the simulation with dual direction coupling seems to provide better results than the model variant without dual direction coupling.

Furthermore, sound radiation into the surrounding fluid is calculated. For this purpose, the ERP model from 4.4.2.4 is used. The surface vibration represents the input variable of the

sound calculation and is the direct transient result of the multibody model.

The emitted sound power is plotted across the spectrum in figure 6.21. The frequency range in which higher vibrations occur can be inferred from these graphs. Such areas should be avoided for operating points since they generate larger pressure fluctuations in the fluid compared to neighboring regions and can therefore also be perceived louder.

One more takeaway from these section is, that there are quite few deviations (marked red in figure 6.21) between ERP and experimental values. Even though the formula is nicely coupled with surface velocities of the structure, it is still just an approximation setup to estimate the sound. It does not consider factors like drag coefficient and surface impedance at the interface for calculation of the acoustic intensities and pressures. Finally, the modified error calculated from equation 6.3 for this plot is found out to be 13.44%.

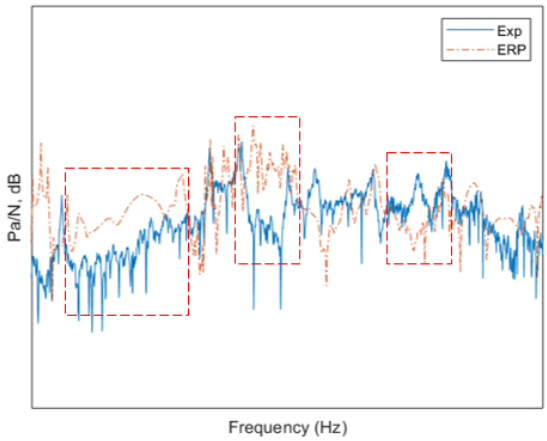

Figure 6.21: Acoustic pressure of microphone obtained at a distance of 500 mm vs. values calculated from the ERP. Experimental setup is described in section 6.2.1.

Results from FE

This part describes the surface velocities and acoustic pressures obtained from the FE simulation methodology as discussed in section 4.4.3.

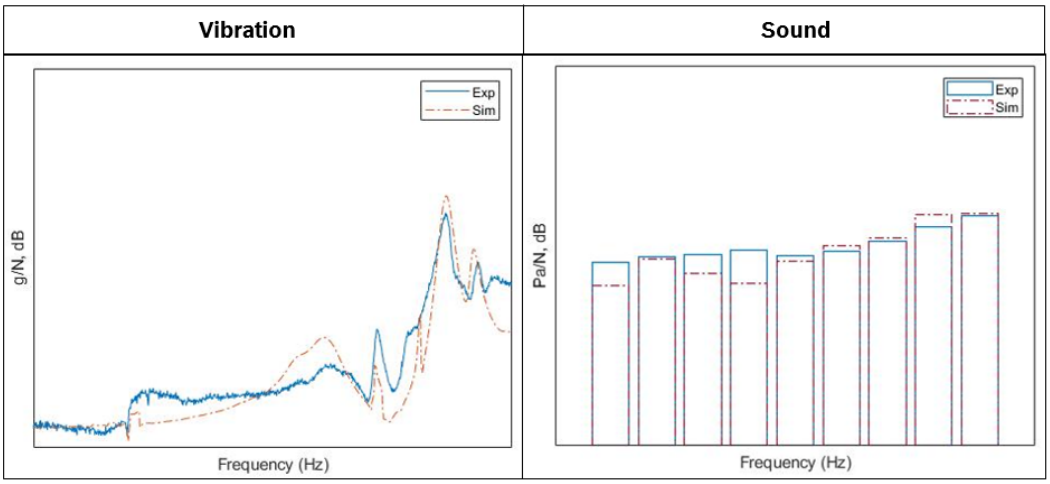

Figure 6.22: Vibration and acoustic pressure of the complete drivetrain for experiment and simulation scaled using factors SF4v and SF4a respectively. FE and experimental schematics are described in sections 4.4.3 (under Single domain) and 6.2.1 respectively.

The graphs in figure 6.22 describe the vibrations and sound plots obtained for the complete

drivetrain assembly using the harmonic analysis. The model parameters acquired earlier from individual and combined structure simulations are used in the drivetrain template to improve the accuracy. Additionally, before performing the steady state analysis, the structures are checked for deformations and nonlinearities using section 6.2.2. Once it is made sure that the deformations lie well within the limits, the models are transferred to the vibration module. Furthermore, the vibration curves are measured at critical areas on the housing surfaces with help of acceleration sensors. The acoustic curves are measured using acoustic camera placed at a distance of 500 mm from the drivetrain.

Although, the values of experiment and simulation don't match completely with 100% accuracy as can be seen by means of diagram 6.22. It is obvious that simulations obtains a decent profile comparable with that of experiment. The deviations between results can be caused by many reasons like experimental deviations or simulation errors. Overall, the modified error values calculated using the equation 6.3 for structure borne and airborne emissions are 5.14% and 3.39% respectively.

Figure 6.23 differentiates the two flows with help of parameters like simulation time, number of CPU's, simplicity and reliability. Although the run time and the cores required to simulate the drivetrain are better for multi-domain calculation. The accuracy of single domain calculation is better across the different models variants compared throughout the thesis. The reason for better reliability can be attributed to the characteristic of detail modeling associated with FE.

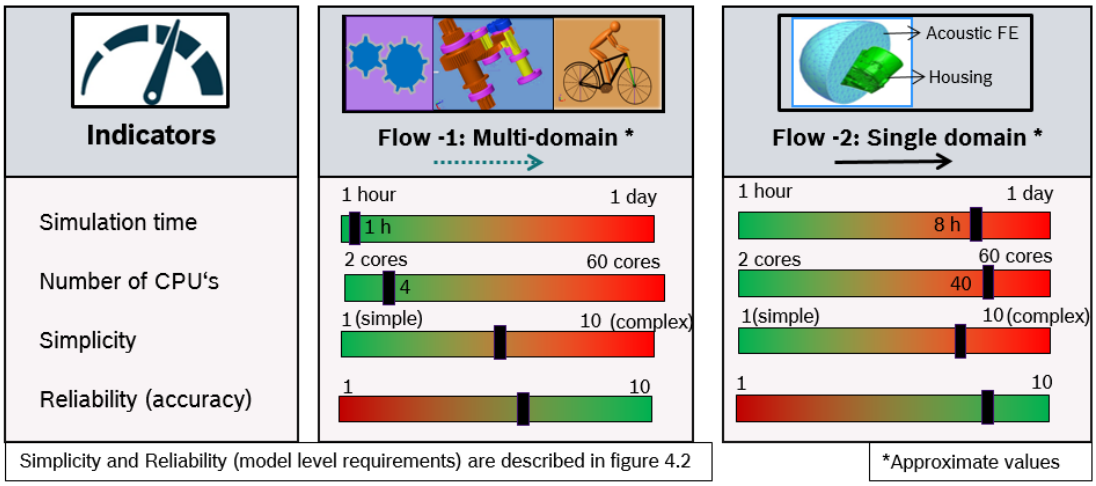

Figure 6.23: Comparison between multi-domain and FE approaches. The domains are described in section 4.4.3.

6.3 Method Verification of the Wear Model

Once the model is validated for the NVH characteristics as depicted in the previous section, the next main question arises from the abrasion. This section tries to address questions like how can one obtain plausible abrasion computations using numerical methods and how can the abrasion domain be linked with the vibration domain for further analysis of its influences.

This particular part of work describes model validation for the abrasion setups discussed in section 4.5. Figure 6.24 illustrates gears, toothed shafts and associated wear at the gear mesh. The drivetrain layout consists of four axles namely: rotor axle, transmission axle 1, transmission axle 2 and crankshaft axle. Additionally, the attached bearings of the corresponding shafts are also represented in this figure.

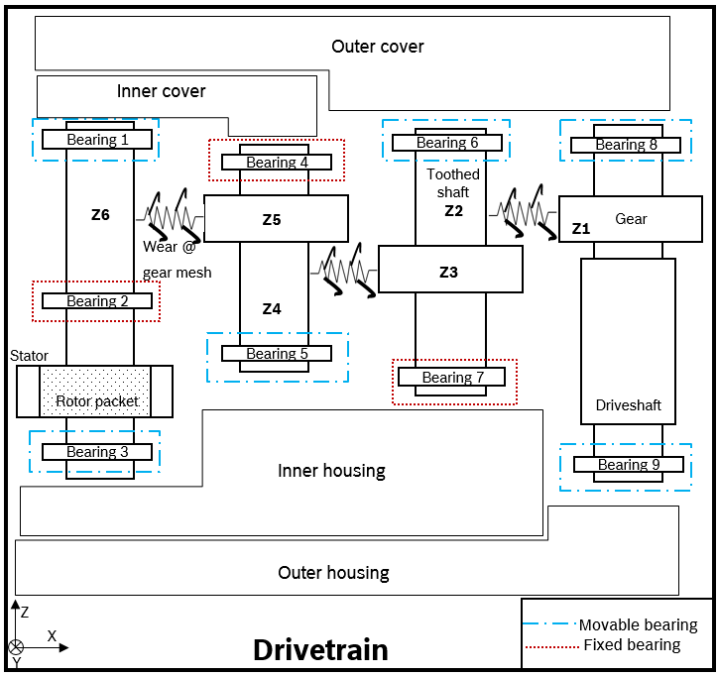

Figure 6.24: Drivetrain layout with wear among the gears and toothed shafts

There are three gear meshes and the wear can occur at all three gear stages. Generally, values obtained at gears on the rotor side can have greater wear rates compared to the driveshaft axle. It is mainly due to the higher RPM present at the motor. The presence of wear among the components changes the vibration characteristics of the drivetrain. Therefore, the noise on the housing structure is represented explicitly in diagram 6.24.

6.3.1 Experimental Setup of the Wear

Figure 6.25 illustrates the simplest schematic view for wear measurements. Keyence VK-X160K microscope is used mainly for making the experimental runs. This Keyence apparatus uses the laser scanning technology to make measurements in regards to surface topology, profile measurement, 3D scanning etc. The profile measurement module is utilized mainly for analyzing and plotting the required results [Key16]. Wear line here is considered as a line along the gear tooth surface, where the measurements are made (also check figure 6.28).

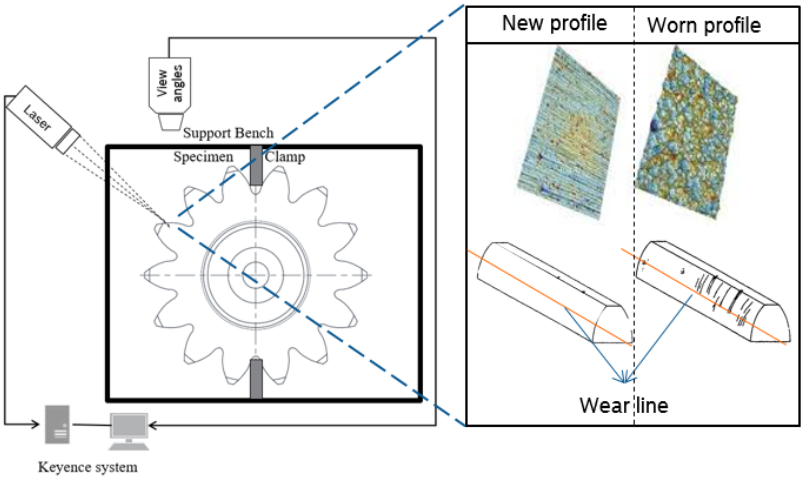

Figure 6.25: Schematic view for the wear experimental setup

6.3.2 Validation of FE Wear Model

Before the implementation of wear subroutine, it is important to analyze the constructed FE model for its plausibility. One of the major tasks here is to determine the correct element lengths. They are found out by a simple convergence study that is described by means of figure 4.32 in section 4.5.2), where the parameter of interest are contact pressures and contact forces, rather than von-Mises stress. The graph 6.26 describes the convergence study plot for one of the gear stages. The two curves represent two individual gears coming into contact.

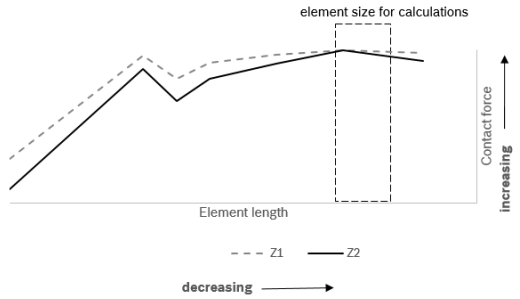

Figure 6.26: Convergence for element lengths calculated using FE simulation method described in sections 4.4.2.2 (under Contact analysis among the gears) and 4.5.2

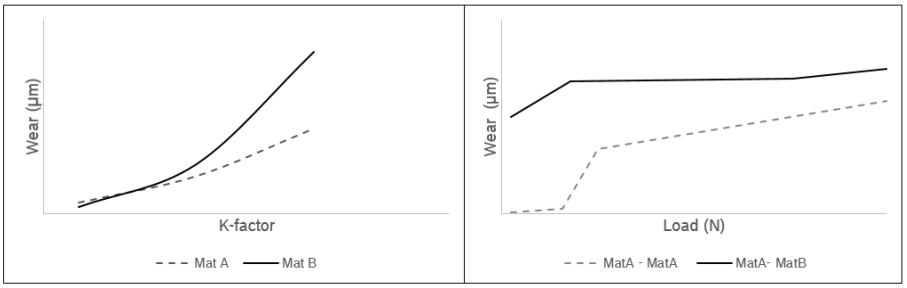

Figure 6.27: Wear map - influence of K-factor and material combinations on wear depth calculated using FE setup shown in section 4.5.2

The wear maps in diagram 6.27 describe the influence of K-factor and the load w.r.t. the abrasion depth obtained from simulations. From the first part, it can be inferred that, a harder material (Mat A) has less wear while keeping the other parameters constant. Similarly, the second part describes that the wear between different materials (Mat A - Mat B) is greater than the same material combination (Mat A - Mat A). It can be argued that the difference in hardness between two materials can increase the occurrence of wear.

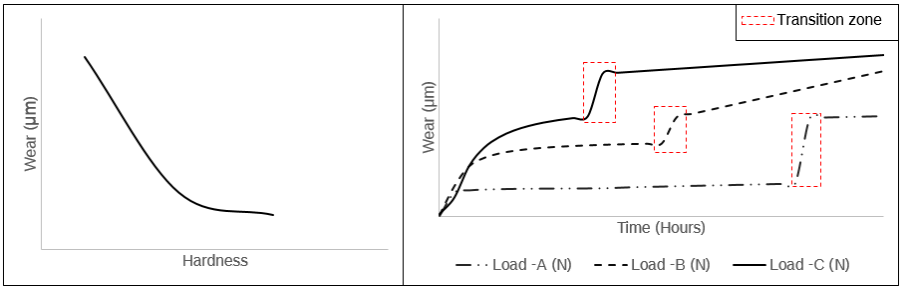

Figure 6.28: Wear map - influence of hardness and load on wear depth estimated using FE setup shown in section 4.5.2

Likewise, the graphs in 6.28 describe wear maps with regard to hardness and time. It can be seen that with the increase in hardness the wear depths and rates decrease exponentially. On the other hand, after certain time, once the plasticity and damage has occurred, the wear moves to transition zone and thereby enters the severe zone. Also the wear process is accelerated with higher loads (Load-A < Load-B < Load-C). The performances are largely impacted once the wear reaches severe zone area and eventually the drivetrain will fail. Note that all the scales of figures 6.27 and 6.28 are not the same.

Furthermore, figures in 6.29 describe certain sections of the wear profile obtained from experiments and simulations. A torque and run time of 1.10 N · m and 600 hours are applied as inputs for the tests. Note that, the graphs represent only certain parts of the flank and face surfaces and not the complete gear tooth.

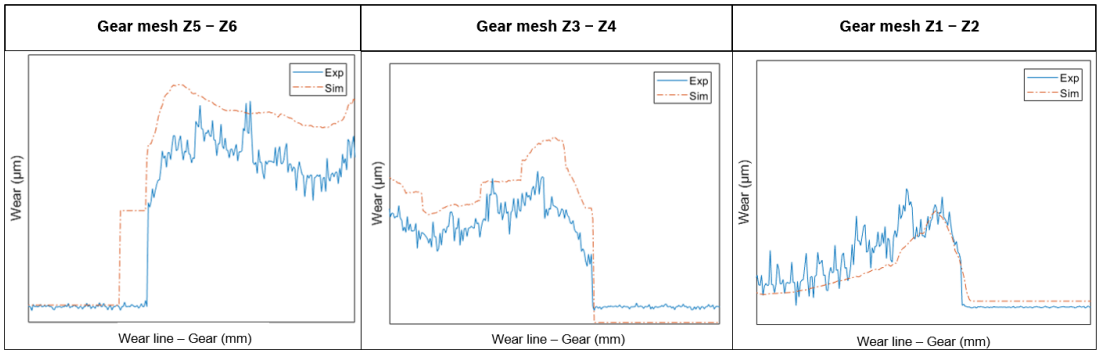

Figure 6.29: Wear profile of gears (and not complete surfaces) Z1, Z3 and Z5 (experiment vs. simulation). Simulation and experimental setups are described in sections 4.5.2 and 6.3.1 respectively.

6.3.3 Results from Uncertainty Quantification and Neural Network

Certainly, these simulation wear maps (figures 6.27 and 6.28) can be coupled with data analytic to comprehend the behavior of parameters impacting the abrasion rates and profiles (check section 4.5.1). The left hand side of the picture represents sensitivity analysis performed using the LHS technique in the UQ toolbox. It is found out that the hardness and K-factor represent the maximum influence on the wear values. The picture on the right-hand side illustrates the change in wear values with hardness and K-factor. It is observed that with decrease in hardness and increase in K-factor the wear increases.

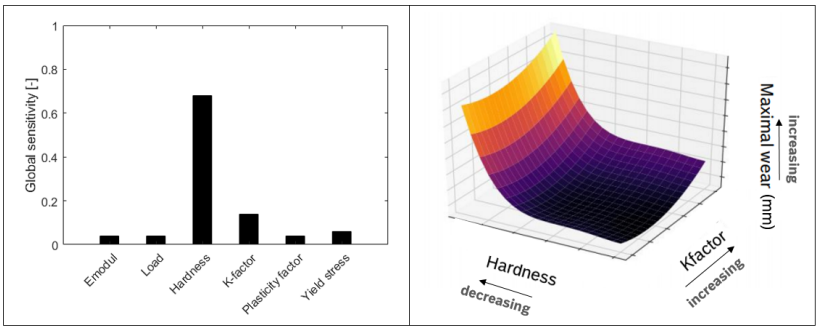

Figure 6.30: Sensitivity values obtained from UQ toolbox (section 4.5.1) and impact of hardness and K-factor on wear depth

The availability of simulation values for larger sets (obtained for various UQ simulations) supports the application of machine learning algorithms. The parameters described in figure 6.30 are

considered as design variables (or predictor data) and the wear depth and rates are represented as design responses (or response data), which helps in construction of the ML algorithms.

Table 6.15 represents various definitions associated with FE and NN used for predicting the wear among the gear components. The NN structure consists of 6 input, 36, 24 hidden and 2 output layers.

FE properties		**NN properties**	
Element length	0.09 mm	**Algorithm type**	Back-propagation
Element shape function	Linear	**Activation function**	Sigmoid
Element type	Hexa	**Layers**	6, 36, 24, 2
Step	Static	**Loss function**	Mean square error
Run time factor	180x	**Run time factor**	1x

Table 6.15: Difference in values calculated using ML algorithms w.r.t. the FE results

The values in table 6.16 describe wear depths obtained using FE and neural networks for certain values of the parameters. The values described here are normalized. The column ϵ_i in table 6.16 shows the deviation of NN values from that of the FE. These values are captured using the equation 6.4. The wear depth values are generally small and hence calculating the relative error would depict larger deviations. Therefore, instead of using the FE value of the corresponding instance, a maximum wear value available among the set is considered for calculation of deviations. Overall, the FE and back-propagation neural networks with Sigmoid activation function are compared for 18 instances and an average error of 6.62% is found out. The main reason for this deviation is due to factors like insufficient quantity, non representative and noisy training data.

Load (N)	**Hardness ratio**	**K-factor**	**Plasticity factor**	**Yield stress (MPa)**	**Wear (μ m)**		**ϵ_i (equation 6.4)(in %)**
					FE	**NN**	
0.41	0.22	0.88	0.09	0.27	0.31	0.34	3.26
0.20	0.22	0.49	0.20	0.46	0.04	0.03	0.23
0.57	0.59	1.00	0.56	1.00	0.51	0.60	9.50
1.00	1.00	0.78	1.00	0.58	0.95	1.00	4.80

Table 6.16: Wear depths calculated using FE and neural network for sets of different parameter ranges (scaled). Definitions of FE and neural network setups are described in sections 4.5.2 and 4.5.3 respectively.

$$\epsilon_i = \frac{|NN\_Value_i - FE\_Value_i|}{Max(NN\_Value, FE\_Value)} \tag{6.4}$$

Figure 6.31 describes the wear depth obtained from the simulation and neural network with Sigmoid activation function for K-factor and hardness. It can be interpreted from the graph that the wear values increase with increasing K-factor and at the same time decrease with increasing hardness of the softer material. The machine learning values are relatively close to the simulation results for most of the test cases. But for few examples tested, the values seem to slightly deviate (marked in red). The average error calculated for the left and right-hand side graphs in figure 6.31 are 5.78% and 6.32% respectively. Furthermore, the geometries of the gears and shafts, for instance, the helix angle, number of tooth, etc., would have nonlinear influence on the wear, which could be better modeled by a NN. Within the scope of the thesis, these parameters could not be included into the design space.

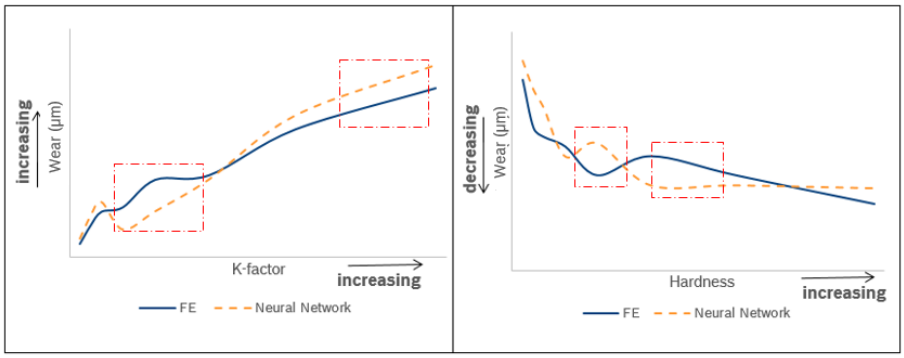

Figure 6.31: Wear values comparison between the FE (section 4.5.2) and NN (section 4.5.3)

6.4 Method Verification of NVH on Wear Model

All the rotating components with repetitive contact loading experience fatigue. Once the material deformations exceed the plastic limits and finds themselves in damage zone, there is a possibility for loss of material. This would have a negative influence on the vibration characteristics of the drivetrain assemblies. Hence, the worn models are first analyzed for their shift in natural frequencies.

Abraded shafts and gears × SF2					
Z1 (Hz)	**Percent diff (%)**	**Z2 (Hz)**	**Percent diff (%)**	**Z3 (Hz)**	**Percent diff (%)**
0.114	-3.61	0.475	-1.37	0.258	-3.89
0.116	-1.59	0.476	-1.38	0.258	-3.87
0.148	-2.48	0.656	-1.42	0.454	-0.53
0.149	-1.95	0.807	-2.73	0.461	-0.79
0.299	-2.63	0.807	-2.74	0.461	-0.79
0.300	-2.69	0.940	-0.54	0.591	-2.60

Table 6.17: Natural frequencies of the abraded shafts scaled with SF2 and percentage deterioration w.r.t. to the original components (table 6.6) - I. Experimental setup for vibrations is described section 6.2.1.

Abraded shafts and gears × SF2					
Z4 (Hz)	**Percent diff (%)**	**Z5 (Hz)**	**Percent diff (%)**	**Z6 (Hz)**	**Percent diff (%)**
0.444	-2.19	0.433	-2.62	0.107	-2.09
0.445	-2.01	0.433	-2.51	0.108	-1.74
0.710	-1.89	0.555	-0.75	0.269	-1.24
0.711	-1.81	0.555	-0.84	0.271	-0.51
0.763	-1.44	0.736	-3.12	0.316	-4.83
0.981	-1.86	0.972	-0.39	0.407	-10.41

Table 6.18: Natural frequencies of the abraded shafts scaled with SF2 and percentage deterioration w.r.t. to the original components (table 6.6) - II. Experimental setup for vibrations is described section 6.2.1.

Tables 6.17 and 6.18 describe the changes in natural frequencies of the abraded components due

to presence of wear at flanks of the teeth. It can be understood that the Eigen frequencies shift to the lower spectrum due to the abrasion mechanism. These values are compared with the modes of original shafts for comprehending the percentage shift w.r.t. the original frequencies displayed in table 6.6.

The modes can later influence the structure and airborne emissions of the complete drivetrain. Figure 6.32 shows surface velocity and acoustic pressure obtained at critical areas of concern for a specific drivetrain. The load profile applied for this example is illustrated in table 6.3 by means of load case 2. The experimental plots are obtained via the setup described in section 6.2.1. The acoustic pressure plot is displayed for the bandwidth of 1/3rd octaves. Overall, a deterioration of 9.75% and 7.93% (from the original) in vibrations and acoustics is found after the wear at gear shafts.

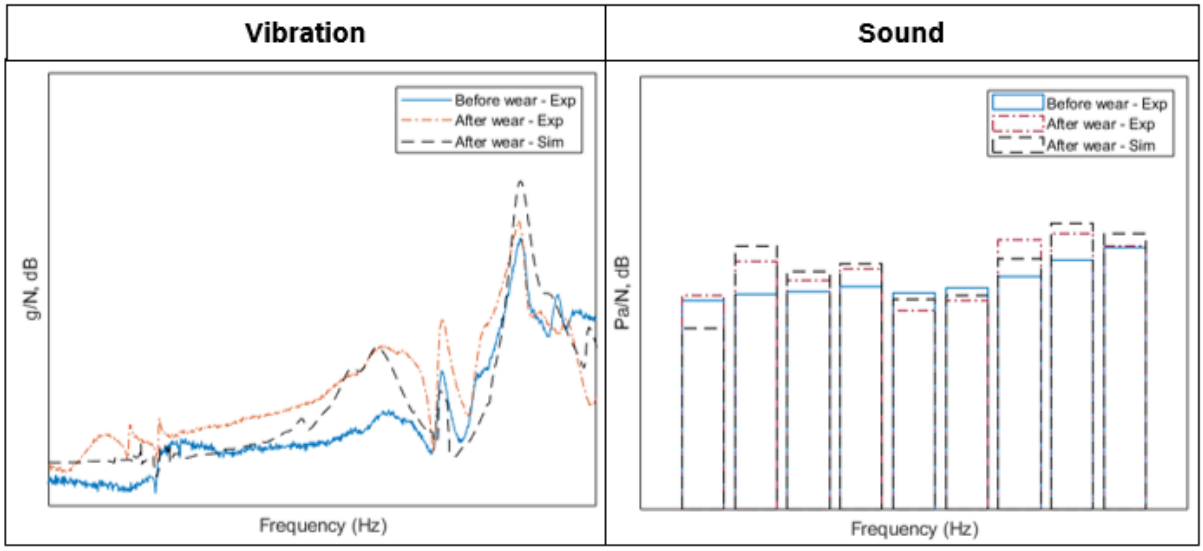

Figure 6.32: Vibration and acoustic pressure measured and simulated for new and old drivetrain with run time of 600 hours scaled using factors SF4v and SF4a respectively. FE and experimental schematics are described in sections 4.4.3 and 6.2.1 respectively.

Additionally, figure 6.32 also illustrates the comparison graphs between experiment and simulation after the process of wear at the gear shafts. Overall, the modified error values calculated using the equation 6.3 for surface velocities and acoustic pressures are found out to be 6.56% and 4.27% respectively.

6.5 Optimization of the Components

Once the NVH behavior of individual components, combined structures and complete drivetrain are made available, those structures can be modified with the objective of improving the dynamics. The related constraint and objective definitions can be found in section 4.8.1.

6.5.1 Design Optimization

This section describes the design improvisations brought onto the structures to reduce the vibration amplitudes and push the frequencies to a higher spectrum. Table 6.19 describes the values of new Eigen frequencies obtained for "Improved - Outer housing + Outer cover" and "Improved - Inner housing + Inner cover" scaled with a factor SF3 and the percentage change from the old structures (check tables 6.7 and 6.8).

Design changes × SF3	Improved - Outer housing + Outer cover		Improved - Inner housing + Inner cover	
	New (Hz)	Improvement (%)	New (Hz)	Improvement (%)
Mode 1	0.213	2.74	0.410	9.41
Mode 2	0.300	4.41	0.557	13.37
Mode 3	0.375	11.07	0.860	12.12
Mode 4	0.404	7.01	0.936	14.35
Mode 5	0.426	-0.30	1.034	12.89
Mode 6	0.464	2.54	1.126	11.22

Table 6.19: Natural frequencies of improved structures scaled with a factor SF3 and the percentage of improvement in frequencies - I. More information about optimization definitions is given in section 4.8.1.

Figure 6.33 describes the acoustic pressure plots obtained for the "Improved - Outer housing + Outer cover" and "Improved - Inner housing + Inner cover". Overall, improvements of 1.45% (left side) and 2.23% (right side) in the acoustic pressures are achieved using these modifications.

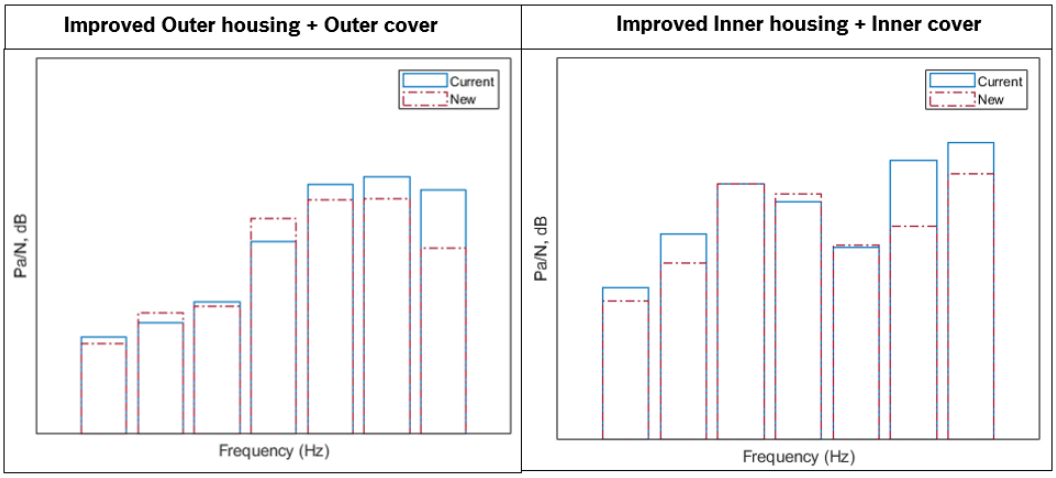

Figure 6.33: Simulated sound octave plots of "Improved - Outer housing + Outer Cover" and "Improved - Inner housing + Inner cover" vs. the current ones scaled with factor SF3a (check section 4.4.2.4).

Design changes × SF3	Outer housing + Outer cover (with Seal)		Outer housing + Motor (with Ring)	
	New (Hz)	Improvement (%)	New (Hz)	Improvement (%)
Mode 1	0.198	-4.63	0.147	-0.49
Mode 2	0.237	-21.15	0.293	-1.68
Mode 3	0.331	-0.78	0.334	1.76
Mode 4	0.410	8.49	0.339	-1.38
Mode 5	0.445	4.03	0.389	-4.11
Mode 6	0.463	2.18	0.450	-0.84

Table 6.20: Natural frequencies of improved structures scaled with a factor SF3 and the percentage of improvement in frequencies - II. More information about optimization definitions is given in section 4.8.1.

Table 6.20 describes values of new frequencies obtained for "Outer housing + Outer Cover + Seal" and "Outer housing + Motor + Ring" scaled with a factor SF3 and the percentage change from their respective old structures (check tables 6.7 and 6.8). Table 6.20 focuses on addition of new components along the transfer path of the vibrations to damp out the amplitudes. Due to addition of extra masses for most of the natural frequencies are moved to lower spectrum but the presence of damping properties inside the materials reduces higher amplitudes of vibrations and acoustic quantities (check figure 6.34).

Figure 6.34 describes the acoustic pressure plots obtained for the "Outer housing + Outer Cover + Seal" and "Outer housing + Motor + Ring". Here, improvements of 1.05% (left side) and 0.89% (right side) are realized by the addition of new components.

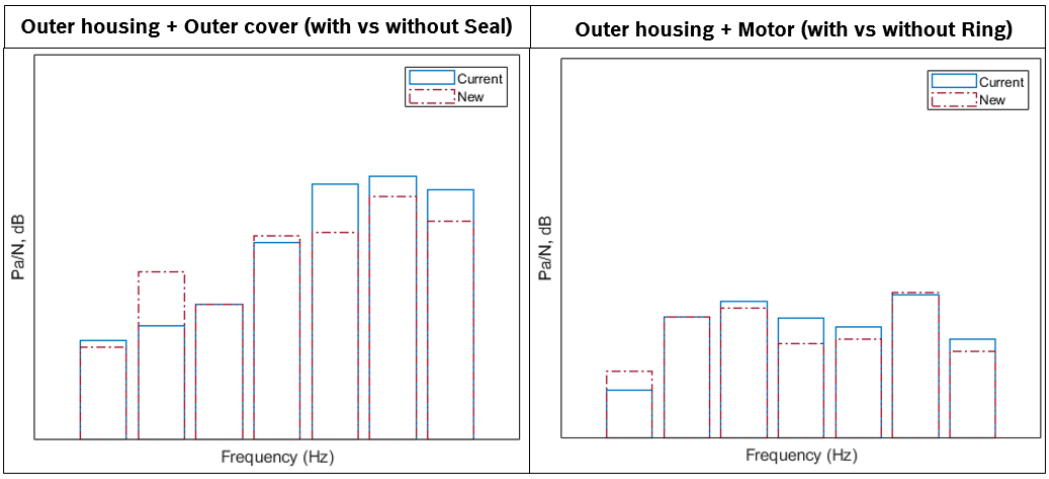

Figure 6.34: Simulated sound octave plots of "Outer housing + Outer Cover + Seal" and "Outer housing + Motor + Ring" vs. the current scaled with factor SF3a (check section 4.4.2.4).

6.5.2 Material Optimization

Table 6.21 describes the influence of materials along the vibration path. Initially, a model with material aluminum (Alu), which transfers complete vibrations due to the similarity in surface impedance is described. Later, aluminum is replaced by a specific kind of vulkollan (Vul), which aids in damping the vibrations along spectrum. From the graphs in 6.35 it can be observed that even though Vulkollan moved the natural modes to lower spectrum, it achieved a positive influence on to the structures.

Material changes × SF3	Outer housing + Damping elements(Alu) + Inner housing		Outer housing + Damping elements(Vul) + Inner housing	
	New (Hz)	Improvement (%)	New (Hz)	Improvement (%)
Mode 1	0.185	-0.44	0.165	-12.48
Mode 2	0.318	-1.70	0.249	-30.26
Mode 3	0.349	-2.08	0.277	-28.56
Mode 4	0.402	-1.92	0.336	-21.88
Mode 5	0.415	-3.14	0.371	-15.37
Mode 6	0.482	-1.16	0.415	-17.30

Table 6.21: Natural frequencies of structures (with additional damping elements) scaled with a factor SF3 and the percentage change in frequencies. More information about optimization definitions is given in section 4.8.1.

Figure 6.35 describes the vibration and acoustic pressure plots obtained for the materials aluminum and Vulkollan. It can be clearly seen that the addition of materials with damping properties like Vulkollan moves the frequencies slightly towards the lower spectrum and at the same time reduces the amplitudes drastically. Overall, mean difference for the vibration and acoustic plots obtained are 22.74% and 13.16% respectively.

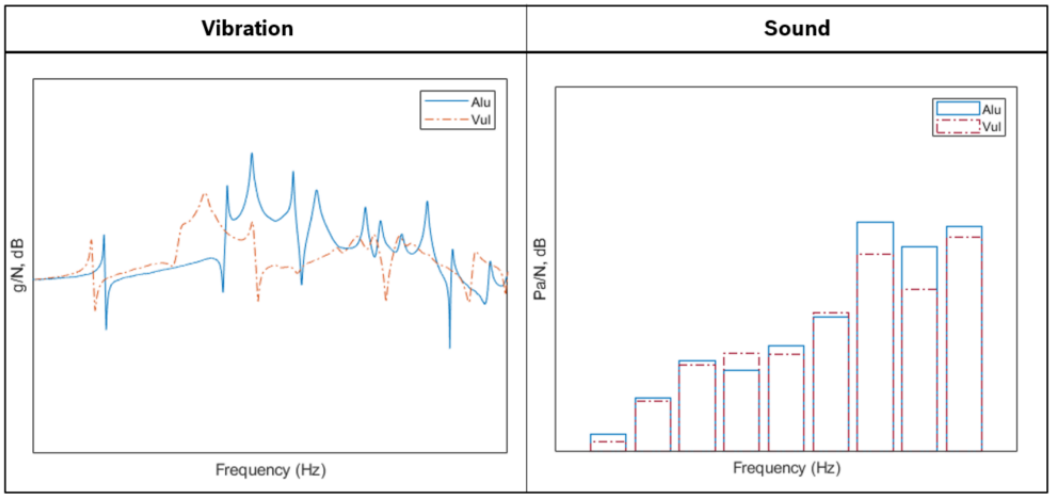

Figure 6.35: Vibration and acoustic pressure simulated for "Outer housing + Damping elements + Inner housing" for aluminum and vulkollan scaled using factors SF3vv and SF3aa (check sections 4.4.2.3 and 4.4.2.4).

Eventually, the design and material improvements discussed above are imported in the current drive unit template, thereby creating an updated simulation model. Figure 6.36 illustrates the improvements in vibration and acoustic for complete drivetrain due to the modifications made. It can be seen that the increase in stiffness of structures due to the design changes and inclusion of better damping elements along the paths of vibration have pushed the frequencies to a higher spectrum and damped the corresponding amplitudes. An overall improvement of 11.87% and 4.85% in surface acceleration and sound has been achieved due to these changes.

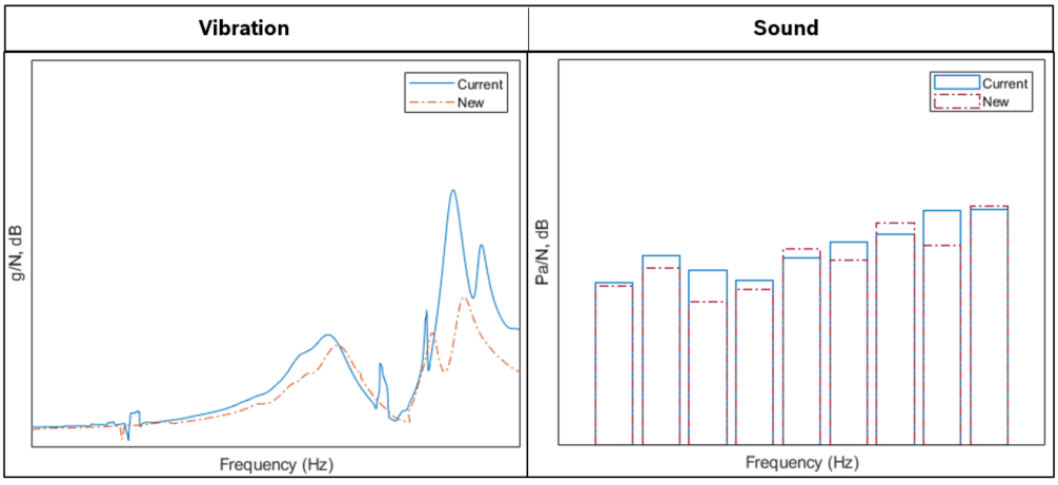

Figure 6.36: Vibration and acoustic pressure of the complete drivetrain for current drivetrain variant vs. the model with improvements (simulation) scaled with factors SF4v and SF4a respectively (check sections 4.4.2.3, 4.4.2.4 and 6.2.3).

6.5.3 Other Possible Optimizations

Apart from the design changes illustrated in the sections 6.5.1 and 6.5.2, steps like improving the surface qualities of the gear faces, altering the helix angle of the gears in contact etc., can bring influence on the acoustic characters of the powertrain. This section describes the other possible potentials to reduce the sound and vibrations in a drive unit.

Tooth errors and surface quality of gear flanks

Tooth defects can occur in manufacturing process or during operation, for example under excessive load. How the error of a single tooth affects the dynamic vibration behavior is examined below. It is based again on the constantly accelerated run-up of the three-stage helical gearbox. The tooth defect leads to a broadband excitation and additional vibrations in the system. In further analysis, the resulting dynamic additional forces in the transmission due to the tooth defect and their effect on the housing vibration can be examined. As a result, it is wise to eliminate the tooth defects in the manufacturing phase.

One more important factor concerning the manufacturing phase is the surface quality. The roughness along the surface profile of the gears can also bring an influence on the dynamic characteristics of drive unit. It can impact the vibrations and thereby noises of the drivetrain. Figure 6.37 describes the reduction in acoustics achieved when the surface profile of the gear is changed from normal to logarithmic. Here, the drivetrain variant discussed in section 6.1.2 is considered. Additionally, the profile of the gears at just one gear mesh is altered and the of the setup is kept unchanged. Improvements of 5.47% and 12.52% are achieved for the load cases 1 and 2 respectively (check table 6.3).

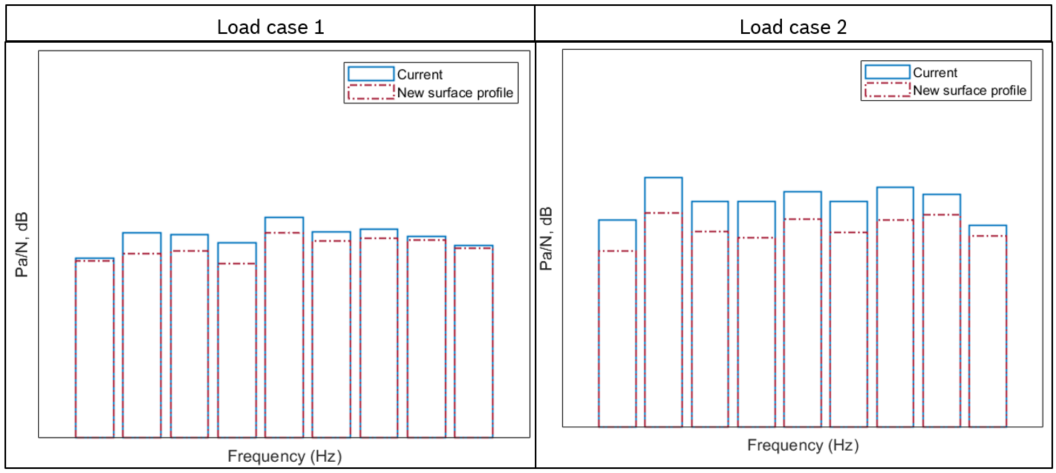

Figure 6.37: Acoustic pressure plots measured for the current model and drivetrain with changed gear flank profiles scaled with factor SF4a. Experimental setup is shown in section 6.2.1.

Impact of helix angle and contact ratio

Another parameter for the gearbox design is the helix angle. If this angle is increased, the degree of contact at the gear stage increases. Due to the resulting lower internal dynamic forces it leads to a smoother running behavior of the gears. However, it increases the axial forces, which will have a counterproductive effect. An example simulation considering numerical values is shown in figure 6.38. The transmission errors are evaluated for two load cases (check section 6.2.1). A constant time interval is shown on the x-axis of the graphs. The y-axis describes the transmission

errors for the helix angles examined. It can be seen that the number of interventions scales with speed. Moreover, the lowest transmission error is found out for the plot with helix angles. This was to be expected since, the degree of coverage increases. In contrast, there are growing axial bearing forces, which should be considered in a more comprehensive analysis. There is also an upper limit with regard to the gear design.

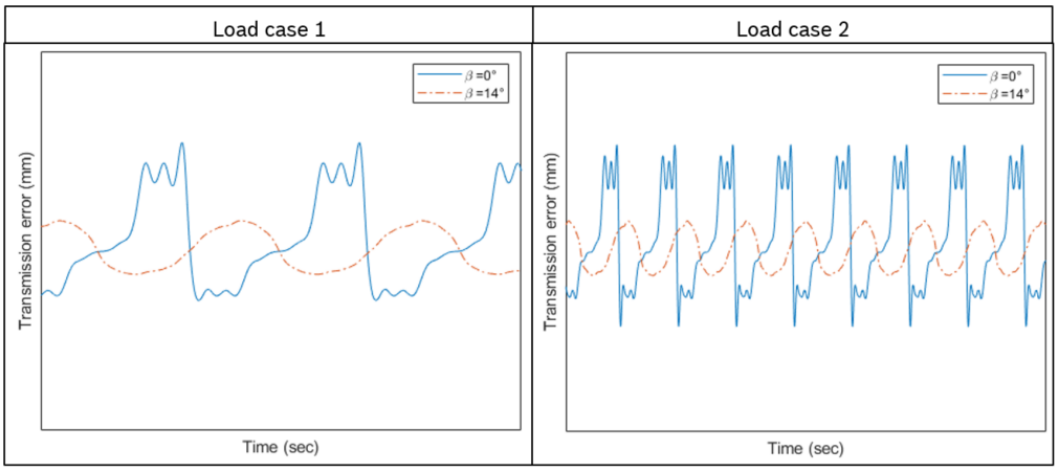

Figure 6.38: Transmission error for spur vs. helical gears at different speeds

Now considering this helix angle, real parts are produced and assembled inside the drivetrain variant to check their influences. Figure 6.39 illustrates the improvements achieved due to the introduction of helical gears at one of the gear stages. Once again, in order to understand the influence of the helical angle, the rest of model setup is kept unaltered. Overall, a reduction of 10.12% and 11.81% for load case 1 and 2 respectively could be achieved.

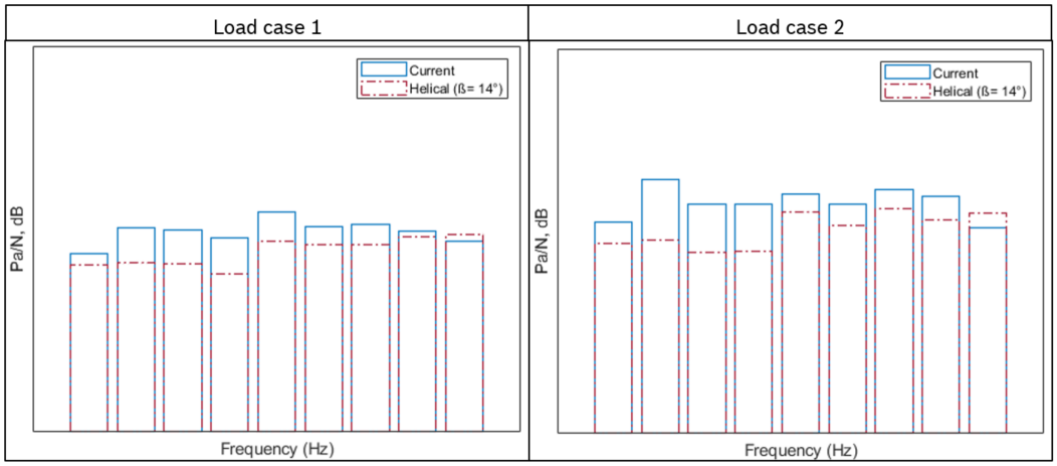

Figure 6.39: Acoustic pressure plots measured for the current and drivetrain with helical gears (at one gear stage) scaled with factor SF4a. Experimental setup is shown in section 6.2.1.

7 Summary and Future Scope

Conclusion

The vibro-acoustic behavior of gears is a complex interplay of different physical mechanisms. If we follow the structure-borne sound path, vibrations are stimulated by the mechanical meshing of teeth, via the gears and toothed shafts to the bearings. The latter transmit the forces to housings and set them in vibration. The bearings present between the shafts and the housing structures are responsible for transferring the vibrations. By deflecting the housing, however, the boundary conditions of the bearings also change and dual directional interaction occurs. At the same time, the surface of the housing emits sound into the surrounding fluid. In addition, the presence of wear can deteriorate the NVH performances of the drivetrain.

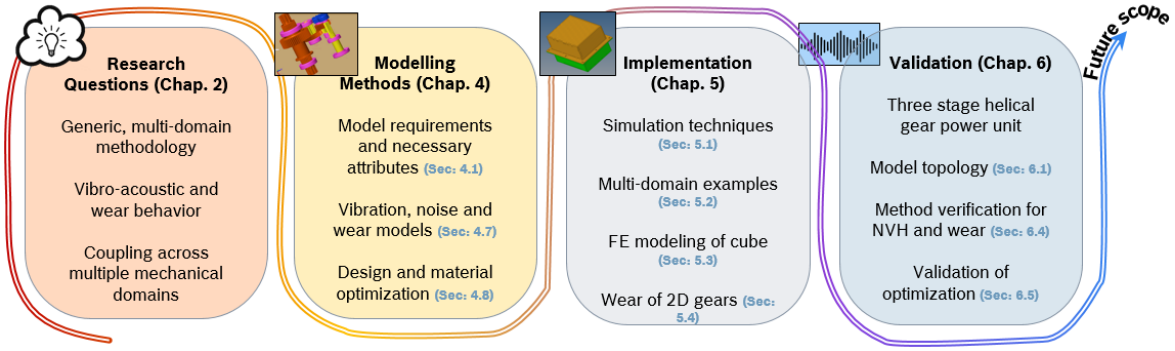

Figure 7.1: Summary of the thesis

Figure 7.1 describes the essential topics discussed through out the work. The main question at the beginning of work was how to provide developers with a comprehensive picture of the effects of a component on vibro-acoustic and abrasion behavior as early as possible and how this knowledge can be continuously expanded through the development process for different transmission variants and system configurations.

The present work provides an extensive answer in the form of a generic, multi-domain methodology for the modeling and simulation of structure borne emissions in power units. The model level requirements for a system and transmission model derived in research methodology are met. The prerequisites in regard to the attributes necessary to predict the vibrations and wear are also met.

In detail, a lumped parameter model is used for the mechanical tooth engagement. The method efficiently and scalably depicts mechanical excitation mechanisms of the transmission vibration in the form of a few system parameters. For the purpose of single domain analysis, the same excitation model was also developed within FE setups as well. A modular application of both the models is possible through the configuration of different levels of detail of the components. As a result, system knowledge can be continuously expanded during product development and an existing simulation model can be expanded. The rotating components of the gearbox are represented by a Multibody simulation. Both macroscopic state variables of the power transmission and high-frequency vibrations of the transmission components can be mapped. The latter are transferred down to the housing, which has a spectrum of natural frequencies and modes due to its structural dynamic properties. The surface vibration generates the sound emitted

into the surrounding fluid, which can be further analyzed using the acoustic FE or the ERP models developed depending on the domain of interest and the accuracy (single vs. multiple). Furthermore, the FE simulations of abrasion among the gear components are also described and later the abrasion domain is linked with the vibrational domain. This connection helps in studying the influences of wear on the NVH characteristics.

The generic, multi-domain methodology is explained in detail by a functional representation of the physical mechanisms and a flowchart for the identification of the system parameters. The verification is carried out using a modeling instance with Simscape and Abaqus as simulators. With the help of the modeling instance, a three stage spur + helical gear is built as a simulation model and validated using experimental measurement results. The main variables used here are macroscopic system states like engine speed, engine torque and surface velocity of the housing structure at different measuring points. Finally, the potential for different parameter optimizations possible for the improvements of vibrations are illustrated.

In the following, the presented methodology for modeling and simulation of vibro-acoustic and wear mechanisms in gears is discussed. The starting point is the questions in the product development process and how system modifications such as the influence of helical angles of the gears, the reduction of structure-borne noise through damping elements along the transfer path or a modification of the housing geometry affects the vibration of surfaces and the acoustic behavior of the gear unit. Since a complex interaction among the different physical mechanisms is involved in this scenario, and also at the same time there is no prototype and only moderate system knowledge at the beginning of product development is available, a modular, configurable system model is best suitable as starting point for studying the influences on the vibrations and wear mechanisms.

This is exactly where the methodology presented in the thesis comes in, since it describes a generic approach for creating a vibro-acoustic and abrasion model (check figures 4.42, 4.44 and 4.45). In contrast to an isolated view of the mechanisms involved, the complete structure-borne sound path including the emitted sound power is mapped within the scope of generic methodology shown. The physical causal relationship is described using component-oriented and FE modeling (check sections 3.2.2, 3.2.3 and 3.4.3) before the formal creation of the qualitative, mathematical model. In regards to the system model, it can be expanded and modified in parallel with the level of product maturity. Whereas for the FE, initial design layouts should be available for the further analysis. The important advantages of system model are that, the analyses are effective and resource-saving at this level and can be accessed and used by experts from other disciplines. On the other hand, FE provides better accurate results.

The model for calculations of vibration and abrasion is shown as an example (three stage spur + helical gear, chapter 6). It is created using a modeling instance of the methodology and thus fulfills the model requirements and necessary attribute from section 4.2. Proof of the correct implementation of the modeling instance is provided in chapter 5 and the validation of physical mechanisms of the model is shown in section 6.4. The modified relative error can be calculated to numerically show that the percentage deviation for the simulation results available in comparison with the experiments is in the low, double-digit range (section 6.2.3 - Results from multi-domain and FE, table 6.14).

The modified error is suitable as an evaluation key figure, since small amplitudes are neglected more with the normal mean error. This property is particularly useful when evaluating the surface vibration, since small speed amplitudes of the surface emit only very little sound into the surrounding fluid and should therefore not be included in the error calculation. Since a large part of the measurement or simulation values are close to zero, the mean relative error is therefore relatively large and can therefore lead to misleading conclusions when interpreting the results. The modified error considers this property and is therefore suitable for the model validation shown.

When modeling physical relationships, the question that arises repeatedly is whether a physical effect must be taken into account in the simulation model or whether it can be neglected under tolerable errors. In general, the reduction of physical effects shown leads to a saving in computing time, which is particularly desirable for large models with many degrees of freedom. In the context of the methodology developed, the dual directional coupling (DD-3 from figure 4.25) represents a potential model simplification in that the dual directional is eliminated and only the power flow from the gearbox to the housing is taken into account. A simulation with the simplified model is carried out as an example (figures 6.19 and 6.20). The simulation time can be reduced by approximately 26.8%. However, the results of the simplified model are in comparison to measurements according to the modified error about 60% worse than that of the variant with feedback. Consequently, the time-variant boundary condition, which represents a bearing that is also moved through the housing, is a physical phenomenon that should be taken into account in the vibro-acoustic modeling. Unlike the system model, for the case of single domain analysis, FE simulations the effect of dual directional coupling is present intuitively within the model solution. For e.g., when a load is applied on the housing structure, it automatically transfers the load on to the bearings and vice versa. Therefore the effect of DD3 is not largely focused within the FE analysis. Note that FE simulation time could be easily 20 to 30 times that of the system model. But it could not be completely disregarded as it would allow to analyze the wear mechanisms and provide better accuracy for the NVH calculations.

The surface vibration of the gear housing generates the sound emitted into the surrounding fluid. In general, the sound is calculated via the kinematic coupling conditions, which considers the normal velocity of the structure and fluid at the interface to be equal. Further, it considers impedances, material properties of the fluid etc., to calculate the acoustic pressures at far field locations. From a system perspective, the ERP technique is mainly used for making the calculations. For the FE results, the acoustic finite, infinite elements are utilized, which are developed based on the Naviers-stokes equations (check figure 4.24). The modified errors of around 15% and 5% in acoustic pressure is calculated for the ERP and FE model respectively. These percentages show the accuracy of FE over the system model simulation.

One more important problem addressed was the wear among gears. Even though the simulation of the wear is much complex, many assumptions are made to tone it down to variant that could be numerically studied. The parameters like hardness, contact properties, friction etc., are analyzed via the UQ approach. Later, the FE simulations are executed to calculate the wear depths and wear rates (check figure 4.30). Also, the values are coupled with machine learning algorithms for further predictions. The modified errors of around 6.56% and 4.27% are obtained for vibrations and acoustic in the abraded simulation model (against the experiments).

In summary, a simulation model created according to the generic, multi-domain methodology enables not only the numerical analysis of modified transmission components, but also the possibility of optimizing different system parameters. Due to the mapping among the multi-domain mechanisms (excitation, transmission and radiation) optimization within the framework of an overall system is achieved. Finally, the effects of parameter changes are shown in section 4.8 and 6.5. Decent 5 to 10% improvements in acoustic quantities are achieved via the suggestions made in those sections.

Future Scope

In this section, few concepts apropos for further steps are depicted. The presented, methodology for the modeling and simulation of structure borne emissions and wear mechanisms in drive-trains opens up new research opportunities. The following questions can be listed as an outlook:

Noise and vibration of the drivetrains

- Although the sound pressure and power level are important acoustical parameters, they do not characterize the customers perception of product sound sufficiently. This work focused in quantifying the acoustic characters like pressure and intensity of the drivetrains. It neglected the sensitivities of realizing the behavior in regards with human ear. Same amplitudes of acoustic pressures can be heard in a completely different manner with change in frequencies. The parameters, e.g., loudness, sharpness, tonality, roughness, fluctuation strength, etc., are much more useful for characterization purposes. The assessment of this kind of airborne sound emission falls in the area of psychoacoustics. For this purpose, the sound behavior can be further analyzed with regard to human impression.
- Better material properties like damping tables, hyperelastic constants etc., for each of the materials and dampings at contact interfaces in the power unit can be further investigated to make the FE simulations perfect.
- The temperature gradients inside the drivetrains can also impact the vibration characteristics. The system models developed can be improved to incorporate the temperature fields, thereby comprehending its influences.
- During the time for measurements and calculations of the acoustic behavior, it was found out that few factors like volumetric drag were vital for obtaining decent results. Few of these acoustic model properties considered were straight out of the literature. For more robust acoustic pressure calculations, the values such as drag coefficient, material characteristic impedance of the fluid and surface impedance at the fluid structure interface can be derived from experiments. Also, the pressure values could be converted into wave files, which enables the user to hear the sounds generated from the simulation data.

Abrasion at the gear components

- Concerning abrasion simulation, more accurate wear model subroutines can be developed (for e.g., specific to the application) to obtain more plausible simulation results. Moreover, the geometries of the gears, for e.g., the number of tooth would have a strong nonlinear influence on the wear. These parameters can be included in the design space, which could be better modeled by a NN.
- Until now, sigmoid kind of nonlinear activation function was used for making the prediction with neural networks. They have a problem of vanishing gradients, i.e., the gradients diminish in value by the time they reach the beginning layers. This can cause problems for developing neural network on to bigger sizes with more layers. In order to avoid this problem and make improved predictions, few alternate activation functions like ReLU or advanced convolutional and temporal neural networks could be tested.
- Within abrasion calculations, one major area is lubrication. The friction models can be developed to include impact of lubrication properties like densities, temperature of the fluids, which further would influence the wear profiles.
- Throughout the thesis, impact of abrasion on vibration characteristics is developed. For the next research node, the reverse coupling of understanding the influence of NVH on wear among the gears can also be analyzed.

Optimization of the structures

- With a view to optimizing different system parameters, multi target sizes can be defined and then optimized as part of multi-domain system simulation.

8 Appendix

Table 8.1 describes various scale factors used throughout chapters 5 and 6 to represent the Eigen frequencies, surface acceleration and acoustic pressure. Note that, all the plots are scaled/ normalized with different factors in order to conceive the plots in a better way.

Scale Factors	**Natural frequency**	**Amplitudes - vibration**	**Amplitudes - acoustic**
Cube (sec 5.3.1)	SF1	SF1v	SF1a
Individual structures (sec 6.2.3)	SF2	-	-
Combined structures (sec 6.2.3)	SF3	SF3v	SF3a
Complete drivetrain (sec 6.2.3)	SF4	SF4v	SF4a
Wear individual structures (sec 6.4)	SF2	-	-
Wear complete drivetrain (sec 6.4)	SF4	SF4v	SF4a
Improved design components (sec 6.5.1)	SF3	-	SF3a
Improved material components (sec 6.5.2)	SF3	SF3vv	SF3aa
Optimized complete drivetrain (sec 6.5)	SF4	SF4v	SF4a
Other possible optimizations (sec 6.5.3)	SF4	SF4v	SF4a

Table 8.1: Various scale factors used in the work for representation of Eigen frequencies and amplitudes

9 Bibliography

[Abi19] Abijhith, S.: *NPTEL- Aocustic and Noise Control - Acoustic analysis of automotive exhaust system*, 2019. https://nptel.ac.in/courses/112106225//.

[Aco16] Acoustics, Head: *Acoustic Camera / Head Visor (code /5000ff) Handbook.*, 2016.

[AH56] Archard, J.F. and W. Hirst: *The Wear of Metals under Unlubricated Conditions.* The Royal Society, 1956.

[AK14] Angeles, J. and A. Kecskemethy: *Kinematics and Dynamics of Multi-body Systems*, volume 360. Springer, 2014.

[Ake01] Akerblom, M.: *Gear Noise and Vibration - A Literature Survey.* Digitala Vetenskapliga Arkivet, pages 1–25, 2001.

[Alt18] Altair: *Vibrations and Acoustics, Hypermesh User's Guide.* Hyperworks, Altair, 2018.

[Ami07] Amirouche, F.: *Fundamentals of Multibody Dynamics: Theory and Applications*, volume 1. Springer Science & Business Media, 2007, ISBN 9780817642365.

[And95] Anderson, J.: *Computational Fluid Dynamics - Introduction to CFD*, volume 206. Springer, 1995, ISBN 9783540534600.

[And14] Anderl, R.: *Simulations with NX - Kinematics, FEM, CFD, EM and Data Management. With Numerous Examples of NX 9.* Hanser eLibrary. Hanser Publications, 2014, ISBN 9781569904794.

[Arc04] Archard, J.F.: *Contact and Rubbing of Flat Surfaces.* Journal of Applied Physics, pages 981–988, 2004.

[Bat07] Bathe, K.J.: *Finite Element Procedures.* Prentice Hall, New Jersey, 2007, ISBN 9783540668060.

[Bhu15] Bhushan, B.: *Introduction to Tribology.* Wiley, 2015.

[BKA04] Bajpai, P., A. Kahraman, and N. Anderson: *A Surface Wear Prediction Methodology for Parallel-Axis Gear Pairs.* Journal of Tribology-transactions of The Asme - J TRIBOL-TRANS ASME, 126:597–605, 2004.

[Bri97] Brigham, E.O.: *FFT - Anwendungen.* Oldenbourg Wissenschaftsv, 1997, ISBN 9783486215670.

[CAN19] CANape, Vector: *CANaoe Software Tools, Analysis, Diagnostics and Simulation Guide*, 2019.

[CFD19] CFD: *CFD model of a car*, 2019. https://www.cfd-online.com/Wiki/DrivAer_Model/.

[Cla04] Clarence, W.: *Mechatronics - An Integrated Approach.* CRC press, 2004.

[Cor15] Corves, B.: *Modal Analysis of the Structures, Mutli Body Dynamics.* IGM Aachen, 2015.

[Cor16] Corp, Dassault Systems Simulia: *Simulia User Assistance Guide 2016 - About submodeling*, 2016. http://abaqus.software.polimi.it/v2016/books/key/default.htm.

[Cor17a] Corp, Dassault Systems Simulia: *Simulia User Assistance Guide 2017 - About dynamic analysis procedures*, 2017. https://abaqus-docs.mit.edu/2017/English/

SIMACAEEXCRefMap/simaexc-c-docproc.htm.

[Cor17b] Corp, Dassault Systems Simulia: *Simulia User Assistance Guide 2017 - Contact formulations, types and algorithms*, 2017. https://abaqus-docs.mit.edu/2017/English/SIMACAEEXCRefMap/simaexc-c-docproc.htm.

[Cor18a] Corp, Dassault Systems Simulia: *Simulia User Assistance Guide 2018 - Infinite element library*, 2018. https://www.3ds.com/support/documentation/resource-library/single/simulia-user-assistance-documentation/.

[Cor18b] Corp, Dassault Systems Simulia: *Simulia User Assistance Guide 2018 - Mesh convergence study*, 2018. https://www.3ds.com/support/documentation/resource-library/single/simulia-user-assistance-documentation/.

[Cor18c] Corp, Dassault Systems Simulia: *Simulia User Assistance Guide 2018 - Terms for optmization*, 2018. https://www.3ds.com/support/documentation/resource-library/single/simulia-user-assistance-documentation/.

[Cor19] Corp, Dassault Systems Simulia: *Simulia User Assistance Guide 2019 - About ALE adaptive meshing*, 2019. https://www.3ds.com/support/documentation/resource-library/single/simulia-user-assistance-documentation/.

[CP14] Carlos, A. and A. Pedro: *Numerical Calculation of Eigenfrequencies and Eigenmodes of 3D Simply Connected Domains using the Method of Fundamental Solutions*. Numerical Methods for Partial Differential Equations, 2014.

[CPZ96] Choy, F.K., V. Polyshchuk, and J.J. Zakrajsek: *Analysis of the Effects of Surface Pitting and Wear on the Vibration of a Gear Transmission System*. Tribology International, 29:77–83, 1996.

[CSA99] Chih, H.J., G. Steyer, and T. Abe: *Gear Noise Reduction through Transmission Error Control and Gear Blank Dynamic Tuning*. Technical Report 1999-01-17660, SAE Technical Paper, 1999.

[Dac16] Dackermann, T.: *Generische domaenenuebergreifende Methodik fuer die Modellierung und Simulation vibroakustischer Mechanismen in Getrieben*. PhD thesis, Goethe University, PhD Thesis, 2016.

[Dar17] Darmstadt, TU: *Support Vector Regression*, 2017. https://www.kma.informatik.tu-darmstadt.de/fileadmin/user_upload/Group_KMA/teaching/se_recommender_systems/Recommender_Systeme_-_Reinforcement_Learning.pdf.

[DB12] Dupont, J.B. and P. Bouvet: *Multiphysics Modelling to Simulate the Noise of an Automotive Electric Motor*. 2012, ISSN 0148-7191.

[DDH15] Dackermann, T., R. Doelling, and L. Hedrich: *Method for System Level Vibro-acoustic Gear Modeling and Simulation of Electro-mechanical Drive Trains*. In *2015 IEEE International Symposium on Systems Engineering (ISSE)*, pages 60–65, 2015.

[Dej85] Dejong, R.G.: *A Study of Vehicle Interior Noise using Statistical Energy Analysis*. Technical Report 850960, SAE Technical Paper, 1985.

[DMH15] Dackermann, T., S. Miller, and L. Hedrich: *Flexible Gear Model Library - Vibration Excitation Mechanisms and Gear Force Calculation*. Modelling, Identification and Control / 827: Computational Intelligence, 2015.

[Doe14] Doering, A.: *Analyse flexibler Korper in der Mehrkorpersimulation*. Fakultat fur Maschinenbau und Mechatronik, Bachelorarbeit, 2014.

[DV05] Desmet, W. and D. Vandepitte: *Finite Element Modeling for Acoustics*. Numerical Acoustics, 2005.

[Ebr06] Ebrahimi, S.and Eberhard, P.: *Rigid-elastic Modeling of Meshing Gear Wheels in Multibody Systems*. Multibody System Dynamics, 16(1):55, 2006, ISSN 1573-272X. https://doi.org/10.1007/s11044-006-9021-7.

[Eco18] Ecotrib: *European COnference on TRIBology*. Austrian Tribology Society, Italian Tribology Association, the Slovenian Society for Tribology and Swiss Tribology, 2007-2018.

[FA97] Flodin, A. and S. Andersson: *Simulation of Mild Wear in Spur Gears*. ScienceDirect, 1997.

[FBS19] Feng, K., P. Borghesani, and W. Smith: *Vibration-based Updating of Wear Prediction for Spur Gears*. Wear, 426-427:1410–1415, 2019.

[Fir38] Firestone, F.A.: *The Mobility Method for Computing The Vibration of Linear mechanical and Acoustical Systems - Mechanical Electrical Analogies*. J. Applied Physics 9, pp. 373- 387, June 1938.

[Flo10] Flodin, A.: *Wear of Spur and Helical Gears*. Royal Institute of Technology, 2010.

[FMJ09] Fritze, D., S. Marburg, and H. Jurgen: *Estimation of Radiated Sound Power - a Case Study on Common Approximation Methods*. Acta Acustica United with Acustica, 95(5):833–842, 2009.

[Fra94] Frank, J.: *Statistical Energy Analysis - A Critical Overview*. Philosophical Transactions of the Royal Society of London A: Mathematical, Physical and Engineering Sciences, 346(1681):431–447, 1994.

[Fri11] Fritz, F.: *Modellierung von Walzlagern als generische Maschinenelemente einer Mehrkorpersimulation*, volume 14. KIT Scientific Publishing, 2011.

[Fri15] Fritzson, A.: *Principles of Object-Oriented Modeling and Simulation with Modelica 3.3 - A Cyber-physical Approach*. 2nd ed., John Wiley and Sons Inc, 2015.

[Ger15] Gerhard, M.: *Continuum Mechanics and Tensor Analysis*. Lehrstuhl fur Baumechanik - TU Munchen, 2015.

[GHS12] Gross, D., W. Hauger, and J. Schroder: *Formeln und Aufgaben zur Technischen Mechanik 4 - Hydromechanik, Elemente der hoheren Mechanik, Numerische Methoden*. Springer-Verlag, 2012.

[GRR03] Glover, R.C., C. Rodney, and G. Rauen: *Gear Transmission Error Metric for use with Gear Inspection Machine*. Technical report, SAE Technical Paper, 2003.

[Hat00] Hatch, M.R.: *Vibration Simulation Using MATLAB and ANSYS*. CRC Press, Inc., Boca Raton, FL, USA, 1st edition, 2000, ISBN 1584882050.

[Hir16] Hirani, H.: *Fundamentals of Engineering Tribology with Applications*, chapter Wear Maps. Cambridge University Press, Delhi, India (2016), 2016. http://nptel.ac.in/syllabus/112102014/.

[HK07] Huali, D. and A. Kahraman: *Interactions Between Nonlinear Spur Gear Dynamics and Surface wear*. Journal of Sound and Vibration - J SOUND VIB, 307:662–679, 2007.

[HOV94] Houser, R., F. Oswald, and M. Valco: *Comparison of Transmission Error Predictions with Noise Measurements for Several Spur and Helical Gears*. National Aeronautics and Space Administration, 1994.

[HPC12] Humbert, L., P. Pellerey, and S. Cristaudo: *Electromagnetic and Structural Coupled Simulation to Investigate NVH Behavior of an Electrical Automotive Powertrain*. SAE International Journal of Alternative Powertrains, 1:395–404, 2012.

[HR04] Hirschberg, A. and S.W. Rienstra: *An Introduction to Aeroacoustics*. PhD thesis, Eindhoven University of Technology, 2004.

[HS12] Hiroaki, E. and N. Sawalhi: *Mechanical Engineering*, chapter Gearbox Simulation Models with Gear and Bearing Faults. intechopen, 2012, ISBN 978-953-51-0505-3.

[ISO16] ISO, 6336: *Calculation of Load Capacity of Spur and Helical Gears*. 2016.

[JWE16] Jan, T., G. D. Welf, and H. Eric: *Acoustical Optimization of a Train Gearbox Based on Overall System Simulation.* INTER-NOISE and NOISE-CON Congress and Conference Proceedings, pages 1–10, 2016.

[JZH12] Jinfu, D., F. Zongde, and D. Hao: *Time Varying Mesh Stiffness of Gear Pair Based on Loaded Tooth Contact Analysis.* Third International Conference on Digital Manufacturing and Automation, 979-982, 2012.

[JZS17] Jun, L., Z. Zhan, and H. Song: *Design Optimization of Vehicle Body NVH Performance Based on Dynamic Response Analysis.* SAE Technical Papers, 2017.

[Kat05] Kato, K.: *Friction and Wear of Passive metals and Coatings.* Tribocorrosion of Passive Metals and Coatings, pages 65–99, 2005.

[KD10] Kahraman, A. and H. Ding: *A Methodology to Predict Surface Wear of Planetary Gears Under Dynamic Conditions.* Mechanics Based Design of Structures and Machines, 38(4):493–515, 2010. https://doi.org/10.1080/15397734.2010.501312.

[KDH19a] Kolluru, Y., R. Doelling, and L. Hedrich: *Numerical Simulations of Vibro-acoustic Behaviors Related to Drive Train Assemblies.* In *2019 International Symposium on Systems Engineering (ISSE)*, pages 1–8, 2019.

[KDH19b] Kolluru, Y., R. Doelling, and L. Hedrich: *Wear Estimation using FEM and Machine Learning Techniques.* In *2019 ECOTRIB conference*, pages 176–178, 2019. https://ecotrib2019.oetg.at/program2.

[KDH20a] Kolluru, Y., R. Doelling, and L. Hedrich: *Generic Methodology for Vibration and Wear Analysis to Understand their Influences in an Electric Drivetrain - accepted for publication.* In *2020 Integrating Seamlessly NVH*, pages 1–12, 2020.

[KDH20b] Kolluru, Y., R. Doelling, and L. Hedrich: *Multi Domain Modeling of NVH for Electromechanical Drives - accepted for publication.* In *2020 Integrating Seamlessly NVH*, pages 1–12, 2020.

[Key16] Keyence: *3D Laser Scanning Confocal Microscope, VK-X Series Measurement Unit*, 2016. https://www.keyence.com/products/measure-sys/3d-measure/vk-x100_x200/models/vk-x160k/index.jsp.

[KHA09] Karl-Heinrich, G. and E.K. Antonsson: *Springer Handbook of Mechanical Engineering*, volume 10. Springer Science & Business Media, 2009.

[Kim15] Kim, N.H.: chapter Finite Element Analysis for Contact Problems, pages 367–426. Springer US, New York, NY, 2015, ISBN 978-1-4419-1746-1. https://doi.org/10.1007/978-1-4419-1746-1_5.

[Kim17] Kim, P.: *MATLAB Deep Learning: With Machine Learning, Neural Networks and Artificial Intelligence.* Apress, 2017, ISBN 9781484228456.

[Kin82] Kinsler, E.: *Sound Radiated Power, in Fundamentals of Acoustics.* John Wiley and Sons Australia, 1982, ISBN 9780471029335.

[KIS16] KISSsys: *Tool for Contact Analysis in KISSsoft.* 2016. https://www.kisssoft.ch/english/home/index.php.

[KK16] Koji, K. and A. Koshi: *Wear Mechanisms.* Tohoku University, 2016.

[KKB89] Kenneth, A., G. Koopmann, and K. Brod: *A Boundary Element Method for Acoustic Radiation Valid for all Wavenumbers.* The journal of the acoustical society of America, 85(1):39–48, 1989.

[KL01] Kuang, J. and A. Lin: *The Effect of Tooth Wear on the Vibration Spectrum of a Spur Gear Pair.* Journal of Vibration and Acoustics, 123, 2001.

[Klo16] Klocke, H.C.F.: *Finite Element Simulation of Cutting Processes.* WZL RWTH Aachen University, 2016.

[Kor07] Korka, Z.: *An Overview of Mathematical Models Used in Gear Dynamics*. RJAV, 2007.

[Kru07] Kruntcheva, M.: *Acoustic Structural Coupling of the Automobile Passenger Compartment*. World Congress on Engineering, 2166:1–6, 2007.

[KSA06] Kollmann, F., T. Schosser, and R. Angert: *Praktische Maschinenakustik*. Springer, 2006.

[KSO06] Kostic, S., C. Snevzana, and M. Ognjanovic: *Excitation of the Modal Vibrations in Gear Housing Walls*. FME Transactions, 34(1):21–28, 2006.

[KWK02] Koike, T., H. Wada, and T. Kobayashi: *Modeling of the Human Middle Ear using the Finite Element Method*. The Journal of the Acoustical Society of America, 111(3):1306–1317, 2002.

[LA87] Lim, S.C. and M.F. Ashby: *Wear Mechanism Maps*, 1987. https://www.sciencedirect.com/science/article/pii/0001616087902094.

[LB10] Linke, H. and J. Borner: *Types of Excitations, Stirnradverzahnung*. Hanser, 2010, ISBN 9783446414648.

[LPW17] Li, R., X. Peng, and W. Wei: *Electromagnetic Vibration Simulation of a 250 MW Large Hydropower Generator with Rotor Eccentricity and Rotor Deformation*. Energies, 10:2155, 2017.

[Lyo14] Lyon, Richard H.: *Theory and Application of Statistical Energy Analysis*. Elsevier, 2014.

[Mar85] Margolis, D.L.: *A Survey of Bond Graph Modelling for Interacting Lumped and Distributed Systems*. Journal of the Franklin Institute, 319(1):125–135, 1985.

[Mar13] Marcus, S.: *Contact Mechanics in Gears*. CHALMERS UNIVERSITY OF TECHNOLOGY, 2013.

[Mat8ba] MathWorks: *Simscape Training Guide*, R2018b.

[Mat8bb] MathWorks: *Simulink Training Guide*, R2018b.

[Mat17] MathWorks: *Neural Network Toolbox Start Up Guide*, 2017. https://www.mathworks.com/help/deeplearning/index.html?s_tid=CRUX_lftnav.

[Mat19] MathWorks: *Matlab Automotive Conference 2018*, 2019. https://www.mathworks.com/company/events/conferences/automotive-conference-stuttgart/2019.html.

[MBR04] Mrazek, T., A.K. Belyaev, and R. Reitbauer: *Versuchsgestutzte Modellierung von Kfz-Stossdampfern fur die Dynamische Mehrkorpersimulation*. e&i Elektrotechnik und Informationstechnik, 121(9):313–318, 2004.

[MDY07] Morgan, J.A., M.R. Dhulipudi, and Yakoub R. Y.: *Gear Mesh Excitation Models for Assessing Gear Rattle and Gear Whine of Torque Transmission Systems with Planetary Gear Sets*. SAE Noise and Vibration Conference and Exhibition, 2007.

[ML94] Meng, H.C. and K.C. Ludema: *Wear Models and Predictive Equations - Their Form and Content*. Elsevier, 1994.

[MMB91] Montbrun, D.J., Delgado M., and C. Brie: *A Survey of Bond Graphs - Theory, applications and programs, pp. 565-606*. Journal of The Franklin Institute, vol. 328, no. 5/6, 1991.

[MOR00] Molinari, J.F., M. Ortiz, and R. Radovitzky: *Finite Element Modeling of Dry Sliding Wear in Metals*. Emerald, 2000.

[MSO15] Millithaler, P., E. Sadoulet, and M. Ouisse: *Structural Dynamics of Electric Machine Stators - Modelling guidelines and identification of three-dimensional equivalent material properties for multi-layered orthotropic laminates*. Journal of Sound

and Vibration, 348, 2015.

[Nik04] Nikishkov, G. P.: *INTRODUCTION TO THE FINITE ELEMENT METHOD*. University of Aizu, 2004.

[NW13] Niemann, G. and H. Winter: *Maschinenelemente - B and 2 - Getriebe allgemein, Zahnradgetriebe-Grundlagen, Stirnradgetriebe*. Springer Verlag, 2013.

[NWH05] Niemann, G., H. Winter, and R. Hoehn: *Maschinenelemente Band 1 - Konstruktion und Berechnung von verbindungen, Lagern, Wellen*. Springer Verlag, 4 a. edition, 2005, ISBN 3-540-25125-1.

[OH88a] Ozguven, H. N. and D. R. Houser: *Mathematical Models used in Gear Dynamics*. Journal of Sound and Vibration 121(3), 1988.

[OH88b] Ozguven, H.N. and D.R. Houser: *Mathematical Models used in Gear Dynamics*. Journal of sound and vibration, 121(3):383–411, 1988.

[PAV00] Parker, R.G., V. Agashe, and S.M. Vijayakar: *Dynamic Response of a Planetary Gear System using a Finite Element/contact Mechanics Model*. Journal of Mechanical Design, 122(3):304–310, 2000.

[Pav18] Pavlov, N.: *Numerical Simulation on the Vibration of a Vehicle Drivetrain with Dual Mass Flywheel*. International Scientific Journals of Scientific Technical Union of Mechanical Engineering Industry 4.0, 2018.

[Paw19] Pawan, S.: *How to Evaluate Gear Mesh Stiffness in a Multibody Dynamics Model*, 2019. https://www.comsol.com/blogs/how-to-evaluate-gear-mesh-stiffness-in-a-multibody-dynamics-model/.

[Pet89] Petersen, D.: *Auswirkung der Lastverteilung auf die Zahnfusstragfahigkeit von hoch uberdeckenden Stirnradpaarungen*. Fakultat Maschinenbau TU Carolo-Wilhelmina zu Braunschweig, 1989.

[Pet00] Peter, S.: *Physically Oriented Modeling of Heterogeneous Systems*. 3rd IMACS Symposium of Mathematical Modelling (MATHMOD), 2000.

[Pet06] Peter, W.: *Computational Contact Mechanics*. Second edition, Springer, 2006.

[Pie89] Pierce, A.: *Acoustics - An Introduction to Its Physical Principles and Applications*, volume 34. Physics Today - PHYS TODAY, 1989, ISBN 0883186128.

[PK14] Patil, S. and S. Karuppanan: *Contact Stress Analysis of Helical Gear Pairs including Frictional Coefficients*. Elsevier, 2014.

[PS97] Priit, P. and A. Soeren: *Wear Simulation with the Winkler Surface Model*. Elsevier, 1997.

[Qev00] Qevist, Mona: *Numerical Simulations of Wear*. Lulea University of Technology, 2000.

[Rav17] Ravindran, B.: *Nptel - Introduction to Machine Learning*, 2017. https://onlinecourses.nptel.ac.in/noc18_cs26/preview.

[Rhe71] Rhee, S.K.: *Wear of Metal-reinforced Phenolic Resins*. Wear Journal, 18:471–477, 1971.

[Rog15] Roger, S.: *Contact Mechanics*. RWTH Aachen University, 2015.

[RPB08] Rodriguez, J., V. Pedro, and A. Belahcen: *Air-gap Force Distribution and Vibration Pattern of Induction Motors Under Dynamic Eccentricity*. Electrical Engineering, 90(3):209–218, 2008, ISSN 1432-0487. https://doi.org/10.1007/s00202-007-0066-2.

[Saw11] Sawodny, O.: *Modellierung und Identifikation Dynamischer Systeme (MIS)*. Institut fuer Systemdynamik (ISYS) der Universität Stuttgart - Umdruck zur Vorlesung zum WS11/12, 2011.

[Sch05] Schmitz, T.L.: *The Difficulty of Measuring Low Friction - Uncertainty Analysis for*

Friction Coefficient Measurements. Journal of Tribology-Transactions of the Asme, pages 673–678, 2005.

[Sie15] Siemens: *LMS Test.lab, Analysis and Structural Design Manual*. Siemens Industry Software, 2015.

[Sie20] Siemens: *What is a Frequency Response Function (FRF)?*, 2020. https://community.sw.siemens.com/s/article/what-is-a-frequency-response-function-frf.

[SIH91] Sundaresan, S., K. Ishii, and D.R. Houser: *A Procedure Using Manufacturing Variance to Design Gears with Minimum Transmission Error*. Journal of Mechanical Design, 113(3):318–324, 1991.

[Ska18] Skansi, S.: *Introduction to Deep Learning - From Logical Calculus to Artificial Intelligence*. Undergraduate Topics in Computer Science. Springer International Publishing, 2018, ISBN 9783319730042.

[SKY01] Sobieszczanski, J., S. Kodiyalam, and R.Y. Yang: *Optimization of Car Body under Constraints of Noise, Vibration, and Harshness (NVH), and Crash*. Structural and Multidisciplinary Optimization, 22(4):295–306, 2001, ISSN 1615-1488. https://doi.org/10.1007/s00158-001-0150-6.

[Smi03] Smith, J. D.: *Gear Noise and Vibration*. Second edition, Marcel Dekker, Inc., 2003.

[Soe90] Soeren, A.: *Prediction of the Sliding wear of Spur Gears*. Wiley, 1990.

[Soe09a] Soederberg, A.: *Evaluation of Dry Sliding Wear Rate and Analysis of Residual Stress*. Shodhganga, 2009.

[Soe09b] Soederberg, A.: *Interface Modeling - Friction and Wear*. Lulea University of Technology, 2009.

[Soe10] Soeren, A.: *Wear Simulation*, 2010. https://www.scribd.com/document/325626346/Wear-Simulation.

[SP05] Saeed, E. and E. Peter: *Rigid-elastic Modeling of Meshing Gear Wheels in Multibody Systems*. Springer Science, 2005.

[SPC06] Singh, A.K., S.S. Panda, and D. Chakraborty: *Predicting Drill Wear Using an Artificial Neural Network*. The International Journal of Advanced Manufacturing Technology, 28(5):456–462, 2006, ISSN 1433-3015. https://doi.org/10.1007/s00170-004-2376-0.

[SR96] Sweeney, P.J. and R.B. Randall: *Gear Transmission Error Measurement Using Phase Demodulation*. Proceedings of the Institution of Mechanical Engineers, Part C: Journal of Mechanical Engineering Science, 210(3):201–213, 1996.

[Ste16] Stephen, M.: *Modern Tribology Handbook*, chapter Wear Maps. 2016.

[Sul16] Sullivan, T.J.: *Introduction to Uncertainty Quantification*. 1st ed., Springer, 2016.

[SWW88] Seybert, A.F., T.W. Wu, and X.F. Wu: *Radiation and Scattering of Acoustic Waves from Elastic solids and Shells using the Boundary Element Method*. The Journal of the Acoustical Society of America, 84(5):1906–1912, 1988.

[Tec19] Technology, Polytec GmbH: *Vibrometer Measurements*, 2019. https://www.polytec.com/eu/vibrometry/technology/.

[Tha10] Tharmakulasingam, R.: *Transmission Error In spur gears - Static and Dynamic Finite Element Modeling and Design Optimization*. PhD thesis, Brunel University School of Engineering and Design PhD Thesis, 2010.

[TL16] Tuononen, A. and A. Lajunen: *Modal Analysis of Different Drivetrain Configurations in Electric Vehicles*. Journal of Vibration and Control, 24:126–136, 2016.

[UW99] Uchtmann, K. and R. Wirth: *Maschinen-diagnose an drehzahlveraenderlichen*

Antrieben mittels Ordnungsanalyse. ANTRIEBSTECHNIK, 38:44–49, 1999.

[VA18] Victor, C. and M. Arnav: *Modeling Flexible Bodies in Simmechanics.* Technical Articles and Newsletters, MathWorks Inc., 2018.

[VD12] Van, N. and N. Dien: *Parametric Vibration Analysis of Transmission Mechanisms Using Numerical Methods.* INTECH Open Access Publisher, 2012.

[VW97] Voigt, P. and G. Wachutka: *Electro-fluidic Microsystem Modeling Based on Kirchhoffian Network Theory.* Dig. of Tech. Papers of Transducers 97, pp. 1019- 1022, 1997.

[WBN55] Weber, C., K. Banaschek, and G. Niemann: *Formanderung und Profilrucknahme bei gerad-und schragverzahnten Radern.* F. Vieweg, 1955.

[WH11] William, K. and S. Herold: *Electroactive Polymer Actuators in Dynamic Applications.* Mechatronics, IEEE/ASME Transactions on, 16(1):24–32, 2011.

[WJ12] Journal Wear: *An International Journal on the Science and Technology of Friction, Lubrication and Wear.* Sciencedirect, 1972-2012. https://www.sciencedirect.com/journal/wear/issues.

[WKB16] Winokur, J., D. Kim, and F. Bisetti: *Sparse Pseudo Spectral Projection Methods with Directional Adaptation For Uncertainty Quantification.* Journal of Scientific Computing Springer, Volume 68, Issue 2, August 2016.

[WM94] Wriggers, P. and K. Miehe: *Heat Formulations at Contact.* Prentice Hall, New Jersey, 1994.

[WO03] Wojnarowski, J. and V. Onishchenko: *Tooth Wear Effects on Spur Gear Dynamics.* Mechanism and Machine Theory, 38:161–178, 2003.

[Woe11] Woernle, C.: *Mehrkorpersysteme - eine Einfuhrung in die Kinematik und Dynamik von Systemen starker Korper.* Springer-Verlag, 2011.

[Wri07] Wriggers, P.: *Contact Mechanics.* Prentice Hall, New Jersey, 2007.

[Yef05] Yefimenko, Y.: *Komponentenorientierte Modellierung elektrischer Systeme in der Mechatronik.* PhD thesis, Otto-von-Guericke-Universitat Magdeburg, Universitatsbibliothek, 2005.

[YF03] Yesilyurt, I. and G. Fengshou: *Gear Tooth Stiffness Reduction Measurement using Modal Analysis and its Use in Wear Fault Severity Assessment of Spur Gears.* NDT and E International, 36:357–372, 2003.

[YTS05] Yuan, G.H., L.C. Teik, and W.S. Shepard: *Experimental Study on Active Vibration Control of a Gearbox System.* Journal of Sound and Vibration, 282(3):713–733, 2005.

[Zei06] Zeitler, A.: *Untersuchung der Hubschrauberinnenakustik mittels der Methode der statistischen Energieanalyse.* PhD thesis, Technische Universitat Munchen, 2006.

[Zel09] Zeller, P.: *Handbuch Fahrzeugakustik.* Springer, 2009.

[ZT17] Zienkiewicz, O.C. and R.L. Taylor: *Computer Procedures for Finite Element Analysis, The Finite Element Method Vol. 2.* McGraw-Hill, , New York, 2017.